Characterization of the Cellular and Molecular profiles of *CDH1*-re-expressed Breast Adenocarcinoma Cells (MDA-MB-231) treated with Zebularine and Trichostatin A followed by Tumour Necrosis Factor-related Apoptosis-inducing Ligand (TRAIL)

SONIA WONG HOW MING_UNIMKL-017629

Supervised by	:	**Dr Eunice Ngai Siew Ching** (School of Biosciences)
Co-supervised by	:	**Dr Fang Chee Mun** (School of Pharmacy)
		Prof Sandy Loh Hwei San (School of Biosciences)
Internal Assessor	:	**Dr Pung Yuh Fen** (School of Pharmacy)

Project write-up submitted to
The University of Nottingham for the degree of
doctor of philosophy
(July 2019)

Abstract

Breast cancer (BC) is a heterogeneous disease of which its definite cure had yet to be discovered. Tumour Necrosis Factor-related Apoptosis-inducing Ligand (TRAIL) is one potential anti-cancer protein with its selective killing on cancerous cells while largely evading the healthy cells. Nonetheless, many cancer cells have built TRAIL resistance, including breast cancer. In this study, the addition of two epigenetic drugs, Trichostatin A (TSA) and Zebularine (Zeb) combined prior to TRAIL treatment (TZT) was shown to induce significant increase in G_0/G_1 cell cycle arrest in MDA-MB-231 (57.78%). With E-cadherin expression, the G_0/G_1-arrested population increased to 74.2% (231-EGFP) and 83.15% (MCF-7). Moreover, TZT had also significantly reduced cell viability of 231-EGFP to 62.12%. The observed cell inhibitory effects might be due to suppression of proliferating cell nuclear antigen (PCNA) and cyclin-dependent kinase 2 (CDK2) mRNA expression. The TZT-induced cell cycle arrest had also driven apoptosis occurrence and it was supported by the up-regulation of p21 and p-p53 (S392) proteins in MDA-MB-231 by TZT. With the *in vitro* re-expression of E-cadherin in 231-EGFP, down-regulation of anti-apoptotic PON2, Catalase, Clusterin, IAPs as well as cell stress proteins had validated the notion that E-cadherin expression enhances the TZT anti-cancer efficacy. Similarly, in E-cadherin-positive MCF-7, TZT treatment had down-regulated the anti-apoptotic proteins, increased the pro-apoptotic SMAC, HTRA2 as well as both the TRAIL receptors, TRAIL-R1 and -R2. On the other hand, the TZT treatment regime had negligible effect on reducing the cell migration rate of the invasive MDA-MB-231 and 231-EGFP cell lines. This was supported by the lack of pro-invasive matrix metalloproteinase 9 (MMP9) down-regulation by the TZT treatment. Therefore, our study showed that TSA and Zeb are potential sensitizers of breast cancer towards TRAIL-induced cell inhibition, cell cycle arrest leading towards apoptosis while having no tangible anti-invasive potential. Nonetheless, from our *ex vivo* findings, TRAIL-R2, TRAIL and E-cadherin markers' anti-cancer functions had been hijacked by BC cells to facilitate their survival (TRAIL) and metastatic potential (TRAIL-R2, E-cadherin). Thus, these markers' over-expression and localization can potentially serve as markers for BC prognosis and treatment regime selection.

List of publications

Wong SHM, Fang CM, Chuah L-H, Leong CO, Ngai SC (2018). E-cadherin: Its dysregulation in carcinogenesis and clinical implications. *Crit Rev Oncol Hematol* 121: 11–22. (**published**)

Wong SHM, Kong WY, Fang CM, Loh HS, Chuah Alice, Abdullah Syahriil, Ngai, SC (2019).
The TRAIL to Cancer Therapy: Hindrances and Potential Solutions *Criti Rev Oncol Hematol* (**published**)

Wong SHM, Fang CM, Loh HS, Ngai SC (2019) Trichostatin A and Zebularine along with E-cadherin Re-expression Enhances Tumour Necrosis Factor-related Apoptosis-inducing Ligand (TRAIL)-induced G_0/G_1 Cell Cycle Arrest in Human Breast Cancer Cells (under review)

Acknowledgement

By the grace of the Lord Jesus Christ that this thesis had been successfully completed. Thank God for He had blessed me with a pair of loving parents who have supported me both financially and mentally in completing my PhD. Of course, with any PhD journey there is always a supportive and dedicated supervisor who had accompanied me till this stage of achievement. I'm proud to name her here as Dr Eunice Ngai. Along my PhD journey, there were also technicians and colleagues who have helped me in one way or another which I would like to express my gratitude towards them here. Also, there was a "Kungfu Panda" who supported me throughout the thesis fine-tuning process. To name a few, there were Kak Siti, Wei Yang, May Zie and many more. Thank you everyone who had showered me with great love which drove me towards the fruition of my PhD journey.

Table of contents

List of Figures **5**

List of Tables **14**

1. Literature Review **15**

1.1 Breast cancer trend, detection and therapeutic strategies 15

1.2 Breast Cancer and Problems associated with Current Therapeutic Strategies 17

1.3 Tumour Necrosis Factor-related Apoptosis Inducing Ligand (TRAIL), an Apoptosis Inducer with Anti-Cancer Potential 19

1.3.1 TRAIL clinical trials to date 21

1.4 The Hindrances that TRAIL faces in the Route to Clinical Application 35

1.4.1 Internalization of TRAIL receptors 35

1.4.2 Post-translational modifications to TRAIL receptors 36

1.4.3 Dysregulation of TRAIL receptors' regulators 37

1.4.4 Disrupted balance of pro- and anti-apoptotic proteins 37

1.5 The proposed research in light of the current literature 40

1.5.1 E-cadherin functions and its role in cancer cells dissemination 40

1.5.2 E-cadherin on cancer cells' growth inhibition and TRAIL-induced apoptosis 43

1.5.3 Epigenetic drugs as TRAIL sensitizers in cancer cells 46

2. Introduction: Aims and Objectives **49**

3. Optimization of E-cadherin (*CDH1*) gene delivery into human breast adenocarcinoma cells, MDA-MB-231 ..... **53**

3.1 Introduction 53

3.2 Materials and method 55

3.2.1 Recovery of EGFP plasmid from *Escherichia coli* bacteria host 55

3.2.2 Cell Culture Maintenance 58

3.2.3 Transfection of MDA-MB-231 cells with EGFP plasmid and pCDNA3.1 empty vector 58

3.2.4 Assessment of E-cadherin-Green Fluorescent Protein (EGFP) expression at the mRNA level 60

3.2.5 Assessment of EGFP expression at the protein level 61

3.2.6 Selection of successful MDA-MB-231 transfectants using Geneticin (G4-18) resistance selectable marker 62

3.3Results 63

3.3.1 Verification of E-cadherin-GFP plasmid integrity by restriction enzyme digestion and agarose gel electrophoresis 63

3.3.2 Transfection of MDA-MB-231 cells with EGFP plasmid and pCDNA3.1 empty vector 66

3.3.3 Selection of successful MDA-MB-231 transfectants using the Geneticin (G4-18) resistance selectable marker 82

3.4Discussion 84

3.4.1 Verification of E-cadherin-GFP plasmid integrity by restriction enzyme digestion and agarose gel electrophoresis 84

3.4.2 Transfection of MDA-MB-231 cells with EGFP plasmid and pCDNA3.1 empty vector 85

3.5Conclusion 89

4. The assessment of the treatment effect of Trichostatin A (TSA) and Zebularine (Zeb) followed by Tumour Necrosis Factor-related Apoptosis-inducing Ligand (TRAIL) on human breast adenocarcinoma cells viability, cell cycle progression and invasiveness 90

4.1Introduction 90

4.2Materials and method 93

4.2.1 Cell Culture Maintenance 93

4.2.2 3-(4,5-Dimethylthiazol-2-yl)-2,5-Diphenyltetrazolium Bromide (MTT) Cell Viability Assay 93

4.2.3 Cell cycle analysis using ethanol fixing and propidium iodide DNA staining method 94

4.2.4 Wound healing assay (scratch assay) 95

4.2.5 RT-PCR assessment of mRNA expression of proliferating cell nuclear antigen (PCNA), cyclin-dependent kinase-2 (CDK2) and matrix metalloproteinase 9 (MMP9) 95

4.3Results 97

4.3.1 MTT cell viability assay screening of inhibitory concentrations (ICs) of TSA and Zeb combined treatment on MDA-MB-231 97

4.3.2 MTT cell viability assay on IC selection for consecutive treatment with TRAIL. 101

4.3.3 TSA and Zeb sensitization along with E-cadherin expression enhanced TRAIL-induced cytotoxicity in 231-EGFP and MCF-7 103

4.3.4 The effect of drug treatment on cell proliferation of MDA MB-231, 231-EV, 231-EGFP and MCF-7 105

4.3.5 Minimal inhibitory effect of drug treatment on cell viability and cell proliferation of MCF10A 108

4.3.6 TSA and Zeb sensitization along with E-cadherin expression increased TRAIL-induced cell cycle phade G_0/G_1 arrest in MDA-MB-231, 231-EGFP and MCF-7 111

4.3.7 TZT along with E-cadherin expression had little effect on reducing the migration rate of MDA-MB-231 and 231-EGFP 119

4.3.8 TZT treatment largely down-regulates PCNA and CDK2 mRNA expression in MDA-MB-231, 231-EGFP and MCF-7 121

4.3.9 TZT treatment had insignificant effect on the down- regulation of MMP-9 in MDA-MB-231 and 231-EGFP 125

4.4Discussion 127

4.4.1 TSA and Zeb sensitization along with E-cadherin expression enhanced TRAIL-induced cytotoxicity in 231-EGFP and MCF-7 while having no significant inhibitory effect on MCF10A 127

4.4.2 TSA and Zeb sensitization along with E-cadherin expression increase TRAIL-induced cell cycle phade G_0/G_1 arrest in MDA-MB-231, 231-EGFP and MCF-7 via the down-regulation of PCNA and CDK2 130

4.4.3 The effect of treatment on cell migration of 231-EV and 231-EGFP 132

4.5Conclusion 134

5. The assessment of the apoptotic profile of human breast adenocarcinoma cells treated with Trichostatin A (TSA) and Zebularine (Zeb) followed by Tumour Necrosis Factor-related Apoptosis-inducing Ligand (TRAIL) 135

5.1Introduction 135

5.2Materials and method 138

5.2.1 Hematoxylin and Eosin staining 138

5.2.2 FITC-Annexin V / Propidium Iodide cellular apoptosis detection 139

5.2.3 Human apoptosis array proteome profiling 140

5.3Results 143

5.3.1 Apoptotic morphological changes: Hematoxylin and Eosin staining 143

5.3.2 The effect of treatment on the cellular apoptosis of MDA MB-231 155

5.3.3 The effect of treatment on the cellular apoptosis of E cadherin re-expressed MDA-MB-231 (231-EGFP) 158

5.3.4 The effect of treatment on the cellular apoptosis of MCF7 160

5.3.5 The effect of treatment on the protein expression of apoptosis-related genes in MDA-MB-231 162

5.3.6 The effect of treatment on the protein expression of apoptosis-related genes in 231-EGFP 174

5.3.7 The effect of treatment on the protein expression of apoptosis-related genes in MCF-7 186

5.4Discussion 198

5.4.1 TZT treatment had induced the up-regulation of cell cycle regulators p21 and p-p53 (S392) in MDA-MB-231 198

5.4.2 TZT had down-regulated anti-apoptotic IAPs and cell stress proteins but induced insignificant apoptotic events in 231-EGFP 202

5.4.3 MCF-7 205

5.5Concluding remarks 208

6. Immunohistochemistry staining of markers TRAIL-R2, CDH1 and TRAIL of sectioned breast cancer tissues and their association with the corresponding clinical parameters 209

6.1Introduction 209

6.2Methodology 211

6.2.1 Bioinformatics and statistical analysis of TRAIL-R2, E cadherin and TRAIL expression on published data 211

6.2.2 Validation of anti-TRAIL-R2, anti-E-cadherin and anti- TRAIL primary antibody specificity using western blotting 211

6.2.3 Immunohistochemistry 212

6.2.4 Statistical analyses 214

6.3Results 215

6.3.1 Bioinformatics and statistical analysis of TRAIL-R2, E-cadherin and TRAIL mRNA expression using RNA sequencing gene counts from TCGA-BRCA data 215

6.3.2 Bioinformatics and statistical analysis of TRAIL-R2, E- cadherin and TRAIL mRNA expression using the microarray transcriptomic expression data from METABRIC and their correlation with the clinico-pathological parameters 218
6.3.3 Validation of the TRAIL-R2, E-cadherin and TRAIL primary antibodies' specificity using western blotting and their immunohistochemistry staining on primary invasive BC series 223
6.3.4 Correlation between the H-scores of immunohistochemistry stained TRAIL-R2, E-cadherin and TRAIL on the primary invasive BC series 229
6.3.5 The association between the protein expression of TRAIL-R2, E-cadherin, TRAIL and the clinico-pathological parameters of the primary invasive BC series 231
6.4Discussion 247
6.5Concluding remarks 252
7. Conclusion and Future Perspectives 253
References 256
Appendices 277

List of Figures

Figure 1	TRAIL-induced apoptosis via the extrinsic pathway and the intrinsic pathway. In the extrinsic pathway, the ligation of TRAIL onto death receptors DR4 and DR5 results in the activation of caspase 8. This induces the activation of effector caspase, caspase 3 and execution of extrinsic apoptotic pathway. Besides, caspase 8 activates the BID proteins to produce a truncated BID (tBID). tBID interacts with Bax and Bak, leading to their oligomerization in the mitochondrial membrane and causes the loss of mitochondrial membrane potential. This in turn results in the release of cytochrome c. Cytochrome c associates with APAF-1 and caspase 9 to induce the activation of caspases. Diagram is self-drawn using Microsoft PowerPoint.	20
Figure 2	TRAIL resistance mechanisms: (A) Internalization of TRAIL-ligated TRAIL receptors; (B) Lack of fucosylation on TRAIL receptors; (C) Activated survival pathway like Akt/PI3K which inhibits positive transcription factor of TRAIL receptors gene like FOXO3a; (D) Disrupted balance of the pro- and anti-apoptotic proteins.	39
Figure 3	E-cadherin physically interacts with TRAIL-ligated receptors facilitating, thereby connecting TRAIL receptors to cytoskeleton via alpha-catenin and facilitates receptor clustering, DISC formation, caspase activation and apoptosis.	45
Figure 4	DNA gel electrophoresis single BamHI digested E-GFP plasmid on 1% (w/v) agarose gel. Lanes 1, 14: 1 kb plus DNA ladder (Invitrogen); Lanes 2, 4, 6, 8, 10, 12: Undigested E-GFP plasmid; Lanes 3, 5, 7, 9, 11, 13: BamHI digested E-GFP plasmid.	64
Figure 5	DNA gel electrophoresis of BamHI and XbaI digested E-GFP plasmid on 1% (w/v) agarose gel. Lanes 1,14: 1 kb plus DNA ladder (Invitrogen); Lanes 2, 4, 6, 8, 10, 12: Undigested E-GFP plasmid; Lanes 3, 5, 7, 9, 11, 13: BamHI and XbaI digested E-GFP plasmid.	65
Figure 6	MDA-MB-231 cells untransfected (control) and transfected with 2%, 3%, 4% Lipofectamine LTX with PLUS reagent for 24 h were extracted its RNA using the NucleoSpin RNA Plus Extraction Kit (Machery-Nagel, Duren, Germany) and subjected to qPCR analysis using the SuperScript™ III Platinum® SYBR® Green One-Step qRT-PCR Kit with ROX (Life Technologies). The relative expression of each sample against beta-actin loading control is shown. Error bars represent standard deviation of ΔCq values from three biological replicates.	68
Figure 7	MDA-MB-231 cells untransfected (control) and transfected with 4% Lipofectamine LTX with PLUSTM reagent for 24 (A-C), 48 (D-F) and 72 h (G-I) were trypsinized, harvested and resuspended in 1× PBS containing 1% (v/v) FBS at 1 × 106 cells/mL. Cell suspension was then subjected to flow cytometric analysis in the FL1-A (530/30nM) channel in a gated 20,000 cell population at slow flow rate. The gates shown in (A), (B), (D), (E), (G) and (H) indicate that events falling below which are due to background auto-fluorescence.	69
Figure 8	MDA-MB-231 cells untransfected (control) and transfected with 4% Lipofectamine LTX with PLUSTM reagent for 24, 48 and 72 h were trypsinized, harvested and resuspended in 1× PBS containing 1% (v/v) FBS at 1 × 106 cells/mL. Cell suspension was then subjected to flow cytometric analysis in the FL1-A (530/30nM) channel in a gated 20,000 cell population at slow flow rate. Data represents mean fluorescence unit (MFU) of 20,000 events collected per sample from single experiment.	70
Figure 9	Untransfected MDA-MB-231 (A, C) and MDA-MB-231 cells transfected with EGFP plasmid using Lipofectamine LTX with PLUSTM reagent (B) at 4% (v/v) and Transit-X2 reagent (D) at 3μL:1μg plasmid for 24h. A minimum of 15,000 events were analyzed and the SSC-A-FSC-A plot was used to determine the percentage of live cells (P1 gate) in the sample. Below is the bar	71

chart representation of the live cell percentage of the respective samples.
Figure 10 Untransfected MDA-MB-231 (A, C) and MDA-MB-231 cells transfected with EGFP plasmid using Lipofectamine LTX with PLUSTM reagent (B) at 4% (v/v) and Transit-X2 reagent (D) at 3µL:1µg plasmid for 24 h. A minimum of 15 000 events were analyzed and the SSC-A-FSC-A plot was used to determine the percentage of live cells (P1 gate) in the sample. Above is the bar chart representation of the live cell percentage of the respective samples. 72
Figure 11 Verification of mRNA expression of CDH1-GFP in transfected MDA-MB-231. Total RNA was extracted from MDA-MB-231 (231), MDA-MB-231 transfected with pCDNA3.1 (231-EV) and MDA-MB-231 transfected with EGFP plasmid (231-EGFP) for 24, 48 and 72 h, converted to cDNA and amplified byPCR using primers targeting CDH1-GFP (491 bp) and beta-actin housekeeping gene (182 bp). 73
Figure 12 Flow cytometric data of MDA-MB-231 cells transfected for 24 (A,B,C), 48 (D,E,F) and 72 h (G,H,I). Percentage of MDA-MB-231 cells falling above the background fluorescence after transfection using TRANSIT-X2 reagent for 24, 48 and 72 h. (A, D, G: untransfected; B, E, H: transfection with pCDNA3.1 empty vector; C, F, I: transfection with E-cadherin-GFP plasmid). A total of 20,000 events were analyzed and the non-transfected served as the gating control for FL1-A channel. 74
Figure 13 MDA-MB-231 cells untransfected (control) and transfected with 4% Lipofectamine LTX with PLUSTM reagent for 24, 48 and 72 h were trypsinized, harvested and resuspended in 1× PBS containing 1% (v/v) FBS at 1 × 106 cells/mL. Cell suspension was then subjected to flow cytometric analysis in the FL1-A (530/30nM) channel in a gated 20000 cell population at slow flow rate. Data represents mean fluorescence unit (MFU) of 20,000 events of triplicates from one independent experiment. 75
Figure 14 231, 231-EV and 231-EGFP cells were captured for GFP fluorescence under the bright field and FITC channel of Axio observer 7 inverted fluorescence microcope (ZEISS, Germany) at the respective time points of 800 µg/mL G4-18 selection for 24, 48 and 72 h. Scale bars represent 100 µm. 76
Figure 15 Untransfected MDA-MB-231 (A, D, G) and MDA-MB-231 cells transfected with pCDNA3.1 empty vector (B, E, H) and EGFP plasmid (C, F, I) using Transit-X2 reagent at 3µL:1µg plasmid for 24, 48 and 72 h. A minimum of 15,000 events were analyzed and the SSC-A-FSC-A plot was used to determine the percentage of live cells (P1 gate) in the sample. 80
Figure 16 Untransfected MDA-MB-231 and MDA-MB-231 cells transfected with pCDNA3.1 empty vector and EGFP plasmid using Transit-X2 reagent at 3µL:1µg plasmid for 24, 48 and 72 h. A minimum of 15,000 events were analyzed and the SSC-A-FSC-A plot was used to determine the percentage of live cells (P1 gate) in the sample. Above is the bar chart representation of the live cell percentage of the respective samples. Data represents means + standard deviations of triplicates from one independent experiment. 81
Figure 17 At 24 h post-transfection, 800µg/mL of Geneticin (G4-18) was added to select the CDH1-GFP-expressing cell population. A minimum of 10,000 events were analysed and the events falling above the gates shown (horizontal line) are taken as the CDH1-GFP-expressing cells. 82
Figure 18 231, 231-EV and 231-EGFP cells were captured for GFP fluorescence under the bright field and FITC channel of Axio observer 7 inverted fluorescence microcope (ZEISS, Germany) at the respective time points of 800 µg/mL G4-18 selection for 6, 15, 21 and 29 days. Scale bars represent 100 µm. 83
Figure 19 EGFP plasmid was digested using BamHI-HF® and XbaI restriction enzymes (New England BioLabs®). After digestion, the theoretically expected band sizes of backbone sequence (6259 84

bp) and (2638 bp) were obtained as shown in Figure 5.

Figure 20 MTT cell viability data of all combinations of TSA (12.5, 25, 50, 100, 200nM TSA) and Zebularine (1, 2, 4, 6, 8, 10μM) concentrations. IC25 of TSA and Zeb combined treatment on MDA-MB-231 for 24 h was determined from the data. The same data is presented as line graph (above) and bar chart (below) representation. Means are from triplicate values of at least three independent experiments. Error bars represent SEM. 98

Figure 21 MTT cell viability data of all combinations of TSA (12.5, 25, 50, 100, 200nM TSA) and Zebularine (1, 2, 4, 6, 8, 10μM) concentrations. IC25 of TSA and Zeb combined treatment on MDA-MB-231 for 48 h was determined from the data. The same data is presented as line graph (above) and bar chart (below) representation. Data represents means + SEM of three independent experiments of triplicates. 99

Figure 22 MTT cell viability data of all combinations of TSA (12.5, 25, 50, 100, 200nM TSA) and Zebularine (1, 2, 4, 6, 8, 10μM) concentrations. IC25 of TSA and Zeb combined treatment on MDA-MB-231 for 72 h was determined from the data. The same data is presented as line graph (above) and bar chart (below) representation. IC25 of TSA and Zebularine combination was determined as shown in the line graph (black line). The IC25 is bolded and underlined in the legend. Data represents means + SEM of three independent experiments of triplicates. 100

Figure 23 IC15 (12.5 nM TSA, 1 μM Zeb), IC20 (12.5 nM TSA, 2 μM Zeb), IC25 (12.5 nM TSA, 4 μM Zeb) and IC30 (12.5 nM TSA, 6 μM Zeb) of the Trichostatin A and Zebularine (TZ) combined treatment were chosen from the 24 h post-treatment cell viability curve of MDA-MB-231. These ICs were used to treat MDA-MB-231 (231) and geneticin selected MDA-MB-231 transfected with pCDNA3.1 empty vector (231-EV) and with E-cadherin-GFP plasmid (231-EGFP) for 12 h followed by TRAIL treatment for 24 h. Data represents means + SEM of three independent experiments of triplicates. 102

Figure 24 MTT cell viability data of different TSA, Zeb and TRAIL drug treatment groups on MDA-MB-231 (231), geneticin selected MDA-MB-231 transfected with pCDNA3.1 empty vector (231-EV) and with E-cadherin-GFP plasmid (231-EGFP) and MCF-7 for (a) 24, (b) 48 and (c) 72 h. All means are average of triplicate values from at least three independent experiments. Error bars represent SEM. One-Way ANOVA test was used to compare means of the different treatment groups. *(P<0.05) and **(P<0.001) are significant and very significant differences from untreated control. 104

Figure 25 MTT proliferation data of different TSA, Zebularine and TRAIL drug treatment groups on (a) MDA-MB-231 (231) (b) geneticin selected MDA-MB-231 transfected with pCDNA3.1 empty vector (231-EV) and with (c) E-cadherin-GFP plasmid (231-EGFP) and (d) MCF7 for 24, 48 and 72 h. All means are average of triplicate values from at least three independent experiments. Error bars represent SEM. One-Way ANOVA test was used to compare means of the different treatment groups. **(P<0.001) are very significant differences from 24 h mean proliferation rates while *(P<0.05 is significant differences from the mean proliferation rate at 48 h. 106

Figure 26 MTT cell viability data of different TSA, Zebularine and TRAIL drug treatment groups on MCF10A for (a) 24 and (b) 48 h. Data represents means + SEM of three independent experiments of triplicates. * represents significant (P<0.05) differences from the untreated control. 109

Figure 27 MTT proliferation data of different TSA, Zebularine and TRAIL drug treatment groups on (a) MCF10A and (b) MCF-7 for 24 and 48 h. *(P<0.05) are significant differences from 24 h mean proliferation rate based on independent sample T-test. Data represents means + SEM are from three independent experiments of triplicates each. 110

Figure 28 Percentage of cell population at G0/G1, S and G2/M from cell cycle analysis of different treatment groups on (a)MDA-MB-231; (b)231-EV; (c)231-EGFP; (d) MCF-7 breast adenocarcinoma cells and (e) MCF10A non-transformed breast epithelial cells for 24 h. Data represents means + SEM of two independent experiments of duplicates. One way ANOVA test was used to compare means of cell population arrested at the cell cycle phades G0/G1, S, and G2/M, respectively after the different treatment groups. (*P<0.05) and **P<0.001) are significant and very significant differences from the untreated group and all other treatment groups, respectively. (#P<0.05) is significant difference from the treatment group, TRAIL. 112

Figure 29 Percentage of cell population at G0/G1, S and G2/M from cell cycle analysis of different treatment groups on (a)MDA-MB-231; (b)231-EV; (c)231-EGFP; (d) MCF7 breast adenocarcinoma cells and (e) MCF10A non-transformed breast epithelial cells for 48 h. Data represents means + SEM of two independent experiments of duplicates. * is significant difference at P<0.05. 115

Figure 30 Percentage of cell population at G0/G1, S and G2/M from cell cycle analysis of different treatment groups on (a) MDA-MB-231; (b) 231-EV; (c) 231-EGFP; (d) MCF7 breast adenocarcinoma cells and (e) MCF10A non-transformed breast epithelial cells for 72 h. Data represents means + SEM of two independent experiments of duplicates. * is significant difference at P<0.05. 117

Figure 31 A cell monolayer formed by (a) MDA-MB-231, (b) 231-EV and (c) 231-EGFP was scratched with a p100 tip along the diameter of a 24-well. Microscopic images of the formed gap were then captured at 0, 3, 6, 12, and 24 h and the gap area was then measured using the ImageJ software. The percentages of gap closure at the respective time points are presented above. Error bars represent SEM from three independent experiments. (*p<0.05) and (**p<0.001) are significant and very significant differences from the untreated control, respectively. 120

Figure 32 Total RNA extraction and RT-PCR on proliferating cell nuclear antigen (PCNA) and cyclin-dependent kinase 2 (CDK2. (a) MDA-MB-231 (231), geneticin selected MDA-MB-231 transfected with pCDNA3.1 empty vector (231-EV) and with E-cadherin-GFP plasmid (231-EGFP), MCF7 were extracted its total RNA for untreated control (UT), TSA, Zeb, TZ, TRAIL and TZT treatment groups at 24 h time point using the RNeasy Mini Kit. The total RNA was DNase I treated and then converted to cDNA prior to PCR amplification using primers specific to PCNA and CDK2. Loading amount was normalized using the housekeeping gene, beta-actin. The respective band intensity was quantified using the ImageJ software. 122

Figure 33 Total RNA extraction and RT-PCR on proliferating cell nuclear antigen (PCNA) and cyclin-dependent kinase 2 (CDK2). (a) MDA-MB-231 (231), geneticin selected MDA-MB-231 transfected with pCDNA3.1 empty vector (231-EV) and with E-cadherin-GFP plasmid (231-EGFP), MCF-7 were extracted its total RNA for untreated control (UT), TSA, Zeb, TZ, TRAIL and TZT treatment groups at 48 h time point using the RNeasy Mini Kit. The total RNA was DNase I treated and then converted to cDNA prior to PCR amplification using primers specific to PCNA and CDK2. Loading amount was normalized using the housekeeping gene, beta-actin. The respective band intensity was quantified using the ImageJ software. 124

Figure 34 Total RNA extraction and RT-PCR on matrix metalloproteinase 9 (MMP9). MDA-MB-231 and 231-EGFP were extracted its total RNA for untreated control (UT), TSA, Zeb, TZ, TRAIL and TZT treatment groups at (a) 24 and (b) 48 h time point using the RNeasy Mini Kit. The total RNA was DNase I treated and then converted to cDNA prior to PCR amplification using primers specific to MMP9. Loading amount was normalized using the housekeeping gene, beta-actin. The respective band intensity was quantified using the ImageJ software. 126

Figure 35 Microscopoic images of hematoxylin and eosin (H and E) stained (A) untreated MDA-MB-231 and MDA-MB-231 treated with (B) TSA, (C) Zeb, (D) TSA and Zeb, (E) TRAIL for 24 h; (F) TSA and Zeb for 12 h followed by TRAIL treatment for 24 h. Scale bars represent 100 μm. The apoptotic morphologies are explained as follows: cell shrinkage and nuclear chromatin condensation (black arrows); cell membrane blebbing (red arrows); nuclear fragmentation (yellow arrows); apoptotic body (light blue arrow). Images were captured at 200× magnification. Scale bars represent 100 μm. 144

Figure 36 Microscopoic images of hematoxylin and eosin (H and E) stained (A) untreated MDA-MB-231 and MDA-MB-231 treated with (B) TSA, (C) Zeb, (D) TSA and Zeb, (E) TRAIL for 48 h; (F) TSA and Zeb for 12 h followed by TRAIL treatment for 48 h. Scale bars represent 100 μm. The apoptotic morphologies are explained as follows: cell shrinkage and nuclear chromatin condensation (black arrows); cell membrane blebbing (red arrows); nuclear fragmentation (yellow arrows); apoptotic body (light blue arrow). Images were captured at 200× magnification. Scale bars represent 100 μm. 145

Figure 37 Microscopic images of hematoxylin and eosin (H and E) stained (A) untreated MDA-MB-231 and MDA-MB-231 treated with (B) TSA, (C) Zeb, (D) TSA and Zeb, (E) TRAIL for 72 h; (F) TSA and Zeb for 12 h followed by TRAIL treatment for 72 h. Scale bars represent 100 μm. The apoptotic morphologies are explained as follows: cell shrinkage and nuclear chromatin condensation (black arrows); cell membrane blebbing (red arrows); nuclear fragmentation (yellow arrows). Images were captured at 200× magnification. Scale bars represent 100 μm. 146

Figure 38 Microscopic images of hematoxylin and eosin (H and E) stained (A) untreated 231-EGFP and 231-EGFP treated with (B) TSA, (C) Zeb, (D) TSA and Zeb, (E) TRAIL for 24 h; (F) TSA and Zeb for 12 h followed by TRAIL treatment for 24 h. Scale bars represent 100 μm. The apoptotic morphologies are explained as follows: cell shrinkage and nuclear chromatin condensation (black arrows); cell membrane blebbing (red arrows); nuclear fragmentation (yellow arrows). Images were captured at 200× magnification. Scale bars represent 100 μm. 148

Figure 39 Microscopic images of hematoxylin and eosin (H and E) stained (A) untreated 231-EGFP and 231-EGFP treated with (B) TSA, (C) Zeb, (D) TSA and Zeb, (E) TRAIL for 48 h; (F) TSA and Zeb for 12 h followed by TRAIL treatment for 48 h. Scale bars represent 100 μm. The apoptotic morphologies are explained as follows: cell shrinkage and nuclear chromatin condensation (black arrows); cell membrane blebbing (red arrows); nuclear fragmentation (yellow arrows). Images were captured at 200× magnification. Scale bars represent 100 μm. 149

Figure 40 Microscopic images of hematoxylin and eosin (H and E) stained (A) untreated 231-EGFP and 231-EGFP treated with (B) TSA, (C) Zeb, (D) TSA and Zeb, (E) TRAIL for 72 h; (F) TSA and Zeb for 12 h followed by TRAIL treatment for 72 h. Scale bars represent 100 μm. The apoptotic morphologies are explained as follows: cell shrinkage and nuclear chromatin condensation (black arrows); cell membrane blebbing (red arrows); nuclear fragmentation 150

(yellow arrows); apoptotic body (light blue arrow). Images were captured at 200× magnification. Scale bars represent 100 µm.
Figure 41 Microscopic images of hematoxylin and eosin (H and E) stained (A) untreated MCF-7 and MCF-7 treated with (B) TSA, (C) Zeb, (D) TSA and Zeb, (E) TRAIL for 24 h; (F) TSA and Zeb for 12 h followed by TRAIL treatment for 24 h. Scale bars represent 100 µm. The apoptotic morphologies are explained as follows: cell shrinkage and nuclear chromatin condensation (black arrows); cell membrane blebbing (red arrows); nuclear fragmentation (yellow arrows); apoptotic body (light blue arrow). Images were captured at 200× magnification. Scale bars represent 100 µm. 152
Figure 42 Microscopic images of hematoxylin and eosin (H and E) stained (A) untreated MCF-7 and MCF-7 treated with (B) TSA, (C) Zeb, (D) TSA and Zeb, (E) TRAIL for 48 h; (F) TSA and Zeb for 12 h followed by TRAIL treatment for 48 h. Scale bars represent 100 µm. The apoptotic morphologies are explained as follows: cell shrinkage and nuclear chromatin condensation (black arrows); cell membrane blebbing (red arrows); nuclear fragmentation (yellow arrows); apoptotic body (light blue arrow). Images were captured at 200× magnification. Scale bars represent 100 µm. 153
Figure 43 Microscopic images of hematoxylin and eosin (H and E) stained (A) untreated MCF-7 and MCF-7 treated with (B) TSA, (C) Zeb, (D) TSA and Zeb, (E) TRAIL for 72 h; (F) TSA and Zeb for 12 h followed by TRAIL treatment for 72 h. Scale bars represent 100 µm. The apoptotic morphologies are explained as follows: cell shrinkage and nuclear chromatin condensation (black arrows); cell membrane blebbing (red arrows); nuclear fragmentation (yellow arrows); apoptotic body (light blue arrow). Images were captured at 200× magnification. Scale bars represent 100 µm. 154
Figure 44 Percentage of cell population which had undergone early apoptosis, late apoptosis and dead from Annexin V-FITC/PI cellular apoptosis assay of different treatment groups on MDA-MB-231 for (a) 24, (b) 48 and (c) 72 h. Data represents means + standard deviation from one independent experiment of triplicates for (a) and (b). Data represents means + SEM from two independent experiments of triplicates each for (c). *($p<0.05$) is significant difference from the untreated (UT) control and TRAIL treatment based on LSD mean separation. 157
Figure 45 Percentage of cell population which are undergoing early apoptosis, late apoptosis and dead from Annexin V-FITC/PI cellular apoptosis assay of different treatment groups on 231-EGFP for (a) 24, (b) 48 and (c) 72 h. Data represents means + standard deviation from one independent experiment of triplicates for (a) and (b). Data represents means + SEM from two independent experiments of triplicates each for (c). *($p<0.05$) is significant difference from the TZ treatment for late apoptosis and from all the other experimental groups for dead cells. 159
Figure 46 Percentage of cell population which are undergoing early apoptosis, late apoptosis and dead from Annexin V-FITC/PI cellular apoptosis assay of different treatment groups on MCF-7 for (a) 24, (b) 48 and (c) 72 h. Data represents means + standard deviation from one independent experiment of triplicates for (a) and (b). Data represents means + SEM from two independent experiments of triplicates each. *($p<0.05$) is significant difference from all other experimental groups for early apoptosis for (c). *($p<0.05$) is significant difference from all other experimental groups for early apoptosis. 161
Figure 47 Bcl-2 family proteins expression in the untreated MDA-MB-231 (UT) and MDA-MB-231 treated with TSA and Zeb (TZ), 50 ng/mL TRAIL (TRAIL) for 72 h and TSA and Zeb for 12 h followed by TRAIL treatment for 72 h (TZT). Data represents mean + standard deviation. *($p<0.05$) is significant difference from UT using the Student's T-test. 163
Figure 48 Extrinsic pathway proteins expression in the untreated MDA-MB-231 (UT) and MDA-MB-231 treated with TSA and Zeb (TZ), 50 ng/mL TRAIL (TRAIL) for 72 h and TSA and Zeb for 12 h followed by TRAIL treatment for 72 h (TZT). Data represents mean + 165

standard deviation. *(p<0.05) and **(p<0.01) are significant and very significant differences from UT using the Student's T-test.
Figure 49 The expression of pro-apoptotic proteins (pro-caspase-3, cleaved caspase-3 and cytochrome c) and anti-apoptotic proteins (catalase, PON2, and clusterin) in the untreated MDA-MB-231 (UT) and MDA-MB-231 treated with TSA and Zeb (TZ), 50 ng/mL TRAIL (TRAIL) for 72 h and TSA and Zeb for 12h followed by TRAIL treatment for 72 h (TZT). Data represents mean ± standard deviation. *(p<0.05) and **(p<0.01) are significant and very significant differences from UT using the Student's T-test. 167
Figure 50 The protein expression of IAP family proteins (cIAP-1, cIAP-2, Livin, Survivin and XIAP) and IAP inhibitors (SMAC and HTRA2) in untreated MDA-MB-231 (UT) and MDA-MB-231 treated with TSA and Zeb (TZ), 50 ng/mL TRAIL (TRAIL) for 72 h and TSA and Zeb for 12h followed by TRAIL treatment for 72 h (TZT). Data represents mean + standard deviation. *(p<0.05) and **(p<0.01) are significant and very significant differences from UT using the Student's T-test. 169
Figure 51 The expression of cell cycle regulators in the untreated MDA-MB-231 (UT) and MDA-MB-231 treated with TSA and Zeb (TZ), 50 ng/mL TRAIL (TRAIL) for 72 h and TSA and Zeb for 12h followed by TRAIL treatment for 72 h (TZT). Data represents mean + standard deviation. *(p<0.05) and **(p<0.01) are significant and very significant differences from UT using the Student's T-test. 171
Figure 52 The protein expression of cell stress proteins in the untreated MDA-MB-231 (UT) and MDA-MB-231 treated with TSA and Zeb (TZ), 50 ng/mL TRAIL (TRAIL) for 72 h and TSA and Zeb for 12h followed by TRAIL treatment for 72 h (TZT). Data represents mean + standard deviation. *(p<0.05) and **(p<0.01) are significant and very significant differences from UT using the Student's T-test. 173
Figure 53 Bcl-2 family proteins expression in the untreated 231-EGFP (UT) and 231-EGFP treated with TSA and Zeb (TZ), 50 ng/mL TRAIL (TRAIL) for 72 h and TSA and Zeb for 12h followed by TRAIL treatment for 72 h (TZT). Data represents mean + standard deviation. *(p<0.05) and **(p<0.01) are significant and very significant differences from UT using the Student's T-test. 175
Figure 54 Extrinsic pathway proteins expression in the untreated 231-EGFP (UT) and 231-EGFP treated with TSA and Zeb (TZ), 50 ng/mL TRAIL (TRAIL) for 72 h and TSA and Zeb for 12h followed by TRAIL treatment for 72 h (TZT). Data represents mean + standard deviation. *(p<0.05) and **(p<0.01) are significant and very significant differences from UT using the Student's T-test. 177
Figure 55 The expression of pro-apoptotic proteins (pro-caspase-3, cleaved caspase-3 and cytochrome c) and anti-apoptotic proteins (catalase, PON2, and clusterin) in the untreated 231-EGFP (UT) and 231-EGFP treated with TSA and Zeb (TZ), 50 ng/mL TRAIL (TRAIL) for 72 h and TSA and Zeb for 12h followed by TRAIL treatment for 72 h (TZT). Data represents mean ± standard deviation. *(p<0.05) and **(p<0.01) are significant and very significant differences from UT using the Student's T-test. 179
Figure 56 The protein expression of IAP family proteins (cIAP-1, cIAP-2, Livin, Survivin and XIAP) and IAP inhibitors (SMAC and HTRA2) in the untreated 231-EGFP (UT) and 231-EGFP treated with TSA and Zeb (TZ), 50 ng/mL TRAIL (TRAIL) for 72 h and TSA and Zeb for 12 h followed by TRAIL treatment for 72 h (TZT). Data represents mean + standard deviation. *(p<0.05) and **(p<0.01) are significant and very significant differences from UT using the Student's T-test. 181
Figure 57 The expression of cell cycle regulators in the untreated 231-EGFP (UT) and 231-EGFP treated with TSA and Zeb (TZ), 50 ng/mL TRAIL (TRAIL) for 72 h and TSA and Zeb for 12 h followed by TRAIL treatment for 72 h (TZT). Data represents mean + standard deviation. *(p<0.05) and **(p<0.01) are significant and very significant differences from UT using the Student's T-test. 183

Figure 58	The protein expression of cell stress proteins in the untreated 231-EGFP (UT) and 231-EGFP treated with TSA and Zeb (TZ), 50 ng/mL TRAIL (TRAIL) for 72 h and TSA and Zeb for 12 h followed by TRAIL treatment for 72 h (TZT). Data represents mean + standard deviation. *($p<0.05$) and **($p<0.01$) are significant and very significant differences from UT using the Student's T-test.	185
Figure 59	Bcl-2 family proteins expression in the untreated MCF-7 (UT) and MCF-7 treated with TSA and Zeb (TZ), 50 ng/mL TRAIL (TRAIL) for 72 h and TSA and Zeb for 12h followed by TRAIL treatment for 72 h (TZT). Data represents mean + standard deviation. *($p<0.05$) and **($p<0.01$) are significant and very significant differences from UT using the Student's T-test.	187
Figure 60	Extrinsic pathway proteins expression in the untreated MCF-7 (UT) and MCF-7 treated with TSA and Zeb (TZ), 50 ng/mL TRAIL (TRAIL) for 72 h and TSA and Zeb for 12 h followed by TRAIL treatment for 72 h (TZT). Data represents mean + standard deviation. *($p<0.05$) and **($p<0.01$) are significant and very significant differences from UT using the Student's T-test.	189
Figure 61	The expression of pro-apoptotic proteins (pro-caspase-3, cleaved caspase-3 and cytochrome c) and anti-apoptotic proteins (catalase, PON2, and clusterin) in the untreated MCF-7 (UT) and MCF-7 treated with TSA and Zeb (TZ), 50 ng/mL TRAIL (TRAIL) for 72 h and TSA and Zeb for 12 h followed by TRAIL treatment for 72 h (TZT). Data represents mean + standard deviation. *($p<0.05$) and **($p<0.01$) are significant and very significant differences from UT using the Student's T-test.	191
Figure 62	The protein expression of IAP family proteins (cIAP-1, cIAP-2, Livin, Survivin and XIAP) and IAP inhibitors (SMAC and HTRA2) in the untreated MCF-7 (UT) and MCF-7 treated with TSA and Zeb (TZ), 50 ng/mL TRAIL (TRAIL) for 72 h and TSA and Zeb for 12 h followed by TRAIL treatment for 72 h (TZT). Data represents mean + standard deviation. *($p<0.05$) and **($p<0.01$) are significant and very significant differences from UT using the Student's T-test.	193
Figure 63	The expression of cell cycle regulators in the untreated MCF-7 (UT) and MCF-7 treated with TSA and Zeb (TZ), 50 ng/mL TRAIL (TRAIL) for 72 h and TSA and Zeb for 12 h followed by TRAIL treatment for 72 h (TZT). Data represents mean + standard deviation. *($p<0.05$) and **($p<0.01$) are significant and very significant differences from UT using the Student's T-test.	195
Figure 64	The protein expression of cell stress proteins in the untreated MCF-7 (UT) and MCF-7 treated with TSA and Zeb (TZ), 50 ng/mL TRAIL (TRAIL) for 72 h and TSA and Zeb for 12 h followed by TRAIL treatment for 72 h (TZT). Data represents mean + standard deviation. *($p<0.05$) and **($p<0.01$) are significant and very significant differences from UT using the Student's T-test.	197
Figure 65	Differentially expressed E-cadherin and TRAIL-R2 across different hormone receptor (ER, PR, HER2) status and between non-tumour and primary breast tumour. Patients were sub-divided depending on the clinicopathological parameters provided by TCGA. Normalized gene counts (gene counts rescaled according to library size) were compiled into a tab-delimited text file for analysis using the RobinA applying the Bioconductor-edgeR software. Data represents means + SEM. *, ** and *** are statistical significant differences at $p<0.05$, $p<0.01$ and $p<0.001$, respectively.	216
Figure 66	Kaplen-Meier survival plots of (A) TNFRSF10B (TRAIL-R2) and (B) CDH1 (E-cadherin) vs breast cancer-specific survival (BCSS) in all cases of the METABRIC cohort. Dichotomization cut-off values of TNFRSF10B and CDH1 mRNA expression were determined using the X-tile software to be at 7.72 and 8.1, respectively.	221

Figure 67	A) Western blot of E-cadherin (CDH1) expression in breast ductal carcinoma (T47D) and adenocarcinoma cell lines (MCF-7 and MDA-MB-231). The 42 kDa band on a separate blot (same gel) depicts the β-actin loading control. B) Immunohistochemical expression of CDH1 in primary invasive breast cancer cores showing (i) negative, (ii) weak, (iii) moderate and (iv) strong staining of CDH1.	224
Figure 68	A) Western blot of TRAIL-R2 (TNFRSF10B) expression in human cervical cancer (HeLa CCL-2), human breast adenocarcinoma (MDA-MB-231, MCF-7), human breast ductal carcinoma (T47D), human acute T cell leukemia (Jurkat) and normal human mammary gland (MCF10A). The 42 kDa band on the same blot depicts the β-actin loading control. B) Immunohistochemical expression of TNFRSF10B in primary invasive breast cancer cores showing (i) negative, (ii) weak, (iii) moderate and (iv) strong staining of TNFRSF10B.	226
Figure 69	A) Western blot of TRAIL (TNFSF10) expression in human cervical cancer (HeLa CCL-2), human breast adenocarcinoma (MDA-MB-231, MCF-7, SkBr3), human breast ductal carcinoma (T47D), human acute T cell leukemia (Jurkat) and normal human mammary gland (MCF10A). The 42 kDa band on the same blot depicts the β-actin loading control. B) Immunohistochemical expression of TNFSF10 in primary invasive breast cancer cores showing (i) negative, (ii) weak, (iii) moderate and (iv) strong staining of TNFSF10.	228
Figure 70	Effect of TNFRSF10B, CDH1 and TNFSF10 protein expression on breast cancer patient outcome. (A) membranous TRAIL-R2 (TNFRSF10B) vs BCSS; (B) nuclear TRAIL-R2 (TNFRSF10B) vs BCSS; (C) cytoplasmic TRAIL-R2 (TNFRSF10B) vs BCSS; (D) membranous E-cadherin (CDH1) vs BCSS; (E) cytoplasmic E-cadherin (CDH1) vs BCSS; (F) cytoplasmic TRAIL (TNFSF10) vs BCSS; (G) nuclear TRAIL (TNFSF10) vs BCSS in all cases. N.B. p-values in bold are significant differences. 0= low expression; 1= high expression	246

List of Tables

Table 1	Representative clinical trials conducted on soluble recombinant human Apo2L/TRAIL (rhTRAIL), as a single therapeutic agent or in combination with the potential sensitizers such as chemotherapeutic drug(s) and monoclonal antibody.	24
Table 2	Representative clinical trials conducted on TRAIL receptor agonists (TRAs) against TRAIL-R1 (DR4) and TRAIL-R2 (DR5), either as single therapeutic agent or in combination with the other potential sensitizer(s) such chemotherapeutic drugs, monoclonal antibody and immunotherapeutic drug.	26
Table 3	The Human Apoptosis Array target proteins, controls and their respective coordinates.	142
Table 4	Pearson correlation test between the normalized gene counts of CDH1 (E-cadherin), TNFRSF10B (TRAIL-R2) and TNFSF10 (TRAIL) from the TCGA data using SPSS analysis.	217
Table 5	Pearson correlation test between the normalized mRNA expression of CDH1 (E-cadherin) and TNFRSF10B (TRAIL-R2) from the METABRIC data using SPSS analysis.	219
Table 6	Chi-square test association of CDH1 (E-cadherin) and TNFRSF10B (TRAIL-R2) expression with the clinico-pathological variables in the METABRIC cohort using SPSS analysis.	219
Table 7	Cox regression analysis on the effect of TRAIL-R2 (TNFRSF10B) and E-cadherin (CDH1) expression along with the prognostic factors, tumour grade, tumour size and lymph node stage on BCSS.	222
Table 8	Pearson correlation test between the H-scores of CDH1 (E-cadherin) with H-scores of TNFRSF10B (TRAIL-R2) and TNFSF10 from the primary invasive BC series using SPSS analysis. N.B. p-values in bold are significant differences.	230
Table 9	Clinicopathological associations of TRAIL-R2 (TNFRSF10B) cytoplasmic, nuclear and membranous expression in breast cancer. N.B. p-values in bold are significant differences.	232
Table 10	Clinicopathological associations of E-cadherin (CDH1) cytoplasmic and membranous expression in breast cancer. N.B. p-values in bold are significant differences.	235
Table 11	Clinicopathological associations of TRAIL (TNFSF10) cytoplasmic and nuclear expression in breast cancer. N.B. p-values in bold are significant differences.	238
Table 12	The cytoplasmic, nuclear and membranous expression of TRAIL-R2 (TNFRSF10B) in breast cancer and the expression of other molecular biomarkers. N.B. p-values in bold are significant differences.	241
Table 13	The cytoplasmic and membranous expression of CDH1 in breast cancer and the expression of other molecular biomarkers. N.B. p-values in bold are significant differences.	243
Table 14	The cytoplasmic and nuclear expression of TRAIL (TNFSF10) in breast cancer and the expression of other molecular biomarkers. N.B. p-values in bold are significant differences.	244

1. Literature Review

1.1 Breast cancer trend, detection and therapeutic strategies

Breast cancer used to be a high-mortality disease in Western countries but the mortality rates have plummeted (Leong *et al.*, 2010). Lamentably, in recent years, breast cancer had been assigned with the dreadful title as the most-recurrent female malignancy in developing countries within the Asian region in place of the uterine cervix cancer (Agarwal *et al.*, 2007). According to the World Health Organization (WHO), in the year of 2018 alone, out of the estimated 9.6 million cancer deaths worldwide in 2018, 627,000 women died from breast cancer and this accounts for 15% of the cancer deaths among women. It was also estimated that nearly one-half and over one-half of the breast cancer cases and deaths, respectively, will come from the Asian population (Bray *et al*, 2018) and the breast cancer incidence rates do not show a decreasing trend in the Asia-Pacific region (Shin *et al*, 2010; Youlden *et al*, 2012, 2014). In Malaysia, according to the WHO Global Cancer Observatory, 7,593 out of the 23,218 (32.7%) new cancer cases among the female come from breast cancer. Therefore, it is easily visualized that breast cancer is still a giant to be tackled in the field of breast cancer research.

Studies have shown that early detection coupled with appropriate adjuvant therapeutic strategies can improve breast cancer survival rates tremendously in the long-term (Berry *et al.*, 2005; Migowski, 2015). Some of the most commonly used early detection tools are mammography, ultrasound imaging, magnetic resonance imaging, positron emission tomography (Wang, 2017). In addition, microwave imaging is another recent advancement for low-cost and safe alternative diagnostic approach to mammography (Kwon and Lee, 2016). Recently, cancer diagnosis had even been brought to the nano-scale whereby graphene films, 3D architectures or nanostructures could be functionalized (Gu *et al.*, 2019) with antibodies (Hong *et al.*, 2012) and aptamer (Azimzadeh *et al.*,

2016) for detection of tumour neovasculature *in vivo* and breast cancer biomarker, mRNA-155, found in clinical samples, respectively.

The establishment of effective neoadjuvant and adjuvant therapies was also in tandem with the advancement of early breast cancer detection tools. Chemotherapy drugs like doxorubicin, cyclophosphamide, methotrexate, and fluorouracil are widely used and estrogen receptor-negative (ER-), triple-negative breast cancer (TNBC) and HER2-positive patients mostly benefit from them (Nounou *et al.*, 2015). Neoadjuvant chemotherapy is the chemotherapy treatment conferred before breast cancer surgery with the aim of increasing breast conservation rate, allowing smaller surgical resection volume for those eligible for breast conservation (Mougalian *et al.*, 2015) as well as providing a model to assess and compare patients' response towards new or standard therapies (Selli and Sims, 2019). Adjuvant chemotherapy, on the other hand, supplements the local therapy in reducing the risk of recurrence and enhancing overall survival. The chemotherapy regimens commonly used include anthracyclines (doxorubicin, epirubicin) and/or taxanes (paclitaxel, docetaxel) which are two effective cytotoxic agent classes against early and advanced stage breast cancer (Anampa *et al.*, 2015).

In addition to chemotherapy, the established adjuvant systemic therapy also includes the targeted endocrine therapy and anti-HER2 therapy. The current standard endocrine therapy comprises pharmacologic ovarian suppression using gonadotropin-releasing hormone (GnRH) agonists (Singh, 2012), selective estrogen receptor modulators (SERMs) and down-regulators (SERDs) like tamoxifen (Criscitiello *et al.*, 2010), fulvestrant (Blackburn *et al.*, 2018), and aromatase inhibitors (AIs) (Li *et al.*, 2019) which all aim to reduce the activity or levels of estrogen in patients with ER+ presentation. On the other hand, for those with presentation of human epidermal growth factor receptor 2 overexpression (HER2+), there are three HER2-targeted agents, namely trastuzumab (Herceptin), lapatinib (Tykerb) and pertuzumab (Perjeta) which

are available to treat HER-2 positive metastatic breast cancer (Jelovac and Emens, 2013).

1.2 Breast Cancer and Problems associated with Current Therapeutic Strategies

Despite the advancements made in early diagnosis and treatment have stabilized its incidence in the West (Kohler *et al.*, 2015), the issue of the less differentiated, more aggressive basal subtype tripe negative breast cancer (TNBC) remains to be solved as the respective targets, ER and HER2, of established hormonal treatment such as tamoxifen and trastuzumab (Scully *et al.*, 2012) are not expressed in this subtype, hence rendering the established targeted treatment ineffective. As research is still actively ongoing to find a suitable targeted treatment for TNBC, patients diagnosed with TNBC are mostly left with the option of standard cytotoxic chemotherapy which is still met with varied responses between different TNBC molecular subtypes (Masuda *et al.*, 2013). The situation in Malaysia and Singapore is aggravated where patients presenting no ER and Progesterone Receptor (PR) constitute 34% of the patients studied, in contrast to data from a registered patient database in the USA reporting only a 21% falling within this group (Pathy *et al.*, 2011). Moreover, TNBC is also packaged with the potential of metastasis and recurrence at distant metastatic sites along with reduced overall survival rate and disease-free survival (Dent *et al.*, 2007, Dent *et al.*, 2009; Lin *et al.*, 2008).

In order to reduce reliance on the standard cytotoxic chemotherapeutic options for TNBC patients, scientists have been placing much effort and focus on better understanding of the different TNBC subtypes and discovering novel therapeutic targets against the differential gene expression profiles. These targets include those involved in angiogenesis, DNA-repair mechanism default, activating mutations of proliferation pathways like Wnt/β-catenin signalling pathway as well as immune regulation (Abramson *et al.*, 2015; Burstein *et al.*, 2015; King *et al.*, 2012; Lehmann *et al.*, 2011). Recently, Ahmed *et al*. (2019)

have even discovered that an anti-leprotic drug, clofazimine, effectively targets the Wnt pathway and is compatible with doxorubicin at moderate dose in TNBC.

Nonetheless, some of the ligand-targeted treatments are still bound with complexities. For instance, inhibitors against the epidermal growth factor (EGF) receptor family (ErbB) have limited efficacy towards TNBC due to the transactivation of AXL, another receptor tyrosine kinase which upon EGF ligation, gives rise to TNBC's motility response (Meyer *et al.*, 2013). Therefore, dual-target therapy can be seen as attractive in the sense that multiple erroneously activated pathways can be targeted by one agent concurrently. This is condoned by a recent finding that a secreted extracellular protein, tubulointerstitial nephritis antigen-like 1 (Tinagl1) suppresses TNBC progression and metastasis through direct binding to integrin α5β1, αvβ1, and epidermal growth factor receptor (EGFR). Besides, it had also simultaneously inhibited the focal adhesion kinase (FAK) and EGFR signalling pathways (Shen *et al.*, 2019).

However, TNBCs are molecularly so diverse that before its molecular stratification based on genetic and gene expression subtyping can be brought to the clinic, targeted therapies currently being researched on might not be extensively active in unselected or non-stratified TNBCs (Turner and Reis-Filho, 2013). Therefore, while TNBC patients are frequently left with the dreadful choice of chemotherapy (Yip *et al.*, 2014), there remains a pressing need for scientists to discover novel drugs which target breast cancer cells with a general mechanism applicable across molecular diversity while at the same time being minimally toxic to patients. Along the same vein, several new promising molecular targets have been identified in TNBC such as androgen receptor, phosphoinositide 3-kinase/protein kinase B (PI3K/AKT), trophoblast antigen 2 (trop2), glycoprotein NMB (gpNMB), programmed cell death 1 (PD1), programmed death ligand 1 (PD-L1) receptors and poly(adenosine diphosphate-ribose) polymerase (PARP) (Vidula and Bardia, 2017).

1.3 Tumour Necrosis Factor-related Apoptosis Inducing Ligand (TRAIL), an Apoptosis Inducer with Anti-Cancer Potential

In this context, Tumour Necrosis Factor-related Apoptosis Inducing Ligand (TRAIL) is likely to become the holy grail of cancer therapy in attribution to its selective induction of apoptosis in cancerous cells, leaving non-malignant cells generally unharmed (Ashkenazi *et al.*, 1999; Fulda, 2015). The recombinant human TRAIL (rhTRAIL) had been tested as generally safe and well tolerated from phade I in-human clinical trial on patients with advanced cancer (Herbst *et al.*, 2010). TRAIL is a unique type II membrane protein of which its gene was cloned back in 1995 and added to the family of Tumour Necrosis Factor (TNF) due to its C-terminal extracellular domain homology to other members of the TNF family (Marsters, 1996; Wiley *et al.*, 1995). Similar to other members of the TNF family, the apoptosis signalling by TRAIL is triggered by an extrinsic pathway of ligand binding to the cell surface TRAIL receptor 1/2 (TRAIL-R1/2) inducing receptor oligomerization. This signal will then be transmitted through binding of the TRAIL-R1/2 cytoplasmic death domain to an adaptor domain called Fas-associated Death Domain (FADD) via homophilic interaction which in turn will associate with initiator procaspase-8 and -10 forming the death inducing signalling complex (DISC). Consequently, the apoptosis signal will then culminate in the apoptotic effector apparatus of executioner caspases-3, -6, and-7 resulting in cellular apoptotic demise (Almasan and Ashkenazi, 2003; Ashkenazi, 2008; Kelley and Ashkenazi, 2004; Schulze-Osthoff *et al.*, 1998).

Beside TRAIL-R1 and –R2, TRAIL also interacts with cell surface TRAIL receptor-3 and -4 (TRAIL-R3 and –R4), also known as decoy receptor-1 and -2 (DcR-1 and -2) but these block the apoptosis signal from being transmitted due to the lack and truncation of the cytoplasmic death domain, respectively (Mérino *et al.*, 2006). Although the expression of these DcRs do not correlate with TRAIL sensitivity or confer resistance of normal cells towards TRAIL-induced apoptosis, they definitely play a vital role in reducing TRAIL apoptosis-

inducing efficacy towards malignant cells, especially the DcRs expressed in the tumour stromal tissue (O'Leary *et al.*, 2016).

Apart from the extrinsic pathway, in most instances of cancer cell lines, scientists have uncovered that TRAIL-induced apoptosis signal requires intensification from the activation of the intrinsic apoptotic pathway vis-à-vis the Bcl-2 regulated mitochondrial pathway (Gonzalvez and Ashkenazi, 2010; Holland, 2013). This requirement distinguishes these cells from Type I cells which can reach apoptosis independent of the mitochondrial pathway, grouping them under the category of Type II cells. The reason of this distinction lies mainly in the presence of X-linked inhibitor of apoptosis protein (XIAP) which inhibits the activation of caspase-3 by caspase-8, hence necessitating the backing from mitochondrial pathway which releases the second mitochondrial activator of caspases (SMAC) to exert inhibitory effect on XIAP (Kantari and Walczak, 2011) for caspase-3 activation. The TRAIL-induced apoptotic pathways are illustrated in (Figure 1).

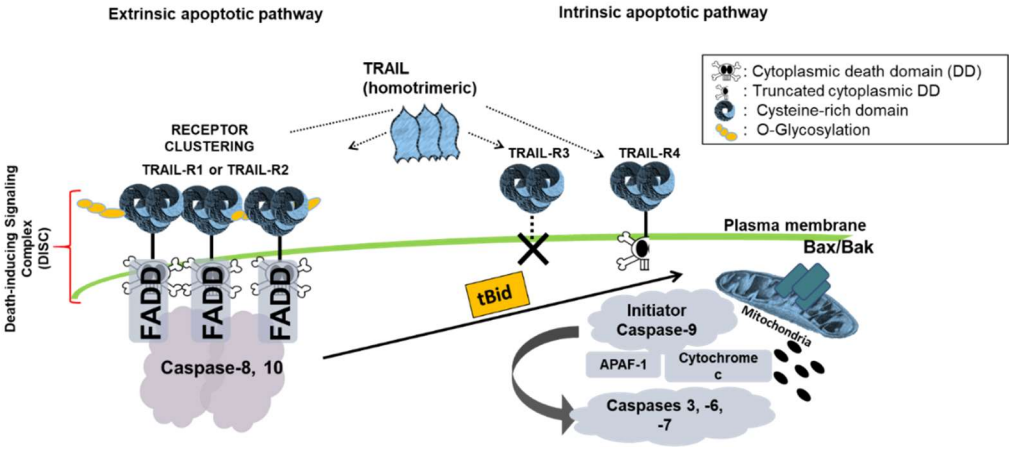


Figure 1 TRAIL-induced apoptosis via the extrinsic pathway and the intrinsic pathway. In the extrinsic pathway, the ligation of TRAIL onto death receptors DR4 and DR5 results in the activation of caspase 8. This induces the activation of effector caspase, caspase 3 and execution of extrinsic apoptotic pathway. Besides, caspase 8 activates the BID proteins to produce a truncated BID (tBID). tBID interacts with Bax and Bak, leading to their oligomerization in the mitochondrial membrane and causes the loss of mitochondrial membrane potential. This in turn results in the release of cytochrome c. Cytochrome c associates with APAF-1 and caspase 9 to induce the activation of caspases. Self-drawn using Microsoft PowerPoint.

1.3.1 TRAIL clinical trials to date

As soon as TRAIL's potential as a selective anti-cancer agent was observed in preclinical studies on its functionalized variants, a great deal of effort had been placed on human clinical trials of TRAIL and monoclonal antibodies against TRAIL receptors (Stuckey and Shah, 2013). The first of such effort was done with the soluble recombinant human Apo2L/TRAIL (rhTRAIL) or dulanermin on 71 patients with metastatic solid tumours in a phade I dose-escalation study. rhTRAIL was demonstrated to be safe and well tolerated at doses up to 30 mg/kg with no observable antibody formation and rhTRAIL-related hepatoxicity (Herbst *et al.*, 2010a). Another phade III clinical trial of recombinant human Apo-2 ligand for injection was conducted on stage IV non-small-cell lung cancer (NSCLC) in 2016. The study was estimated to be completed in June 2018, however, no results have been posted as yet (NCT03083743 at http://www.clinicaltrials.gov).

Beside acting as a single therapeutic agent, dulanermin had also been tested in combination with various chemotherapeutic drugs like paclitaxel, carboplatin, bevacizumab, vinorelbine, cisplatin and FOLFOX regimen in clinical trials for advanced NSCLC and locally advanced, recurrent, or metastatic colorectal cancer (Table 1). In a phade 1b study for advanced NSCLC treated with a combination of rhTRAIL with paclitaxel, carboplatin and bevacizumab (PCB), the treatment regimen was well tolerated with no increase in toxicity; the overall response rate was 58% and the median progression-free survival (PFS) time was 7.2 months (Soria *et al.*, 2010). In another phade III study for advanced NSCLC treated with the combination of dulanermin with vinorelbine and cisplatin, the treatment regimen significantly improved PFS and objective response rate (ORR) (Ouyang *et al.*, 2018). However, in a phade II study on the advanced NSCLC treated with dulanermin with paclitaxel, carboplatin (PC) and bevacizumab (PCB), adverse events were common and the treatment regimen did not improve the patients' clinical outcome (Soria *et*

al., 2011). These contradicting results warrant further research in obtaining consistent objective response and positive patients' clinical outcomes.

The current limitations of either TRAIL as single therapeutic agent or in combination of chemotherapeutic agent have instigated the development and advancement of several TRAIL receptor agonists (TRAs) in phade I clinical trials as single therapeutic agent or in combination with other sensitizers such as chemotherapeutic drug, immunotherapeutic agent, monoclonal antibody, therapeutic proteasome inhibitor and tyrosine kinase inhibitor (Table 2). One of the earliest TRAs was mapatumumab which is a human agonistic monoclonal antibody targeted against DR4. Both the phade I clinical trials on advanced cancers gave promising outcome of excellent safety and tolerability profile and prolonged plasma mapatumumab terminal half-life. Nonetheless, no objective responses were obtained except for the achievement of stable disease in approximately 30% of the study patients (Hotte *et al.*, 2008; Tolcher *et al.*, 2007). On the other hand, TRAs against DR5 also progressed to phade I clinical trials. Conatumumab (Doi *et al.*, 2011; Herbst *et al.*, 2010b), lexatumumab (Plummer *et al.*, 2007; Wakelee *et al.*, 2010) and drozitumab (apomap) (Camidge *et al.*, 2010) have been reported as safe in multiple phade I clinical trials on advanced cancers but likened to TRAs against DR4, they generally displayed no objective responses in patients. On the basis of TRAs displaying a generally safe and tolerable profile even at high doses of 10 to 30 mg/kg, these TRAs were not given up on clinical trials and some have even been developed to phade II clinical trials either as single agents or combined with other potential TRAIL-sensitizers (Table 2).

When combined with chemotherapy or other potential TRAIL-sensitizers, TRAs showed improved efficacy in terms of pathological response. For instance, mapatumumab combined with gemcitabine and cisplatin gave a partial response in 12/49 patients (Mom *et al.*, 2009) while in the combination with

paclitaxel and carboplatin, 5/27 patients responded partially (Leong *et al.*, 2009) in phade I clinical studies. Nonetheless, randomized-controlled phade II trials of mapatumumab combined with bortezomib and chemotherapy on patients with multiple myeloma (Belch *et al.*, 2010) and lung cancer (von Pawel *et al.*, 2014), respectively, did not yield significant anticancer activity in terms of response rate, PFS or overall survival. Recently, an ongoing randomized phade II trial of mapatumumab combined with sorafenib on patients with advanced hepatocellular carcinoma had shown no significant improvement in time to (radiologic) progression or other efficacy end points, pointing towards inferior clinical feasibility of mapatumumab (Ciuleanu *et al.*, 2016). Similar trend of poor response rate and insignificant anti-tumour activity was observed in phade I and phade II trials of TRAs against DR5 like conatumumab, lexatumumab, tigatuzumab, drozitumab and LBY-135 in combination with chemotherapy (Table 2). Some of the ongoing clinical trials on TRAs combined with other anti-cancer entities targeted against proliferation, angiogenesis and immune checkpoint inhibitors are summarized in Table 2.

.

In short, TRAIL and its receptor agonists have been successful clinically by the consistency of safe and tolerable profile even at high-dose administration to cancer patients. By supplementing the standard chemotherapy, TRAIL performed better in terms of response rate. Nevertheless, along the fact that TRAIL in combination with standard chemotherapy did not produce a favorable clinical outcome in randomized controlled trials, novel potential TRAIL-sensitizers and TRAIL functionalization will still be an important research area before TRAIL can ace in the clinical setting.

Table 1 Representative clinical trials conducted on soluble recombinant human Apo2L/TRAIL (rhTRAIL), as a single therapeutic agent or in combination with the potential sensitizers such as chemotherapeutic drug(s) and monoclonal antibody.

Cancer type	Intervention	Dosage	Outcome	Phade (Status)	Reference
Soluble recombinant human TRAIL (rhTRAIL)/Dulanermin					
Advanced cancer	Soluble recombinant human Apo2L/TRAIL (rhTRAIL)	**0.5-30 mg/kg/d** intravenously (IV) on days 1 to 5 of each 21-day cycle	rhTRAIL was safe and well tolerated; dose escalation up to serum concentrations on par with preclinical anti-tumour efficacy	I (ongoing as of 2010)	(Herbst *et al.*, 2010a)
Stage IV non-small-cell lung cancer (NSCLC)	Recombinant human Apo-2 ligand (injection)	**150µg/kg/d** IV, on days 1 to 7 of each 21-day cycle	(ongoing)	III (active, not recruiting)	+NCT03083743
In combination with the potential sensitizer(s)					
Advanced NSCLC (with no prior treatment)	Combination of rhTRAIL with paclitaxel, carboplatin and bevacizumab (PCB)	Paclitaxel, carboplatin (IV), and bevacizumab (IV) on day 1 followed by **4 or 8 mg/kg/d dulanermin (IV)** for 5 days or **20 mg/kg/d dulanermin (IV)** for 2 days of each 21-day cycle	Well tolerated with no increase in toxicity; overall response rate was 58%; the median PFS time was 7.2 months	Ib (ongoing with long term follow-up as of 2008)	(Soria *et al.*, 2010)
Follicular and low-grade $CD20^+$, B-cell Non-Hodgkin's Lymphoma (NHL)	Combination of dulanermin with rituximab	**4 or 8 mg/kg/d** dulanermin (IV) on days 1 to 5 of each 21-day cycle; 375 mg/m^2 rituximab (IV) weekly for up to 8 doses	Improved PFS with combination therapy (17.9 months) compared to dulanermin alone (6.9 months).	Ib, II (terminated with results)	+NCT00400764
Advanced NSCLC	Combination of dulanermin with paclitaxel and carboplatin (PC) and	**PC (IV) with dulanermin 8 mg/kg/d** for 5 days (squamous NSCLC); **PCB (IV) with dulanermin 8**	Grade ≥3 adverse events were common; elevated caspase-cleaved cytokeratin-18	II (ongoing as of 2009)	(Soria *et al.*, 2011)

	bevacizumab (PCB)	**mg/kg/d** for 5 days or **20 mg/kg/d** for 2 days (nonsquamous NSCLC)	after dulanermin treatment; did not improve patient outcomes.		
Stage IIIb to IV NSCLC	Combination of dulanermin with vinorelbine and cisplatin	Vinorelbine (25 mg/m^2) (IV) on days 1 and 8; cisplatin (30 mg/m^2) (IV) on days 2 to 4 for up to six cycles plus **dulanermin (75 µg/kg) (IV)** on days 1 to 14 in every 21 days	Significantly improved PFS and objective response rate (ORR); similar adverse events AE profile across placebo and treatment	III (completed in 2012)	(Ouyang *et al.*, 2018)
Locally Advanced, Recurrent, or Metastatic Colorectal Cancer	Dulanermin Administered in Combination With the FOLFOX Regimen and Bevacizumab	Drug: FOLFOX regimen IV repeating dose (dose not stated) Drug: bevacizumab IV repeating dose (dose not stated) Drug: dulanermin IV repeating dose (dose not stated)	No results posted	1 (completed in 2014)	†NCT00873756

Note: †NCT represents the clinical trial identifier which had been registered at https://www.clinicaltrials.gov, as accessed on 4th September 2018.

Key for abbreviations: Progression-free survival (PFS); Adverse events (AE); Objective response rate (ORR); Intravenous (IV).

Table 2 Representative clinical trials conducted on TRAIL receptor agonists (TRAs) against TRAIL-R1 (DR4) and TRAIL-R2 (DR5), either as single therapeutic agent or in combination with the other potential sensitizer(s) such chemotherapeutic drugs, monoclonal antibody and immunotherapeutic drug.

Cancer type	Intervention	Dosage	Outcome	Phade	Reference
TRAIL receptor agonists against TRAIL-R1(DR4)					
Single agent					
Advanced cancers	Mapatumumab	**0.01 to 20.0 mg/kg (IV)**	AE events were mostly grade 1 or 2; no ORR observed; 12 patients had stable disease for 1.9 to 29.4 months.	I (completed)	(Hotte *et al*., 2008)
Advanced solid malignancies	Mapatumumab	**0.01 to 10 mg/kg (IV)**	Mild AE events of grade 1 or 2;19 patients had stable disease; attained plasma mapatumumab concentrations active in preclinical models	I (completed)	(Tolcher *et al*., 2007)
Colorectal cancer	Mapatumumab	**20 mg/kg** every 14 days followed by **10 mg/kg IV** every 14 days.	12 patients achieved stable disease of a median of 2.6 months; median PFS was 1.2 months; plasma concentrations on par with phade I-predicted values; no clinical activity.	II (completed)	(Trarbach *et al*., 2010)

Stage IIIb/IV recurrent NSCLC	Mapatumumab	**10 mg/kg IV** every 21 days	No objective single agent activity based on Response Evaluation Criteria in Solid Tumours (RECIST) criteria; no evidence of renal or hepatic toxicity; 21% of patients achieved stable disease	II (completed)	(Greco *et al.*, 2008)
In combination with the potential sensitizers					
Advanced solid malignancies	Combination of mapatumumab with paclitaxel and carboplatin	**3, 10, 20 mg/kg IV** with standard doses of paclitaxel and carboplatin (IV) every 21 days	5 patients had confirmed radiologic partial response; 12 patients had stable disease	I (completed in 2006)	(Leong *et al.*, 2009)
Advanced solid tumours	Combination of mapatumumab with gemcitabine and cisplatin	**1, 3, 10, 20, 30 mg/kg (IV)** with gemcitabine (1250 mg/m^2) on days 1 and 8 and cisplatin (80 mg/m^2) on day 1 of each 21-day cycle	12 patients had partial response; 25 patients achieved stable disease; safe and well tolerated for doses up to 30 mg/kg	I (completed in 2009)	(Mom *et al.*, 2009)
Stage IIIb or IV advanced primary NSCLC	Combination of mapatumumab with paclitaxel	Paclitaxel (200 mg/m^2) (IV) + carboplatin area under curve (AUC)	Balanced AE events across treatment groups; no	II (completed)	(von Pawel *et al.*, 2010; von Pawel *et al.*, 2014)

	and carboplatin	6.0 mg·min/mL (IV) + mapatumumab (**10mg/kg** or **30 mg/kg IV**) of 21-day cycle for up to 6 cycles	improved response rate or PFS		
Relapsed/refractory multiple myeloma	Combination of mapatumumab with bortezomib	Brotezomib (1.3 mg/m^2) (IV) on days 1, 4, 8, 11 + **10 or 20 mg/kg (IV)** on day 1 of 21-day cycle	Balanced AE events across treatment groups; no improvement in response rate, PFS or duration of response	II (completed)	(Belch *et al.*, 2010)
Advanced hepatocellular carcinoma	Combination of mapatumumab with sorafenib	Sorafenib (400 mg orally, twice daily) and placebo or **30 mg/kg (IV)** mapatumumab on day 1 of 21-day cycle	Comparable AE events across treatment arms; no improvement in time to (radiologic) progression or other efficacy end points	II (completed in 2013)	(Ciuleanu *et al.*, 2016)
TRAIL receptor agonists against TRAIL-R2 (DR5)					
Single agent					
Advanced solid tumours	Conatumumab	**0.3, 1, 3, 10 or 20 mg/kg (IV)** every 14 days	1 NSCLC patient had partial response at 0.3 mg/kg; 1 colorectal carcinoma patient had stable disease and 24% reduction	I (completed in 2008)	(Herbst *et al.*, 2010b)

			in tumour size by RECIST; safe and well tolerated at doses up to 20 mg/kg		
Advanced solid tumours	Conatumumab	**3, 10, 20 mg/kg (IV)** every 14 days	Well tolerated at doses up to 20 mg/kg once every 14 days; 9/18 patients achieved stable disease	I (completed)	(Doi *et al.*, 2011)
Advanced solid malignancies	Lexatumumab	**0.1-20 mg/kg (IV)** every 21-day cycle	Stable disease was sustained in 12/37 patients; safe and well tolerated up to 10 mg/kg every 21 days	I (completed in 2006)	(Plummer *et al.*, 2007)
Advanced solid tumours	Lexatumumab	**0.1-10 mg/kg (IV)** every 14 days	9/31 patients achieved stable disease; safe and tolerated at 10 mg/kg every 14 days	I (completed)	(Wakelee *et al.*, 2010)
Paediatric patients with recurrent or progressiv	Lexatumumab	**3, 5, 8, 10 mg/kg (IV)** once every 14 days	5/24 patients achieved stable disease for 3-24 cycles; no complete	I (completed)	(Merchant *et al.*, 2012)

e solid tumours			or partial response observed; some anti-tumour activity was evident		
Advanced malignancies	PRO95780 (Drozitumab)	**1-20 mg/kg (IV)** every 14 days	3 minor responses observed in patients with ovarian cancers (4 mg/kg) and chondrosarcoma (10 mg/kg); safe and well tolerated at doses up to 20 mg/kg	I (completed)	(Camidge *et al.*, 2010)
Advanced solid tumours	DS-8273a	**2, 8, 16, 24 mg/kg (IV)** once every 21 days	Well demonstrated and showed linear pharmacokinetics; no objective responses were observed	I (completed in 2015)	(Forero *et al.*, 2017)
Relapsed/refractory carcinomas or lymphoma	Tigatuzumab	**1, 2, 4, 8 mg/kg (IV)** weekly	No study-drug-related toxicities; no ant-tigatuzumab responses; 7/17 patients had stable disease (response duration from 81 to 798 days)	I (completed)	(Forero-Torres *et al.*, 2010)
In combination with the potential sensitizer(s)					
Advanced solid tumours;	Combination of conatumumab	**1, 3, 15 mg/kg (IV)** conatumumab	No ORR observed; 28 (36%)	I/II (completed in 2010)	(Tabernero *et al.*, 2015)

NSCLC, colorectal cancer, sarcoma, pancreatic cancer, ovarian cancer	with ganitumab (monoclonal antibody to IGF1R)	with ganitumab (18 mg/kg) on day 1 every 21 days	patients had stable disease; well tolerated with no new toxicities		
Metastatic or locally advanced unresectable soft tissue sarcomas	Combination of conatumumab with doxorubicin	Phade I: Doxorubicin (75 mg/m^2) with conatumumab (**15 mg/kg**)* every 21-day cycle Phade II: Double blind conatumumab 15 mg/kg (conatumumab-doxotubicin)* or placebo (placebo-doxorubicin)* *administration route not stated	No unexpected AE observed; no significant improvement of post-chemotherapy response from conatumumab dosing	I/II (completed)	(Demetri *et al.*, 2012)
Metastaic pancreatic cancer	Combination of conatumumab or ganitumab with gemcitabine	Gemcitabine (1000 mg/m^2) (IV) on days 1, 8 and 15 of each 28-day cycle with ganitumab (12 mg/kg) (IV) every 14 days or double-blind conatumumab (10 mg/kg) (IV) or double-blind placebo	59% of patients receiving the conatumumab-gemcitabine treatment showed anticancer activity based on the 6-months survival rate	II (completed in 2009)	(Kindler *et al.*, 2012)
Advanced solid tumours	Combination of conatumumab and/or ganitumab with or without bevacizumab	Oxaliplatin (100 mg/m^2) (IV), leucovorin (400 mg/m^2) (IV), fluorouracil (400 mg/m^2) (IV) combined with conatumumab	(no results posted)	II (active, not recruiting)	$^+$NCT01327612

		and/or ganitumab, with or without bevacizumab on day 1 of every 14 days			
Various cancer types	Combination of lexatumumab with gemcitabine and FOLFIRI or pemetrexed and doxorubicin	**5 or 10 mg/kg (IV)** with (gemcitabine and FOLFIRI) (IV) every 14 days or (pemetrexed and doxorubicin) (IV) every 21 days	Well tolerated; tumour shrinkage was observed; partial response in the FOLFIRI and doxorubicin arms.	Ib (completed)	(Sikic *et al.*, 2007)
Locally advanced recurrent or metastatic colorectal cancer	Combination of drozitumab (IV) with first-line mFOLFOX6 plus bevacizumab (IV)	(dose not stated)	2 patients had partial response	Ib (completed)	(Rocha Lima *et al.*, 2012)
Chemotherapy-naïve, unresectable or metastatic pancreatic cancer	Combination of tigatuzumab with gemcitabine	**8 mg/kg loading dose followed by 3 mg/kg weekly (IV)** tigatuzumab and gemcitabine (1000 mg/m^2) (IV) once weekly for 21 days followed by 1 week of rest	PFS rate at 16 weeks was 52.5%; ORR was 13.1%; 45.9% patients had stable disease; treatment was well tolerated	II (completed in 2010)	(Forero-Torres *et al.*, 2013)
Chemotherapy-naïve, metastatic or unresectable NSCLC	Combination of tigatuzumab with carboplatin/paclitaxel	Tigatuzumab **(10 or 8 mg/kg)** or placebo **(IV)** with carboplatin (AUC 6mg/mL min) (IV) / paclitaxel (175 mg/m^2) (IV) every 21 days for 6 cycles	Median PFS was 5.4 months for tigatuzumab compared to 4.3 months for placebo; both the placebo and	II (completed)	(Reck *et al.*, 2013)

			tigatuzumab cohorts had similar partial response rate; well tolerated but no improvement in efficacy of carboplatin/paclitaxel treatment		
Metastatic, triple negative breast cancer	Combination of tigatuzumab with abraxane	Abraxane (100 mg/m^2) (IV) on days 1, 8, and 15 of 28-day intervals; **10 mg/kg (IV)** loading dose of tigatuzumab followed by **5 mg/kg (IV)** for the first cycle and then every other week on days 1 and 15 for subsequent cycles.	No serious AE observed; no improvement in PFS compared to abraxane alone	II (completed in 2017)	+NCT01307891
Advanced colorectal cancer	Combination of DS-8273a with nivolumab (anti-PD1)	Nivolumab (240 mg) (IV) once every two weeks on days 1 and 14 of each 28-day cycle; DS-8273a administration after nivolumab IV in ascending doses up to **1200 mg (IV)**	(No results posted)	I (terminated)	+NCT02991196
Unresectable stage III or stage IV melanoma	Combination of DS-8273a with nivolumab	**2, 4, 8, 16, 24 mg/kg (IV)** DS-8273a with nivolumab (5 mg/kg) (IV) every 21 days	(No results posted)	I (recruiting)	+NCT02983006
Advanced solid tumours	Combination of LBY135	Arm 1: **0.3, 1, 3, 10, 15, 20, 40 mg/kg (IV)** LBY135 on	Arm1: 21/38 patients	I/II (completed in 2008)	(Sharma *et al.*, 2014)

	with capecitabine	day 1 of a 21-day cycle Arm 2: **1, 3, 10, 15, 20, 40 mg/kg (IV)** LBY135 on day 1 of a 21-day cycle in combination with oral capecitabine (1000 mg/m^2) twice daily, 2 weeks on and 1 week off	had stable disease Arm2: 3 dose-limiting toxicities (each of grade 3) have been observed at 1, 20 and 40 mg/kg; 22% patients were detected with immunoge-nicity; well tolerated up to maximum dose of 40 mg/kg; no appreciabl e clinical activity was observed		

Note: †NCT represents the clinical trial identifier which had been registered at https://www.clinicaltrials.gov, as accessed in 4th September 2018.
Key for abbreviations: Progression-free survival (PFS); Adverse events (AE); Objective response rate (ORR); Intravenous (IV).

1.4 The Hindrances that TRAIL faces in the Route to Clinical Application

Despite being such a promising anti-tumour candidate drug, TRAIL, notwithstanding the extensive research being done on it, still had a far distance to travel from bench to bedside. This distance is largely bridged by various cancer cells having varied response to TRAIL-arbitrated apoptosis due to different intrinsic and acquired resistance built up by cancer cells over the course of tumour evolution (Dimberg *et al.*, 2013; Stuckey and Shah, 2013). These include internalization of TRAIL receptors, post-translational modifications to TRAIL receptors, dysregulation of TRAIL receptors' regulators and the disrupted balance of pro- and anti-apoptotic proteins (Figure 2).

1.4.1 Internalization of TRAIL receptors

TRAIL resistance can be developed via down-regulation of surface expression of TRAIL-R1 and –R2 and this had been demonstrated with TRAIL sensitivity being restored after TRAIL-R1 and –R2 up-regulation in breast cancer cells (Di *et al.*, 2013; Portanova *et al.*, 2013; Yan *et al.*, 2012). In spite of MDA-MB-231 human breast adenocarcinoma cells being TRAIL-sensitive (Butler *et al.*, 2006; Zhang and Zhang, 2008), the surface expression levels of TRAIL-R1 and –R2 can be reduced by the event of TRAIL-induced endocytosis, thereby attenuating the TRAIL-stimulated apoptosis signal, especially in the case of repeated treatments with subtoxic doses of rhTRAIL (0.1-2 ng/mL) (Yoshida *et al.*, 2009; Zhang *et al.*, 2009). This TRAIL-induced endocytosis of TRAIL-ligated receptors initiates from the activation of initiator caspase-8 which then triggers spikes of Ca^{2+} through ryanodine receptor calcium channels, thereby activating calcineurin, and in turn dephosphorylating dynamin-1 to promote cargo-selective endocytosis of TRAIL–ligated receptors (Reis *et al.*, 2017).

In the same vein, immunohistochemistry on breast tumours showed that all the TRAIL receptors were mislocalized to either cytoplasm or nucleus and their subcellular localization correlated with TRAIL's growth-inhibition activity (Chen

et al., 2012). Moreover, a recent finding that the *in vitro* circulating tumour cells model, breast cancer suspension culture, resulted in TRAIL resistance owing to autophagic removal of TRAIL-R2 receptor from the surface (Twomey and Zhang, 2019) confirms the notion that TRAIL receptors internalization mediates TRAIL resistance in breast cancer.

1.4.2 Post-translational modifications to TRAIL receptors

One of the post-translational modifications, glycosylation, involves the attachment of glycans to specific protein site, most commonly at asparagine (N-linked) and/or serine/threonine (O-linked) (Trivedi and Mishra, 2015; Twomey *et al.*, 2015). Intriguingly, recently researchers have unearthed findings that O glycosylation of TRAIL-R1 and –R2 are crucial determinants of receptor's membrane stability from endocytosis, clustering after TRAIL ligation and subsequently, DISC assembly followed by caspase-8 activation (Twomey *et al.*, 2015; Wagner *et al.*, 2007). On the other hand, fucosylation is the attachment of an L-fucose residue to an oiligosaccharide or protein (Moriwaki and Miyoshi, 2010). To this end, mutational and cell rescue studies of GDP-mannose-4,6-dehydratase (GMDS), one of the vital fucosylating enzymes, in colon cancer cell line have revealed the possibility that deficiency of fucosylation paved the way for TRAIL resistance, evasion from natural killer cell-mediated tumour surveillance and ultimately cancer progression (Moriwaki *et al.*, 2009; Moriwaki *et al.*, 2011; Miyoshi *et al.*, 2012).

In addition, based on a genotype and immunohistochemistry screening of 127 patients diagnosed with breast invasive ductal carcinoma (IDC), loss of α1,3/4-fucosyltransferase (FUT3) enzyme expression was found to be correlated with IDC (do Nascimento *et al.*, 2015). Furthermore, fucosylation was recently shown to selectively restore TRAIL-R2-mediated apoptosis, DISC assembly and caspase 8 activation in colorectal carcinoma cells (Zhang *et al.*, 2019) This further supports the notion that the suppression of TRAIL death-receptor-O-

glycosylation had evolved to be another adaptive defence added to the list of TRAIL resistance mechanisms acquired during tumourigenesis.

1.4.3 Dysregulation of TRAIL receptors' regulators

In addition to TRAIL-ligated receptor internalization regulating TRAIL receptors level at the cell surface, various transcription factors, both activators and suppressors, also make up the concoction of TRAIL-R1 and –R2 expression regulation. For example, the forkhead transcription factor FOXO3a activated downstream of the inhibition of protein kinase B / phosphoinositide 3-kinase (AKT/PI3K) pathway was shown to upregulate TRAIL-R1 and –R2 expression in colon cancer cell in the presence of TRAIL sensitizer. Therefore, suppressing FOXO3a, the activator of TRAIL-R1 and –R2, via AKT/PI3K pathway activation is one of the TRAIL resistance mechanisms pitched by cancer cells (Prabhu *et al.*, 2015; Shoeb *et al.*, 2013). Apart from FOXO3a, some of the other transcription factors like NF-κB, CHOP and AP-1 which induce the TRAIL-R1 and –R2 transcription were discovered by scientists during the investigation of the mechanism behind TRAIL resistance (Chen *et al.*, 2003; Guan *et al.*, 2002; Jin *et al.*, 2014; Ravi *et al.*, 2001). When various potential TRAIL sensitizers were administered to breast cancer cell lines, the upregulation or activation of these transcription factors had revealed them as the vital players in reverting the TRAIL resistance developed in those cancer cells (Pennati *et al.*, 2015; Portanova *et al.*, 2013; Singh *et al.*, 2005).

1.4.4 Disrupted balance of pro- and anti-apoptotic proteins

As aforementioned, upon TRAIL ligation, Type II cells require the mitochondrial signal amplification loop in enhancing the caspase 3 activation for sufficient apoptosis execution. Therefore, it can be envisioned that players of the intrinsic apoptosis pathway will have a regulatory role on TRAIL-induced apoptosis in Type II cells. Apoptosis is a process orchestrated by the balance between the pro- and anti-apoptotic proteins. One such orchestra is played between the pro- and anti-apoptotic members of the Bcl-2 family of proteins. Bcl-2 proteins

regulate cell death primarily by their binding interactions which result in mitochondrial outer membrane permeabilization (MOMP), leading to release of pro-apoptotic intermembrane space proteins like cytochrome *c* and second mitochondria-derived activator of caspases/direct IAP-binding protein with low PI (SMAC/DIABLO) (Zhou *et al.*, 2005), caspase activation and apoptosis (Kale *et al.*, 2018). Since Bax and Bak oligomerization mediates the loss of MOMP, the anti-apoptotic Bcl-2 family members like Bcl-xL, Mcl-1, and A1 inhibits apoptosis via their heterodimerization with Bax (Sedlak *et al.*, 1995) and Bak (Sattler *et al.*, 1997) via their highly conserved BH1 and BH2 domains.

The significance of Bcl-2 family proteins in the regulation of TRAIL-induced apoptosis was highlighted by a recent finding that the expression of Harakiri, a pro-apoptotitc BH3-only protein of the Bcl-2 family, was increased by a histone deacetylase inhibitor (MS-275) when added as TRAIL sensitizer in glioblastoma multiforme while its pro-apoptotic effect was reversed by forced expression of Bcl-2 and Bcl-xL (Kaya-Aksoy *et al.*, 2019). Moreover, TRAIL sensitivity of the NSCLC cell line, NCI-H460 was induced to become a highly TRAIL resistant phenotype by only 3 fold overexpression of the anti-apoptotic Bcl-2 protein (Danish *et al.*, 2018). Thus, the check-and-balance of the pro- and anti-apoptotic Bcl-2 family members serves as a valuable trove of targets for TRAIL-based cancer therapy.

Along the same vein, inhibitor of apoptosis (IAP) protein family is another group of caspase inhibitors which prominently influence the downstream signalling of both the intrinsic and extrinsic pathways. Their over-expression is commonly associated with worse prognosis, chemo-resistance and reduced survival among cancer patients (Engesæter *et al.*, 2011; Hussain *et al.*, 2017; Zhang *et al.*, 2011). These IAPs are namely Xlinked IAP (XIAP), cellular IAP protein 1 (cIAP-1), cellular IAP protein 2 (cIAP-2) and Survivin, inhibiting caspase activities either through attachment to the active pocket of caspases -3, -7 and -9, thereby ablating its pro-apoptotic activities (Gyrd-Hansen and Meier, 2010;

Silke and Meier, 2013) or by causing the ubiquitination of caspases via E3 ligase activities followed by their proteasomal degradation (Lemke *et al.*, 2014; Rathore *et al.*, 2017).

In the intrinsic apoptosis arm, SMAC/DIABLO which is released from mitochondria promotes apoptosis by directly inhibiting IAPs (Martinez-Ruiz *et al.*, 2008; Zhang and Fang, 2005). In this regard, IAP inhibitors which are SMAC mimetics were developed to antagonize IAP proteins' activities, thereby, sensitizing cancer cells towards TRAIL-induced apoptosis. For example, SMAC-7 (AVPIAQK) was shown to enhance TRAIL-induced apoptosis in B-Cell acute lymphoblastic leukemia by down-regulating XIAP and cIAP-1, thereby increasing poly (ADP-ribose) polymerase (PARP) cleavage (Saraei *et al.*, 2018). The importance of IAPs in regulating TRAIL resistance had also repeatedly been revealed in various cancers such as inflammatory breast cancer (Allensworth *et al.*, 2013), pancreatic carcinoma (Stadel *et al.*, 2010), ovarian cancer (Petrucci *et al.*, 2012) and glioblastoma (Lincoln *et al.*, 2018).

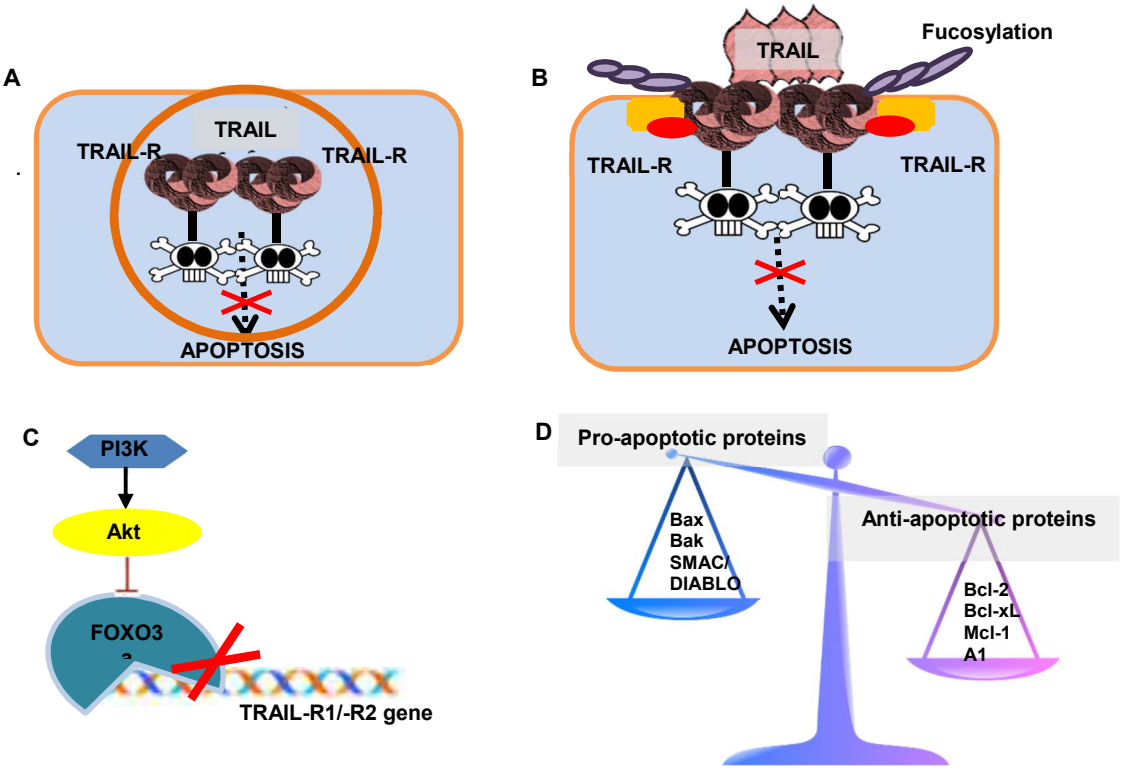


Figure 2 TRAIL resistance mechanisms: **(A)** Internalization of TRAIL-ligated TRAIL receptors; **(B)** Lack of fucosylation on TRAIL receptors; **(C)** Activated survival pathway like Akt/PI3K which inhibits positive transcription factor of TRAIL receptors gene like FOXO3a; **(D)** Disrupted balance of the pro- and anti-apoptotic proteins. Self-drawn using Microsoft PowerPoint.

1.5 The proposed research in light of the current literature

Based on the literature reviewed above, it can be summarized that TRAIL is a potential anti-cancer candidate. However, in order to harness its potential into practical application in the clinical settings of breast cancer therapy, an in-depth research on the TRAIL resistance mechanism behind and stratagem to combat the resistance fortress is compulsory.

1.5.1 E-cadherin functions and its role in cancer cells dissemination

E-cadherin protein is transcribed from *CDH1* gene into a precursor polypeptide of 135 kDa. The precursor segment carries a prosequence harbouring the consensus protease cleavage site (Arg-Arg-Gln-Lys-Arg) which facilitates its proteolytic processing into a mature and functional protein with adhesive properties. The mature E-cadherin protein is a 120 kDa, Ca^{2+}-dependent transmembrane glycoprotein which binds normal and polarized epithelial cells together at lateral surface via adherens junction (AJ) (Ogou *et al.*, 1983; Jiang, 1996; Wheelock and Johnson, 2003; Capaldo *et al.*, 2014). The amino terminal of E-cadherin houses five extracellular cadherin domains between which the Ca^{2+} ions bind and its adhesive activity lies (Pećina-Šlaus, 2003). Ca^{2+} ions-binding then induces the stiffening of the entire span of its extracellular domain (Nagar *et al.*, 1996; Harrison *et al.*, 2011) and promotes protease resistance (Leckband and Prakasam, 2006). The stiffening of the extracellular domain provides a vital role for three-dimensional domain swapping which is at the core of E-cadherin's homophilic *trans* dimer formation between apposed cells as part of AJ.

Mature AJs are formed between cells by E-cadherin binding to beta-catenin via its distal cytoplasmic domain, forming an E-cadherin-beta-catenin complex which then links to the actin cytoskeleton via α-catenin and its interacting protein, α-actinin (Hülsken *et al.*, 1994; Jou *et al.*, 1995; Nieset *et al.*, 1997). In addition, p120 interaction with the juxtamembrane core domain (JMD_{core}) also

forms part of the mature AJs (Ishiyama *et al.*, 2010). p120-JMD_{core} interaction blocks the dileucine endocytosis motif on E-cadherin, thereby preventing its endocytosis and prolonging its functionality on the cell surface (Davis *et al.*, 2003; Fujita *et al.*, 2002). These structural entities are collectively involved in the core function of E-cadherin as the adhesion protein in epithelial cells by maintaining the stability of AJs.

Literature from as early as two decades ago had developed the notion that E-cadherin serves an important role as an invasion suppressor as various reports have associated the loss of E-cadherin expression with the invasive and dedifferentiated or poorly differentiated carcinomas (Frixen *et al.*, 1991; Vleminckx *et al.*, 1991; Mayer *et al.*, 1993; Oka *et al.*, 1993; Sawada *et al.*, 2008; Luo *et al.*, 2013). Nonetheless, in recent years, scientists have discovered that the breast cancer metastases or metastatic foci originating from breast cancer cells that have undergone EMT appear more differentiated and have elevated E-cadherin expression compared to their primary counterpart (Chao *et al.*, 2010; Chao *et al.,* 2012a; Chen *et al.*, 2015). Similarly, studies in pancreatic cancer whereby stabilized E-cadherin expression ironically hadtened the tumour invasion rate and metastatic lesion production in liver have been reported (Liu *et al.*, 2014). Moreover, prostate cancer cells that have undergone EMT re-express E-cadherin when co-cultured with hepatocytes and form heterotypic interaction with them (Yates *et al.*, 2007). Therefore, it is apparent that EMT which was induced for cancer cells dissemination is plastic and mesenchymal-epithelial reversal transition (MErT) can potentially happen via the re-expression of E-cadherin when metastatic cells start to colonize a secondary site (Gunasinghe *et al.*, 2012; Tsai and Yang, 2013).

It is still questionable as to why disseminated tumour cells (DTCs) undergo MET through E-cadherin re-expression after extravasation into a propitious secondary site for colonization? One of the postulated reasons is that DTCs

require physical attachment to the secondary organ site prior to cellular proliferation for the establishment of the secondary metastasis. This hypothesis is corroborated by the finding that E-cadherin-negative MDA-MB-231 breast cancer cells re-expressed E-cadherin when co-cultured with hepatocytes. This increased their heterotypic attachment to hepatocytes followed by activation of pro-survival pathways like extracellular signal-regulated kinases/mitogen-activated protein kinases and protein kinase B (Chao *et al.*, 2012b). In the same vein, expression of E-cadherin along with the functional self-renewal gene program contribute to anoikis resistance or anchorage-independent growth of prostate and bladder cancer cells, hence conferring post-extravasation survivability of DTCs, facilitating their secondary metastasis establishment (Celià-Terrassa *et al.*, 2012). In addition, the self-renewal capacities or stem cell capabilities (SSC) of DTCs are reflected by their ability to form spheroids in suspension cultures and spheroid assay had been actively used to assess cancer cells' SSC (Tang *et al.*, 2012; Fisher *et al.*, 2016). E-cadherin expression had shown to be important in conferring stem cells their SSC in prostate, bladder and breast cancer cells based on its importance in the spheroid formation of these cells (Celià-Terrassa *et al.*, 2012; Iglesias *et al.*, 2013). Therefore, all these evidences steer us towards the understanding that despite E-cadherin loss being required for cancer cells to undergo EMT in gaining invasiveness, the re-expression of E-cadherin and subsequent MET are imperative for its successive survival and colonization to form secondary metastasis (Louie *et al.*, 2013; Yao *et al.*, 2013). Furthermore, this hypothesis is supported by evidence from *in vivo* tracking studies on GFP and luciferase-labelled clonal metastatic breast tumour cells that MET via E-cadherin re-expression provides the tumour cells with higher likelihood of establishing the secondary tumour (Palen *et al.*, 2016).

1.5.2 E-cadherin on cancer cells' growth inhibition and TRAIL-induced apoptosis

Despite the fact that E-cadherin enhances the survival of post-dissemination cancer cells for secondary metastases formation, E-cadherin expression had also been associated with the induction of cancer cells apoptosis. For instance, the spontaneous apoptosis of gallbladder carcinoma undergoing invasion is strongly correlated with E-cadherin expression, displaying potential influence of E-cadherin on the apoptosis of invading cancer cells (Sasatomi *et al.*, 1996). A similar finding had been reported in a three-dimensional skin construct whereby E-cadherin-re-expressed melanoma cells showed typical apoptosis marks like DNA fragmentation, nuclear condensation and apoptotic bodies (Hsu *et al.*, 2000). In addition, the involvement of E-cadherin in apoptosis-inducing drug sensitivity (Ferreira *et al.*, 2005) or drug's mechanism of action in cancer cells (Li *et al.*, 2008) is suggestive of its regulatory role on cancer cells' apoptosis.

Scientists have proposed several mechanisms behind the correlation between E-cadherin expression and apoptosis induction in cancer cells. Besides binding to E-cadherin (Figure 3), β-catenin when activated by the Wnt signaling pathway, also acts as a transcription activator by interacting with those of the LEF-1/TCF family (Daniels and Weis, 2005). This interaction upregulates target genes like c-Myc (He *et al.*, 1998) and cyclin-D1 (Tetsu and McCormick, 1999), leading to cell proliferation and neoplastic transformation. However, in the absence of Wnt-signal, the degradative complex made up of Axin, adenomatous polyposis coli, casein kinase 1, and glycogen synthade kinase 3 is activated to polyubiquitinate beta-catenin, targeting it for proteasomal degradation, thereby preventing the nuclear accumulation of beta-catenin as transcription factor (MacDonald *et al.*, 2009). Since E-cadherin binds β-catenin as part of its adhesion complex, it also serves to negatively regulate β-catenin function by sequestering them, thus minimizing their nuclear localization (Hülsken *et al.*, 1994; Stockinger *et al.*, 2001). As a result, the aforementioned

correlation between E-cadherin and apoptosis in cancer cells can be partially explained by the growth inhibitory effect exhibited through E-cadherin/β-catenin binding (Lowy *et al.*, 2002).

In addition to the constraint placed on the intracellular signal for cell proliferation mediated by β-catenin, E-cadherin was also shown to regulate the transmission of apoptosis signal through the extrinsic apoptotic pathway. The extrinsic apoptosis signal is initiated by a cognate ligand binding to cell surface death receptors and transmitted through the assembly of the DISC and a cascade of caspases activation (Fulda and Debatin, 2006). One of the death ligands is TRAIL and its cognate receptors TRAIL-R1 and TRAIL-R2 (Gonzalvez and Ashkenazi, 2010). Recently, Lu *et al.* (2014) discovered that E-cadherin supports the clustering of TRAIL-R1/–R2 into DISC via its association with the actin cytoskeleton, thereby enabling enhanced apoptosis effect in lung, pancreatic, and colon carcinoma cells at lower TRAIL ligand concentrations. Therefore, the correlation between E-cadherin expression and apoptosis induction can be explained by its coupling of TRAIL death receptors to the actin cytoskeleton for the efficient DISC formation in this case (Figure 3). E-cadherin can thus serve as a potential biomarker for the sensitivity of cancer cells towards pro-apoptotic receptor agonists (PARA) developed against TRAIL receptors (Ashkenazi, 2015).

Since MDA-MB-231 develops resistance towards the administration of TRAIL over time owing to the endocytosis of its surface receptors, TRAIL-R1 and TRAIL-R2 (Yoshida *et al.*, 2009; Zhang *et al.*, 2009), along with the coupling of TRAIL receptors to the actin filaments by E-cadherin, this research aims to answer the question which remains as to whether the dynamic expression of E-cadherin can serve as a marker of TRAIL treatment efficacy in the context of breast cancer, just as its potential as a marker had been demonstrated in the aforementioned carcinomas.

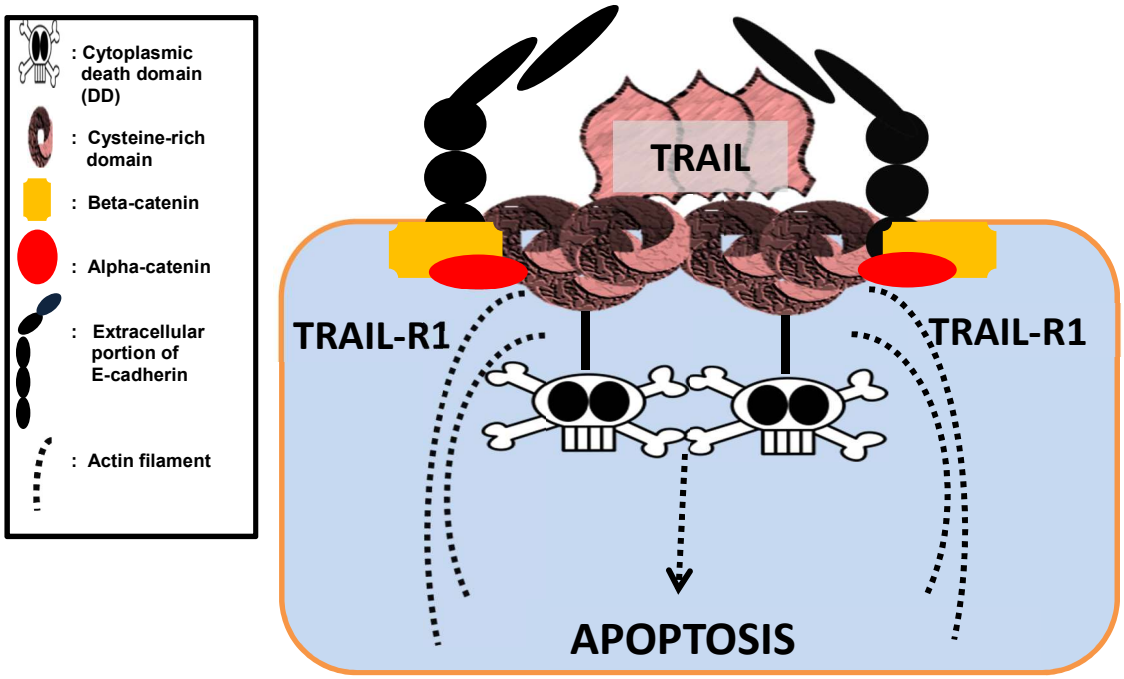


Figure 3 E-cadherin physically interacts with TRAIL-ligated receptors facilitating, thereby connecting TRAIL receptors to cytoskeleton via alpha-catenin and facilitates receptor clustering, DISC formation, caspase activation and apoptosis.

1.5.3 Epigenetic drugs as TRAIL sensitizers in cancer cells

The anti-cancer potential of epigenetic drugs lies in their function as gene regulators by reversing heterochromatin, a tightly packed form of DNA which favours gene suppression, to euchromatin, a lightly packed form of DNA which favours gene expression. Therefore, tumour suppressor genes (TSGs) which have been suppressed by cancer cells can potentially be re-expressed by epigenetic drugs treatment. In the facet of TRAIL-induced apoptosis, epigenetic drugs have also been reported to be one of the many effective sensitizers of various cancer cells towards the apoptotic effect of TRAIL. One of the commonly studied epigenetic drugs aimed as TRAIL sensitizer is the histone deacetylase inhibitors (HDACi) which reverse the gene suppression effected by histone deacetylating enzymes. HDACi have shown excellent cooperation with TRAIL in the killing of a panel of cancer cell types including breast, lung, colon, prostate, renal cell carcinoma and melanoma (Fulda and Debatin, 2005).

Some of the commonly studied HDACi are suberoylanilide hydroxamic acid (SAHA), m-carboxycinnamic acid bis-hydroxamide (CBHA), MS-275 and trichostatin A (TSA). One of the earliest elucidated mechanisms behind the TRAIL-sensitizing effect of HDACi is the upregulation of TRAIL-R1, TRAIL-R2 and proapoptotic Bcl-2 members (Singh *et al.*, 2005; VanOosten *et al.*, 2005a). Besides, HDACi also exhibit pro-TRAIL regulatory effect on cell cycle-related genes, growth factors and their cognate receptors in breast cancer cell line (Zhou *et al.*, 2016). In light of the finding that some of the TRAIL-sensitizing effects of HDACi were also observed without the upregulation of TRAIL receptors (Inoue *et al.*, 2004), it illuminates the fact that there are TRAIL resistance mechanisms which can be targeted beyond the receptor level.

As aforementioned, the rapid internalization of TRAIL-ligated receptors is one of the resistance mechanisms pitched by cancer cells against TRAIL-induced killing (Zhang and Zhang, 2008). Intriguingly, prior treatment with HDACi,

depsipeptide, had enhanced the sensitivity of prostate tumour cells to TRAIL-induced apoptosis by redistributing DR4 and DR5 to membrane lipid rafts (VanOosten *et al.*, 2005b). In addition, the combinatorial treatment of HDACi and TRAIL had also combated the TRAIL resistance in breast cancer via various methods such as downregulation of c-FLIP (Frew *et al.*, 2008), suppression of c-Myc TRAIL-deactivating function by its acetylation (Nebbioso *et al.*, 2017) and fine-tuning the regulation of genes related to the mitochondrial pathway (Morales *et al.*, 2010), so as to engage the intrinsic pathway for better TRAIL anti-cancer efficacy.

Since chromatin architecture is not only regulated by histone deacetylation but also DNA methylation in CpG rich region of gene promoter, scientists have also placed their research focus on another group of epigenetic drug known as DNA methyltransferase inhibitors (DNMTi). Both DNMTi and HDACi work against TRAIL resistance via different mechanisms. For instance, in contrast to the upregulation of TRAIL receptors by HDACi, DNMTi, Zebularine, was shown to enhance TRAIL-induced apoptosis in breast cancer cells by increasing cellular fucosylation level, thereby enhancing the TRAIL-receptor fucosylation-facilitated receptor clustering and apoptosis induction, while the TRAIL receptors level remaining unchanged (Moriwaki *et al.*, 2010).

Nonetheless, growing evidence shows that DNA methylation and histone deacetylation are inter-correlated. For example, attachment of methyl binding protein MeCP2 to methylated sites is followed by recruitment of HDACs which eventually leads to heterochromatin formation (Li, 2002; Sharma *et al.*, 2009). Therefore, dual therapy of HDACi and DNMTi can be envisioned as a TRAIL-sensitizing combination with great potential based on the inter-correlation between the two types of chromatin modifications. This notion had been supported by the cooperative restoration of caspase-8 expression in small cell lung carcinoma (SCLC) by prior treatment of HDACi, valproic acid (VPA) or CI-994 and DNMTi, decitabine, followed by TRAIL treatment (Kaminskyyy *et al.*,

2011). It is also evident from this finding that prior treatment rather than concurrent treatment provided a platform for the re-expression of genes important for TRAIL sensitivity before the TRAIL treatment itself. Both Zebularine (Zeb) and Trichostatin A (TSA) increase TRAIL death receptor fucosylation (Nascimento *et al.*, 2015) and upregulate TRAIL receptors (Singh *et al.*, 2005), respectively, targeting distinctive mechanism of TRAIL resistance in breast cancer cells. In short, combinatorial addition of DNMTi and HDACi prior to TRAIL treatment displays more diverse sensitizing effects on cancer cells to TRAIL-induced apoptosis as compared to the respective single TRAIL-sensitizer.

Therefore, the growth inhibitory effects and apoptosis of E-cadherin-re-expressed MDA-MB-231 human breast carcinoma induced by the proposed sequential treatment of TSA and Zeb followed by TRAIL alongside the potential reduction of the cells' invasiveness will be assessed according to the aims and objectives of this project arrayed in the next chapter.

2. Introduction: Aims and Objectives

This project aims to re-express the E-cadherin gene, *CDH1*, in MDA-MB-231 which does not express or basally express *CDH1* and to sequentially treat *CDH1*-re-expressed MDA-MB-231 with TSA and Zeb combination followed by TRAIL. Subsequently, this project aspires to characterize the cell cycle distribution, invasiveness and apoptosis of *CDH1*-re-expressed MDA-MB-231 at the morphological, cellular and molecular levels after the aforementioned treatment and compare them with MDA-MB-231 (non-transfected control), MCF-7 (*CDH1*-positive control) and MCF10A (epithelial, non-tumourigenic control) cell lines. In addition to the *in vitro* studies, the protein expression of the three main biomarkers in this study, TRAIL-R2, TRAIL and E-cadherin, will also be studied using established mRNA expression data via bioinformatics and compared with immunohistochemistry on formalin-fixed paraffin-embedded (FFPE) tissue microarray on an independent breast cancer cohort (n=2000).

In Chapter 3, in order to deliver the *CDH1* gene into MDA-MB-231, it will be transfected with the E-cadherin-Green Fluorescent Protein (EGFP) plasmid using both the Lipofectamine LTX reagent and *Trans*IT-X2® reagent. The research objectives were as follow:

- To transfect MDA-MB-231 cells with E-cadherin Green Fluorescent Protein (EGFP) plasmid using Lipofectamine LTX reagent and *Trans*IT-X2® reagent;
- To verify the successful delivery of E-cadherin-GFP (*CDH1*-GFP) gene into MDA-MB-231 at the mRNA level of expression using RT-PCR;
- To verify the successful delivery of *CDH1*-GFP gene into MDA-MB-231 at the protein level of expression using flow cytometry;
- To compare the transfection efficiencies between Lipofectamine LTX reagent and *Trans*IT-X2® reagent;
- To compare the live cell percentage given by transfection using the Lipofectamine LTX reagent and the *Trans*IT-X2® reagent;

- To select one between the two transfection reagents of Lipofectamine LTX reagent and *Trans*IT-X2® reagent.

MDA-MB-231 (231), 231-EGFP, MCF-7, MCF10A as well as the empty vector-transfected control (231-EV) will be tested in Chapter 4. The research objectives were as follow:

- To obtain the TSA and Zeb combined treatment (TZ) cell viability curve of MDA-MB-231 for the time points of 24, 48 and 72 h;
- To assess the best inhibitory concentration (IC) of TZ treatment based on the reduction in cell viability obtained by TSA and Zeb combined treatment followed by TRAIL (TZT);
- To use the chosen IC in the MTT cell viability assay of MDA-MB-231, 231-EV, 231-EGFP, MCF-7 and MCF10A in testing the six experimental treatment groups of untreated control, single TSA, single Zeb, TZ, single TRAIL and TZT treatment for the time points of 24, 48 and 72 h;
- To assess the effect of the six experimental treatment groups on the cell cycle distribution of MDA-MB-231, 231-EV, 231-EGFP, MCF-7 and MCF10A via ethanol fixing, propidium iodide (PI) staining and flow cytometry;
- To assess the effect of the six experimental treatment groups on the cell migration rate of MDA-MB-231, 231-EV and 231-EGFP via the wound healing assay;
- To assess the mRNA expression of genes regulating cell cycle progression (PCNA and CDK2) and cell invasiveness (MMP-9).

After the cell cycle distribution had been assessed both at the cellular and molecular levels in Chapter 4, 231, 231-EGFP and MCF-7 will be assessed for the apoptosis induced by the groups of untreated and treated with TZ, TRAIL and TZT, both at the morphology level via Hematoxylin and Eosin (H and E) staining and at the cellular level using Annexin V-FITC/PI cellular apoptosis flow cytometric assay in Chapter 5.

The research objectives were as follow:

- To assess the TSA and Zeb combined followed by TRAIL (TZT) treatment apoptosis-induction in MDA-MB-231, 231-EGFP and MCF-7 at the morphology level via Hematoxylin and Eosin (H and E) staining;
- To assess the TSA and Zeb combined followed by TRAIL (TZT) treatment apoptosis-induction in MDA-MB-231, 231-EGFP and MCF-7 at the cellular level via Annexin V-FITC/PI cellular apoptosis flow cytometric assay;
- To assess the TSA and Zeb combined followed by TRAIL (TZT) treatment apoptosis-induction in MDA-MB-231, 231-EGFP and MCF-7 at the molecular level via Human Apoptosis Proteome Profiling of 35 apoptosis-related proteins.

In the final experimental chapter (Chapter 6), the expression patterns of TRAIL-R2, TRAIL and E-cadherin will be studied at both the mRNA and protein levels using the bioinformatics and immunohistochemistry approaches, respectively. The research objectives were as follow:

- To obtain the RNA sequencing data from The Cancer Genome Atlas (TCGA) breast invasive carcinoma data repository for normalized gene counts (mRNA) of TRAIL-R2, TRAIL, E-cadherin and conduct statistical analysis;
- To obtain the Molecular Taxonomy of Breast Cancer International Consortium (METABRIC) microarray mRNA expression data of TRAIL-R2, TRAIL, E-cadherin and conduct statistical analysis;
- To validate the specificity of anti-TRAIL-R2, anti-TRAIL and anti-E-cadherin monoclonal antibody using Western blotting;
- To stain the primary invasive breast cancer patients' formalin-fixed paraffin-embedded (FFPE) tissue sections via immunohistochemistry of the heat-induced epitope retrieval method;
- To score the immunohistochemically stained images of TRAIL-R2, TRAIL, and E-cadherin for H-scores calculation using the formula: (Percentage value × 3) + (Percentage value × 2) + (Percentage value × 1) + (Percentage value × 0)

whereby 0=negative; 1=weak staining; 2=moderate staining; 3=strong staining) and conduct statistical analysis.

Last but not least, the final concluding chapter will outline the main findings obtained from this study and several potential future research directions to be taken from this project onwards.

3. Optimization of E-cadherin (*CDH1*) gene delivery into human breast adenocarcinoma cells, MDA-MB-231

3.1 Introduction

E-cadherin (CDH1) is one of the important cell-cell adhesion proteins expressed in normal epithelial cells including breast cells. It is a tumour suppressor gene of which the aberrant expression had caused malignancies such as gastric cancer (Guilford *et al*., 1998; Huiping *et al*., 2001), prostate cancer (Cheng *et al.*, 1996; Barber *et al.*, 2015), lung cancer (Bremnes *et al.*, 2002; Kim *et al.*, 2014), colon and colorectal cancer (Palmer *et al.*, 2001; Fang *et al.*, 2015) as well as breast cancer.

CDH1 is located at chromosome 16q22.1 and is approximately 100 kb long. The gene region comprises of 16 exons sized between 115 and 2245 base pairs (bp) intervened by 15 introns in total. Comparison of the human *CDH1* exon borders across different species and different cadherin types revealed noteworthy conservation of their splice sites, implying gene duplication or conversion along the coevolution process between cadherin types. Intron 2 at 65 kb is the longest among all while intron 1 along with its juxtaposed exons house a unique long CpG island which possibly serves to regulate the dynamic E-cadherin expression via CpG island methylation (Berx *et al.*, 1995).

E-cadherin protein is transcribed from the *CDH1* gene into a precursor polypeptide of 135 kDa. The precursor segment carries a prosequence harbouring the consensus protease cleavage site (Arg-Arg-Gln-Lys-Arg) which facilitates its proteolytic processing into a mature and functional protein with adhesive properties. This proteolytic processing happens in the Golgi apparatus and yields the mature E-cadherin protein starting with a conserved amino terminal sequence of (Asp/Glu)-Trp-Val-(Ile/Met)-Pro-Pro-Ile which is transported to the plasma membrane (Ozawa and Kemler, 1990; Häussinger *et al.*, 2004). The mature E-cadherin protein is a 120 kDa, Ca^{2+}-dependent transmembrane glycoprotein found within adherens junctions located at the

lateral surface of polarized epithelial cells (Ogou *et al.*, 1983; Jiang, 1996; Wheelock and Johnson, 2003; Capaldo *et al.*, 2014).

This chapter serves as the fundamental milestone of optimizing the delivery of *CDH1* gene into MDA-MB-231 cells using both the Lipofectamine LTX reagent and the *Trans*IT-X2® reagent. The successful delivery of the E-cadherin-green fluorescent protein (EGFP) plasmid into MDA-MB-231 will be verified at the mRNA and protein levels using reverse transcription-polymerase chain reaction (RT-PCR) and flow cytometry, respectively.

The research objectives were as follow:

- To transfect MDA-MB-231 cells with E-cadherin Green Fluorescent Protein (EGFP) plasmid using Lipofectamine LTX reagent and *Trans*IT-X2® reagent;
- To verify the successful delivery of E-cadherin-GFP (*CDH1*-GFP) gene into MDA-MB-231 at the mRNA level of expression using RT-PCR;
- To verify the successful delivery of *CDH1*-GFP gene into MDA-MB-231 at the protein level of expression using flow cytometry;
- To compare the transfection efficiencies between Lipofectamine LTX reagent and *Trans*IT-X2® reagent;
- To compare the live cell percentage given by transfection using the Lipofectamine LTX reagent and the *Trans*IT-X2® reagent;
- To select one between the two transfection reagents of Lipofectamine LTX reagent and *Trans*IT-X2® reagent.

3.2 Materials and method

3.2.1 Recovery of EGFP plasmid from *Escherichia coli* bacteria host

3.2.1.1 Streaking *Escherichia coli* bacteria host for single colony formation

The E-cadherin-Green Fluorescent Protein (EGFP) plasmid (Addgene plasmid #28009), a gift from Jennifer Stow, was obtained commercially from Addgene as an *E. coli* stab culture. The full plasmid map is shown in Appendix A. The plasmid is sized 8897 base pairs (bp) and it harbours an ampicillin resistance gene in the region of 7045 to 7905 bp. To recover the plasmid, the *E. coli* stab culture (as received) was dipped with a sterile inoculating loop and subsequently streaked onto Luria Bertani (LB) agar plate (1% (w/v) NaCl, 1% (w/v) tryptone, 0.5% (w/v) yeast extract, 1.5% (w/v) agar) (Amresco, USA) containing 100μgmL^{-1} ampicillin. The plate was then incubated at 37˚C for 24 hours (h) for single colony establishment.

3.2.1.2 Expansion of clonal *Escherichia coli* host in Luria Bertani (LB) broth

LB broth (1% (w/v) NaCl, 1% (w/v) tryptone, 0.5% (w/v) yeast extract) (Amresco, USA) (10 mL) containing 100 μgmL^{-1} ampicillin was prepared in 50 mL centrifuge tube with sterile technique. A single colony was picked using a sterile inoculating loop and inoculated into the prepared LB broth (10 mL per colony). The tube was then incubated in an incubator shaker for 16 h at 37˚C with rotation at 200 rpm to obtain a dense culture of *E. coli* containing the EGFP plasmid. Successful *E. coli* culture was indicated by cloudy and opaque appearance.

3.2.1.3 E-cadherin Green Fluorescent Protein (EGFP) plasmid extraction from *E. coli LB broth culture*

The EGFP plasmid was extracted from the dense *E. coli* culture using the PureLink® Quick Plasmid Miniprep Kit (Invitrogen, USA) according to the manufacturer's guidelines with minor alterations. Briefly, *E. coli* cells were harvested via centrifugation at 4˚C and resuspended in Resuspension Buffer containing RNase A. Lysis Buffer was then added to lyse and disintegrate the plasma membrane. Subsequently, Precipitation Buffer was added to precipitate cellular components other than the plasmid DNA. After centrifugation, the supernatant containing the plasmid DNA was bound to a spin column and processed through several washings using Wash Buffer with ethanol. Eventually, the EGFP plasmid was eluted using nuclease-free water into clean recovery tube and stored at -20˚C.

3.2.1.4 Quantification and quality assessment of the extracted EGFP plasmid

The extracted EGFP plasmid was quantified using BioTek Take3 Micro-Volume Plate Reader at 3 µL per reading. The absorbance values of the eluted EGFP plasmid solution at 260 (A_{260nm}) nm and 280 nm (A_{280nm}) wavelengths were also obtained simultaneously. All extracted plasmids with A_{260nm}:A_{280nm} ratio ranging from 1.8 - 2.0 were considered as excellent quality and were used for the subsequent restriction enzyme digestion verification of the plasmids' integrity.

3.2.1.5 *Bam*HI-HF® and *Xba*I restriction enzyme diagnostic digestion of EGFP plasmid

The EGFP plasmid had a *Bam*HI-High Fidelity® (*Bam*HI-HF®) restriction recognition site at 5159 bp and an *Xba*I restriction recognition site at 2521 bp (Appendix A). Therefore, *Bam*HI-HF® and *Xba*I restriction enzymes (New England BioLabs®, USA) were used for the diagnostic digestion of EGFP plasmid to ensure its integrity. The restriction reaction was conducted in CutSmart buffer (New England BioLabs®, USA) at 37˚C for 3 h. Subsequently, the restricted product was then mixed with 1×DNA loading dye (Thermo Fisher Scientific, USA) and separated on 1.5% (w/v) agarose gel electrophoresis at 75 V, 300 mA for 45 minutes (min). After agarose gel electrophoresis, the gel was then exposed to UV radiation for image capture of the DNA bands using Bio-Rad Gel Doc XR (Bio-Rad, U.S.A.).

3.2.1.6 Agarose gel electrophoresis of the *Bam*HI-HF® and *Xba*I restriction enzyme digested products

The *Bam*HI-HF® and *Xba*I restricted product was then mixed with 1× DNA loading dye (Thermo Fisher Scientific, USA) and separated on 1.5% (w/v) agarose gel electrophoresis at 75 V, 300 mA for 45 min. The agarose gel was then exposed to UV radiation for image capture of the DNA bands using Bio-Rad Gel Doc XR.

3.2.2 Cell Culture Maintenance

Human breast adenocarcinoma cell line, MDA-MB-231, was maintained on culture with Dulbecco's Modified Eagle Medium (DMEM) (Corning, U.S.A.) supplemented with 10% (v/v) of fetal bovine serum (FBS) (Gibco Life Technologies, U.S.A.) and 1% (v/v) penicillin-streptomycin (Gibco Life Technologies, U.S.A.) at 37˚C and 5% CO_2, 95% O_2 atmosphere. MDA-MB-231 was transfected (steps as below) with pCDNA3.1(+) empty vector (#2903) (231-EV) and E-cadherin-Green Fluorescent Protein (EGFP) plasmid, a gift from Jennifer Stow (Addgene plasmid #28009) (231-EGFP), respectively, and maintained under the same condition with the addition of Geneticin (G4-18) (Thermo Fisher Scientific, U.S.A.).

3.2.3 Transfection of MDA-MB-231 cells with EGFP plasmid and pCDNA3.1 empty vector

3.2.3.1 Lipofectamine® LTX and PLUS™ Reagent

MDA-MB-231 cells were seeded at 1.25×10^5 cells or 2.5×10^5 cells per well in 24-well or 6-well, respectively. Transfection was conducted after 24 h when cells have fully attached to the well surface. First, Lipofectamine® LTX reagent (Invitrogen, USA) was diluted with Opti-MEM® medium (Invitrogen, USA) at 2, 3, 4% (v/v), respectively. The concentration of Lipofectamine® LTX reagent which gives the highest *CDH1*-GFP expression level based on real-time quantitative polymerase chain reaction (qPCR) data will then be used for subsequent transfections. EGFP plasmid was mixed with the PLUS™ reagent at 1 µg:1 µL ratio prior to diluting the plasmid in Opti-MEM® medium (Invitrogen, USA) at concentration of 0.02 µg/µL. The mixture was incubated at room temperature for 15 min. Subsequently, diluted DNA was added to diluted Lipofectamine® LTX reagent at 1:1 ratio and incubated at room temperature for 20 min for the DNA-lipid complex to form. The DNA-lipid complex was then added to 24-well or 6-well of seeded cells at 100 ng or 2500 ng plasmid per well, respectively. Cells were then incubated for the stipulated duration prior to

assessment of the *CDH1*-GFP expression levels using the methods stated below.

3.2.3.2 *Trans*IT-X2® Dynamic Delivery System

MDA-MB-231 cells were seeded at 1.25 × 10^5 cells or 2.5 × 10^5 cells per well in 24-well or 6-well, respectively. Transfection was conducted after 24 h when cells have fully attached to the well surface. First, *Trans*IT-X2® reagent (Mirus Bio, USA) was warmed to room temperature and vortexed briefly. Opti-MEM I Reduced-Serum Medium (Invitrogen, USA) was mixed with plasmid DNA (EGFP plasmid or pCDNA3.1 empty vector) at 1 µg DNA:100 µL medium in a sterile tube. *Trans*IT-X® reagent was added to the diluted DNA mixture at 3 µL per 1µg of plasmid used. The mixture was incubated at room temperature for 30 min to allow sufficient time for the complexes to form. Subsequently, the *Trans*IT-X2®: DNA complexes were added dropwise to different areas of the wells. Even distribution of the complexes was ensured by gently rockling the plate back and forth and from side to side. The plate was then incubated for 24, 48 and 72 h.

3.2.4 Assessment of E-cadherin-Green Fluorescent Protein (EGFP) expression at the mRNA level

3.2.4.1 Real time Quantitative Polymerase Chain Reaction (qPCR)

GFP is fused at the carboxyl terminal of the *CDH1* open reading frame 3 (ORF3) and was used as a reporter gene. At 24 h post-transfection, MDA-MB-231 cells were lysed and RNA was extracted using NucleoSpin RNA Plus Extraction Kit (Machery-Nagel, Duren, Germany) according to the manufacturer's protocol. cDNA synthesis and amplification were accomplished in a single reaction tube using the SuperScript™ III Platinum® SYBR® Green One-Step qRT-PCR Kit with ROX (Invitrogen, USA) according to the manufacturer's protocol. Beta-actin amplification was done to ensure equal loading amount across samples. The oligonucleotide primers specific for the connecting region of *CDH1*-GFP: forward 5'-GTCGTGCTGCTTCATGTGGT-3', reverse 5'-CGACGTAAACGGCCACAAGT-3' (Integrated DNA Technologies, USA) and beta-actin: forward 5'CCCAGGACTCTCTTCTCTGACC-3', reverse 5'TCCAAGGCCGCTTTACACCA-3' (Integrated DNA Technologies, USA) have been designed using the NCBI Primer-BLAST online tool.

3.2.4.2. Reverse-transcription Polymerase Chain Reaction (RT-PCR)

At 24, 48 and 72 h post-transfection, MDA-MB-231 cells were lysed and total RNA was extracted using the Trizol conventional RNA extraction method. RNA purity and quantity was assessed using the BioTek Take3 Micro-Volume Plate Reader at 2 µL per reading. The absorbance ratios of (A_{260}/A_{280}) and (A_{260}/A_{230}) were obtained, 1.8 - 2.0 and 2.0 - 2.2, respectively, is considered as the range of excellent RNA quality. The good quality total RNA samples were treated with DNase I (Promega, USA) to remove any genomic DNA contamination. Thereafter, DNAse I-treated RNA was reverse transcribed into cDNA using the First Strand cDNA Synthesis Kit ProtoScript II Reverse Transcriptase. Subsequently, the synthesized first strand cDNA was then subjected to PCR amplification using the primer sequence forward: 5'-

GCTCCTGGACGTAGCCTTC-3' and reverse: 5'-GAAAGCGGCTGATACTGACC-3' targeting the *CDH1* gene with the condition as follows:

Initial denaturation:	94˚C – 2 min	
Denaturation:	94 ˚C – 30 seconds (sec)	35 cycles
Annealing:	55 ˚C – 20 sec	
Extension:	72 ˚C - 20 sec	
Final extension:	72 ˚C -5 min	

The final PCR product of *CDH1* gene amplification was subjected to 1% (w/v) agarose gel electrophoresis. Gel image of targeted band was captured using the Bio-Rad GelDoc Imager.

3.2.5 Assessment of EGFP expression at the protein level

3.2.5.1 Flow cytometry

At 24, 48, and 72 h post-transfection, MDA-MB-231 cells were trypsinized for 2 min and added with DMEM with 10% (v/v) FBS to deactivate the trypsin. Then, the mixture was centrifuged at 1800 rpm for 5 min and supernatant was discarded. Cell count was performed. Pellet was then resuspended in 1× Phosphate Buffered Saline (PBS) (Vivantis Technologies, Malaysia) containing 1% (v/v) FBS to constitute 1 × 10^6 cells/mL and transferred to a 1.5 mL microcentrifuge tube. Samples were then analyzed on BD Accuri C6 Flow-cytometer using the 20,000 cells gate and FL-1 channel to capture GFP fluorescence. Non-transfected cells served as background signal for the normalization of data. Cell population distribution and mean fluorescence unit of FL1-A (MFU FL1-A) were analyzed using the BD Accuri™ C6 software.

3.2.5.2 Fluorescence microscopy

At 24, 48 and 72 h post-transfection under G4-18 selection, MDA-MB-231 cells were washed thoroughly with 1× PBS for three times prior to capturing microscopic images under the bright field and the FITC channel of Axio observer 7 inverted fluorescence microcope (ZEISS, Germany). Images were also captured at the respective time points of G4-18 selection for 6, 15, 21, 29 days post-selection (d.p.s.). The images captured under the bright field and the FITC channel were merged using the ZEISS imaging software (ZEISS, Germany).

3.2.6 Selection of successful MDA-MB-231 transfectants using Geneticin (G4-18) resistance selectable marker

At 24 h post-transfection, cells were cultured with DMEM with 10% (v/v) FBS added with 800μg/mL Geneticin (G4-18) to select for the successful transfectants. The transfected cells were expanded and maintained on culture with the G4-18 selection.

3.3 Results

3.3.1 Verification of E-cadherin-GFP plasmid integrity by restriction enzyme digestion and agarose gel electrophoresis

The E-cadherin-GFP plasmid (EGFP) (#28009) recovered from the commercial *E. coli* stab culture was quantified. The eluted plasmids with A260nm:A280nm of 1.8 to 2.0 were selected as of excellent quality and were digested with BamHI-HF® and XbaI (New England BioLabs®) restriction enzymes to verify its integrity. The plasmid full length sequence consists of 8897 bp. It had a BamHI-HF® restriction recognition site at 5159 bp and an XbaI restriction recognition site at 2521 bp (Appendix A). Therefore, after digestion with single BamHI-HF®, a linearized band of 8891 bp was obtained (Figure 4). On the other hand, after restriction by both the BamHI-HF® and the XbaI enzymes, the expected band sizes are 2638 bp and 6259 bp, respectively. The gel image presented here shows two DNA bands of their expected sizes in the digested lanes and not in the undigested lanes (Figure 5).

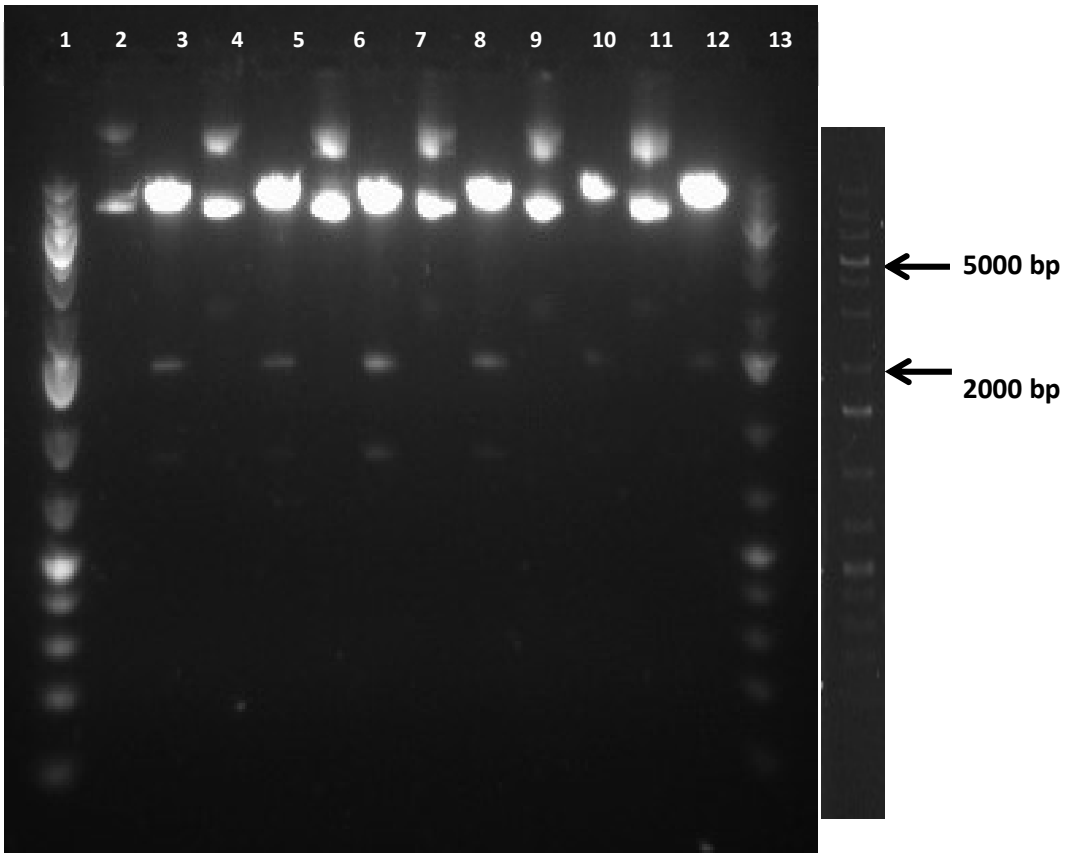


Figure 4 DNA gel electrophoresis single *Bam*HI digested E-GFP plasmid on 1% (w/v) agarose gel.
Lanes 1, 14: 1 kb plus DNA ladder (Invitrogen); Lanes 2, 4, 6, 8, 10, 12: Undigested E-GFP plasmid; Lanes 3, 5, 7, 9, 11, 13: *Bam*HI digested E-GFP plasmid. N.B. The additional 1kb plus DNA ladder image shown on the right is taken from another gel electrophoresis to better visualize the DNA ladder bands separation.

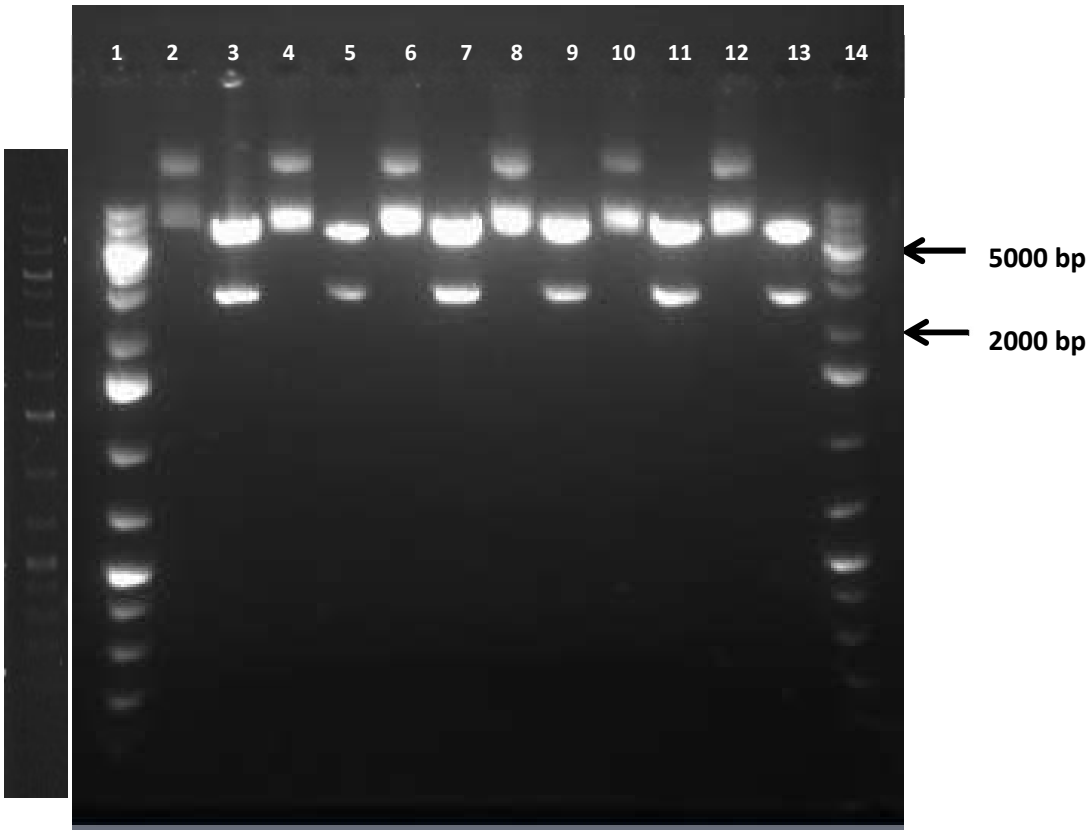


Figure 5 DNA gel electrophoresis of *Bam*HI and *Xba*I digested E-GFP plasmid on 1% (w/v) agarose gel.
Lanes 1,14: 1 kb plus DNA ladder (Invitrogen); Lanes 2, 4, 6, 8, 10, 12: Undigested E-GFP plasmid; Lanes 3, 5, 7, 9, 11, 13: *Bam*HI and *Xba*I digested E-GFP plasmid. N.B. The additional 1kb plus DNA ladder image shown on the left is taken from another gel electrophoresis to better visualize the DNA ladder bands separation.

3.3.2 Transfection of MDA-MB-231 cells with EGFP plasmid and pCDNA3.1 empty vector

EGFP carrying the *CDH1* gene fused to GFP (*CDH1*-GFP) was transfected into the *CDH1*-negative human breast adenocarcinoma cells, MDA-MB-231, using Lipofectamine LTX reagent at 2%, 3%, 4%, and 5%, respectively with PLUS reagent at DNA amount:PLUS reagent ratio of 1:1. Transfection with Lipofectamine LTX reagent at 5% induced considerable amount of cell death as visualized by floating cells under the microscope (result not shown). After transfection, both the non-transfected control and transfected samples were subjected to RNA extraction using the NucleoSpin RNA Plus Extraction Kit (Machery-Nagel, Duren, Germany) and excellent quality RNA samples with A260nm:A280nm of 1.8-2.0 and A260nm/A230nm of 2.0-2.2 were used for the qPCR reaction. From the qPCR result, *CDH1*-GFP mRNA expression level increases with the increase of Lipofectamine LTX reagent concentration from 0% (v/v) (untransfected) to 4% (v/v). The highest relative expression of 214.26 compared to untransfected control was given by transfection at 4% (v/v) lipofectamine LTX reagent (Figure 6). The melt curve analysis is shown in Appendix B.

Besides, both the non-transfected control and transfected samples were also harvested and resuspended in 1× PBS containing 1% (v/v) FBS at 1 × 106 cells/mL for flow cytometric analysis of GFP fluorescence in the FL1-A (530/30 nm) channel. At 48 h post-transfection, there is an increase in the mean fluorescence unit (MFU) of FL1-A channel of the gated 20000 cell population from 3027.85 (non-transfected control) to 10121.4 (4% (v/v) Lipofectamine transfected cells) (Figure 8). However, as shown in (Figure 7E), only 11.5% of the cell population shifted away from the auto-fluorescence region. At 24 h and 72 h post-transfection, there was no appreciable difference in MFU of the gated 20000 cell population between control and transfected sample (Figure 8).

Nonetheless, transfection of MDA-MB-231 cells with 4% (v/v) Lipofectamine LTX reagent gave a marked reduction in live cell population at 24 h post-transfection. The live cell population was only 25.3% (Figure 9A and 9B; Figure 10).

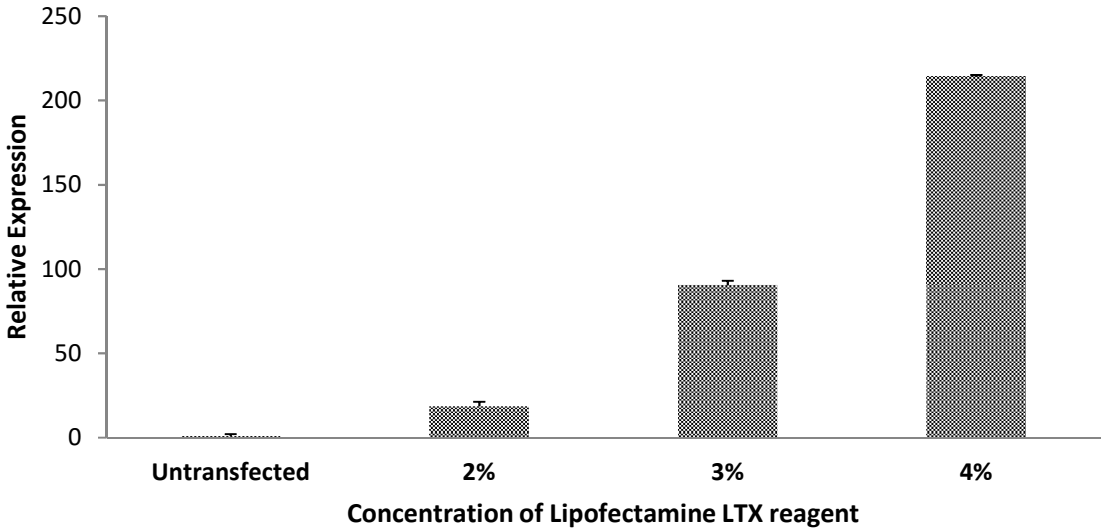


Figure 6 MDA-MB-231 cells untransfected (control) and transfected with 2%, 3%, 4% Lipofectamine LTX with PLUS reagent for 24 h were extracted its RNA using the NucleoSpin RNA Plus Extraction Kit (Machery-Nagel, Duren, Germany) and subjected to qPCR analysis using the SuperScript™ III Platinum® SYBR® Green One-Step qRT-PCR Kit with ROX (Life Technologies). The relative expression of each sample against beta-actin loading control is shown. Error bars represent standard deviation of ΔCq values from three biological replicates.

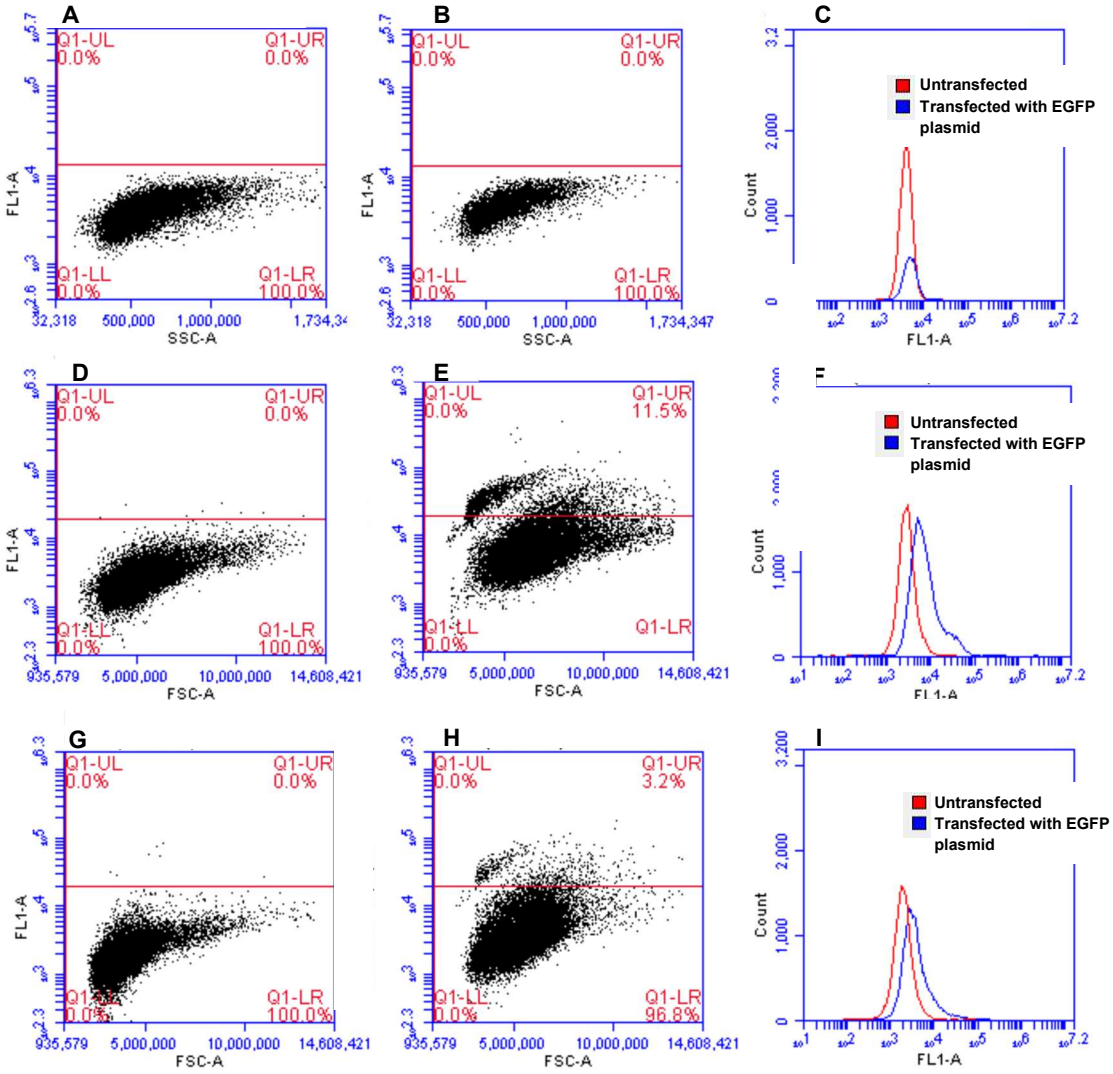


Figure 7 MDA-MB-231 cells untransfected (control) and transfected with 4% Lipofectamine LTX with PLUS™ reagent for 24 (A-C), 48 (D-F) and 72 h (G-I) were trypsinized, harvested and resuspended in 1× PBS containing 1% (v/v) FBS at 1 × 10^6 cells/mL. Cell suspension was then subjected to flow cytometric analysis in the FL1-A (530/30nM) channel in a gated 20,000 cell population at slow flow rate. The gates shown in (A), (B), (D), (E), (G) and (H) indicate that events falling below which are due to background auto-fluorescence.

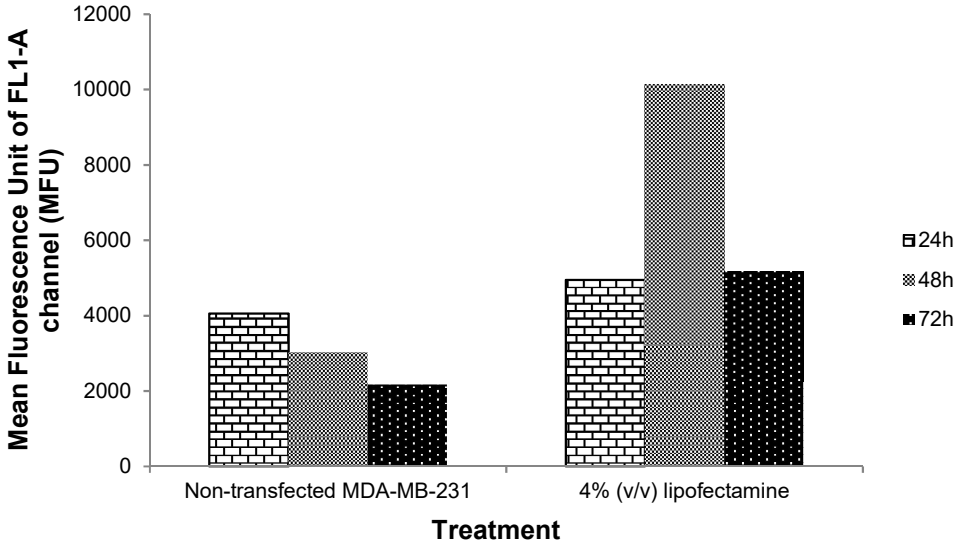


Figure 8 MDA-MB-231 cells untransfected (control) and transfected with 4% Lipofectamine LTX with PLUS^{TM} reagent for 24, 48 and 72 h were trypsinized, harvested and resuspended in 1× PBS containing 1% (v/v) FBS at 1 × 10^6 cells/mL. Cell suspension was then subjected to flow cytometric analysis in the FL1-A (530/30nM) channel in a gated 20,000 cell population at slow flow rate. Data represents mean fluorescence unit (MFU) of 20,000 events collected per sample from single experiment.

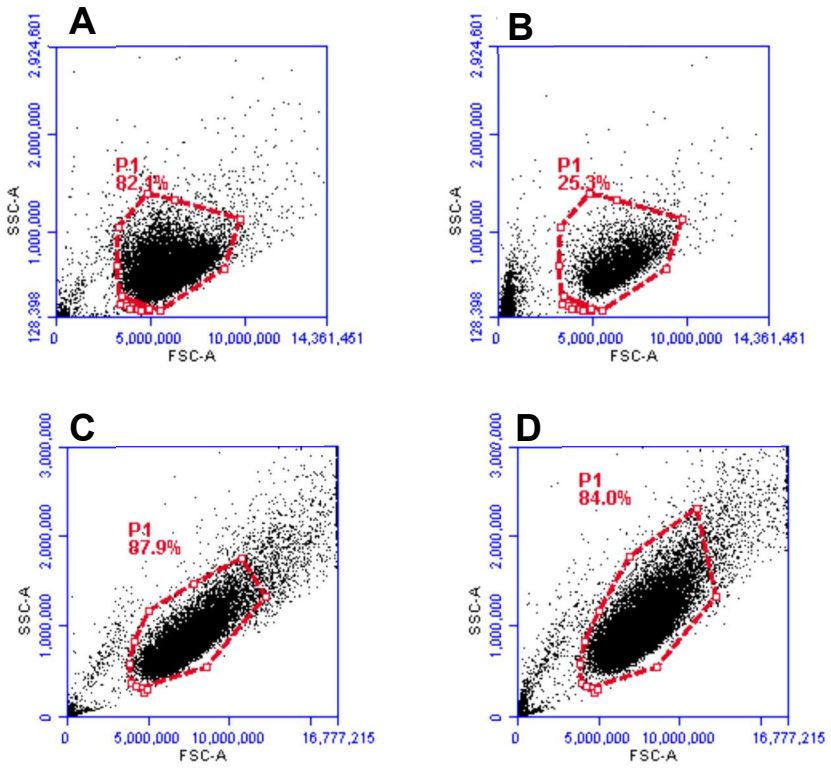


Figure 9 Untransfected MDA-MB-231 (A, C) and MDA-MB-231 cells transfected with EGFP plasmid using Lipofectamine LTX with PLUS™ reagent (B) at 4% (v/v) and Transit-X2 reagent (D) at 3µL:1µg plasmid for 24h. A minimum of 15,000 events were analyzed and the SSC-A-FSC-A plot was used to determine the percentage of live cells (P1 gate) in the sample. Below is the bar chart representation of the live cell percentage of the respective samples.

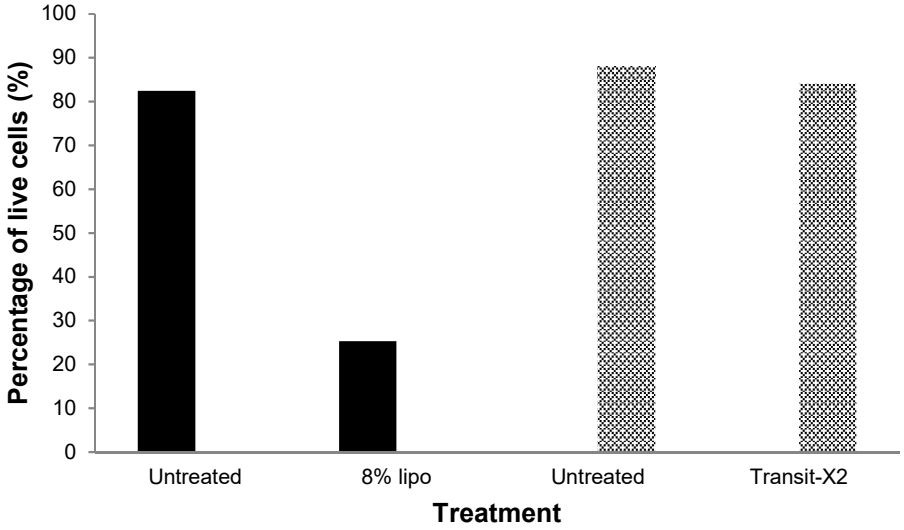


Figure 10 Untransfected MDA-MB-231 (A, C) and MDA-MB-231 cells transfected with EGFP plasmid using Lipofectamine LTX with PLUS™ reagent (B) at 4% (v/v) and Transit-X2 reagent (D) at 3µL:1µg plasmid for 24 h. A minimum of 15 000 events were analyzed and the SSC-A-FSC-A plot was used to determine the percentage of live cells (P1 gate) in the sample. Above is the bar chart representation of the live cell percentage of the respective samples.

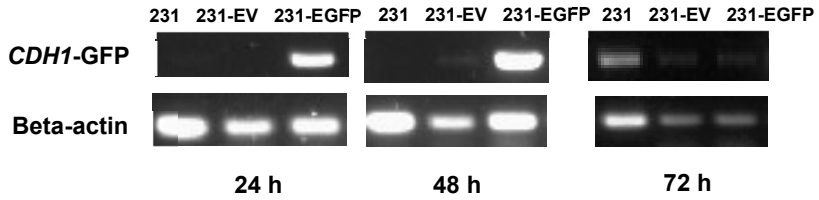


Figure 11 Verification of mRNA expression of *CDH1*-GFP in transfected MDA-MB-231. Total RNA was extracted from MDA-MB-231 (231), MDA-MB-231 transfected with pCDNA3.1 (231-EV) and MDA-MB-231 transfected with EGFP plasmid (231-EGFP) for 24, 48 and 72 h, converted to cDNA and amplified by PCR using primers targeting *CDH1*-GFP (491 bp) and beta-actin housekeeping gene (182 bp).

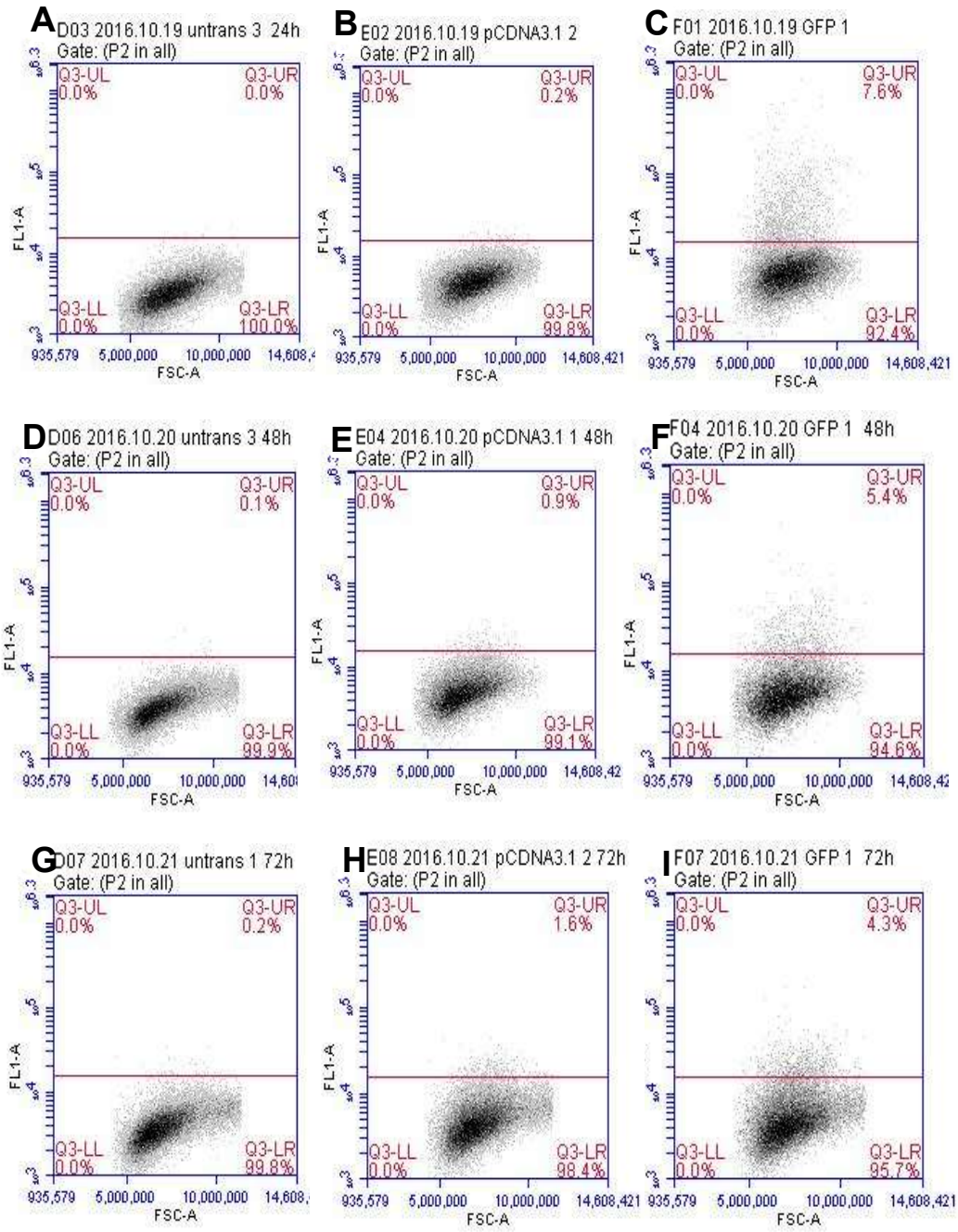


Figure 12 Flow cytometric data of MDA-MB-231 cells transfected for 24 (A,B,C), 48 (D,E,F) and 72 h (G,H,I). Percentage of MDA-MB-231 cells falling above the background fluorescence after transfection using TRANSIT-X2 reagent for 24, 48 and 72 h. (A, D, G: untransfected; B, E, H: transfection with pCDNA3.1 empty vector; C, F, I: transfection with E-cadherin-GFP plasmid). A total of 20,000 events were analyzed and the non-transfected served as the gating control for FL1-A channel.

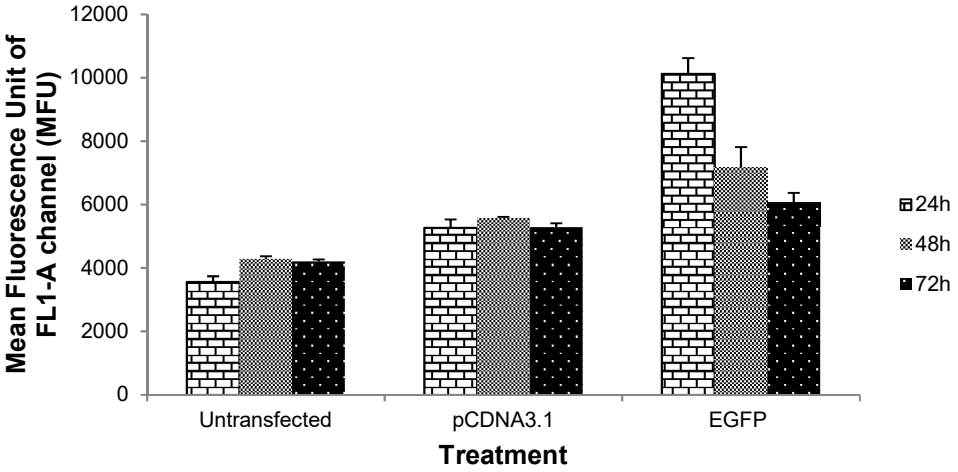
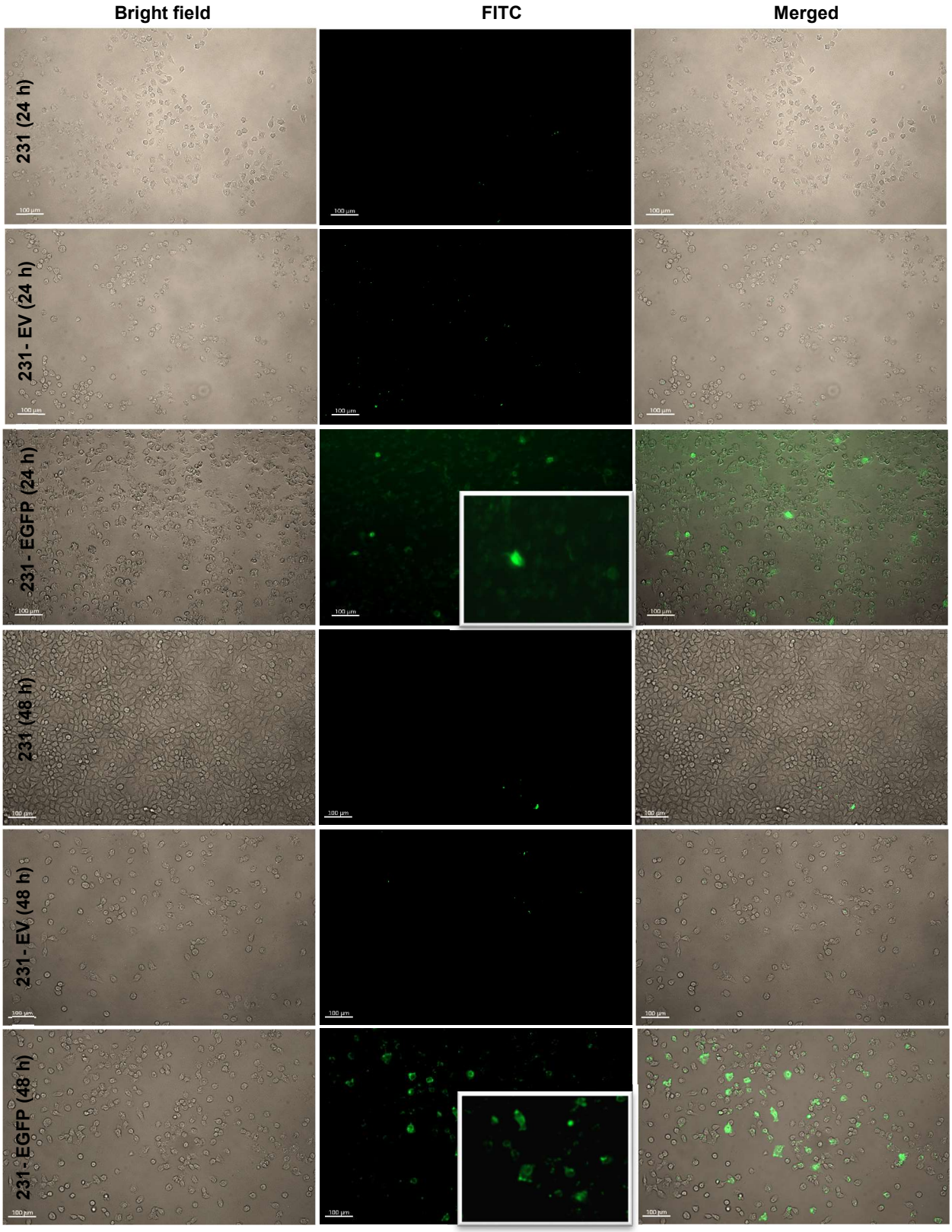


Figure 13 MDA-MB-231 cells untransfected (control) and transfected with 4% Lipofectamine LTX with PLUS™ reagent for 24, 48 and 72 h were trypsinized, harvested and resuspended in 1× PBS containing 1% (v/v) FBS at 1 × 10^6 cells/mL. Cell suspension was then subjected to flow cytometric analysis in the FL1-A (530/30nM) channel in a gated 20000 cell population at slow flow rate. Data represents mean fluorescence unit (MFU) of 20,000 events of triplicates from one independent experiment.


Bright field
FITC
Merged
231 (24 h)
231- EV (24 h)
231- EGFP (24 h)
231 (48 h)
231- EV (48 h)
231- EGFP (48 h)

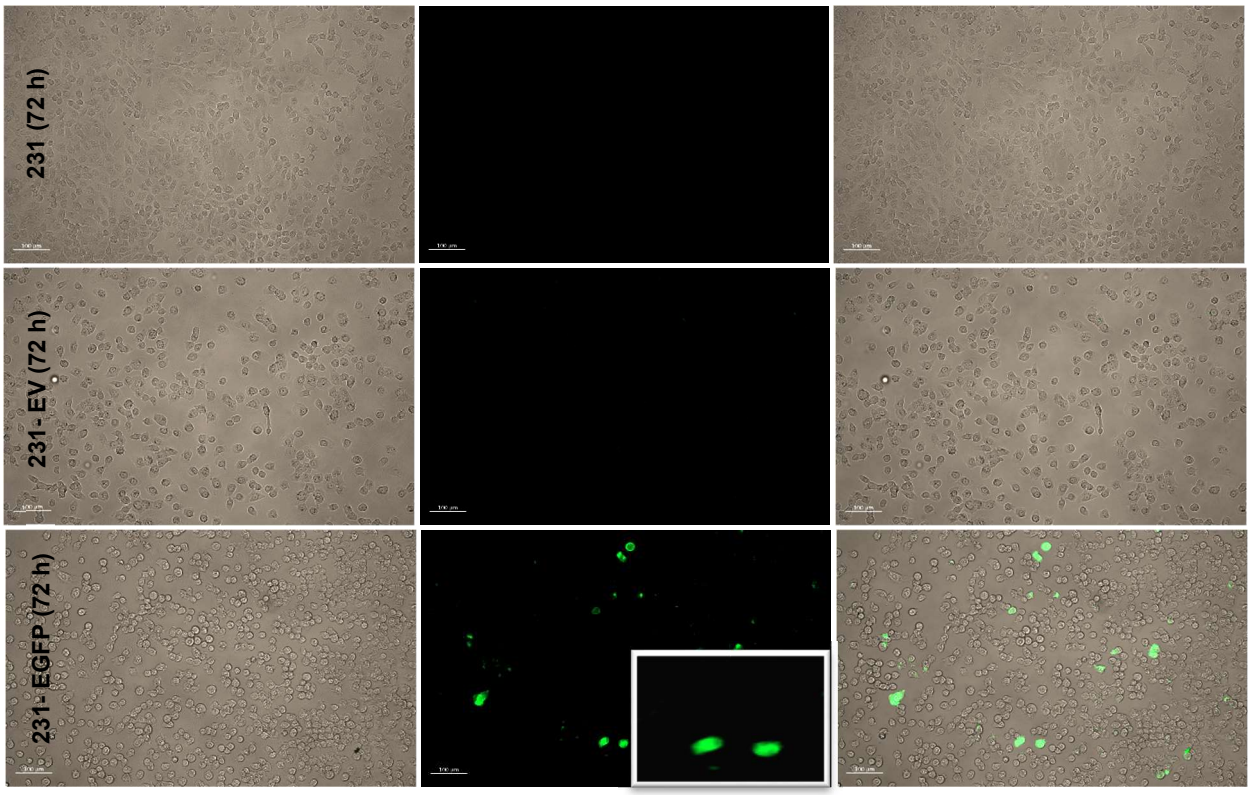


Figure 14 MDA-MB-231 (231), 231-EV and 231-EGFP cells were captured for GFP fluorescence under the bright field and FITC channel of Axio observer 7 inverted fluorescence microcope (ZEISS, Germany) at the respective time points of 800 µg/mL G4-18 selection for 24, 48 and 72 h. Scale bars represent 100 µm. Insets are of the same photo at higher magnification for clearer view.

Since transfection using lipofectamine LTX reagent greatly inhibited MDA-MB-231 cells growth, other mean of delivering EGFP plasmid into the cell line was attempted. The *Trans*IT-X2® reagent was used as an alternative transfection reagent. As shown in Figure 11, *Trans*IT-X2® reagent successfully delivered the *CDH1*-GFP gene into MDA-MB-231 and it was expressed at the mRNA level as the expected band of *CDH1*-GFP (491 bp) was obtained from RT-PCR at 24 and 48 h post-transfection, respectively. However, at 72 h post-transfection, the expression of *CDH1*-GFP had decreased.

From the flow cytometry data, 24 h of transfection with *Trans*IT-X2® reagent successfully delivered the *CDH1*-GFP gene into MDA-MB-231 and expression was detectable based on the reporter gene GFP expression. However, only 7.6% of the cell population was shifted above the background fluorescence threshold, indicating transfectants harbouring *CDH1*-GFP expression (Figure 12). The percentage of successfully transfected cells declined progressively to 5.4% and 4.3% at 48 and 72 h, respectively. The successful delivery of *CDH1*-GFP gene was also verified by the increase in mean fluorescence unit (MFU) in EGFP-transfected sample (10116.68) as compared to the non-transfected control (3563.29) and the pCDNA3.1 empty vector-transfected control (5269.17) (Figure 13). Fluorescence images captured under the FITC channel shows that the delivery of *CDH1*-GFP gene was successful but not homogeneous (Figure 14).

On the other hand, from the FSC-A vs SSC-A plot derived from the same sample (Figure 15), the mean percentages of live cell given by 24 h transfection with *Trans*IT-X2® was 75.2% and 72.7% for pCDNA3.1 empty vector and EGFP plasmid, respectively (Figure 16). This is in stark contrast with 25.3% given by Lipofectamine LTX with PLUS™ reagent transfection for 24 h (Figure 10).

Despite Lipofectamine LTX with PLUS™ reagent giving an enhanced 3.9% transfection efficiency as compared to Transit-X2® reagent, the latter was chosen for the subsequent experiments due to less cell death incurred based on the flow cytometric data. Since 24 h transfection was most efficient and least inhibitory towards MDA-MB-

231 cell growth, it was chosen as the duration for subsequent transfections prior to G4-18 selection for both the cellular and molecular assays.

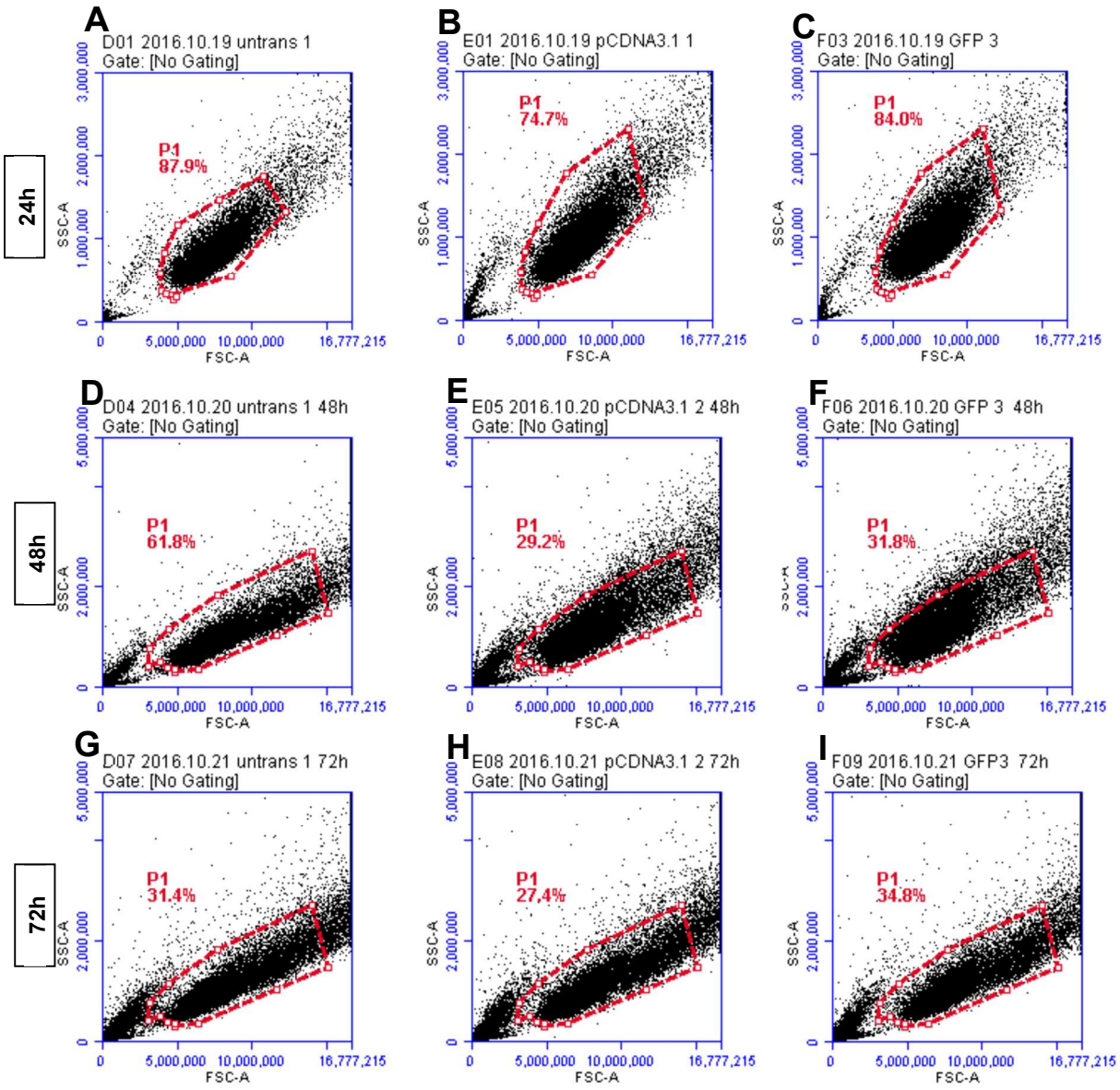


Figure 15 Untransfected MDA-MB-231 (A, D, G) and MDA-MB-231 cells transfected with pCDNA3.1 empty vector (B, E, H) and EGFP plasmid (C, F, I) using Transit-X2 reagent at 3µL:1µg plasmid for 24, 48 and 72 h. A minimum of 15,000 events were analyzed and the SSC-A-FSC-A plot was used to determine the percentage of live cells (P1 gate) in the sample

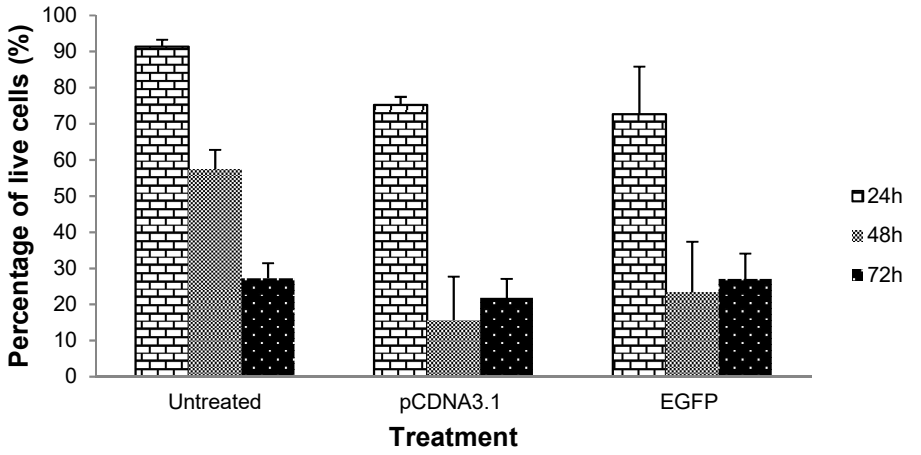


Figure 16 Untransfected MDA-MB-231 and MDA-MB-231 cells transfected with pCDNA3.1 empty vector and EGFP plasmid using Transit-X2 reagent at 3µL:1µg plasmid for 24, 48 and 72 h. A minimum of 15,000 events were analyzed and the SSC-A-FSC-A plot was used to determine the percentage of live cells (P1 gate) in the sample. Above is the bar chart representation of the live cell percentage of the respective samples. Data represents means ± standard deviations of triplicates from one independent experiment.

3.3.3 Selection of successful MDA-MB-231 transfectants using the Geneticin (G4-18) resistance selectable marker

Geneticin (G4-18) was added to the transfected MDA-MB-231 cells at 24 h post-transfection to select for successful transfectants expressing the gene, *CDH1*-GFP. On the 34th day post-selection, the percentage of transfected cells is 4.4% (Figure 17) which is similar to that obtained at 72 h post-transfection (Figure 12). However, further selection up to 104th day did not sustain the *CDH1*-GFP expressing population as the percentage of *CDH1*-GFP expressing cells dropped to 0.4% (Figure 17). Fluorescence images captured under the FITC channel also confirm that *CDH1*-GFP expression was sustained up till 29th day post-G4-18 selection (Figure 18).

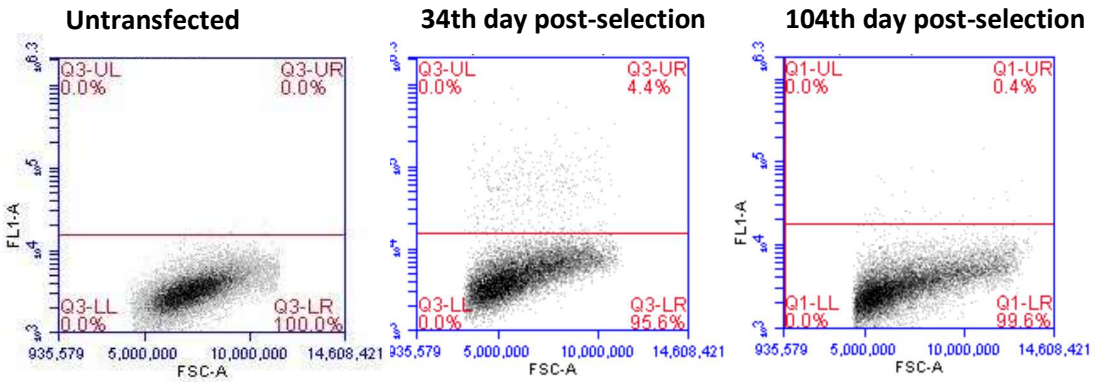


Figure 17 At 24 h post-transfection, 800µg/mL of Geneticin (G4-18) was added to select the *CDH1*-GFP-expressing cell population. A minimum of 10,000 events were analysed and the events falling above the gates shown (horizontal line) are taken as the *CDH1*-GFP-expressing cells.

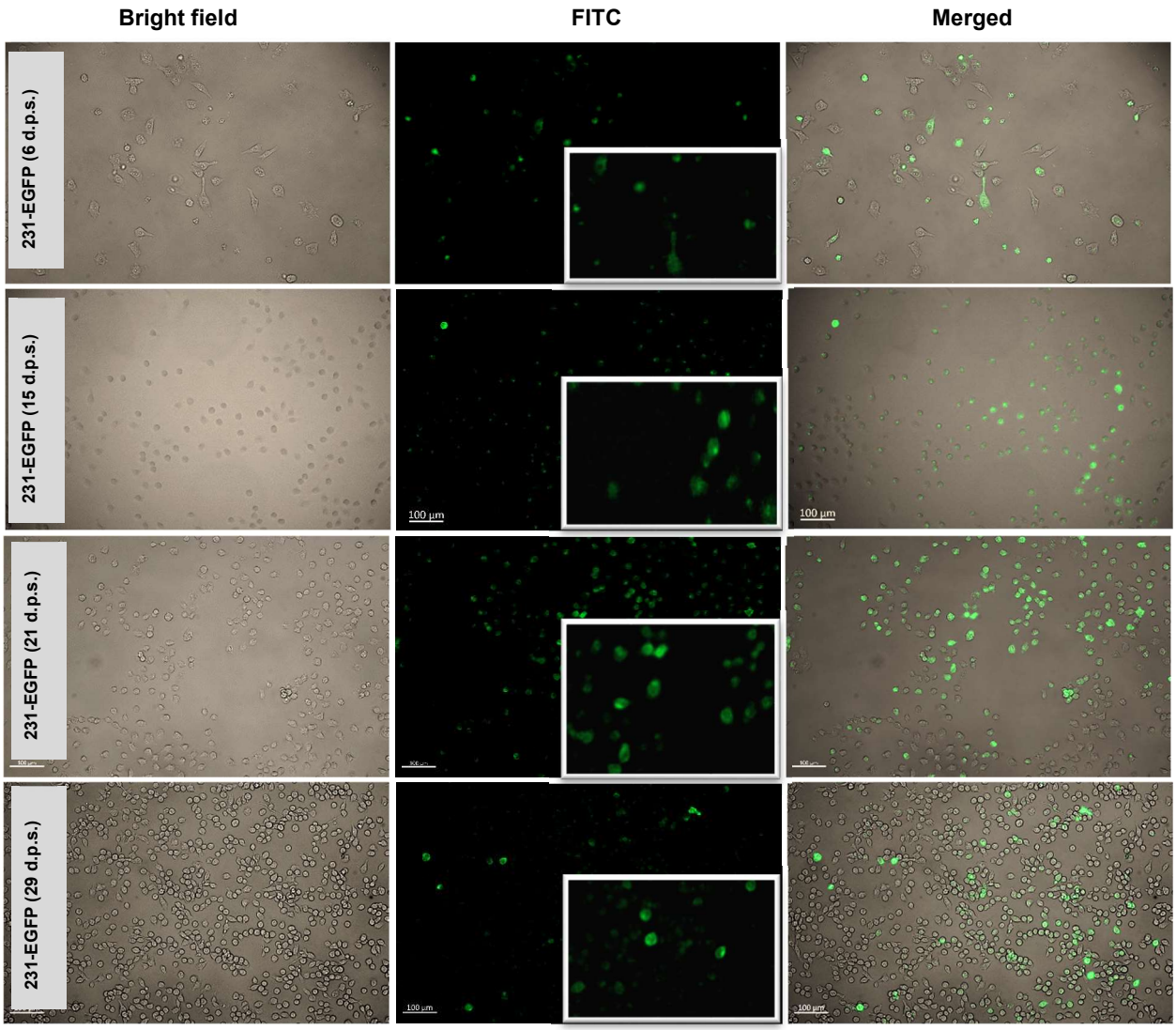


Figure 18 231-EGFP cells were captured for GFP fluorescence under the bright field and FITC channel of Axio observer 7 inverted fluorescence microcope (ZEISS, Germany) at the respective time points of 800 µg/mL G4-18 selection for 6, 15, 21 and 29 days post-selection (d.p.s.). Scale bars represent 100 µm. Insets are of the same photo at higher magnification for clearer view.

3.4 Discussion

3.4.1 Verification of E-cadherin-GFP plasmid integrity by restriction enzyme digestion and agarose gel electrophoresis

The EGFP plasmid is commercially available as *Escherichia coli* stab culture. After the recovery steps from *E. coli* single colony establishment, LB broth culture expansion to plasmid extraction from the dense *E. coli* LB culture, the quality of the plasmid had been confirmed with A_{260nm}:A_{280nm} ratio ranging from 1.8 - 2.0 (Kim *et al.*, 1997).The concentration of the eluted EGFP plasmid solution ranged from 600 - 900 ng/µL. Based on the plasmid sequence map (Appendix A), there is a *Bam*HI and *Xba*I restriction enzyme recognition sequence at 5159 bp and 2521 bp, respectively. After digestion with *Bam*HI and *Xba*I restriction enzymes, the plasmid should yield a backbone sequence of 6259 bp and a shorter spanning sequence between the two restriction sites of 2638 bp (Figure 19).

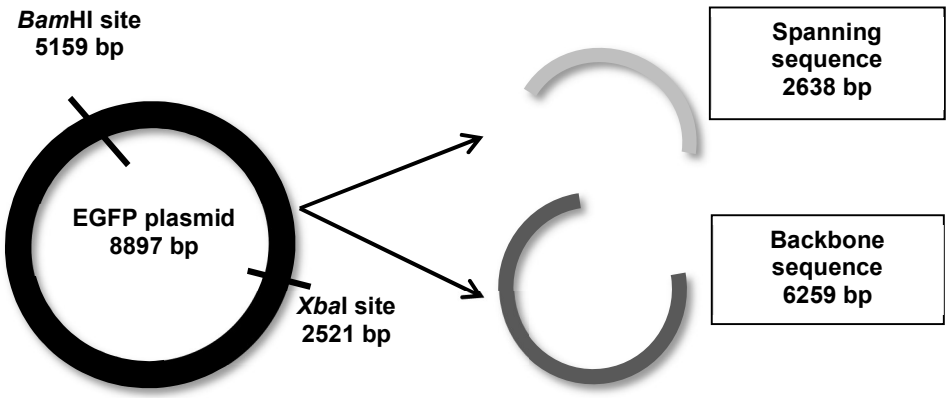


Figure 19 EGFP plasmid was digested using *Bam*HI-HF® *and Xba*I restriction enzymes (New England BioLabs®). After digestion, the theoretically expected band sizes of backbone sequence (6259 bp) and (2638 bp) were obtained as shown in Figure 5.

3.4.2 Transfection of MDA-MB-231 cells with EGFP plasmid and pCDNA3.1 empty vector

There are various methods of gene delivery into mammalian cells. One of them is harnessing the positively charged liposomes in delivering gene of interest into mammalian host cell. Despite being inferior in terms of transduction efficiency, cationic liposomes are seen as attractive non-viral vector alternative to viral vector which are less or non-immunogenic and are mostly not restricted by the size of the gene to be delivered (Mady, 2011). As both the DNA and plasma membrane are negatively charged, cationic liposomes serve well as a mediator to mask the negative charge of DNA by binding to them, forming DNA-lipid complexes. These DNA-lipid complexes then, with the help of neutral helper lipids, bind and fuse with the plasma membrane for gene delivery and efficient escape from endosomal destabilization (Balaz and Godbey, 2011). Lipofectamine® LTX used in this study is a cationic polysome commercially available which are widely used in gene delivery into various mammalian cell lines (Kosaka *et al.*, 2013; Park *et al.*, 2013; Pribic and Brazill, 2012).

After transfection, both the non-transfected control and transfected samples were assayed for the transgene *CDH1* expression using the GFP reporter protein tagged to it at the carboxyl terminal. This is to examine the transfection efficiency. From the qPCR results, there was an increase in the *CDH1*-GFP mRNA expression level with the increase of Lipofectamine LTX reagent concentration from 2% (v/v) (untransfected) to 4% (v/v) while there is no expression in the non-transfected control. This indicates that the EGFP plasmid had successfully entered the nuclei of cells, accessing to its transcription machineries for mRNA production (Zuhorn *et al*, 2002). Since the highest relative expression of 214.26 compared to untransfected control was given by transfection at 4% (v/v) Lipofectamine LTX reagent (Figure 6), 4% (v/v) was chosen for the subsequent transfection experiments.

In addition, both the non-transfected control and transfected sample were also assayed for gene expression at the protein level. Based on the flow cytometric analysis of GFP fluorescence in the FL1-A (530/30 nm) channel, there is a 3.3-fold increase in the mean fluorescence unit (MFU) of FL1-A channel of the gated population of transfected cells at 48 h post-transfection as compared to the non-transfected control (Figure 8). However, the dot plot of FL1-A versus side scatter (SSC) shows only a small percentage of the cell population (11.5%) shifted away from the auto-fluorescence region. This shows that transfection was successful but not efficient as most of the cell population (88.5%) did not express GFP fluorescence above that of the threshold gate (Figure 7D, 7E and 7F). The less efficient transfection can be a result of multiple factors. One of them is insufficient amount of DNA added to each well but the recommended amount had been added. Another factor is the mass ratio of DNA:lipofectamine, which had been recommended to range 1:2 to 1:3 (Dalby *et al.*, 2004). However, a 1:1 ratio had been employed in this study based on the recommended ratio provided from the manufacturer (Life Technologies).

In addition, at 72 h post-transfection, the MFU of the gated 20,000 cell population declined sharply to the level of auto-fluorescence (Figure 8). There was also no remarkable shift of cell population to the region above the threshold gate of auto-fluorescence (Figure 7G, 7H and 7I). Therefore, the result shows that although the transfection was successful and mediated transgene *CDH1*-GFP expression up to the transcriptional level, the transgene could have been silenced in the post-transcriptional route which affected the protein synthesis machineries while not affecting the mRNA level (Bartel, 2004; Kim *et al.*, 2004a).

Reports have revealed that many miRNAs govern breast cancer invasiveness. For instance, miR-9 and miR-92a targets the 3'-untranslated region region (3'-UTR) of *CDH1*, thereby repressing its translation elongation or termination in this case (Chen *et al.*, 2011; Ma *et al.*, 2010). This is further supported by the

fact that when the miRNAs bind with imperfect match to the 3'UTR of an exogenously expressed gene, the gene could be silenced by translational repression without mRNA degradation (Saxena *et al.*, 2003). Therefore, from the result presented above, it is speculated that at 24 h post-transfection, mRNA transcript of the *CDH1*-GFP had been produced. However, from 24 to 48 h, due to the proposed post-transcriptional miRNA-mediated translational repression of the transgene, a portion of the produced *CDH1*-GFP transcripts had progressed to complete the translation process, giving the rise in GFP fluorescence (MFU) at 48 h (Figure 7D, 7E and 7F) while most of them were inhibited at halfway through the translation process. In addition, the descent of GFP fluorescence at 72 h could be due to the short-lived nature of the *CDH1*-GFP which is subjected to protein clearance by the ubiquitin-proteasome pathway (Dantuma *et al.*, 2000; Hochstrasser, 1996; Mizushima *et al.*, 2002).

Despite Lipofectamie LTX reagent being the "gold standard" among chemical-based transfection reagents and giving high transfection efficiency by its ability to evade the entrapment and subsequent lysosomal degradation of its payload, DNA:lipid complexes, via its vesicles' random Brownian movement within the cytosol (Cardarelli *et al.*, 2016), it had induced pronounced toxicity in cells transfected with EGFP plasmid. The live cell percentages were 25.3%, 4.2% and 18.7% at 24 h (Figure 10), 48 and 72 h post-transfection, respectively (data not shown). This is in agreement with a comparative study done by another group investigating the toxicity induced by transfection using different transfection reagents. Lipofectamine LTX reagent was shown to significantly inhibit HeLa CCL-2 cell proliferation at the highest tested concentration of 0.1 µL per well and induced the expression of heat shock protein 70 (Hsp70) at 72 h post-transfection. These findings indicate that Lipofectamine LTX-mediated transfection had actually induced certain level of stress in the transfected cells (Antczak *et al.*, 2014). Nonetheless, our results showed earlier drastic cytotoxicity at 24 h post-transfection (Figure 9) and this might be explained by

the 5-fold higher concentration of the Lipofectamine LTX reagent used at 2.5 mL per well.

Since Lipofectamine LTX reagent is not the ideal option in this study due to its strong inhibition on MDA-MB-231 cell growth, *Trans*IT-X2® reagent was tested out in delivering both pCDNA3.1 empty vector and EGFP plasmid into MDA-MB-231 cells. *Trans*IT-X2® was chosen as the alternative transfection reagent as it is claimed by the manufacturer as a non-lipid based polymeric system that efficiently delivers both DNA and RNA out of endosomes, overcoming the critical nucleic acid delivery barrier while being of minimal toxicity to cells. Optimization findings from transfection using 3 µL *Trans*IT-X2® reagent per 1 µg of plasmid DNA showed that MDA-MB-231 cells transfected for 24 h maintained the live cell percentages of 75.2% and 72.7% for pCDNA3.1 empty vector and EGFP plasmid, respectively. However, the live cell percentage decreased up to 80% as the transfection duration increased to 48 and 72 h (Figure 15). Thus, transfection condition of 3 µL *Trans*IT-X2® reagent per 1 µg of plasmid DNA for 24 h was chosen for the subsequent transfection steps.

In order to obtain MDA-MB-231 cell line which stably express the *CDH1*-GFP gene to be used for the subsequent drug treatment, cellular and molecular assays, the Geneticin resistance was used as the selectable marker (Appendix A). With regards to G4-18 selection for transfectants harbouring the *CDH1*-GFP gene expression, the *CDH1*-GFP expressing population could only be sustained up to approximately a month's time (Figure 17, Figure 18). The finding that the *CDH1*-GFP expressing population dropped to 0.4% on the 104th day post-selection (approximately 3 months' time) (Figure 17) shows that the earlier speculation of post-transcriptional and translational silencing of the transgene might be valid.

3.5 Conclusion

The non-viral, chemical-based transfection method was chosen to deliver the *CDH1*-GFP gene into MDA-MB-231 cells due to its low cytotoxicity and better versatility. Lipofectamine LTX reagent gave an 11.5% of transfection efficiency while *Trans*IT-X2® reagent produced only 7.6% of transfection efficiency. Although Lipofectamine LTX reagent was superior in terms of transfection efficiency, *Trans*IT-X2® reagent was opted due to the much less cytotoxicity induced on the transfected MDA-MB-231 cells. Due to MDA-MB-231 cells carrying miRNAs which might contribute to the *CDH1*-GFP transgene silencing despite successful gene delivery into the cells, the low *CDH1*-GFP expressing MDA-MB-231 cell population could only be maintained under G4-18 selection for up to a month's time possibly because the expression was transient. Therefore, after transfection, selection and expansion of *CDH1*-GFP expressing MDA-MB-231 cell population, all following cellular and molecular assays will be conducted within a month before another transfection of delivering the gene *CDH1*-GFP into MDA-MB-231 cells is performed and followed by the cellular and molecular assays.

4. The assessment of the treatment effect of Trichostatin A (TSA) and Zebularine (Zeb) followed by Tumour Necrosis Factor-related Apoptosis-inducing Ligand (TRAIL) on human breast adenocarcinoma cells viability, cell cycle progression and invasiveness

4.1 Introduction

Tumour Necrosis Factor-related Apoptosis-inducing Ligand (TRAIL) is a promising anti-neoplastic agent produced by our very own immune system. It is a ligand which serves as an immunosurveillant protein targeted against transformed and malignant cells. Due to the multiple redundant pathways that make up the TRAIL resistance defence in normal, healthy cells (van Dijk *et al.*, 2013), healthy cells are safeguarded from the apoptosis-induction by TRAIL, making TRAIL a very unique anti-cancer candidate as compared to other standard chemotherapeutic drugs which are harmful to other healthy cells in the body. Nonetheless, before TRAIL can be widely used as a useful targeted drug against breast cancer, TRAIL resistance in breast cancer had to first be resolved.

The epigenetic drugs Trichostatin A (TSA) and Zebularine (Zeb) have individually shown synergism with TRAIL in enhancing the apoptosis-inducing effect TRAIL had on breast cancer cells. TSA was shown to upregulate the expression of TRAIL receptors, TRAIL-R1 and –R2 while Zebularine increased TRAIL sensitivity in breast cancer cells by increasing the fucosylation of the TRAIL receptors whereby it correlates with TRAIL sensitivity (Moriwaki *et al.*, 2010; Singh *et al.*, 2005). However, how these two drugs work together with the same aim of synergism with TRAIL is worth investigating.

On the other hand, E-cadherin had been extensively studied on its dysregulated expression linking to cancer cells invasiveness and metastatic potential while there is still lack in literature on how it regulates apoptosis in the anti-neoplastic feat. Literature had suggested that MDA-MB-231, despite being a TRAIL-sensitive human breast adenocarcinoma cell line, can develop TRAIL

resistance at sub-toxic TRAIL doses via endocytosis which progressively amasses TRAIL receptors from the plasma membrane, dampening the apoptosis signals transmitted via these receptors (Yoshida *et al.*, 2009; Zhang and Zhang, 2008). In this regard, E-cadherin was shown to physically associate with TRAIL receptors at the cell surface, coupling them to the actin cytoskeleton, thereby facilitating the enhanced assembly of death-inducing silencing complex (DISC) which leads to the culmination of cellular apoptosis (Lu *et al.*, 2014).Therefore, it is interesting to inspect on the potential of TSA and Zeb working towards enhanced TRAIL sensitivity with the expression of *CDH1*.

With the outcome of Chapter 1, *CDH1*-re-expressed MDA-MB-231 cells (231-EGFP) will serve as the raw material for this chapter. Cellular assays assessing the cell viability, cell proliferation, cell cycle distribution as well as cell migration shall be investigated on 231-EGFP as well as MDA-MB-231 and MDA-MB-231 transfected with pCDNA3.1 empty vector (231-EV). RT-PCR assessment of mRNA expression of genes regulating cell cycle progression (Proliferating Cell Nuclear Antigen, PCNA and Cyclin-dependent Kinase 2, CDK2) and cell invasiveness (Matrix metalloproteinase 9, MMP-9) will also be carried out.

The research objectives were as follow:

- To obtain the TSA and Zeb combined treatment (TZ) cell viability curve of MDA-MB-231 for the time points of 24, 48 and 72 h;
- To assess the best inhibitory concentration (IC) of TZ treatment based on the reduction in cell viability obtained by TSA and Zeb combined treatment followed by TRAIL (TZT);
- To use the chosen IC in the MTT cell viability assay of MDA-MB-231, 231-EV, 231-EGFP, MCF-7 and MCF10A in testing the six experimental treatment groups of untreated control, single TSA, single Zeb, TZ, single TRAIL and TZT treatment for the time points of 24, 48 and 72 h;

- To assess the effect of the six experimental treatment groups on the cell cycle distribution of MDA-MB-231, 231-EV, 231-EGFP, MCF-7 and MCF10A via ethanol fixing, propidium iodide (PI) staining and flow cytometry;
- To assess the effect of the six experimental treatment groups on the cell migration rate of MDA-MB-231, 231-EV and 231-EGFP via the wound healing assay;
- To assess the mRNA expression of genes regulating cell cycle progression (PCNA and CDK2) and cell invasiveness (MMP-9).

4.2 Materials and method

4.2.1 Cell Culture Maintenance

Human breast adenocarcinoma cell line, MDA-MB-231, MDA-MB-231 transfected with pCDNA3.1(+) (#2903) (231-EV) and E-cadherin-Green Fluorescent Protein (EGFP) plasmid, a gift from Jennifer Stow (Addgene plasmid #28009) (231-EGFP) were maintained as reported in Chapter 3. MCF-7 was maintained on culture with Dulbecco's Modified Eagle Medium (DMEM) (Corning, U.S.A.) supplemented with 10% (v/v) of fetal bovine serum (FBS) (Gibco Life Technologies, U.S.A.) and 1% (v/v) penicillin-streptomycin (Gibco Life Technologies, U.S.A.) at 37˚C and 5% CO_2, 95% O_2 atmosphere. The non-tumourigenic human breast epithelial cell line, MCF10A, was maintained by DMEM/F-12 (Corning, U.S.A.) supplemented with 5% equine serum (RMBIO, U.K.), 20 ng/mL epidermal growth factor (EGF) (Sigma-Aldrich, U.S.A.), 0.5 µg/mL hydrocortisone (Nacalai Tesque, Japan), 10 µg/mL insulin and 1% (v/v) penicillin-streptomycin at the same physical condition as above. For experimental assays on MCF10A, the DMEM/F-12 medium was supplemented with all the aforementioned components except epidermal growth factor.

4.2.2 3-(4,5-Dimethylthiazol-2-yl)-2,5-Diphenyltetrazolium Bromide (MTT) Cell Viability Assay

MDA-MB-231 cells were seeded at 5×10^4 cells per well in 96-well plate. At 24 h post-seeding, cells were treated with Trichostatin A (12.5, 25, 50, 100, 200 nM TSA) and Zebularine (1, 2, 4, 6, 8, 10 µM Zeb) at all possible combination of concentrations for 24, 48 and 72 h. At the respective post-treatment time-point, medium was removed from each well and the wells were washed with 100 µL of 1× PBS. MTT solution (1 mg/ml) was added at 100 µL per well. After 4 h of incubation at 37˚C, MTT solution was removed and 150 µL of dimethyl sulfoxide was added to each well to dissolve the purple formazan crystals formed by MTT reduction. The absorbance values at 570 nm and 630 nm were measured. The normalized absorbance value is taken from the formula A_{570} –

A_{630}. The percentage of cell viability compared to untreated control was calculated as follows:

$$\frac{\text{Normalized absorbance value (treated)}}{\text{Normalized absorbance value (untreated)}} \times 100\%$$

The IC_{25} of TSA and Zeb combination was obtained from the cell viability graph obtained from this assay. The IC_{25} of single TSA and single Zeb were obtained from previous optimization results. The experimental treatment groups of (i) untreated, (ii) IC_{25} TSA (TSA), (iii) IC_{25} Zeb (Zeb), (iv) IC_{25} TSA and Zeb (TZ), (v) 50 ng/μL TRAIL (TRAIL) treatment for 24, 48 and 72 h and (vi) IC_{25} TSA and Zeb for 12 h followed by 50 ng/μL TRAIL (TZT) treatment for 24, 48 and 72 h were tested in terms of cytotoxicity on MDA-MB-231, 231-EV, 231-EGFP, MCF-7, and non-tumourigenic human breast epithelial cell line, MCF10A.

4.2.3 Cell cycle analysis using ethanol fixing and propidium iodide DNA staining method

MDA-MB-231, 231-EV and 231-EGFP were seeded at 2.3 × 10^5 cells per well while MCF-7 and MCF10A were seeded at 3.25 × 10^5 cells per well of 6-well plate. The cells were treated with the indicated treatment groups as above. At 24, 48 and 72 h post-treatment, cells were trypsinized and harvested as pellet. The chilled ethanol [70% (v/v)] was added at 500 μL per sample tube and tubes were kept at -20˚C for a week for cell fixing. Subsequently, the cell pellet was harvested again via centrifugation at 2000 rpm for 5 min. After the supernatant had been removed, the propidium iodide (PI) staining solution (0.1% (v/v) Triton X-100 (Nacalai Tesque, Japan), 50 μg/ml PI (Sigma-Aldrich, U.S.A.) and 100 μg/mL DNase-free RNase A (Nacalai Tesque, Japan) in 1× PBS) was added at 500 μL per sample to stain the cellular DNA. After incubation at room temperature for at least 30 min, the cellular DNA content was assessed using the FL-2 channel of the BD Accuri C6 flow cytometer (BD Biosciences, U.S.A.) At least 10,000 events were recorded per sample. The percentage distribution

of cells across the cell cycle phades of G0/G1, S and G2/M were quantified using the ModFit LTTM software (Verity Software House, U.S.A.).

4.2.4 Wound healing assay (scratch assay)

MDA-MB-231, 231-EV, and 231-EGFP were seeded at 1 × 10^5 cells per well of 24-well plate to form a confluent monolayer. Thereafter, the cell monolayer was wounded with a p200 tip at consistent pressure and pipette tip angle to keep the wound consistent (Jonkman *et al*., 2014). The scratch edge was smoothened by washing of cells once with 1 mL of 1× PBS. Untreated wells were added with DMEM with 10% (v/v) FBS while treated wells were added with the indicated treatment groups as above. Microscope images were captured after incubation at 37˚C for 0, 3, 6, 12 and 24 h. The area of the gap formed by the scratch was quantified using ImageJ and statistically analysed.

4.2.5 RT-PCR assessment of mRNA expression of proliferating cell nuclear antigen (PCNA), cyclin-dependent kinase-2 (CDK2) and matrix metalloproteinase 9 (MMP9)

At 24 and 48 h after the indicated treatments as above, total RNA was extracted from MDA-MB-231, 231-EGFP and MCF-7. The total RNA was subjected to qualitative and quantitative assessments using the ratios of A_{260}/A_{280} and A_{260}/A_{230} with 1.8 – 2.0 as the range of good RNA quality. The total RNA of good quality was then subjected to RQ1 RNase-free DNase I (M6101) (Promega, U.S.A.) treatment to remove any trace of genomic DNA contamination. The DNase I-treated RNA was converted to cDNA via the First Strand cDNA Synthesis Kit using ProtoScript II Reverse Transcriptase (M0368) (New England Biolabs, U.S.A.). Subsequently, the synthesized first strand cDNA was then subjected to PCR amplification using the PCR reagents kit (Bioline, U.S.A.) with primers targeting proliferating cell nuclear antigen (PCNA), cyclin-dependent kinase-2 (CDK2), matrix metalloproteinase 9 (MMP9) and the housekeeping beta-actin (β-actin) gene. The primer sequences are as follows:

Gene	Primer sequence
PCNA	**Forward:** 5'-CCATCCTCAAGAAGGTGTTGG-3' **Reverse:** 5'-GTGTCCCATATCCGCAATTTTAT-3'
CDK2	**Forward:** 5'-CATGAGGTGGTGACCCTGTG-3' **Reverse:** 5'-CAAATAGCCCAAGGCCAAGC-3'
MMP9	**Forward:** 5'-GATGCGTGGAGAGTCGAAAT-3' **Reverse:** 5'-CACCAAACTGGATGACGATG-3'
β-actin	**Forward:** 5'-AGAGCTACGAGCTGCCTGAC-3' **Reverse:** 5'-AGCACTGTGTTGGCGTACAG-3'

The PCR condition was 94˚C for 2 min, 35 cycles of 94˚C for 30 s, 55˚C for 20 s and 72˚C for 20 s, and 72˚C for 5 min. The respective PCR amplicons were subjected to 1% agarose gel electrophoresis and visualized using SyBr safe staining. Gel image of targeted band was captured using the Bio-Rad GelDoc Imager (Bio-Rad, U.S.A.).

4.3 Results

4.3.1 MTT cell viability assay screening of inhibitory concentrations (ICs) of TSA and Zeb combined treatment on MDA-MB-231

Based on the results from MTT cell viability assay after the combined treatment of Trichostatin A (TSA) and Zebularine (Zeb), dose reduction was achieved for both drugs. IC_{25} of TSA when in combination with Zeb was halved from 25 nM (Appendix C) to 12.5 nM (Figure 20) for 24 h treatment. However, IC_{25} of TSA when in combination with Zeb in treating MDA-MB-231 cells increased to 25 nM at the 72 h time-point (Figure 22). On the other hand, dose reduction of Zeb was slightly less as the IC_{25} of Zeb was only reduced from 4.75 µM (Appendix D) to 4 µM at the 24 h time-point (Figure 20). High concentrations of TSA and Zeb starting from 200 nM TSA and 4 µM Zeb gave significantly ($P<0.05$) decreased cell viability compared to the untreated MDA-MB-231 as early as 24 h post-treatment (Figure 20) and progressively gave very significantly ($P<0.001$) lower cell viability compared to untreated control at 72 h post-treatment (Figure 22).

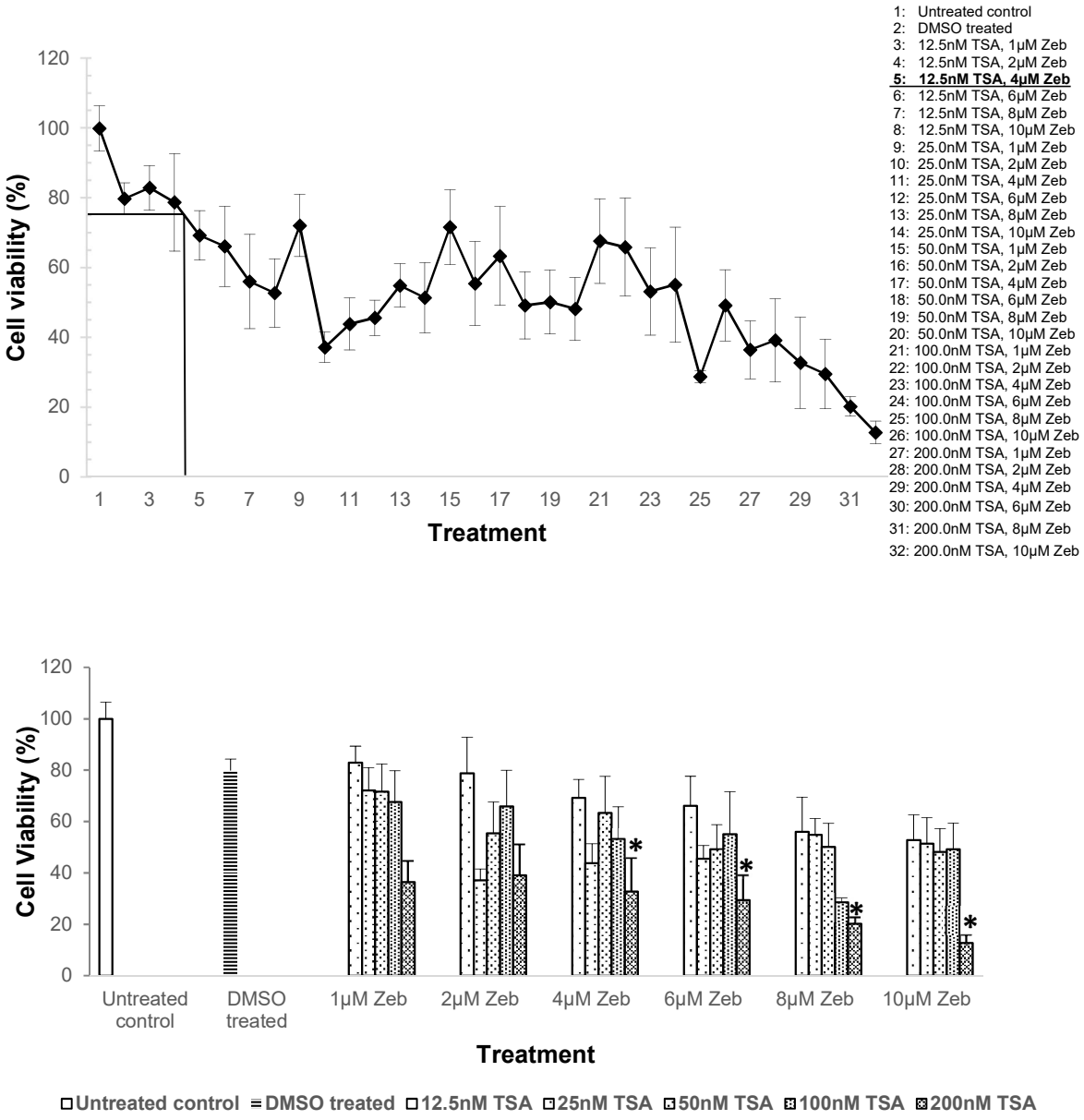


Figure 20 MTT cell viability data of all combinations of TSA (12.5, 25, 50, 100, 200nM TSA) and Zebularine (1, 2, 4, 6, 8, 10μM) concentrations. IC_{25} of TSA and Zeb combined treatment on MDA-MB-231 for **24 h** was determined from the data. The same data is presented as line graph (above) and bar chart (below) representation. Means are from triplicate values of at least three independent experiments. Error bars represent SEM.

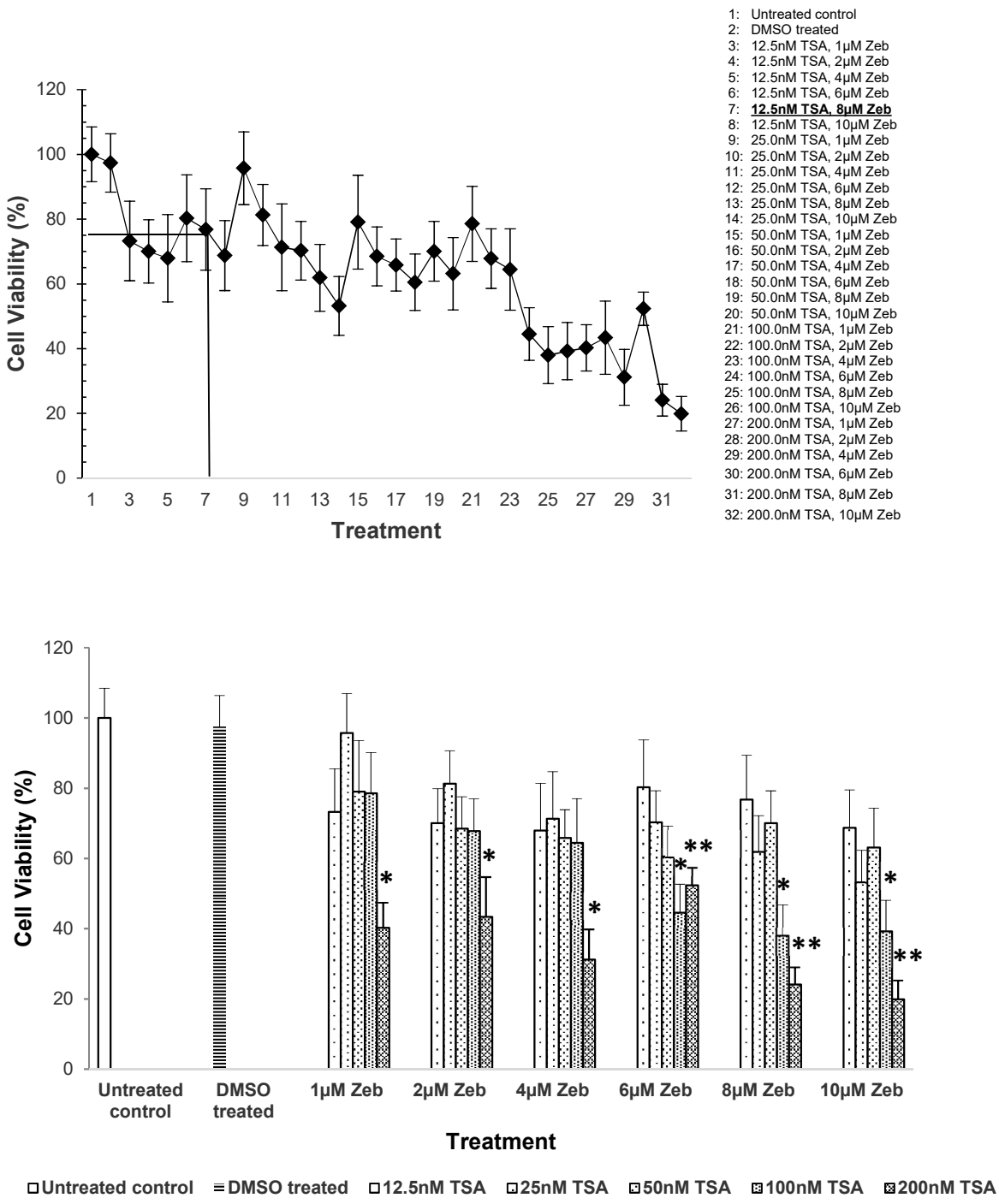


Figure 21 MTT cell viability data of all combinations of TSA (12.5, 25, 50, 100, 200nM TSA) and Zebularine (1, 2, 4, 6, 8, 10μM) concentrations. IC_{25} of TSA and Zeb combined treatment on MDA-MB-231 for **48 h** was determined from the data. The same data is presented as line graph (above) and bar chart (below) representation. Data represents means ± SEM of three independent experiments of triplicates.

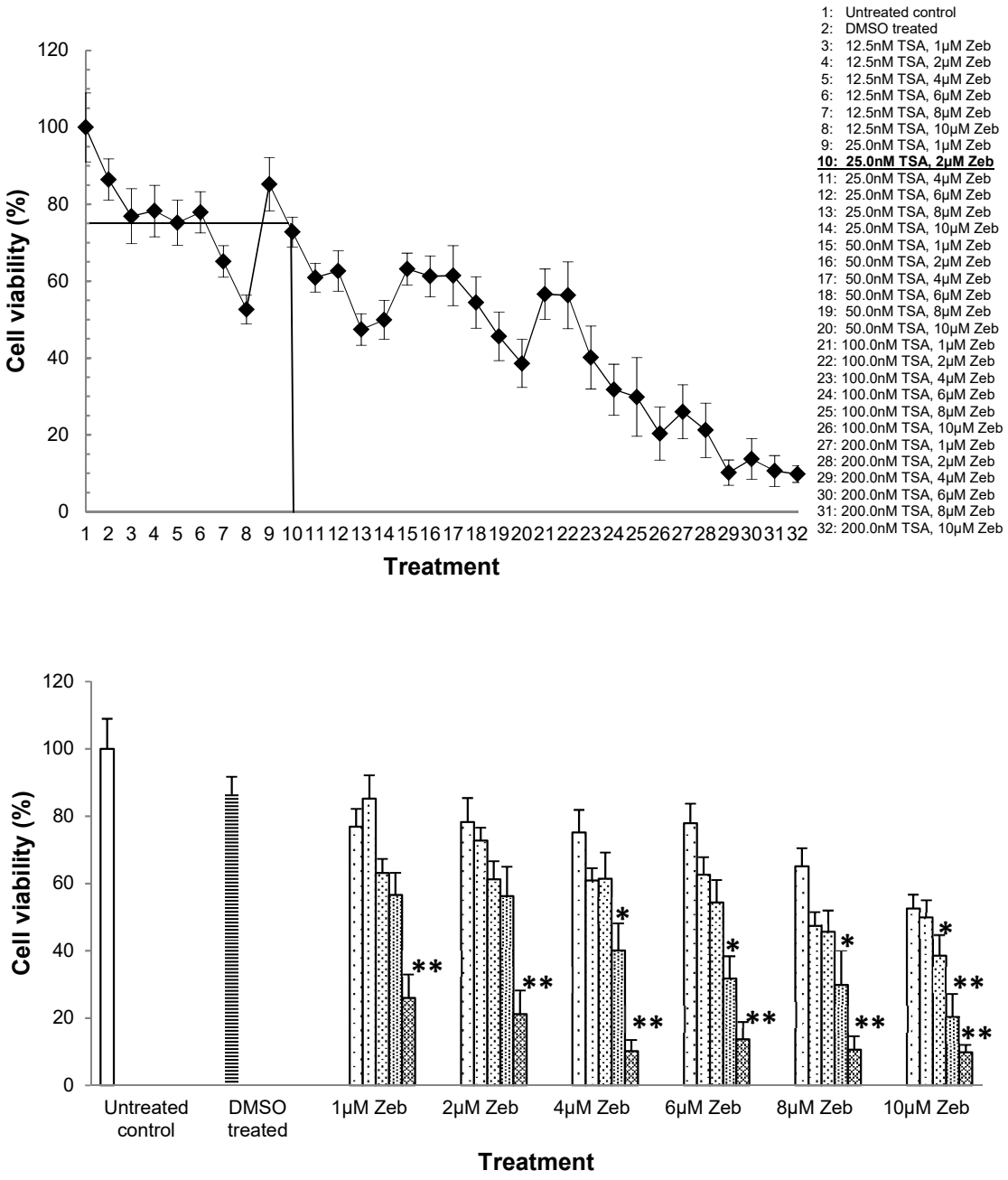


Figure 22 MTT cell viability data of all combinations of TSA (12.5, 25, 50, 100, 200nM TSA) and Zebularine (1, 2, 4, 6, 8, 10μM) concentrations. IC_{25} of TSA and Zeb combined treatment on **MDA-MB-231 for 72 h** was determined from the data. The same data is presented as line graph (above) and bar chart (below) representation. IC_{25} of TSA and Zebularine combination was determined as shown in the line graph (black line). The IC_{25} is bolded and underlined in the legend. Data represents means ± SEM of three independent experiments of triplicates.

4.3.2 MTT cell viability assay on IC selection for consecutive treatment with TRAIL

From the IC screening test of TSA and Zeb (TZ) combinations, in order to select an optimal sub-toxic IC for the consecutive treatment with TRAIL, IC_{15}, IC_{20}, IC_{25}, and IC_{30} of TSA and Zeb combination which are 12.5 nM TSA and 1 μM, 2 μM, 4 μM, 6 μM Zeb, respectively were extracted from the cell viability curve of 24 h treatment (Figure 20) to perform the consecutive treatment with TRAIL. One Way ANOVA analysis and Tukey post-hoc test revealed that there is no significant differences ($P>0.05$) among the chosen ICs. Nonetheless, 12.5 nM TSA and 4 μM Zeb (IC_{25}) were chosen as this sub-toxic dose for TZ combination inhibited the 231-EGFP cell growth to the greatest extent, giving a post-treatment cell viability of 82.7% in contrast to 91.97%, 92.52% and 85.71% given by IC_{15}, IC_{20} and IC_{30}, respectively (Figure 23).

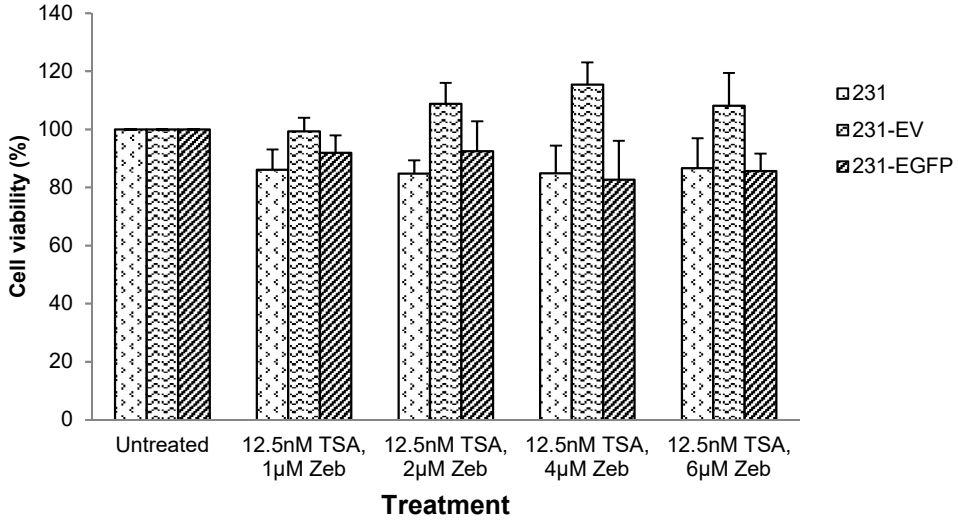


Figure 23 IC_{15} (12.5 nM TSA, 1 μM Zeb), IC_{20} (12.5 nM TSA, 2 μM Zeb), IC_{25} (12.5 nM TSA, 4 μM Zeb) and IC_{30} (12.5 nM TSA, 6 μM Zeb) of the Trichostatin A and Zebularine (TZ) combined treatment were chosen from the 24 h post-treatment cell viability curve of MDA-MB-231. These ICs were used to treat MDA-MB-231 (231) and geneticin selected MDA-MB-231 transfected with pCDNA3.1 empty vector (231-EV) and with E-cadherin-GFP plasmid (231-EGFP) for 12 h followed by TRAIL treatment for 24 h. Data represents means ± SEM of three independent experiments of triplicates.

4.3.3 TSA and Zeb sensitization along with E-cadherin expression enhanced TRAIL-induced cytotoxicity in 231-EGFP and MCF-7

As shown in Figure 24, all 6 treatment groups of IC_{25} TSA (TSA), IC_{25} Zeb (Zeb), IC_{25} TSA and Zeb combined (TZ), 50ng/mL TRAIL (TRAIL) and IC_{25} TSA and Zeb followed by 50 ng/mL TRAIL (TZT) did not yield significantly lower cell viability as compared to the untreated control of the respective cell lines, MDA-MB-231 and geneticin (G4-18) selected MDA-MB-231 transfected with pCDNA3.1 empty vector (231-EV) at 24 h time point. Nonetheless, MDA-MB-231 cells transfected with the EGFP plasmid harbouring the *CDH1*-GFP gene (231-EGFP) had significantly ($P<0.05$) reduced cell viability of 70.3% and 79% after both TZ and TRAIL treatment for 24 h. Furthermore, TZT had further reduced the cell viability to 62.12% ($P<0.001$) (Figure 24a). On the other hand, there was no significant reduction in cell viability of MCF-7 across the untreated and treatment groups at the 24 h time-point. However, TZT-treated MCF-7 had a cell viability of 66.13% which is similar to TZT-treated 231-EGFP which had a cell viability of 62.12% (Figure 24a). At 48 and 72 h post-treatment, both single TRAIL and TZT treatments did not yield significant reduction in all cell lines except MCF-7 in which the TZT and TRAIL treatment have significantly ($P<0.05$) inhibited its cell viability at 48 and 72 h, respectively (Figure 24b and 24c).

On the other hand, the epigenetic drug, TSA treatment significantly ($P<0.05$) reduced cell viability of MDA-MB-231 and 231-EV at 48 and 72 h post-treatment, respectively while both the single TSA and single Zeb treatment gave significant reduction of MCF-7 cell viability at 48 h post-treatment (Figure 24b and 24c). In addition, TZ treatment had significant effect in reducing cell viability of all cell lines at 72 h (Figure 24c).

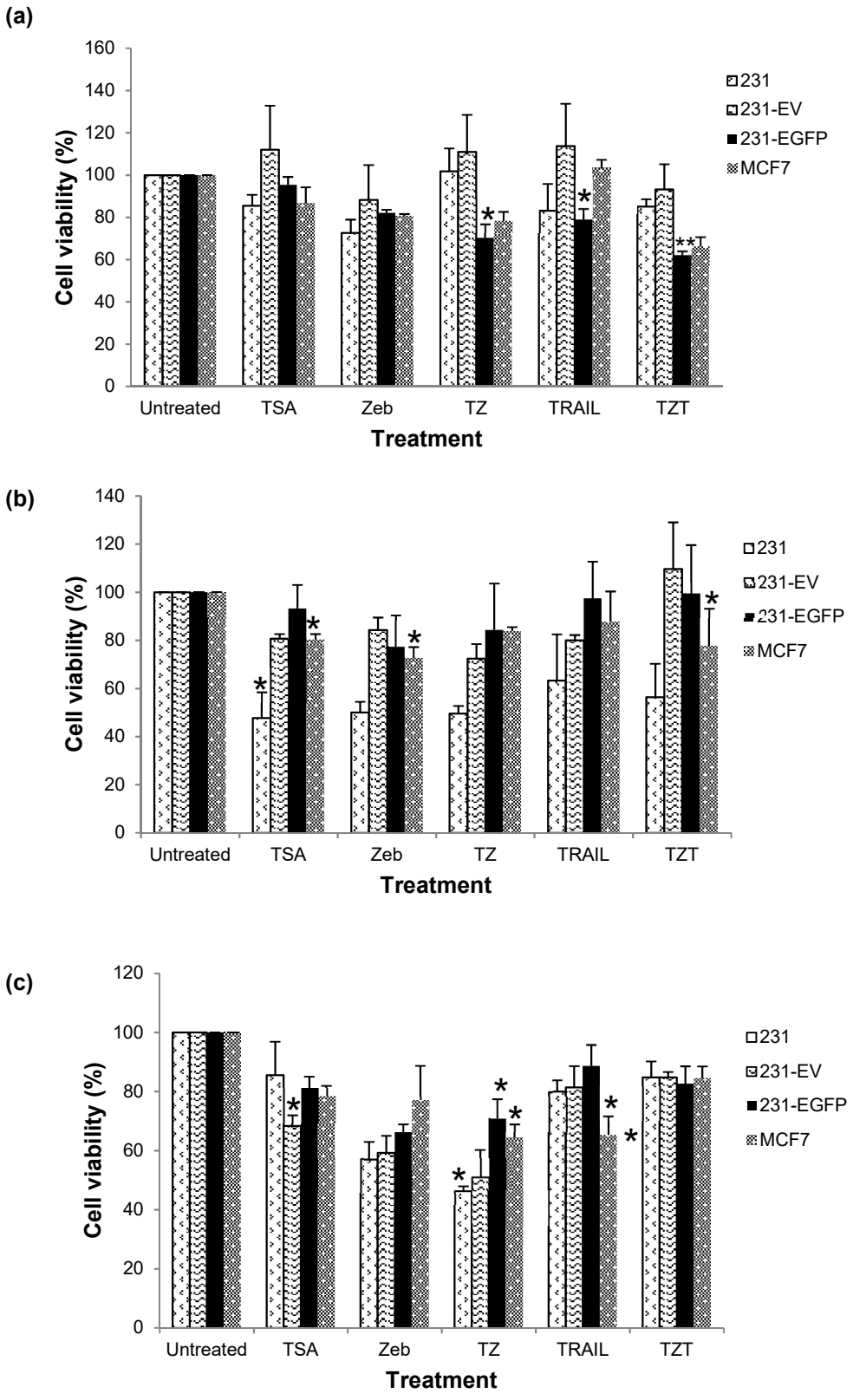
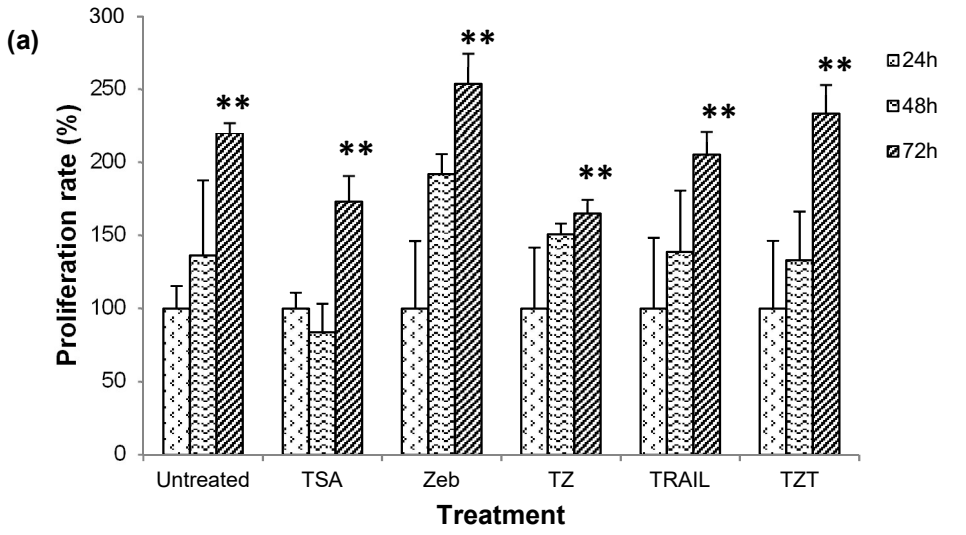


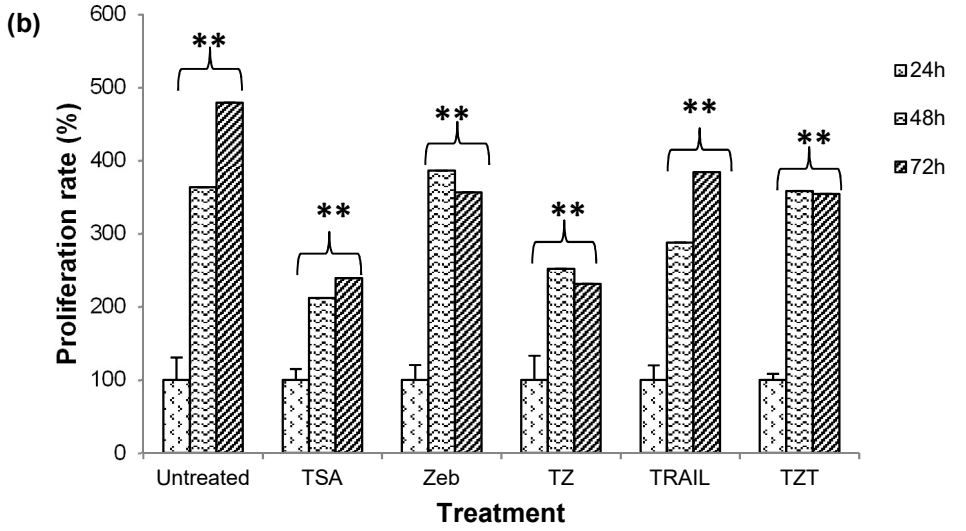
Figure 24 MTT cell viability data of different TSA, Zeb and TRAIL drug treatment groups on MDA-MB-231 (231), geneticin selected MDA-MB-231 transfected with pCDNA3.1 empty vector (231-EV) and with E-cadherin-GFP plasmid (231-EGFP) and MCF-7 for **(a) 24, (b) 48 and (c) 72 h**. All means are average of triplicate values from at least three independent experiments. Error bars represent SEM. One-Way ANOVA test was used to compare means of the different treatment groups. *(P<0.05) and **(P<0.001) are significant and very significant differences from untreated control.

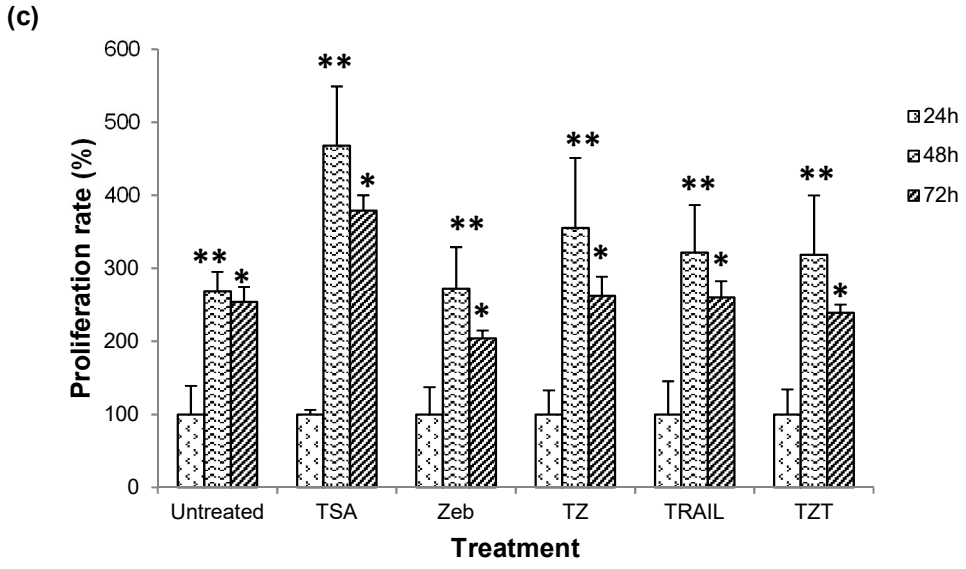
4.3.4 The effect of drug treatment on cell proliferation of MDA MB-231, 231-EV, 231-EGFP and MCF-7

In order to assess the effect of drug treatment on cell proliferation in the cell lines, the proliferation rate (%) was calculated with reference to the respective normalized absorbance values of MTT assay of each sample where 100% = no proliferation; < 100% = cell toxicity and >100% = proliferation. Figure 25a shows that the control MDA-MB-231 cells were highly proliferative with the proliferation rate significantly ($P<0.001$) higher at 72 h compared to that at 24 h across all treatment groups. In addition, 231-EV maintained significantly ($P<0.001$) higher proliferation rate at both 48 and 72 h post-treatment.

On the other hand, in 231-EGFP cells, there was an initial spike in proliferation rate across all experimental groups at 48 h. However, there was a significant ($P<0.05$) decrease in cell proliferation rate across all treatment groups from 48 to 72 h post-treatment (Figure 25c). With regards to MCF-7, the proliferation rate remained low but was significantly ($P<0.05$) increased at 72 h across all treatment groups (Figure 25d).


(a)
Proliferation rate (%)
300
250
200
150
100
50
0
**
24h
48h
72h
Untreated
TSA
Zeb
TZ
TRAIL
TZT
Treatment


(b)
Proliferation rate (%)
600
500
400
300
200
100
0
**
24h
48h
72h
Untreated
TSA
Zeb
TZ
TRAIL
TZT
Treatment


(c)
Proliferation rate (%)
600
500
400
300
200
100
0
**
*
24h
48h
72h
Untreated
TSA
Zeb
TZ
TRAIL
TZT
Treatment

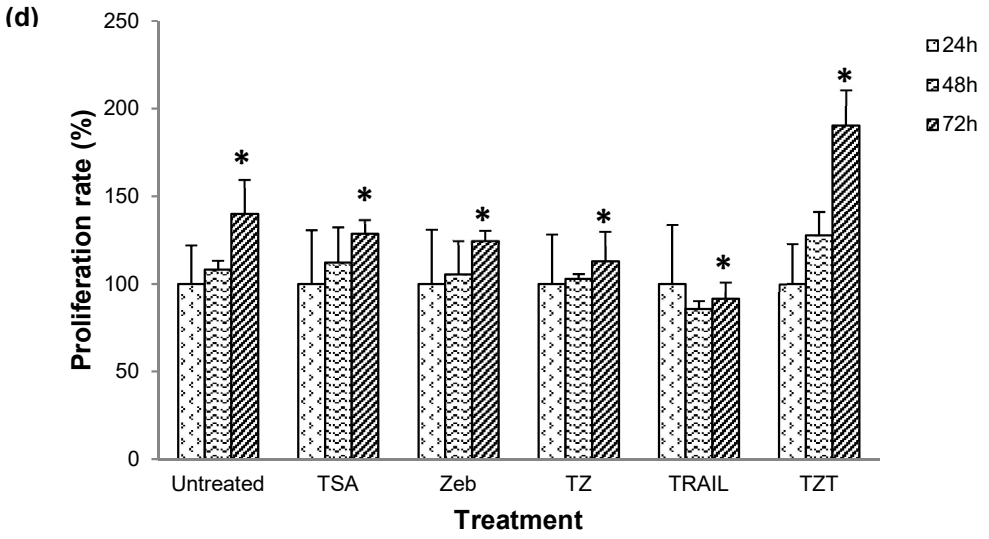


Figure 25 MTT proliferation data of different TSA, Zebularine and TRAIL drug treatment groups on (a) MDA-MB-231 (231) (b) geneticin selected MDA-MB-231 transfected with pCDNA3.1 empty vector (231-EV) and with (c) E-cadherin-GFP plasmid (231-EGFP) and (d) MCF7 for **24, 48** and **72 h**. All means are average of triplicate values from at least three independent experiments. Error bars represent SEM. One-Way ANOVA test was used to compare means of the different treatment groups. $^{**}(P<0.001)$ are very significant differences from 24 h mean proliferation rates while $*(P<0.05$ is significant differences from the mean proliferation rate at 48 h.

4.3.5 Minimal inhibitory effect of drug treatment on cell viability and cell proliferation of MCF10A

MCF10A is a non-tumourigenic human breast epithelial cell line used as a control in this study to assess the toxicity of the proposed treatment. As shown in Figure 26a, all treatment groups, TSA, Zeb, TZ, TRAIL and TZT have significantly ($P<0.05$) reduced the cell viability of MCF10A at 24 h post-treatment. However, the reduction of cell viability ranged only from 20% to 30% and there was no significant difference in the reduction of cell viability between all treatment groups. At 48 h post-treatment, there was no significant reduction in cell viability of MCF10A as induced by all treatment groups (Figure 26b).

There was no significant inhibition of cell proliferation for MCF10A except for the TRAIL treatment group (Figure 27).

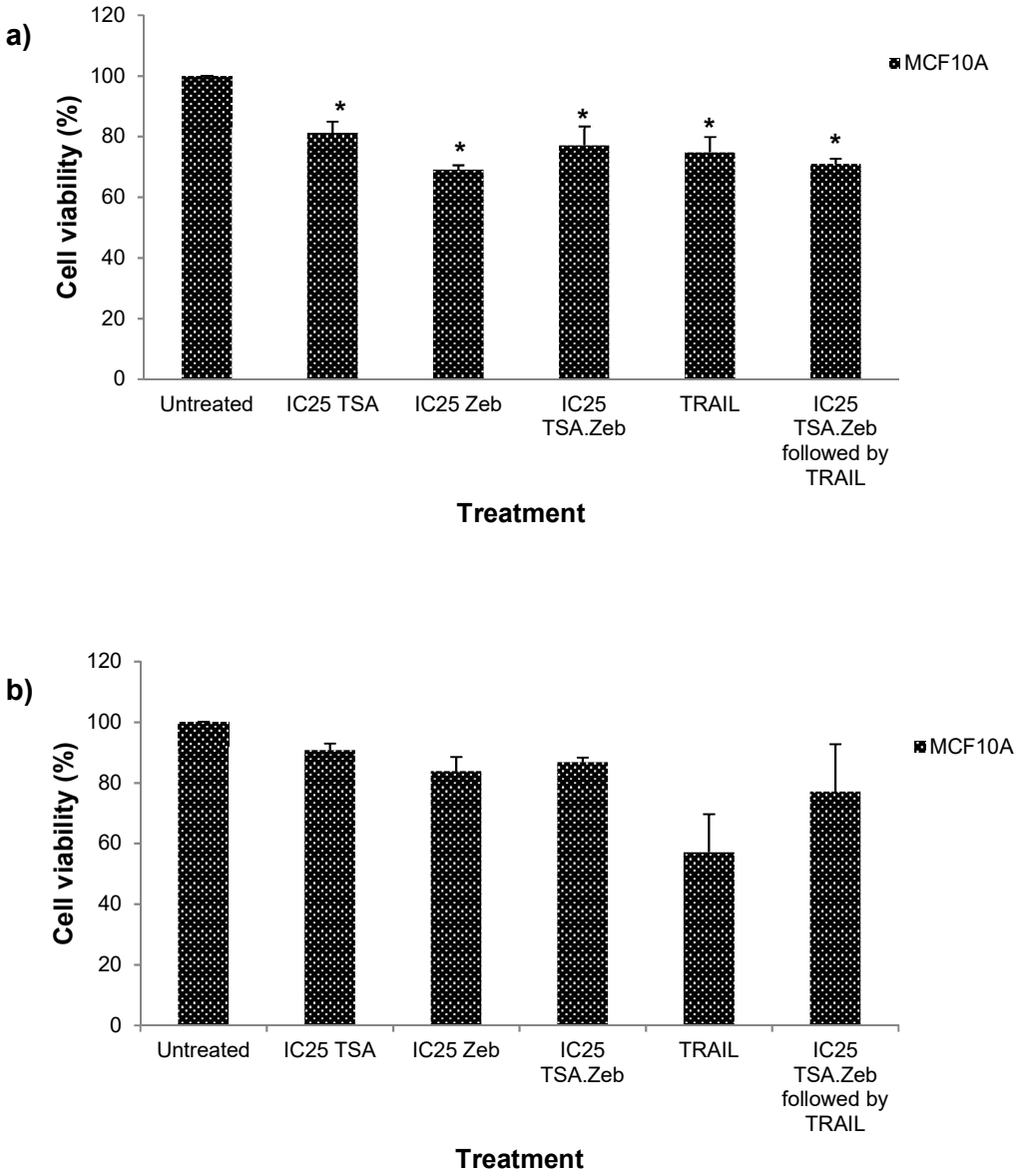


Figure 26 MTT cell viability data of different TSA, Zebularine and TRAIL drug treatment groups on MCF10A for (a) **24** and (b) **48 h**. Data represents means ± SEM of three independent experiments of triplicates. * represents significant ($P<0.05$) differences from the untreated control.

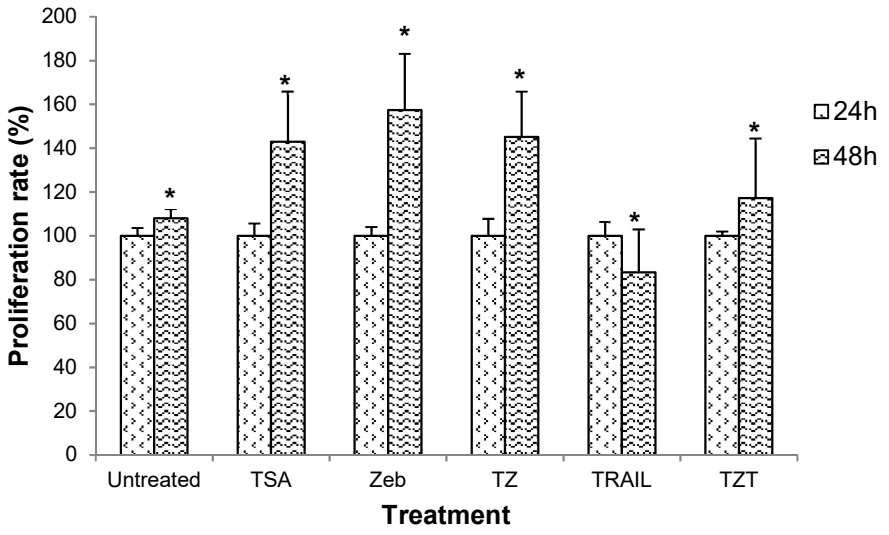


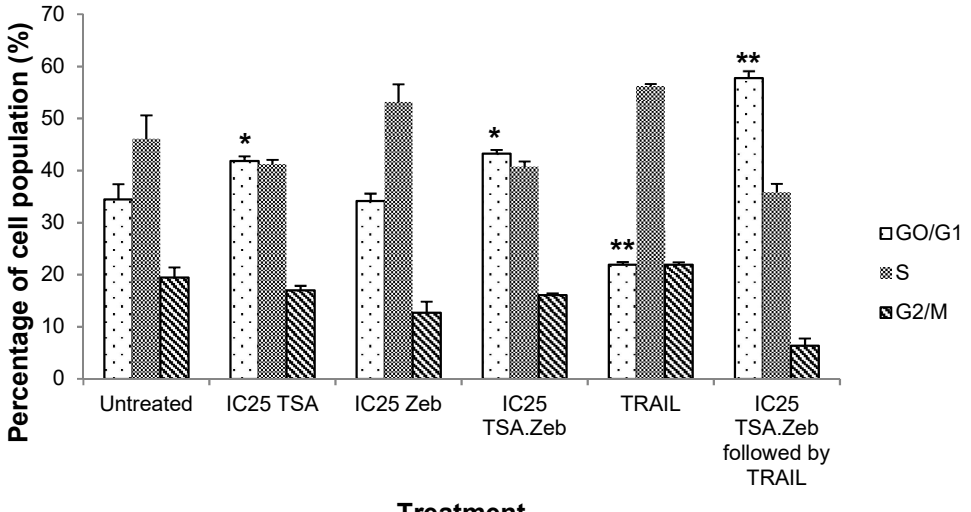
Figure 27 MTT proliferation data of different TSA, Zebularine and TRAIL drug treatment groups on (a) MCF10A and (b) MCF-7 for **24** and **48 h**. *($P<0.05$) are significant differences from 24 h mean proliferation rate based on independent sample T-test. Data represents means ± SEM are from three independent experiments of triplicates each.

4.3.6 TSA and Zeb sensitization along with E-cadherin expression increased TRAIL-induced cell cycle phade G_0/G_1 arrest in MDA-MB-231, 231-EGFP and MCF-7

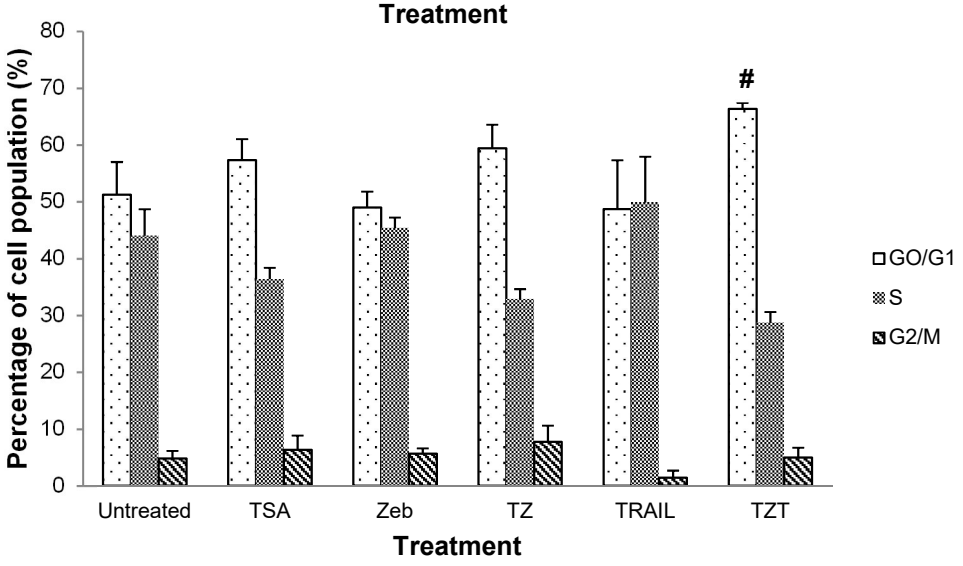
The favourable inhibition of MDA-MB-231 cell viability achieved by TZT treatment with the re-expression of E-cadherin had guided us to further analyze its anti-cancer effect in the aspect of cell cycle distribution. At 24 h post-treatment, TZT treatment had significantly ($P<0.001$) arrested 57.8% of MDA-MB-231 cells in the G0/G1 phade. TSA and TZ have arrested 41.8% ($P<0.05$) and 43.2% ($P<0.05$) of MDA-MB-231, respectively, in the G_0/G_1 phade (Figure 28a). Interestingly, both TRAIL and Zeb treatments have induced a significant ($P<0.05$) S-phade arrest in contrast with all the other treatments which induced G_0/G_1 arrest (Figure 28a). In addition, TZT treatment had also arrested 66.3% ($P<0.05$) of 231-EV in the G_0/G_1 phade, having similar trend with MDA-MB-231 (Figure 28b). On the other hand, with the re-expression of E-cadherin in 231-EGFP, a significant 74.2% ($P<0.05$) arrest of 231-EGFP at G_0/G_1 phade had been achieved by the TZT treatment (Figure 28c). With regards to MCF-7 which inherently expresses E-cadherin, both TZ and TZT have significantly ($P<0.05$) arrested 82% and 83.1% of MCF-7 cells in the G0/G1 phade while TRAIL alone did not increase the G_0/G_1 arrest appreciably from the untreated control (Figure 28d).

On the other hand, the G_0/G_1 percentage of MCF10A cell population was not significantly altered by any of the treatment groups (Figure 28e). The representative histograms of cellular DNA content distribution of MDA-MB-231 231-EV, 231-EGFP, MCF-7 and MCF10A across the G_1/G_0, S and G_2/M phades of cell cycle after each treatment group at 24 h post-treatment are presented in Appendices E, F, G, H and I, respectively.

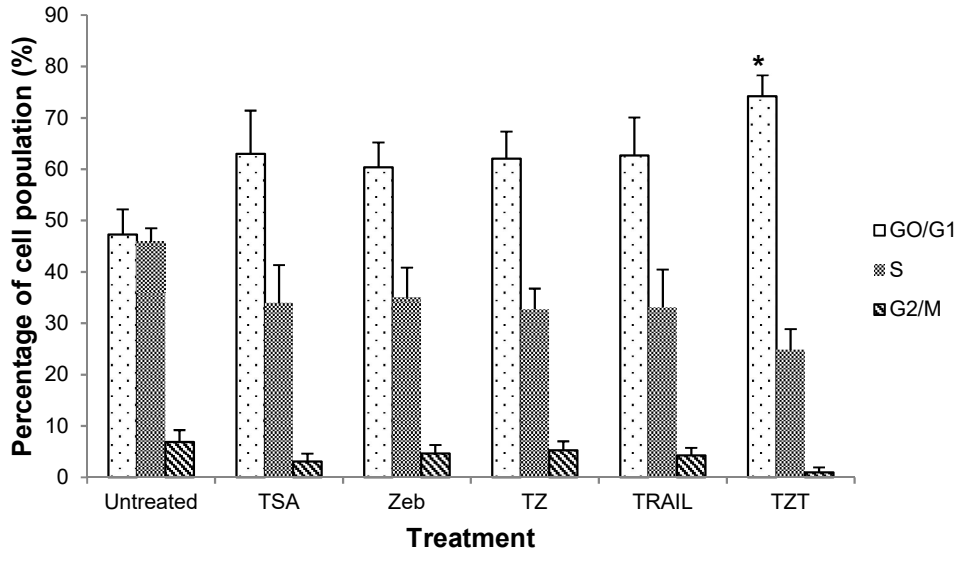
(a)


Percentage of cell population (%)
70
60
50
40
30
20
10
0
*
*
**
**
Untreated
IC25 TSA
IC25 Zeb
IC25 TSA.Zeb
TRAIL
IC25 TSA.Zeb followed by TRAIL
Treatment
GO/G1
S
G2/M

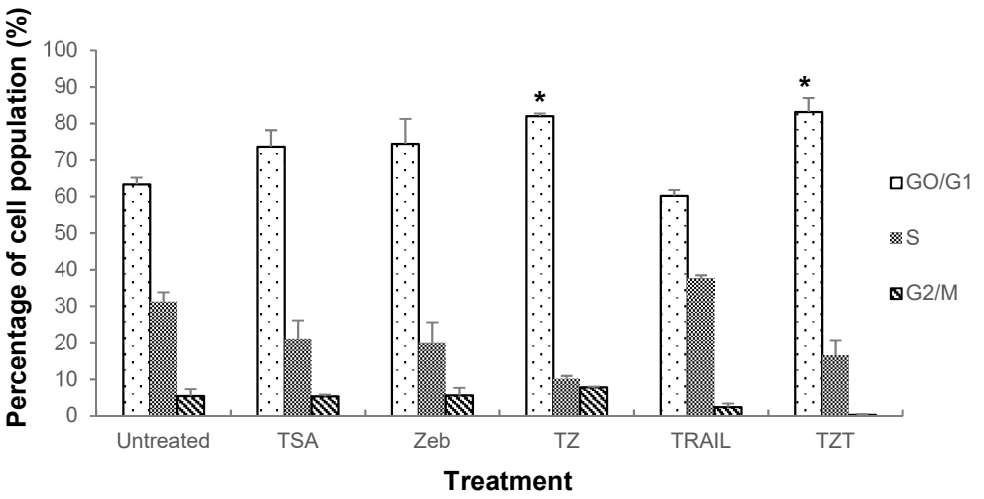
(b)


Percentage of cell population (%)
80
70
60
50
40
30
20
10
0
#
Untreated
TSA
Zeb
TZ
TRAIL
TZT
Treatment
GO/G1
S
G2/M

(c)


Percentage of cell population (%)
90
80
70
60
50
40
30
20
10
0
*
Untreated
TSA
Zeb
TZ
TRAIL
TZT
Treatment
GO/G1
S
G2/M

(d)



(e)

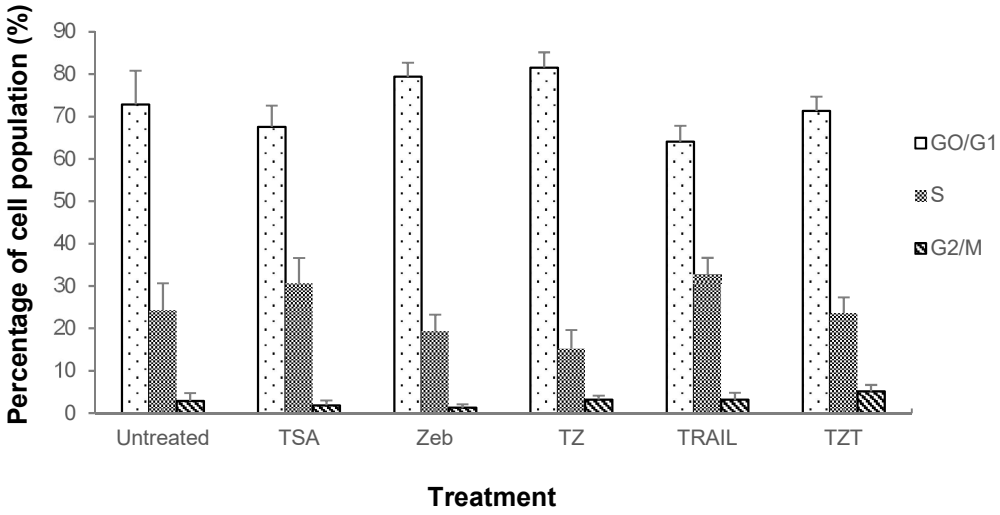


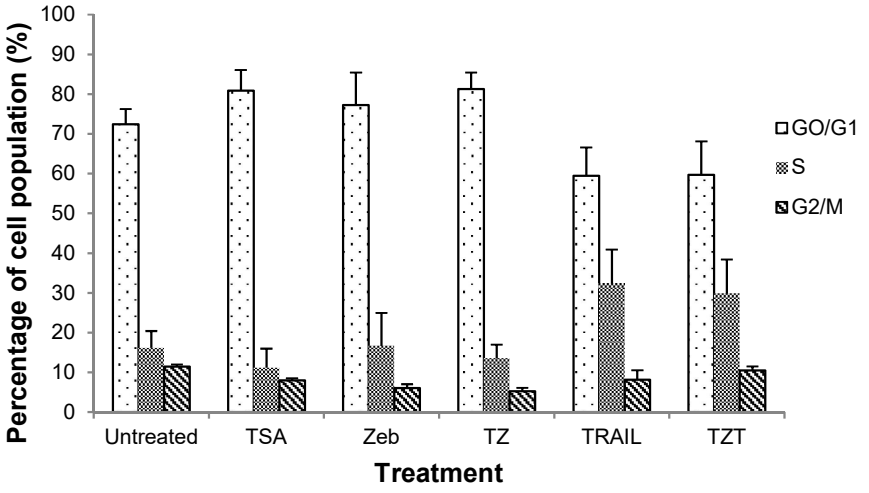
Figure 28 Percentage of cell population at G_0/G_1, S and G_2/M from cell cycle analysis of different treatment groups on **(a)MDA-MB-231; (b)231-EV; (c)231-EGFP; (d) MCF-7** breast adenocarcinoma cells and **(e) MCF10A** non-transformed breast epithelial cells for **24 h**. Data represents means ± SEM of two independent experiments of duplicates. One way ANOVA test was used to compare means of cell population arrested at the cell cycle phases G_0/G_1, S, and G_2/M, respectively after the different treatment groups. (*P<0.05) and **P<0.001) are significant and very significant differences from the untreated group and all other treatment groups, respectively. (#P<0.05) is significant difference from the treatment group, TRAIL.

As the treatment was prolonged to 48 h, all the treatment groups did not have significant alteration on the cell cycle distribution across G_0/G_1, S and G_2/M phades in MDA-MB-231 (Figure 29a). In 231-EV, the TSA, Zeb and TZ treatments have significantly ($P<0.05$) increased approximately 20% of cells being arrested in the G_0/G_1 phade in comparison with the TZT treatment (Figure 29b). Similarly, with the re-expression of *CDH1*-GFP in 231-EGFP, 20% higher ($P<0.05$) of G_0/G_1 arrest was achieved by TZ as compared to the TZT treatment (Figure 29c). Similar observation of TZ and Zeb inducing significantly ($P<0.05$) higher G_0/G_1 arrest was also made in *CDH1*-expressing MCF-7 cells (Figure 29d). Despite being ineffective in inducing G_0/G_1 arrest in the other cell lines, TZT had significantly ($P<0.05$) induced the highest percentage of cells in the G_2/M phade in MCF-7 in comparison with the untreated control (Figure 29d)

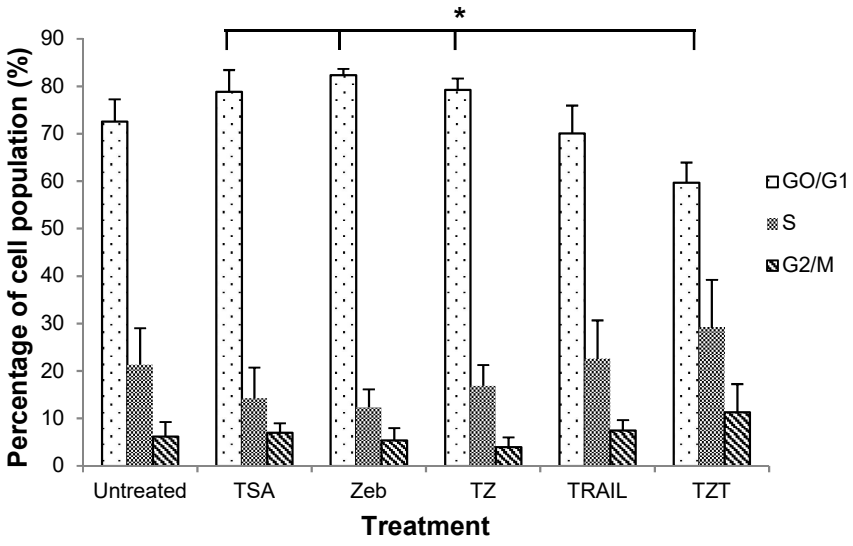
On the other hand, the percentages of G_0/G_1 arrest induced by both the TRAIL and the TZT treatments are intriguingly lower ($P<0.05$) than the untreated control while TRAIL alone had significantly ($P<0.05$) induced the highest percentage of cells in the S-phade among the untreated control and the other treatment groups in MCF10A (Figure 29e).

At the 72 h treatment time point, both the untreated and all the treated cells showed G_0/G_1 arrest and there is no significant difference between the untreated and all the treatment groups in MDA-MB-231, 231-EV, 231-EGFP and MCF10A, respectively (Figure 30a, b, c and e). However, Zeb had induced significant ($P<0.05$) 70.11% G_0/G_1 arrest in comparison with the untreated, TZ, TRAIL and TZT groups in MCF-7 (Figure 30d).

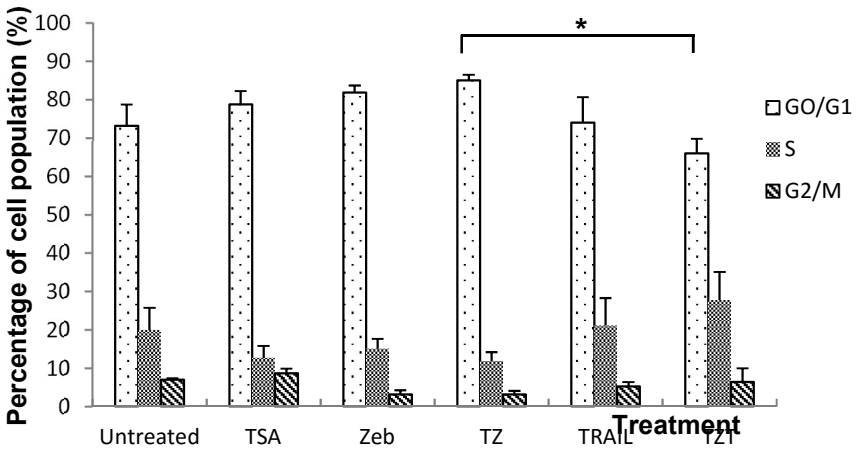
(a)


Percentage of cell population (%)
100
90
80
70
60
50
40
30
20
10
0
Untreated
TSA
Zeb
TZ
TRAIL
TZT
Treatment
GO/G1
S
G2/M

(b)


*
Percentage of cell population (%)
90
80
70
60
50
40
30
20
10
0
Untreated
TSA
Zeb
TZ
TRAIL
TZT
Treatment
GO/G1
S
G2/M

(c)


*
Percentage of cell population (%)
100
90
80
70
60
50
40
30
20
10
0
Untreated
TSA
Zeb
TZ
TRAIL
TZT
Treatment
GO/G1
S
G2/M

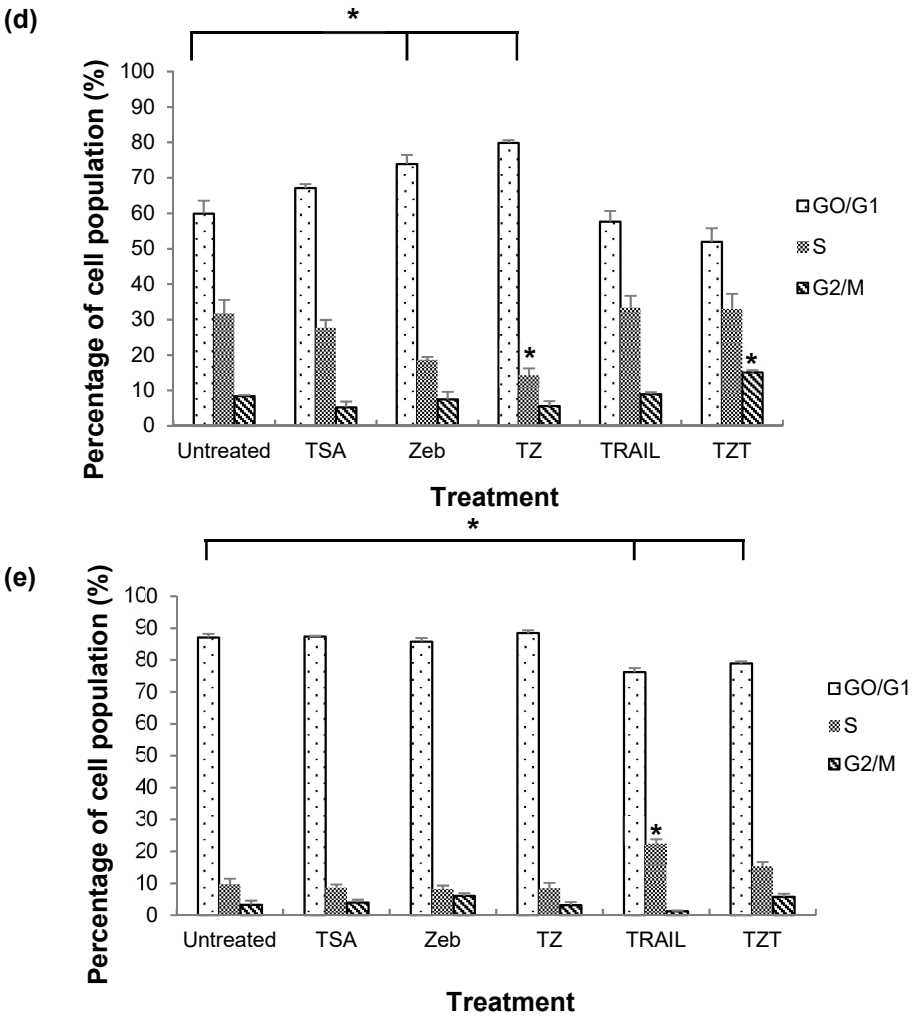
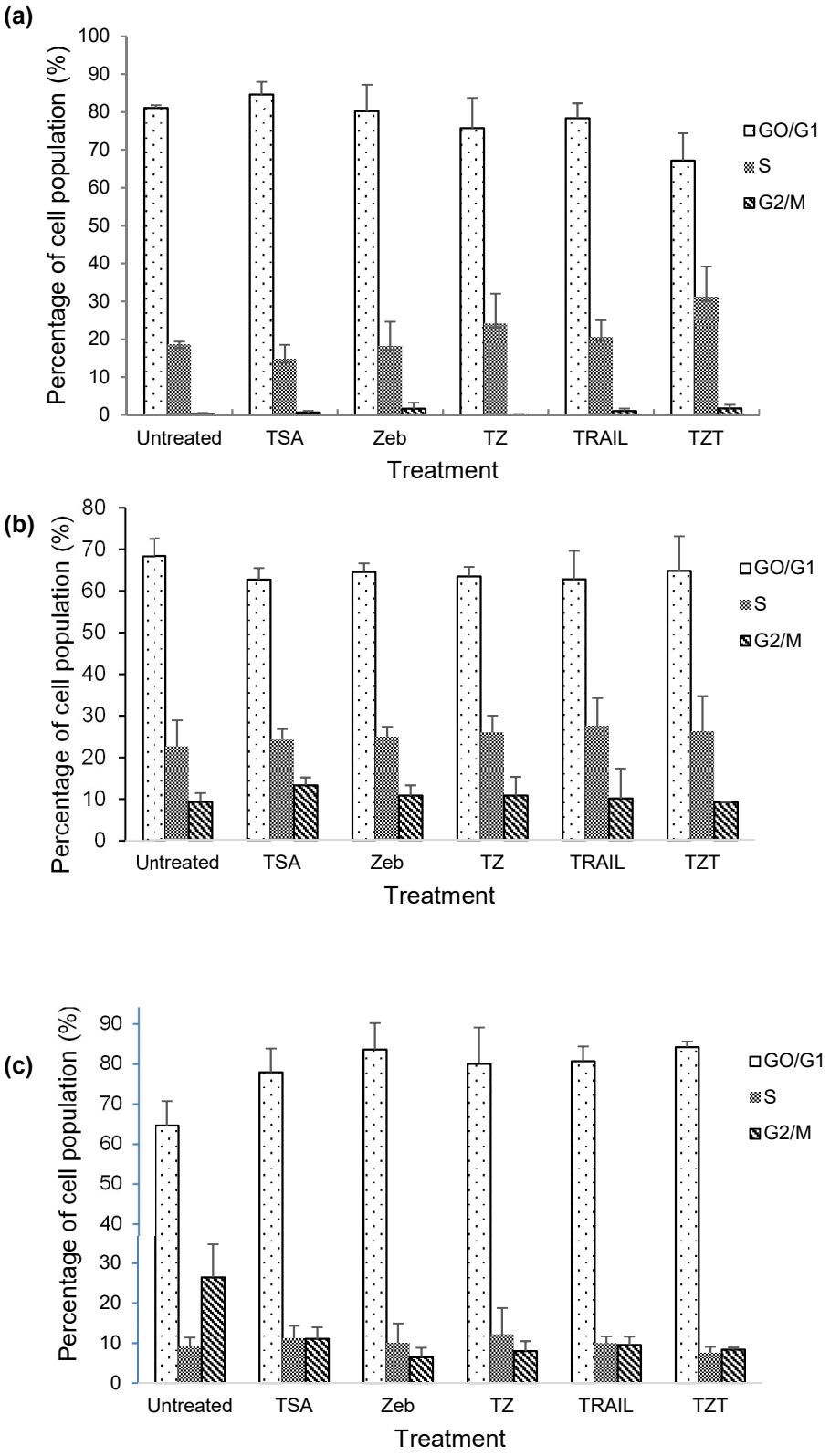


Figure 29 Percentage of cell population at G_0/G_1, S and G_2/M from cell cycle analysis of different treatment groups on **(a)MDA-MB-231; (b)231-EV; (c)231-EGFP; (d) MCF7** breast adenocarcinoma cells and **(e) MCF10A** non-transformed breast epithelial cells for **48 h**. Data represents means ± SEM of two independent experiments of duplicates. * is significant difference at $P<0.05$.


(a)
Percentage of cell population (%)
100
90
80
70
60
50
40
30
20
10
0
Untreated
TSA
Zeb
TZ
TRAIL
TZT
Treatment
GO/G1
S
G2/M
(b)
Percentage of cell population (%)
80
70
60
50
40
30
20
10
0
Untreated
TSA
Zeb
TZ
TRAIL
TZT
Treatment
GO/G1
S
G2/M
(c)
Percentage of cell population (%)
90
80
70
60
50
40
30
20
10
0
Untreated
TSA
Zeb
TZ
TRAIL
TZT
Treatment
GO/G1
S
G2/M

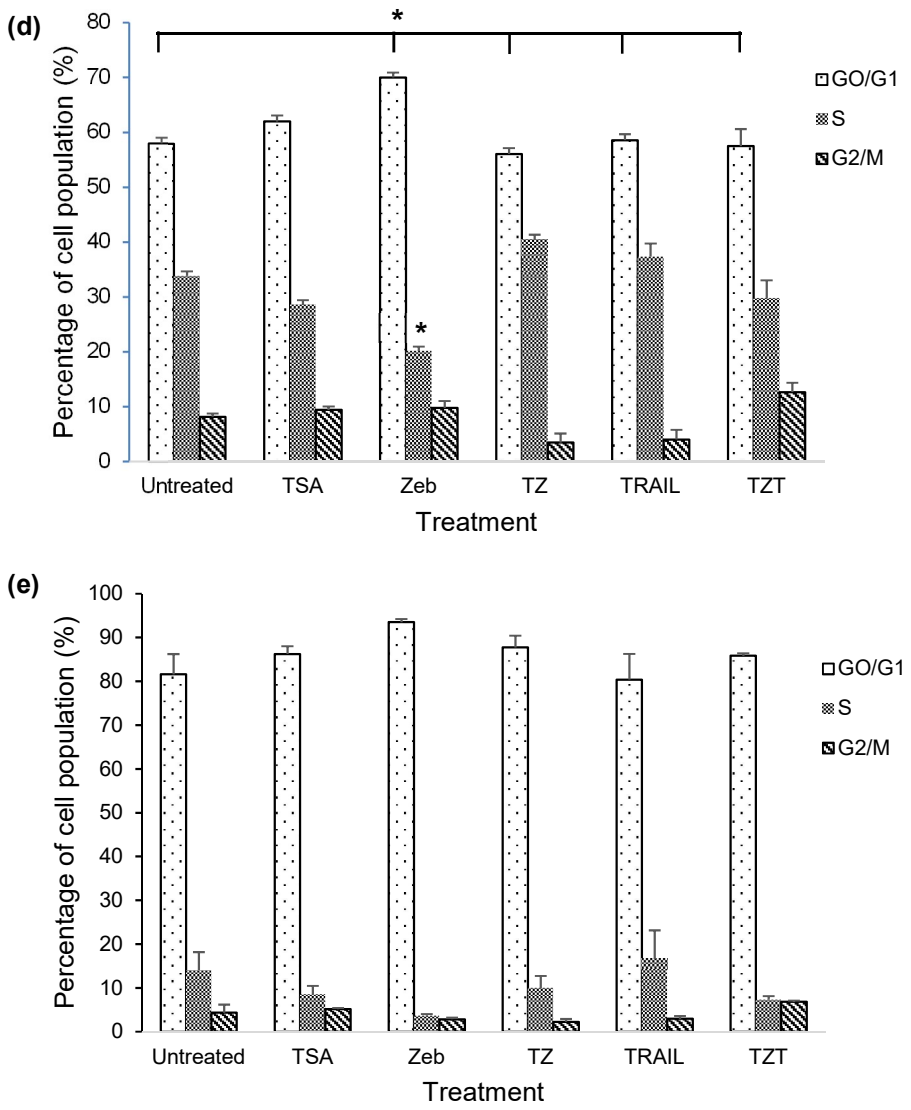


Figure 30 Percentage of cell population at G_0/G_1, S and G_2/M from cell cycle analysis of different treatment groups on **(a) MDA-MB-231; (b) 231-EV; (c) 231-EGFP; (d) MCF7** breast adenocarcinoma cells and **(e) MCF10A** non-transformed breast epithelial cells for **72 h**. Data represents means ± SEM of two independent experiments of duplicates. * is significant difference at $P<0.05$.

4.3.7 TZT along with E-cadherin expression had little effect on reducing the migration rate of MDA-MB-231 and 231-EGFP

There is one scientific report that shows TRAIL suppressing CXCR4-cell migration in MDA-MB-231 (Wang et al., 2013) albeit the numerous findings that support the pro-invasiveness role of TRAIL (Fritsche *et al.*, 2015; Wang *et al.*, 2014). MDA-MB-231 cells are highly invasive and migratory while MCF-7, on the other hand, is mostly poorly invasive *in vitro* (Perrot-Applanat and Di Benedetto, 2012) due to the lower expression of vascular endothelial growth factor (VEGF) (Comşa *et al.*, 2015). Therefore, it is justifiable to explore the effect of TRAIL and TZT treatment, with or without E-cadherin re-expression, on MDA-MB-231, 231-EV and 231-EGFP.

Based on the results from the wound healing assay shown in Figure 31a, all treatment groups did not significantly reduce MDA-MB-231 cell migration rate except for the TZ treatment group which significantly ($P<0.05$) reduced the cell migration rate at 3, 6, 12 and 24 h as compared to the untreated control. For 231-EV, the cell migration rate was significantly ($P<0.05$) reduced for TZ and TZT treatments at 3, 6 and 12 h post-treatment. Nonetheless, TRAIL treatment significantly ($P<0.05$) reduced the cell migration rate of 231-EV only at 3 and 6 h post-treatment (Figure 31b). On the other hand, in 231-EGFP, Zeb significantly ($P<0.05$) reduced its cell migration rate at 6, 12 and 24 h post-treatment. TZ treatment also significantly reduced ($P<0.05$) the cell migration rate at 6 and 12 h post-treatment but the reduction is very significant ($P<0.001$) at 24 h post-treatment (Figure 31c).

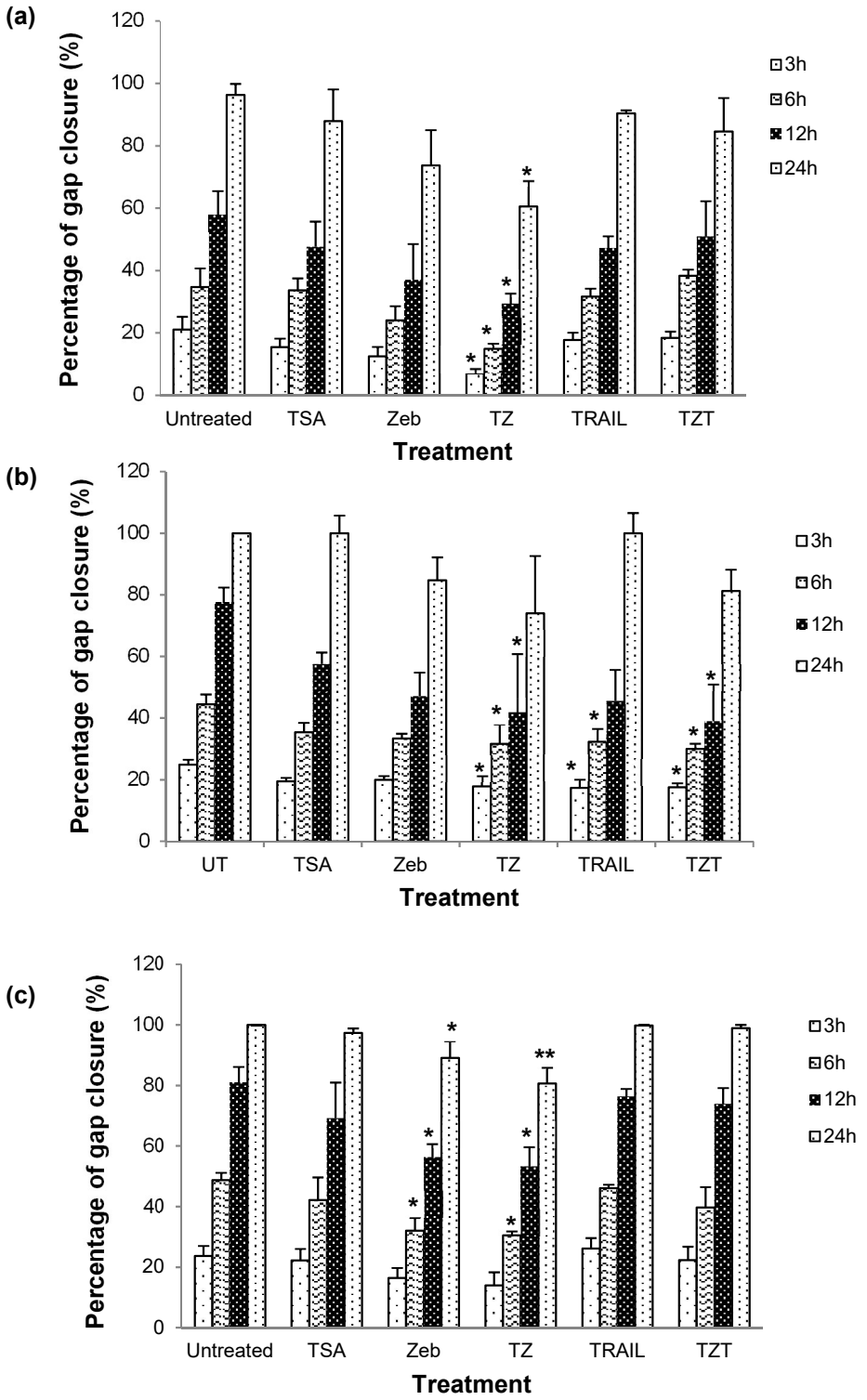


Figure 31 A cell monolayer formed by **(a) MDA-MB-231, (b) 231-EV and (c) 231-EGFP** was scratched with a p100 tip along the diameter of a 24-well. Microscopic images of the formed gap were then captured at 0, 3, 6, 12, and 24 h and the gap area was then measured using the ImageJ software. The percentages of gap closure at the respective time points are presented above. Error bars represent SEM from three independent experiments. ($^{*}p<0.05$) and (**$p<0.001$) are significant and very significant differences from the untreated control, respectively.

4.3.8 TZT treatment largely down-regulates PCNA and CDK2 mRNA expression in MDA-MB-231, 231-EGFP and MCF-7

As shown in the findings from the cell viability assay and cell cycle analysis above, TZT treatment had successfully inhibited cell growth and induced G_0/G_1 arrest in a significant percentage of cell population of MDA-MB-231, 231-EGFP and MCF-7. This had enticed our interest to elucidate the molecular mechanisms by which TZT treatment exerts its anti-cancer effects on the indicated cell lines. Previous report had stated that histone deacetylase inhibitor, MS-275, along with TRAIL had inhibited breast tumour cell proliferation as evidenced by decreased proliferating cell nuclear antigen (PCNA) immunoreactivity (Srivastava et al., 2010). In addition, cyclin-dependent kinase 2 (CDK2), an important positive regulator of G1-S progression in breast cancer cells (Sweeney et al., 1997), was shown to be down-regulated by Zebularine (Nakamura et al., 2013).

From the RT-PCR findings, there were 7- and 10-fold up-regulation of PCNA in MDA-MB-231 treated with TZ and TRAIL for 24 h, respectively, as compared to that of the untreated control (0.01) (Figure 32). However, Zeb and TZT largely suppressed PCNA expression to 0.03. Similar observation was made in 231-EGFP on which Zeb and TZT have largely suppressed PCNA expression to 0.05 in comparison with 0.85 in the untreated control. Nonetheless, in MCF-7, Zeb only induced approximately 2-fold downregulation of PCNA while TZT had downregulated PCNA expression to 14-fold lower than the untreated control (1.12).

On the other hand, both TSA and TZ treatments induced upregulation of CDK2 in MDA-MB-231 while Zeb, TRAIL and TZT treatments maintained low expression of CDK2, with the lowest expression given by TZT (0.04). In 231-EGFP, all treatment groups have downregulated CDK2 while CDK2 was completely and largely suppressed by Zeb and TZT, respectively. Interestingly, all treatment groups have upregulated CDK2 in MCF-7 but TZT maintained the

lowest CDK2 expression at 0.06 among all. All these findings (Figure 32) are in concordance with the cell cycle analysis results (Figure 28) showing TZT being the most effective treatment in arresting the breast cancer cell lines at G_0/G_1. Nonetheless, the obtained mRNA expression data had to be appropriately verified by the full-quantitative real time qPCR because the digital analysis of PCR amplicons using this study method was not performed at the exponential phade of PCR amplification reaction, making this method semi-quantitative at best (Antiabong *et al.*, 2016). Therefore, these preliminary RT-PCR findings will further be supported by antibody array analyses of other cell cycle regulators' protein expression which will be reported in Chapter 5.

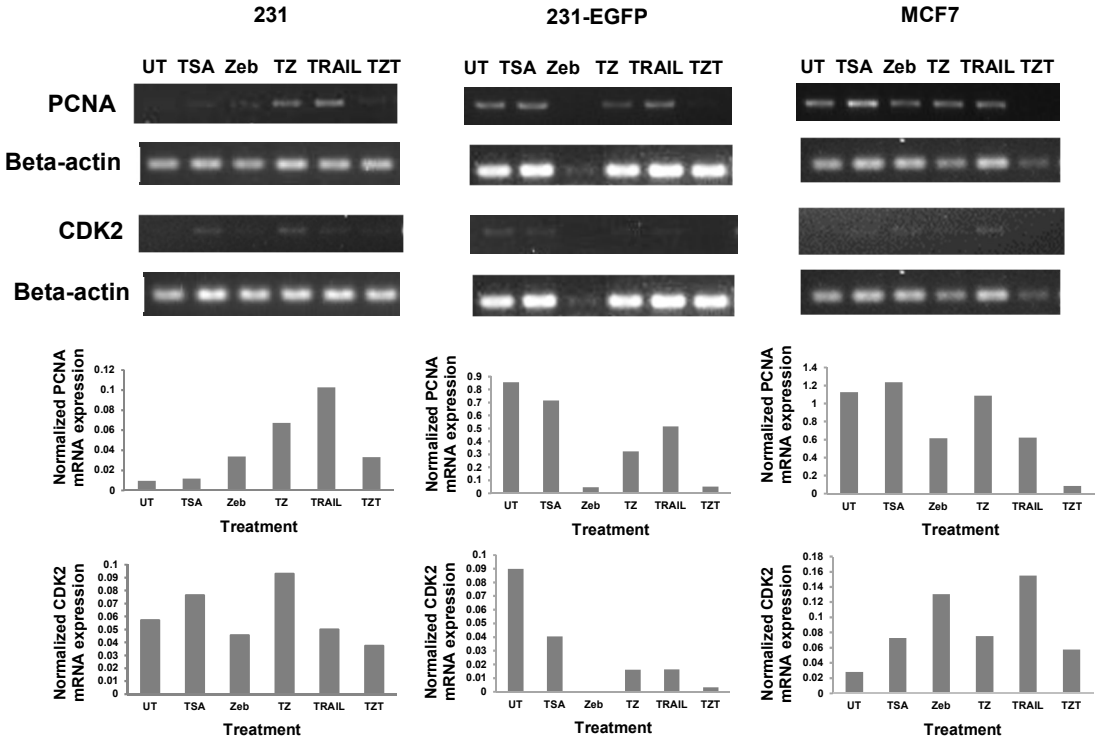


Figure 32 Total RNA extraction and RT-PCR on proliferating cell nuclear antigen (PCNA) and cyclin-dependent kinase 2 (CDK2. (a) MDA-MB-231 (231), geneticin selected MDA-MB-231 transfected with pCDNA3.1 empty vector (231-EV) and with E-cadherin-GFP plasmid (231-EGFP), MCF7 were extracted its total RNA for untreated control (UT), TSA, Zeb, TZ, TRAIL and TZT treatment groups at **24 h** time point using the RNeasy Mini Kit. The total RNA was DNase I treated and then converted to cDNA prior to PCR amplification using primers specific to PCNA and CDK2. Loading amount was normalized using the housekeeping gene, beta-actin. The respective band intensity was semi-quantified using the ImageJ software.

Similarly, at 48 h post-treatment, Zeb maintained the PCNA expression at 0.03 as at 24 h treatment time point while TZT had further reduced PCNA expression to 0.009 which is 10-fold lower than the background expression at 0.09 of the untreated MDA-MB-231 (Figure 33). On the other hand, in 231-EGFP, both the TZ and TZT have induced 7-fold and 2.5-fold down-regulation of PCNA expression, respectively, as compared to the untreated control. In the *CDH1*-expressing MCF-7, all TSA, Zeb and TZ treatments have no appreciable effect in suppressing PCNA expression while TRAIL and TZT treatments have suppressed over 90% of the basal PCNA expression in MCF-7 (Figure 33).

In terms of CDK2 expression, all TSA, Zeb and TZT treatments have induced 2-fold down-regulation of CDK2 expression in MDA-MB-231 while there was no CDK2 down-regulation induced by single TRAIL treatment (Figure 33). In the event of E-cadherin expression, only TSA and TZ treatments have induced down-regulation of CDK2 expression at 2-fold and 7-fold, respectively, while TRAIL and TZT treatments only maintained CDK2 expression at its basal level (Figure 33). On the other hand, in MCF-7, only Zeb induced an appreciable 2.5-fold down-regulation of CDK2 expression (Figure 33).

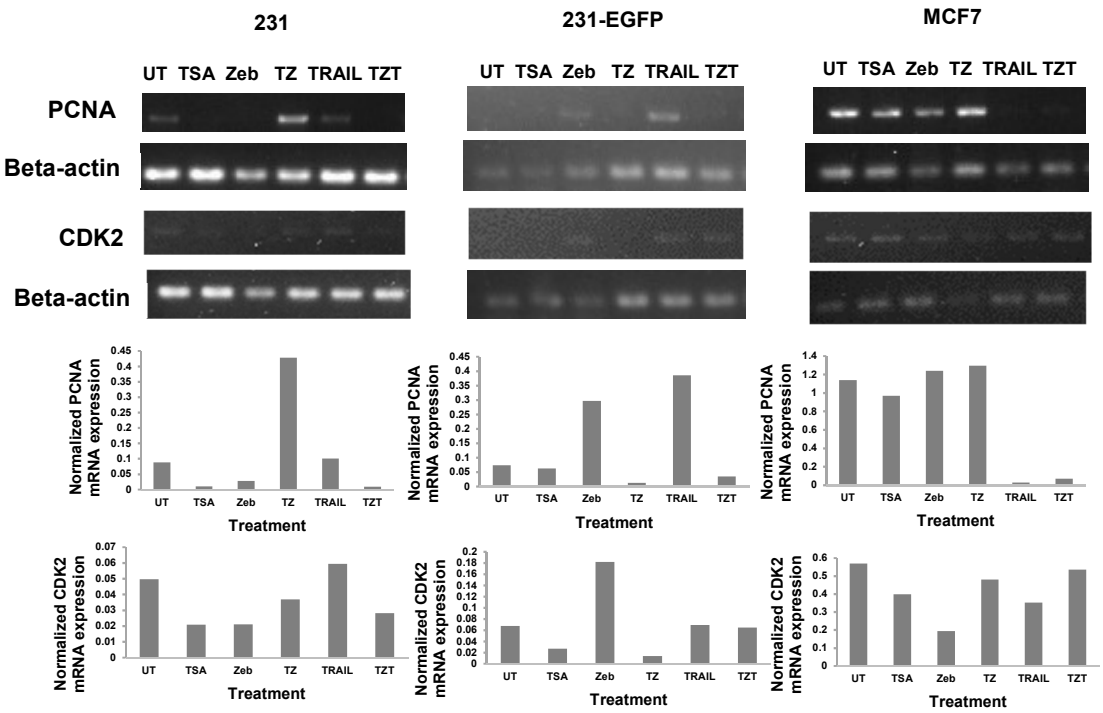


Figure 33 Total RNA extraction and RT-PCR on proliferating cell nuclear antigen (PCNA) and cyclin-dependent kinase 2 (CDK2). (a) MDA-MB-231 (231), geneticin selected MDA-MB-231 transfected with pCDNA3.1 empty vector (231-EV) and with E-cadherin-GFP plasmid (231-EGFP), MCF-7 were extracted its total RNA for untreated control (UT), TSA, Zeb, TZ, TRAIL and TZT treatment groups at **48 h** time point using the RNeasy Mini Kit. The total RNA was DNase I treated and then converted to cDNA prior to PCR amplification using primers specific to PCNA and CDK2. Loading amount was normalized using the housekeeping gene, beta-actin. The respective band intensity was semi-quantified using the ImageJ software.

4.3.9 TZT treatment had insignificant effect on the down-regulation of MMP-9 in MDA-MB-231 and 231-EGFP

Matrix metalloproteinase-9 (MMP-9) is expressed significantly higher in MDA-MB-231 than in human normal breast cell line (HS578Bst) and is closely related to tumour metastasis of breast cancer tissue (Li *et al*., 2017). TZT did not suppress MMP-9 expression in both MDA-MB-231 and 231-EGFP while Zeb and TZ maintained low MMP-9 expression in MDA-MB-231 and reduced MMP-9 expression to almost 2-fold lower than its basal expression in 231-EGFP (Figure 34a). At 48 h post-treatment, MMP9 remained being largely suppressed by Zeb and TZ treatments in both MDA-MB-231 and 231-EGFP (Figure 34b). These data corroborate the findings from the cell migration assay reported above (Figure 31a and Figure 31c). Similarly, the obtained mRNA expression data had to be appropriately verified by the full-quantitative real time qPCR because the digital analysis of PCR amplicons using this study method was not performed at the exponential phade of PCR amplification reaction, making this method semi-quantitative at best (Antiabong *et al*., 2016).

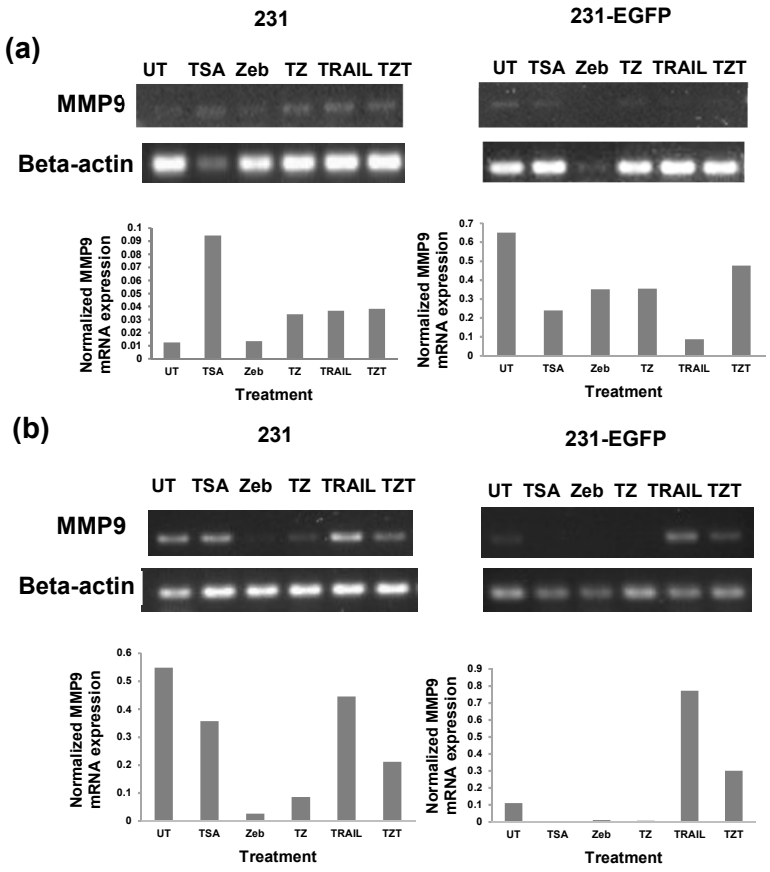


Figure 34 Total RNA extraction and RT-PCR on matrix metalloproteinase 9 (MMP9). MDA-MB-231 and 231-EGFP were extracted its total RNA for untreated control (UT), TSA, Zeb, TZ, TRAIL and TZT treatment groups at (a) **24** and (b) **48 h** time point using the RNeasy Mini Kit. The total RNA was DNase I treated and then converted to cDNA prior to PCR amplification using primers specific to MMP9. Loading amount was normalized using the housekeeping gene, beta-actin. The respective band intensity was semi-quantified using the ImageJ software.

4.4 Discussion

4.4.1 TSA and Zeb sensitization along with E-cadherin expression enhanced TRAIL-induced cytotoxicity in 231-EGFP and MCF-7 while having no significant inhibitory effect on MCF10A

In this report, the research work focuses on the effect of TSA and Zeb sensitization, with and without the re-expression of E-cadherin, on TRAIL-induced inhibition of cell growth in MDA-MB-231. MCF-7 which inherently expresses E-cadherin was tested alongside to compare the treatment effects on both *CDH1* transfected and non-transfected human breast adenocarcinoma cell lines.

Based on the findings presented in Figure 24, the consecutive treatment of Trichostatin A (TSA) and Zebularine (Zeb) combination followed by TRAIL (TZT) worked optimally at the 24h time-point. However, this is only the case for the *CDH1*-re-expressed cells, 231-EGFP as the other two cell lines, MDA-MB-231 and 231-EV showed no significant reduction in cell viability after the administration of TZT treatment. As for the 48 and 72 h treatment duration, the TZT treatment resulted in reduction of cell viability which was of no significant difference with all other treatment groups across all three cell lines.

The nominal effect of the TZT treatment on MDA-MB-231 cells can be explained by the literature's support on how the MDA-MB-231 cells which are TRAIL-sensitive can develop resistance towards sub-toxic doses of TRAIL via the endocytosis of its TRAIL-ligated cell surface receptors, TRAIL-R1 (DR4) and TRAIL-R2 (DR5) (Yoshida *et al.*, 2009; Zhang *et al.*, 2009). The internalization of DR4 and DR5 via the TRAIL ligation-induced endocytosis leads to dampening of the transmitted apoptosis signal, resulting in abated sensitivity of MDA-MB-231 towards TRAIL-induced apoptosis. In addition, a recent study in TRAIL-resistant breast cancer cell lines, BT474 and AU565, shows that the accrual of basal autophagosomes can give rise to TRAIL resistance by sequestering the DR4 and DR5 population from cell surface to

cell interior and the proposed theory had been verified in MDA-MB-231 (Di *et al.*, 2013). Intriguingly, both TSA and Zeb were shown to induce autophagy (He *et al.*, 2014; Yang *et al.*, 2013) which can potentially be the source of basal autophagosomes accumulation in this case. Therefore, despite TSA being able to upregulate DR4 and DR5, the concurrent accretion of autophagosomes through its autophagy induction might have potentially withdrawn the DR4 and DR5 from their active, surface localization, thereby causing the deteriorated TRAIL-mediated apoptosis signal.

In contrast, the post-treatment cell viability of 231-EGFP with *CDH1* re-expressed had been significantly ($P<0.05$) reduced after treatment of IC_{25} TSA and Zeb combination (TZ) and TRAIL while TZT treatment gave very significant ($P<0.001$) decline in the post-treatment 231-EGFP cells (Figure 24a). In the *CDH1*-expressing MCF-7, TZT had reduced its cell viability to 66.13% which is similar to the reduction achieved in 231-EGFP at 62.12% (Figure 24a). In addition, despite being non-significant, *CDH1* re-expression in 231-EGFP consistently reduced the proliferation to the initial rate across all treatment groups (Figure 25c). This could potentially be explained by *CDH1* interaction with the TRAIL receptors, DR4 and DR5. Lu *et al.* (2014) had provided evidence that E-cadherin interacts physically with TRAIL-ligated DR4 and DR5 at the plasma membrane, maintains the cell surface localization of the receptors and also links them to the cytoskeleton via its association with α-actin. This therefore enhances the assembly of the death-inducing silencing complex (DISC), caspase activation and subsequent apoptosis execution.

With respect to the epigenetic drugs, TZ, treatment, the sub-toxic IC_{25} might be too low to induce appreciable growth inhibition on MDA-MB-231 cells in a short duration of 24 h. However, with *CDH1* re-expressed, *CDH1* with its known function as beta-catenin negative regulator might have complemented TSA and Zeb in giving rise to the significant growth inhibition by negatively regulating the proliferative Wnt-signaling pathway (Hulsken *et al.*, 1994). Our

finding is in agreement with the postulation that E-cadherin expression serves to enhance TRAIL-mediated apoptosis and the effect is more evident with the additional mechanisms of TRAIL resistance reversal via the administration of the epigenetic drugs, TSA and Zeb prior to TRAIL treatment.

At the same time of being an effective inhibitory treatment on the aforementioned human breast cancer cell lines, all the treatment groups did not exert significant inhibitory effect on the cell viability and cell proliferation of the non-tumourigenic breast epithelial cell line, MCF10A (Figure 26 and Figure 27). A study had shown that epidermal growth factor receptor (EGFR) activation by EGF enhances the sensitivity of non-transformed human breast epithelial cells to TRAIL-induced apoptosis by down-regulating cellular FLICE (FADD-like IL-1β-converting enzyme)-inhibitory protein (c-FLIP) expression (Yerbes *et al.*, 2012). To exclude this factor in our studies, MCF10A is deprived of EGF in all experimental assays, and this could potentially justify its initial reduction of 20 - 30% cell viability (Figure 26).

4.4.2 TSA and Zeb sensitization along with E-cadherin expression increase TRAIL-induced cell cycle phade G_0/G_1 arrest in MDA-MB-231, 231-EGFP and MCF-7 via the down-regulation of PCNA and CDK2

The positive effect 24 h TZT treatment had on MDA-MB-231 re-expressed with *CDH1* had guided us to analyse the cell cycle distribution of the post-treatment MDA-MB-231, 231-EV and 231-EGFP at the time point of 24 h. Despite having non-significant reduction in cell viability of TZT-treated MDA-MB-231 (Figure 22), the TZT treatment for 24 h had induced significant ($P<0.05$) and very significant ($P<0.001$) escalation in the percentage of cells being arrested in the G_0/G_1 phade to 57.8% from the TZ treatment group and all other treatment groups, respectively (Figure 28a). Studies have shown that tumour cells, including breast cancer, induced with G_1 cell cycle arrest are more sensitized towards TRAIL-apoptosis inducing effect (Florean *et al.*, 2016; Lu *et al.*, 2005; Quast *et al.*, 2015). Besides, literature also reported that the epigenetic drugs, TSA and Zeb used in this study have induced cell cycle arrest in various neoplastic cells including breast cancer (Billam *et al*, 2010; Damaskos *et al.*, 2017; Hrgovic *et al.*, 2016).

Our result is in agreement with these reports as both TSA and TZ treatments have significantly ($P<0.01$) increased G_0/G_1 arrest in MDA-MB-231 as compared to the untreated control (Figure 28a). Zeb (Cheng *et al*, 2004) and TSA (Hrgovic *et al*, 2016) hade also been reported to induce p21 expression which can bind to PCNA and arrest the DNA replication in response to DNA damage. In this regard, our finding that Zeb and TZT have largely suppressed PCNA mRNA expression (Figure 32) concurs with the notion that TZT growth-inhibitory effect stems from the p21 DNA damage response pathway. On the other hand, our data showed that TRAIL significantly ($P<0.05$) induced S-phade arrest with the concomitant decrease in Go/G1 and G2/M population at the 24 h time point (Figure 28a). TRAIL treatment maintained low CDK2 expression in MDA-MB-231 and 231-EGFP at 24 h post-treatment (Figure 32),

thus is in agreement with the finding that S-phade arrest occurs with reduced CDK2 expression in human breast cancer cells (Laezza *et al*., 2006).

Therefore, it is hypothesized that the delayed reduction in cell viability of MDA-MB-231 on TRAIL and TZT treatment at 48 h (Figure 24b) is explainable by the cell cycle arrest induced from the first 24 h of the treatment. This is a promising finding as TRAIL can be developed to target against the resting, non-proliferative tumour cells which are usually recalcitrant towards treatment and stimulate relapse after an extended period of time (Ehrhardt *et al.*, 2015). Since MDA-MB-231 is highly proliferative, it is postulated that the efficiency of the prior treatment with TSA and Zeb followed by TRAIL in this study can be enhanced by prolonging the TSA and Zeb prior treatment to 24 h, allowing sufficient time for the induction of cell cycle arrest prior to TRAIL treatment for the subsequent 24 h.

On the other hand, 231-EGFP cells showed consistent increase in arrest at G_0/G_1 across all treatment groups while TZT have also significantly arrested MCF-7 in the G_0/G_1 phade at 24 h post-treatment (Figure 28c and Figure 28d). This could be explained by increased E-cadherin expression inactivating epidermal growth factor- receptor mitotic pathway (St Croix *et al*., 1998) and concurrently inducing cell cycle G_0/G_1 phade arrest by the upregulation of cdk inhibitor, $p27^{KIP1}$ and the suppression of the cyclin E–Cdk2 complex activity (Wong *et al*., 2018). However, only TZT treatment significantly ($P<0.05$) arrested 231-EGFP cells in the G_0/G_1 phade (Figure 28c). This is in agreement with the finding that all treatment groups have down-regulated CDK2 expression while its expression was largely suppressed by Zeb and TZT treatments at 24 h (Figure 32). Both PCNA and CDK2 expression have also been suppressed by TZT treatment at 24 h in MCF-7 (Figure 32). Moreover, TZT had induced 16.4% more G_0/G_1 arrest in 231-EGFP cells with *CDH1*-re-expressed than that induced in MDA-MB-231 with basal or no E-cadherin expression (Figure 28a and Figure 28c), further proving the enhanced anti-

proliferative function of TRAIL with the supplementation of TSA and Zeb alongside the re-expression of E-cadherin.

4.4.3 The effect of treatment on cell migration of 231-EV and 231-EGFP

In terms of cell migration reduction, Zeb and TZ worked effectively (Figure 31c) in reducing the cell migration rate as compared to the other treatment groups and this is corroborated by the downregulation of MMP-9 by Zeb and TZ in 231-EGFP (Figure 34a and Figure 34b). In the control 231-EV cells without *CDH1* expression, both TRAIL and TZT treatment groups significantly reduced cell migration rate compared to the untreated control as early as 12 h post-treatment. However, the cells regained their initial migration rate from 12 h to 24 h post-wounding as the migration rate is similar across untreated and all treatment groups at 24 h post-wounding. This suggested that both TRAIL and TZT treatments were effective in reducing the migration rate at the initial stage post-treatment but the effect was temporary. This result was reasonable as TRAIL anti-neoplastic action mainly stems from apoptosis induction. However, Wang *et al.* (2013) had suggested anti-invasiveness potential of TRAIL by their group's observation that TRAIL suppressed a key player in MDA-MB-231 cell invasiveness, CXC chemokine receptor 4 (CXCR4) by up-regulating miR-146a expression through NF-κB signalling pathway. Our result was in agreement with Wang *et al.* (2013) as this group had also observed TRAIL-induced reduction in cell migration rate within the post-wounding duration of 18 h.

Notwithstanding the decline in migration rate induced by TRAIL treatment in the early post-wounding hours, the majority of the literature still supports a pro-invasiveness role played by TRAIL via the same NF-κB signalling pathway (Azijli *et al.* 2013). TRAIL-R2 seems to be the key receptor that cancer cells like breast cancer (Fritsche *et al*, 2015) and non-small cell lung cancer harness (Azijli et al. 2012) in the event of TRAIL-induced cellular invasiveness. Moreover, despite the earlier literature supporting an anti-invasive role of E-

cadherin, recent literature advancements have backed the notion that E-cadherin expression increases cancer cell invasiveness and metastatic potential at the secondary metastatic sites (Chao et al. 2010; Chao et al. 2012; Chen et al. 2015). The aforementioned hypothesis was also supported by our finding that both TRAIL and TZT treatment could not reduce the migration rate of 231-EGFP cells to a significant extent, even at 12 h post-wounding (Figure 31c), showing that E-cadherin's growth inhibitory role was more evident than anti-invasive role in this study. Only Zeb- and TZ-treated 231-EGFP (Figure 31c) as well as TZ-treated MDA-MB-231 (Figure 31a) showed significant reduction in migration rate up till the 24 h time point and this was corroborated by their inhibitory effect on cell migration reported in other instances (Zhou *et al.*, 2012; Han *et al.*, 2014) as well as MMP9 down-regulation by Zeb and TZ in our study (Figure 34). Moreover, epigenetic data from literature had also suggested that the multi-layered epigenetic regulation of MMPs, tissue inhibitors of MMPs and collagens can actually serve as a trove of promising epigenetic drug targets in the anti-cancer field (Chernov and Strongin, 2012).

4.5 Conclusion

This study shows the promising potential of E-cadherin expression in boosting the efficacy of epigenetic drugs, TSA and Zeb sensitization of MDA-MB-231 human breast adenocarcinoma cells towards TRAIL anti-cancer effects which include growth inhibition and G_0/G_1 cell cycle arrest by the TZT treatment. The anti-cancer effects were shown to be mediated by the suppression of PCNA and CDK2 expression by the TZT treatment alongside E-cadherin expression. Further assessment in the aspect of apoptosis and its underlying molecular mechanisms on the feasibility of E-cadherin expression in augmenting TZT anti-cancer treatment efficacy in breast cancer is warranted. Nonetheless, future prospective study design on TRAIL should not neglect the pro-invasiveness nature of TRAIL in order that TRAIL can be applied to the cancer therapy field effectively.

5. The assessment of the apoptotic profile of human breast adenocarcinoma cells treated with Trichostatin A (TSA) and Zebularine (Zeb) followed by Tumour Necrosis Factor-related Apoptosis-inducing Ligand (TRAIL)

5.1 Introduction

Following chapter 2 of this thesis, the results showed that TSA and Zeb have sensitized MDA-MB-231 human breast adenocarcinoma cells towards enhanced TRAIL-induced anti-cancer effects via TZT-induced growth inhibition and G_0/G_1 cell cycle arrest mediated by PCNA and CDK2 suppression. Similar observations had been made in 231-EGFP which had E-cadherin re-expressed *in vitro* and in MCF-7 which inherently expresses E-cadherin. Therefore, these observations had guided us to further investigate on the anti-cancer efficacy of TZT treatment in the aspect of apoptosis.

Apoptosis is a programmed cell death induced by cytochrome c release from mitochondria which is driven by caspases and apoptosomes (Pandey *et al.*, 2018). Apoptosis signalling is mostly aberrant in cancer cells and the aberrance stems mainly from unbalanced expression of pro- and anti-apoptotic proteins. Apoptosis signalling aberrance drives cancer cells survivability and tumour aggressiveness (Chen *et al.*, 2018). Therefore, drug candidate which can induce apoptosis in cancer cells is the “Holy Grail” that’s heavily pursued by cancer researchers. As aforementioned, TRAIL is an anti-cancer agent of high potential due to its selective killing of cancerous or transformed cells and the healthy cells are generally escaped from its killing effect (Stuckey and Shah, 2013). Hence, it could serve as a promising replacement or enhancement of standard non-selective and genotoxic chemotherapeutic drugs efficacy in cancer therapy (Nagane *et al.*, 2001).

Albeit the great potential of TRAIL as a selective anti-cancer agent, most cancer cells have evaded its apoptosis induction and have thrived with various mechanisms of TRAIL resistance (Wang *et al.*, 2014a). First of all, for Type II

cells which require mitochondrial intensification in addition to DISC assembly and caspase-8 activation for apoptosis execution (Ozören and El-Deiry, 2002), dysregulation of the Bcl-2 family proteins was shown to play a role in the regulation of TRAIL-induced apoptosis. Their regulatory role had been supported by the abolishment of TRAIL-induced apoptosis blockage by compound administration that sequestered and down-regulated the Bcl-2 pro-survival proteins level in various cancer cell types (Hetschko *et al.*, 2008; Huang *et al.*, 2009; Kisim *et al.*, 2012).

In addition, despite the lack of correlation between TRAIL R1 and TRAIL R2 expression levels and TRAIL sensitivity in breast cancer (Chen *et al.*, 2012; Rahman *et al.*, 2009), its frequent mislocalization from cell surface instead had contributed to TRAIL resistance (Chen *et al.*, 2012). Since Lu *et al.* (2014) had reported that E-cadherin had a positive role on TRAIL R1 and TRAIL R2 via its interaction and sustenance of their surface expression in colon and pancreatic cancer cell lines, it was hypothesized that it could function similarly in breast cancer cells as well. Therefore, the *in vitro* E-cadherin re-expressed MDA-MB-231 (231-EGFP) and inherently E-cadherin expressed MCF-7 were used as the models in our study to assess the TZT treatment efficacy with E-cadherin expression.

Besides, inhibitor of apoptosis (IAP) proteins are prominent in influencing the downstream signalling of both the extrinsic and the intrinsic apoptotic pathways through inhibition of caspase activities by the occurrence of one to three Baculovirus IAP Repeat (BIR) domains binding to pockets of caspases-3, -7, and -9 (Gyrd-Hansen and Meier, 2010; Silke and Meier, 2013). Similarly, down-regulation or elimination of these pro-survival IAPs had ablated their caspase inhibition and augmented TRAIL-induced apoptosis in cancer cells (Allensworth *et al.*, 2012; Lopes *et al.*, 2007).

On the other hand, the molecular determinants of various TRAIL sensitizers in cancer cells include several cell cycle regulators like p21 (Azijli *et al.*, 2014;

Conticello *et al.*, 2008) and p27 (Li *et al.*, 2007). In addition, the phosphorylated forms of p53 at serine residues of 46 (p-p53 (S46)) and 392 (p-p53 (S392)) were also shown to play a part in apoptosis induction (Castrogiovanni *et al.*, 2018; Wu *et al.*, 2016). Last but not least, hypoxic condition (Mayes *et al.*, 2005) and several cell stress proteins (Wang *et al.*, 2014b) have also been implicated in the regulation of TRAIL sensitivity.

Hence, aside from assessing the apoptosis induction of the treatment groups of TSA, Zeb, TZ, TRAIL and TZT at the morphology level, selected treatment groups of TZ, TRAIL and TZT have also been subjected to Annexin V-FITC/Propidium Iodide (PI) cellular apoptosis assay and Human Apoptosis Proteome Profiling which comprises 35 apoptosis-related apoptosis markers of the categories: Bcl-2 family, extrinsic apoptosis pathway, pro-/anti-apoptotic proteins, IAPs and their inhibitors, cell cycle regulators and cell stress proteins.

The research objectives were as follow:

- To assess the TSA and Zeb combined followed by TRAIL (TZT) treatment apoptosis-induction in MDA-MB-231, 231-EGFP and MCF-7 at the morphology level via Hematoxylin and Eosin (H and E) staining;
- To assess the TSA and Zeb combined followed by TRAIL (TZT) treatment apoptosis-induction in MDA-MB-231, 231-EGFP and MCF-7 at the cellular level via Annexin V-FITC/PI cellular apoptosis flow cytometric assay;
- To assess the TSA and Zeb combined followed by TRAIL (TZT) treatment apoptosis-induction in MDA-MB-231, 231-EGFP and MCF-7 at the molecular level via Human Apoptosis Proteome Profiling of 35 apoptosis-related proteins.

5.2 Materials and method

5.2.1 Hematoxylin and Eosin staining

MDA-MB-231 and 231-EGFP cells were seeded at 3 × 10^5 cells per well while MCF-7 cells were seeded at 3.25 × 10^5 cells per well on one sterile cover slip placed on each well of 6-well plate. After cells have attached to the cover slips, the cells were treated with TSA, Zeb, TZ, TRAIL and TZT. At 24, 48 and 72 h post-treatment, the culture media were removed from each well and cells were washed gently with 1× PBS for twice. The cover slips were gently picked using a tip under sterile condition and placed into separate 55 x 14mm petri dishes according to the treatment groups. Cells were then fixed with ice-cold methanol for 10 min at -20°C and rehydrated at decreasing ethanol concentrations, rinsed, stained and dehydrated as follows:

Reagent	Description
100% ethanol	3 washes at 3 min each
90% ethanol	2 washes at 3 min each
70% ethanol	1 wash for 3 min
Distilled water	1 rinse for 5 min
Mayer's Hematoxylin solution	3 min
Scott's tap water	1 rinse for 5 min
95% ethanol	1 wash for 1 min
Eosin Y solution	2 min
95% ethanol	2 washes for 1 min each
100% ethanol	2 washes for 1 min each

*Mayer's Hematoxylin (50 g Aluminum potassium sulphate (alum), 1000 mL distilled water, 1 g hematoxylin, 0.2 g sodium iodate, 20 mL glacial acetic acid); 1% (m/v) Eosin Y stock solution (10 g Eosin Y, 200 mL distilled water, 800 mL 95% ethanol); 0.25% (v/v) Eosin Y working solution (250 mL Eosin Y stock solution, 750 mL 80% ethanol, 5 mL glacial acetic acid).

Slides were cleared with Xylene twice, each for 2 min before being air-dried under a fume hood. Permount solution was dropped onto a microscope slide and the cover slip was placed with the side of attached cells in contact with the Permount solution and the edges of the cover slip were sealed using nail polish. Slides were then viewed under a light microscope at 100× magnification (Nikon, Japan).

5.2.2 FITC-Annexin V / Propidium Iodide cellular apoptosis detection

MDA-MB-231 and 231-EGFP cells were seeded at 2.3 × 10^5 cells per well while MCF-7 cells were seeded at 3.25 × 10^5 cells per well of 6-well plate. Upon reaching semi-confluency, the cells were treated with TZ, TRAIL and TZT. At 24, 48 and 72 h post-treatment, the floating cells were collected from the culture media of both the untreated and the treated wells via centrifugation at 2000 rpm at room temperature. The adherent cells were trypsinized and collected into the tubes separated by the treatment groups. The total cells were washed twice with cold 1× PBS and then resuspended in 50 µL of 1× Binding Buffer. FITC Annexin V and Propidium Iodide (PI) from the FITC Annexin V Apoptosis Detection Kit I (BD Pharmingen, U.S.A.) were added at 5 µL each per sample. The cells were then vortexed gently and incubated for 15 min at room temperature in the dark. Subsequently, 450 µL of 1× Binding Buffer was added to each tube and samples were analysed by BD Accuri C6 Flow Cytometer (BD Biosciences, U.S.A.) within 1 hr.

5.2.3 Human apoptosis array proteome profiling

5.2.3.1 Cell lysate preparation from the untreated and treated MDA-MB 231, 231-EGFP and MCF-7

MDA-MB-231 and 231-EGFP cells were seeded at 4.6×10^5 cells per mL while MCF-7 cells were seeded at 6.5×10^5 cells per mL in T-25 flask. Upon reaching semi-confluency, the cells were treated with TZ, TRAIL and TZT. At 72 h post-treatment, both the floating and the adherent cells were pelleted via centrifugation at 2000 rpm for 5 min and washed with 1× PBS. After removing the residual 1× PBS, the cells were solubilized with 100 µL of Lysis Buffer 17 (provided by the Proteome Profiler™ Array human apoptosis array kit, RnD Systems, U.S.A.) supplemented with 10 µg/mL Aprotinin (Nacalai Tesque, Japan), 10 µg/mL Leupeptin Hemisulfate (Nacalai Tesque, Japan) and 10 µg/mL Pepstatin A (Sigma-Aldirch, U.S.A.) for 30 min. Samples were homogenized with vortex at 10 min interval. The lysates were then microcentrifuged at 16,000 g for 20 min and the supernatant was then transferred to clean 1.5 mL microcentrifuge tubes.

5.2.3.2 Bicinchoninic acid (BCA) protein quantification assay

Each total cell lysate sample prepared from 5.2.3.1 was added at 10 µL per well of a 96-well microplate. The BCA working reagent (50:1, BCA Reagent A: BCA Reagent B) was added at 200 µL per sample per well and the plate was mixed thoroughly on a plate shaker for 30 s. The plate was covered and incubated at 37°C for 30 min. The plate was cooled to room temperature prior to absorbance reading at 562 nm. Three technical replicate readings were taken for each sample.

A standard curve of final diluted bovine serum albumin (BSA) standards concentration against their respective A_{562} value was plotted to determine the concentration of each protein sample.

5.2.3.3 Human apoptosis array processing

The human apoptosis antibody array which consists of 35 apoptosis-related proteins (Table 3) was processed according to the manufacturer's guidelines. First, 2 mL of Array Buffer 1 which serves as the block buffer was pipetted into each well of the 4-well Multi-dish. One array was placed into each well of the 4-well Multi-dish using flat-tip tweezers and the dish was incubated for 1 h on a rocking platform shaker with its lid on. After removing Array Buffer 1, each lysate sample of the untreated, TZ, TRAIL and TZT treatment was added at 200 µg per array in 1.25 mL of Array Buffer 1 with adjustment to a final volume of 1.5 mL with Lysis Buffer 17 followed by overnight incubation at 4°C on a rocking platform shaker.

On the following day, each array was then subjected to three 1× Wash Buffer washes of 10 min each. Subsequently, the reconstituted Detection Antibody Cocktail was added to 1.5 mL of 1× Array Bufer 2/3 at 100-fold dilution per well of the 4-well Multi-dish. Each array was then returned to the 4-well Multi-dish and incubated for 1 h on a rocking platform shaker. Each array was then subjected to three 1× Wash Buffer washes of 10 min each followed by 30 min incubation on a rocking platform shaker with Streptavidin-Horseradish peroxidase (HRP) diluted in 2 mL 1× Array Buffer 2/3 at dilution factor of 1:2000. Subsequently, each array was then subjected to three 1× Wash Buffer washes of 10 min each. Each array was then removed and excess Wash Buffer was allowed to drain from the membrane to paper towel. Each array was placed on a piece of transparent plastic sheet with the identification number facing up. Chemi Reagent mix (200 µL) was pipetted evenly onto each array membrane and another piece of transparent plastic sheet was used cover and spread the Chemi Reagent Mix evenly without any bubbles formation. It was incubated for 1 min prior to exposure of 1-10 min and image capturing using the Chemi Hi-sensitivity feature of Bio-Rad Gel Doc XR (Bio-Rad, U.S.A.).

Table 3 The Human Apoptosis Array target proteins, controls and their respective coordinates.

Coordinate		Target/Control	Coordinate	Target/Control
A1, A2		Reference Spots	C13, C14	HO-2/HMOX2
A23, A24		Reference Spots	C15, C16	HSP27
B1, B2		Bad	C17, C18	HSP60
B3, B4		Bax	C19, C20	HSP70
B5, B6		Bcl-2	C21, C22	HTRA2/Omi
B7, B8		Bcl-x	C23, C24	Livin
B9, B10		Pro-Caspase-3	D1, D2	PON2
B11, B12		Cleaved Caspase-3	D3, D4	p21/CIP1/CDKN1A
B13, B14		Catalase	D5, D6	p27/Kip1
B15, B16		cIAP-1	D7, D8	Phospho-p53 (S15)
B17, B18		cIAP-2	D9, D10	Phospho-p53 (S46)
B19, B20		Claspin	D11, D12	Phospho-p53 (S392)
B21, B22		Clusterin	D13, D14	Phospho-Rad17 (S635)
B23, B24		Cytochrome c	D15, D16	SMAC/Diablo
C1, C2		TRAIL R1/DR4	D17, D18	Survivin
C3, C4		TRAIL R2/DR5	D19, D20	TNF R1/TNFRSF1A
C5, C6		FADD	D21, D22	XIAP
C7, C8		Fas/TNFRSF6/CD95	D23, D24	PBS (Negative Control)
C9, C10		HIF-1α	E1, E2	Reference Spots
C11, C12		HO-1/HMOX1/HSP32		

5.3 Results

5.3.1 Apoptotic morphological changes: Hematoxylin and Eosin staining

Apoptosis is a genetically programmed cell death that occurs with a series of hallmark morphological changes initiated from cell shrinkage and nuclear chromatin condensation followed by nuclear fragmentation and plasma membrane blebbing (He *et al.*, 2009). The process then culminates in the components of the cell being packed into membrane-bound bodies called apoptotic bodies which will then be endocytosed by macrophages and/or neighbouring cells (Abou-Ghali and Stiban, 2015).

At 24 h post-treatment, the morphological changes of apoptosis such as cell shrinkage, nuclear chromatin condensation and plasma membrane blebbing have been observed in MDA-MB-231 treated with all treatments of TSA, Zeb, TZ, TRAIL and TZT (Figure 35). The later stage of morphological changes such as nuclear fragmentation was observed in MDA-MB-231 treated with Zeb, TZ, TRAIL and TZT. Nonetheless, apoptotic bodies were only captured in MDA-MB-231 treated with TZT (Figure 35).

At 48 h post-treatment, similar trend as that of 24 h treatment was observed across all treatment groups. However, nuclear fragmentation and apoptotic body formation were more evident in MDA-MB-231 treated with TZT (Figure 36). At the time point of 72 h, the untreated MDA-MB-231 started to shrink and its nuclear chromatin condensed. Cell shrinkage, nuclear chromatin condensation and plasma membrane blebbing consistently occurred in the treatment groups of TSA, Zeb, TZ, TRAIL and TZT. TSA-treated MDA-MB-231 showed slight occurrence of nuclear fragmentation while TZT-treated MDA-MB-231 displayed more evident nuclear fragmentation and apoptotic body formation in addition to the earlier morphological changes of cell shrinkage and nuclear chromatin condensation (Figure 37)

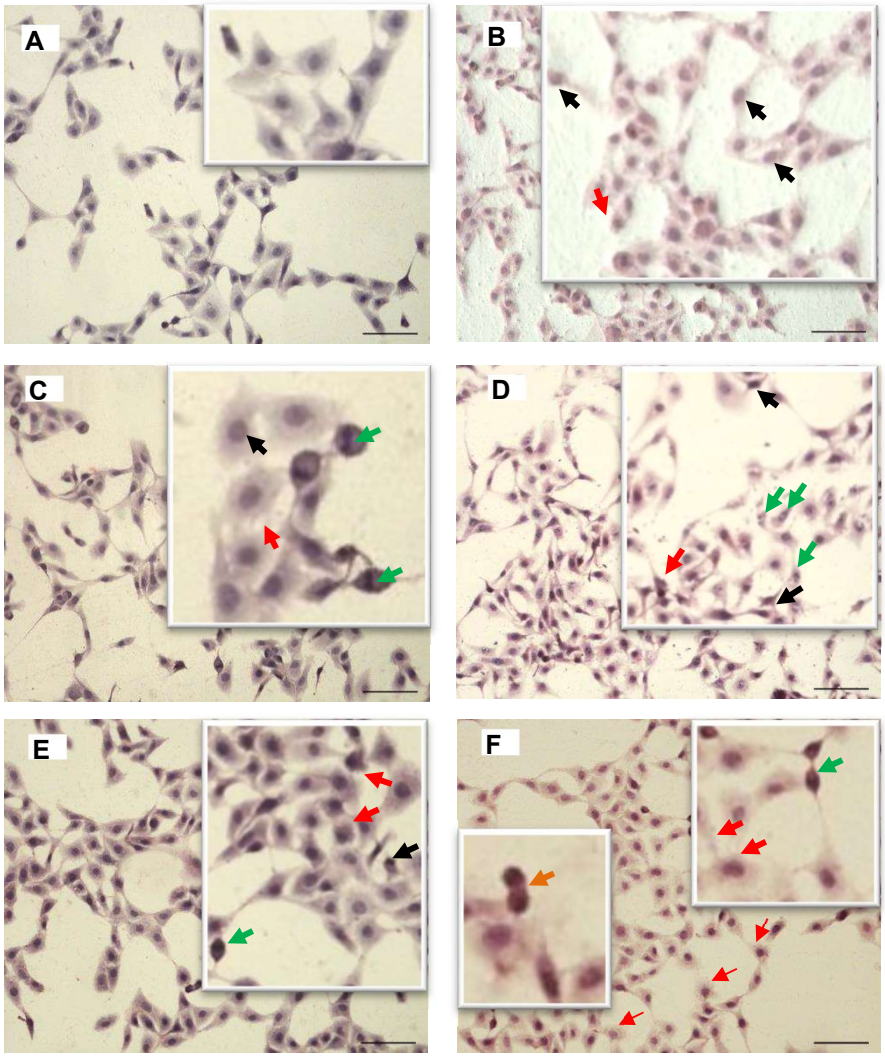


Figure 35 Microscopoic images of hematoxylin and eosin (H and E) stained (A) untreated **MDA-MB-231** and **MDA-MB-231** treated with (B) TSA, (C) Zeb, (D) TSA and Zeb, (E) TRAIL for **24 h**; (F) TSA and Zeb for 12 h followed by TRAIL treatment for **24 h**. Scale bars represent 100 µm. The apoptotic morphologies are explained as follows: cell shrinkage and nuclear chromatin condensation (black arrows); cell membrane blebbing (red arrows); nuclear fragmentation (green arrows); apoptotic body (orange arrow). Images were captured at 20× magnification. Scale bars represent 100 µm. Insets are of same photo at higher magnification for clear view.

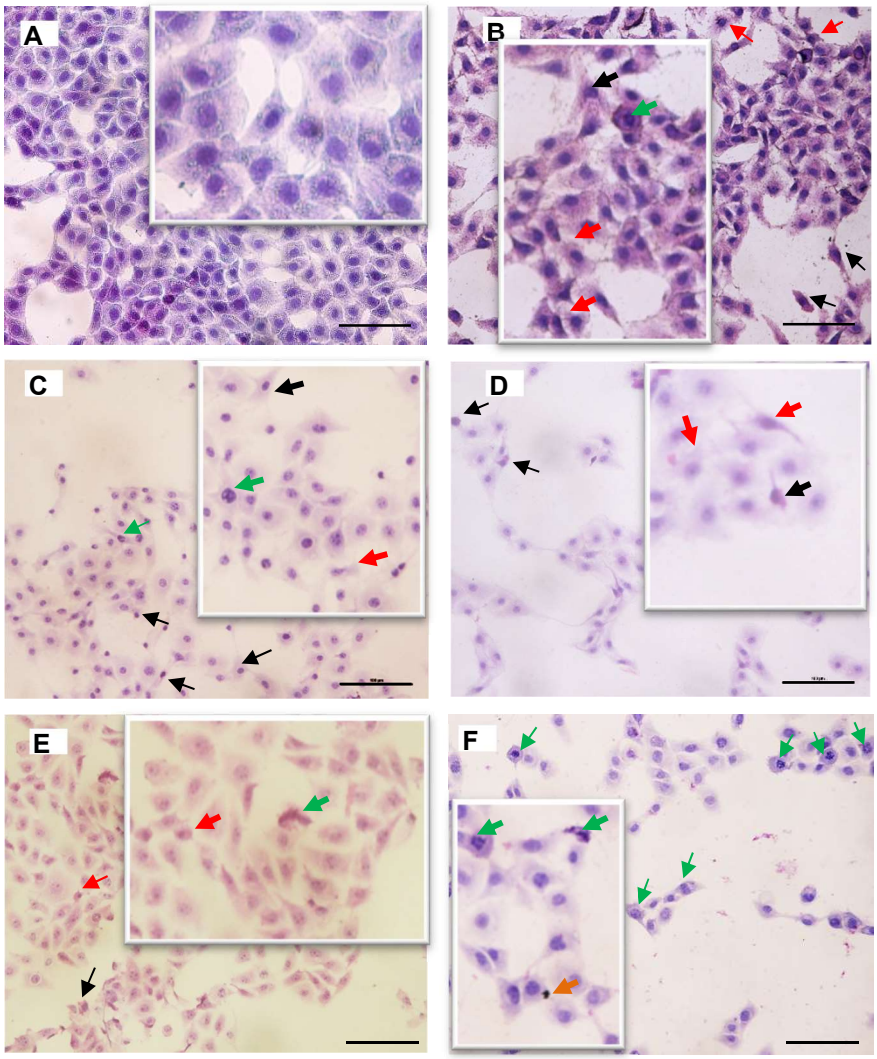


Figure 36 Microscopoic images of hematoxylin and eosin (H and E) stained (A) untreated **MDA-MB-231** and **MDA-MB-231** treated with (B) TSA, (C) Zeb, (D) TSA and Zeb, (E) TRAIL for **48 h**; (F) TSA and Zeb for 12 h followed by TRAIL treatment for 48 h. Scale bars represent 100 µm. The apoptotic morphologies are explained as follows: cell shrinkage and nuclear chromatin condensation (black arrows); cell membrane blebbing (red arrows); nuclear fragmentation (green arrows); apoptotic body (orange arrow). Images were captured at 20× magnification. Scale bars represent 100 µm. Insets are of same photo at higher magnification for clear view.

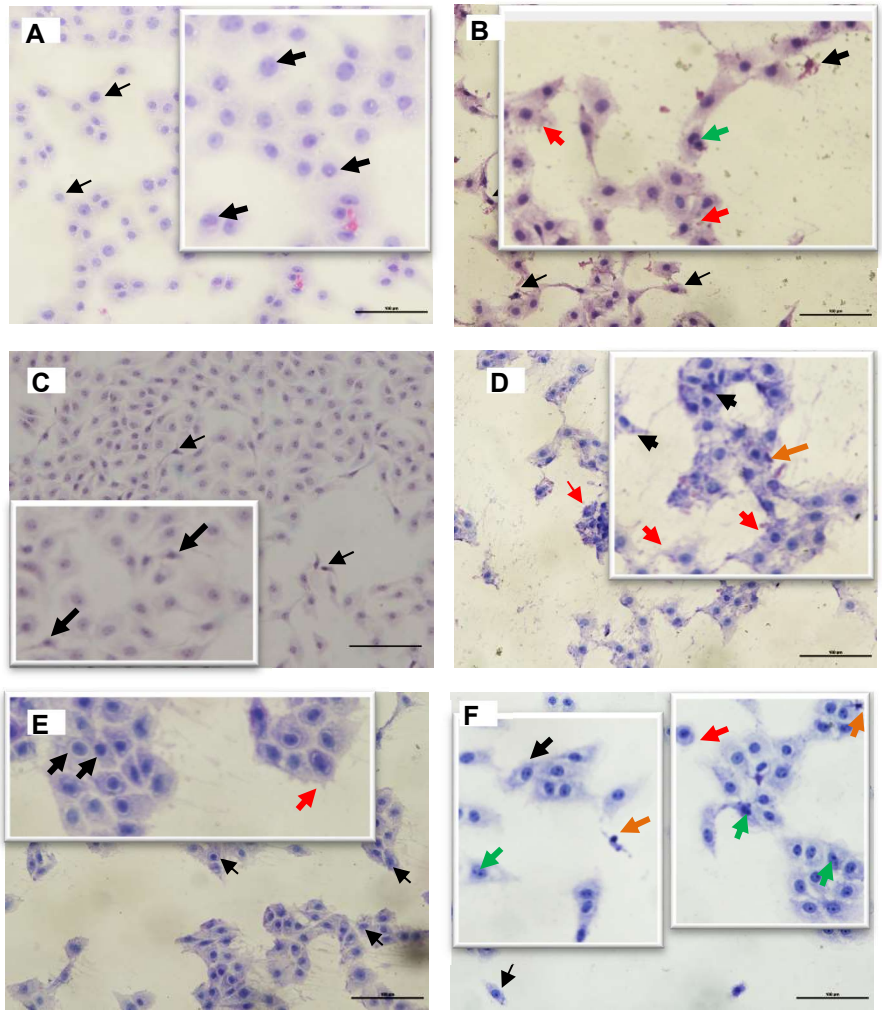


Figure 37 Microscopic images of hematoxylin and eosin (H and E) stained (A) untreated **MDA-MB-231** and **MDA-MB-231** treated with (B) TSA, (C) Zeb, (D) TSA and Zeb, (E) TRAIL for **72 h**; (F) TSA and Zeb for 12 h followed by TRAIL treatment for **72 h**. Scale bars represent 100 µm. The apoptotic morphologies are explained as follows: cell shrinkage and nuclear chromatin condensation (black arrows); cell membrane blebbing (red arrows); nuclear fragmentation (green arrows); apoptotic body (orange arrow). Images were captured at 20× magnification. Scale bars represent 100 µm. Insets are of same photo at higher magnification for clear view.

In 231-EGFP which expresses E-cadherin, at the treatment time point of 24 h, some nuclear fragmentation were observed in the untreated control. In comparison with MDA-MB-231, more nuclear fragmentation had been observed across all treatment groups while TZT maintained the highest occurrence of nuclear fragmentation. All treatment groups had also induced cell shrinkage, nuclear chromatin condensation and plasma membrane blebbing in 231-EGFP (Figure 38).

At 48 h post-treatment, TSA, Zeb and TZ treatment had induced similar extent of cell shrinkage, nuclear chromatin condensation and plasma membrane blebbing in 231-EGFP. Single TRAIL treatment had induced mostly cell shrinkage and nuclear chromatin condensation along with some evidence of nuclear fragmentation in 231-EGFP. However, in TZT-treated 231-EGFP, the cell morphology had switched towards more evidence of nuclear fragmentation, late stage plasma membrane blebbing and apoptotic body formation (Figure 39).

As the treatment duration was extended to 72 h, high incidences of cell shrinkage, nuclear chromatin condensation and plasma membrane blebbing along with some apoptotic body formation had been observed in the untreated and TSA-treated 231-EGFP. Zeb and TZ treatments had induced nuclear fragmentation in addition to the aforementioned cell morphological changes. On the other hand, TZT treatment havd induced more evident apoptotic morphological changes than TRAIL alone in terms of higher occurrences of cell shrinkage, nuclear chromatin condensation, plasma membrane blebbing and apoptotic body formation (Figure 40).

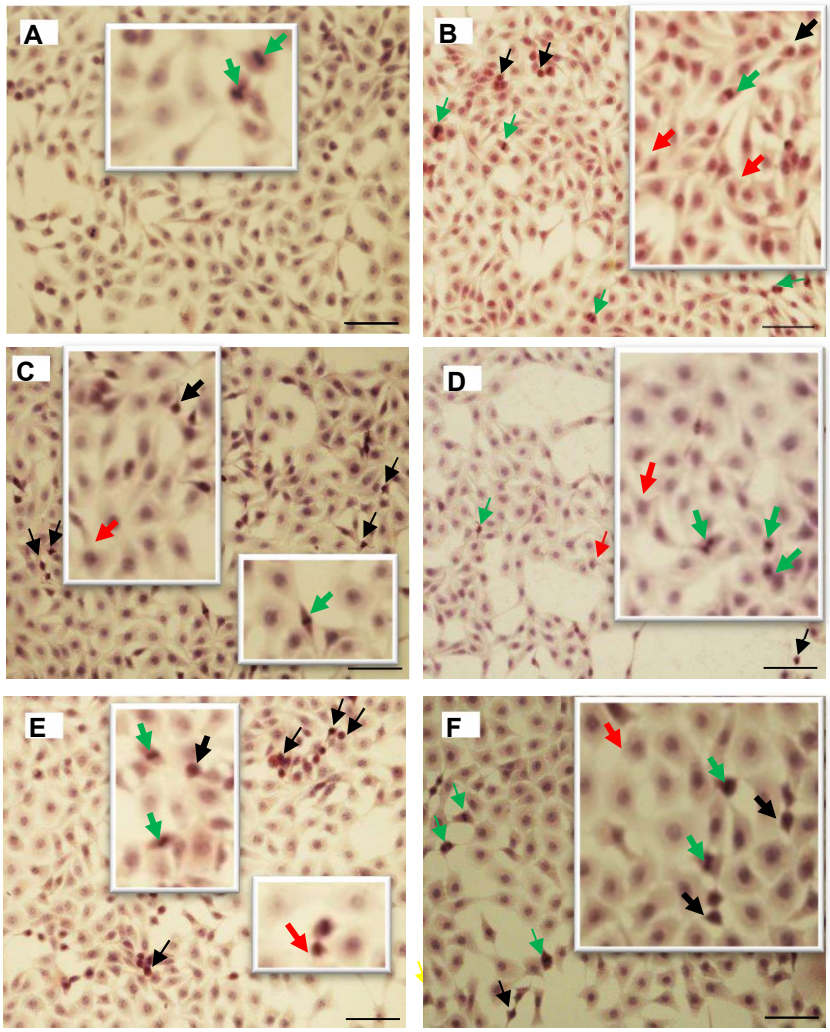


Figure 38 Microscopic images of hematoxylin and eosin (H and E) stained (A) untreated **231-EGFP** and **231-EGFP** treated with (B) TSA, (C) Zeb, (D) TSA and Zeb, (E) TRAIL for **24 h**; (F) TSA and Zeb for 12 h followed by TRAIL treatment for **24 h**. Scale bars represent 100 µm. The apoptotic morphologies are explained as follows: cell shrinkage and nuclear chromatin condensation (black arrows); cell membrane blebbing (red arrows); nuclear fragmentation (green arrows). Images were captured at 20× magnification. Scale bars represent 100 µm. Insets are of same photo at higher magnification for clear view.

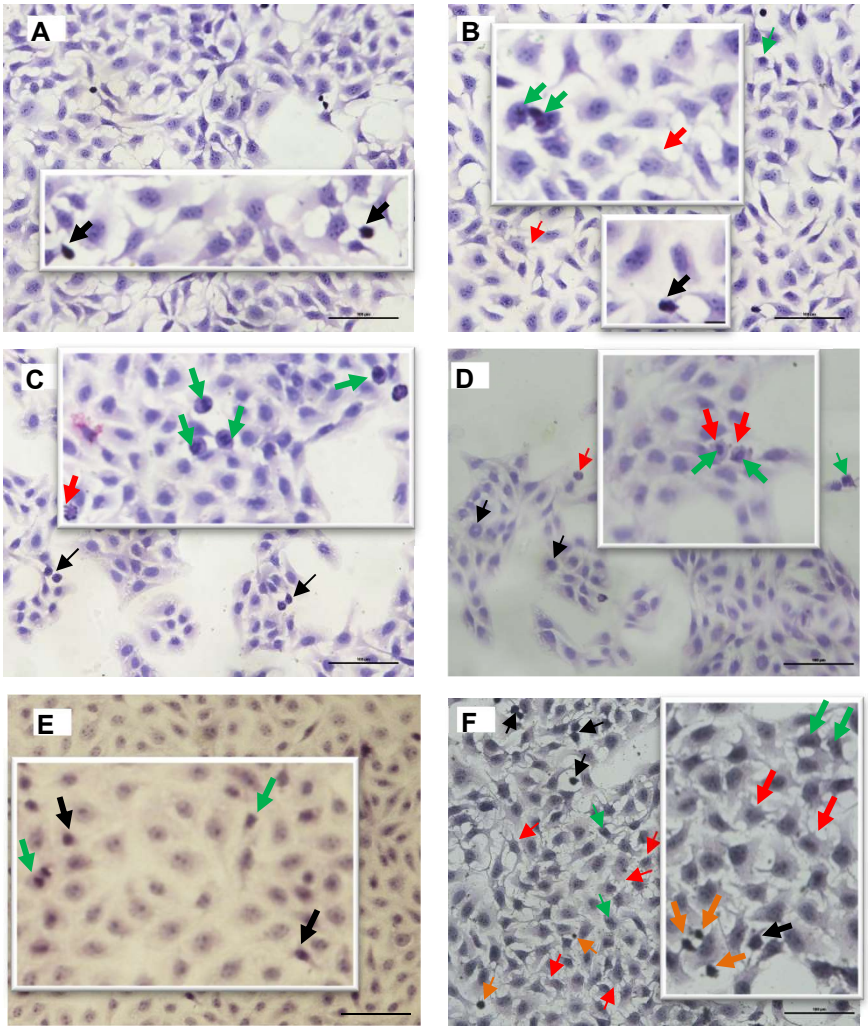


Figure 39 Microscopic images of hematoxylin and eosin (H and E) stained (A) untreated **231-EGFP** and **231-EGFP** treated with (B) TSA, (C) Zeb, (D) TSA and Zeb, (E) TRAIL for **48 h**; (F) TSA and Zeb for 12 h followed by TRAIL treatment for **48 h**. Scale bars represent 100 µm. The apoptotic morphologies are explained as follows: cell shrinkage and nuclear chromatin condensation (black arrows); cell membrane blebbing (red arrows); nuclear fragmentation (green arrows); apoptotic body (orange arrow). Images were captured at 20× magnification. Scale bars represent 100 µm. Insets are of same photo at higher magnification for clear view.

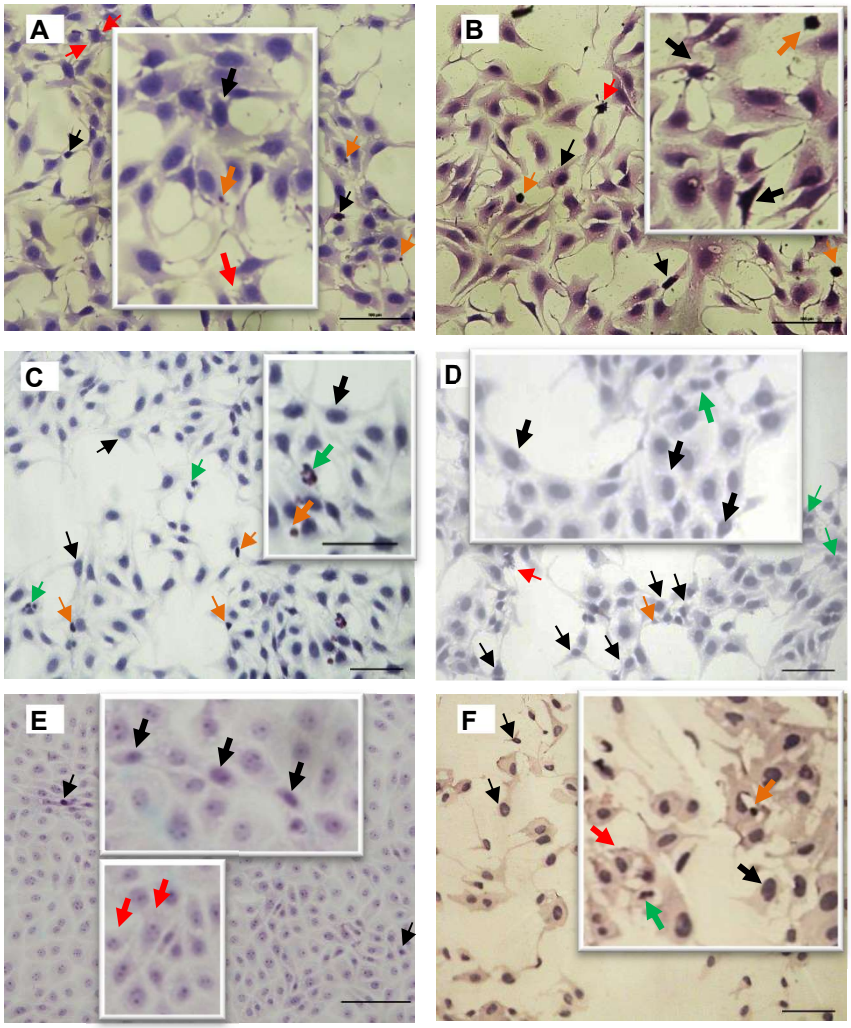


Figure 40 Microscopic images of hematoxylin and eosin (H and E) stained (A) untreated **231-EGFP** and **231-EGFP** treated with (B) TSA, (C) Zeb, (D) TSA and Zeb, (E) TRAIL for **72 h**; (F) TSA and Zeb for 12 h followed by TRAIL treatment for **72 h**. Scale bars represent 100 µm. The apoptotic morphologies are explained as follows: cell shrinkage and nuclear chromatin condensation (black arrows); cell membrane blebbing (red arrows); nuclear fragmentation (green arrows); apoptotic body (orange arrow). Images were captured at 20× magnification. Scale bars represent 100 µm. Insets are of same photo at higher magnification for clear view.

In MCF-7 which inherently expresses E-cadherin, both TSA and Zeb treatments had induced similar extent of early apoptosis morphological changes like nuclear chromatin condensation, cell shrinkage, plasma membrane blebbing and slight nuclear fragmentation at the 24 h time point (Figure 41b and c). TZ treatment showed similar morphological changes as aforementioned with the addition of the appearance of apoptotic bodies (Figure 41d). On the other hand, both TRAIL and TZT treatments had induced nuclear chromatin condensation along with late-stage nuclear fragmentation and apoptotic bodies' formation with TRAIL-induced morphological changes at higher incidence as compared to TZT-induced (Figure 41E and F).

At 48 h post-treatment, nuclear chromatin condensation, nuclear fragmentation, slight plasma membrane blebbing and apoptotic bodies' formation were the apoptotic morphological changes observed in the TSA, Zeb and TZ treatment groups (Figure 42b, c and d). In addition, both TRAIL and TZT treatments have caused mostly nuclear chromatin condensation, nuclear fragmentation and apoptotic bodies' formation in MCF-7. However, comparatively more nuclear fragmentation and apoptotic bodies' formation were observed in the TZT treatment group in MCF-7 at 48 h post-treatment (Figure 42E and F).

At 72 h post-treatment, TSA-, Zeb- and TZ-treated showed morphological traces of apoptosis like plasma membrane blebbing, nuclear chromatin condensation, nuclear fragmentation, and apoptosis bodies' formation (Figure 43b, c and d). On the other hand, TRAIL- and TZT-treated showed morphological changes like nuclear fragmentation, nuclear chromatin condensation and apoptotic bodies' formation without tangible plasma membrane blebbing (Figure 43E and F).

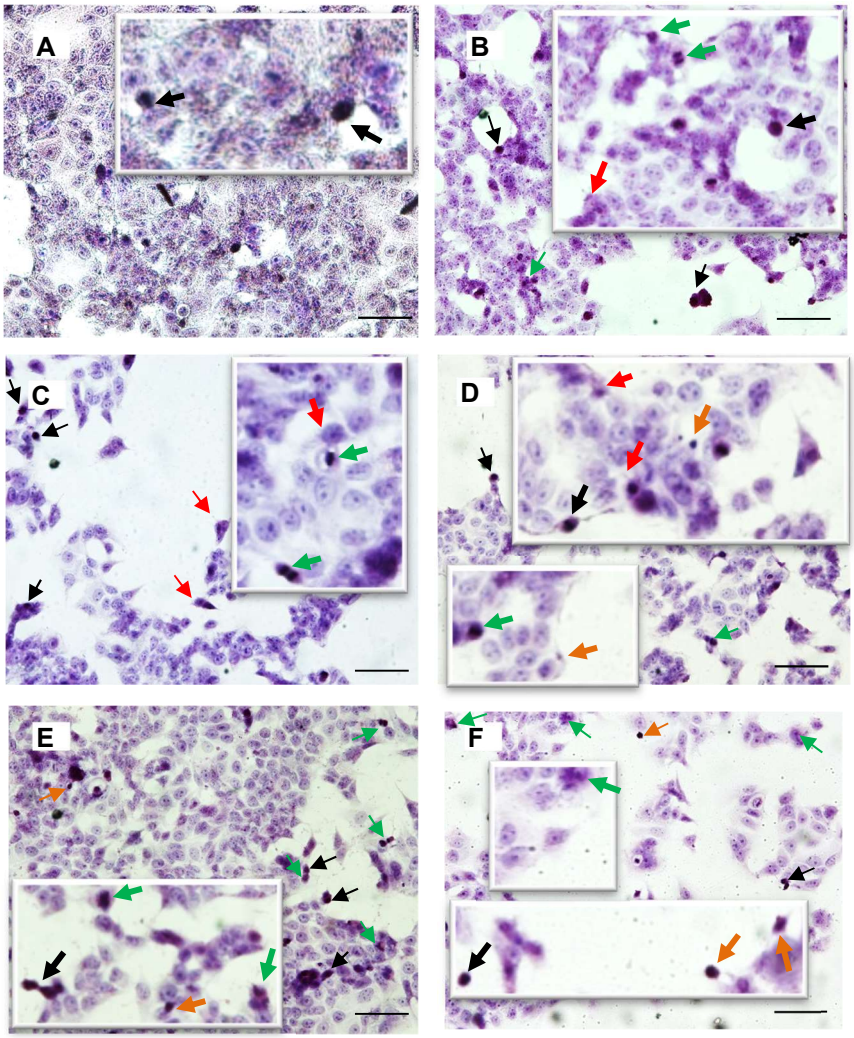


Figure 41 Microscopic images of hematoxylin and eosin (H and E) stained (A) untreated **MCF-7** and **MCF-7** treated with (B) TSA, (C) Zeb, (D) TSA and Zeb, (E) TRAIL for **24 h**; (F) TSA and Zeb for 12 h followed by TRAIL treatment for **24 h**. Scale bars represent 100 µm. The apoptotic morphologies are explained as follows: cell shrinkage and nuclear chromatin condensation (black arrows); cell membrane blebbing (red arrows); nuclear fragmentation (green arrows); apoptotic body (orange arrow). Images were captured at 20× magnification. Scale bars represent 100 µm. Insets are of same photo at higher magnification for clear view.

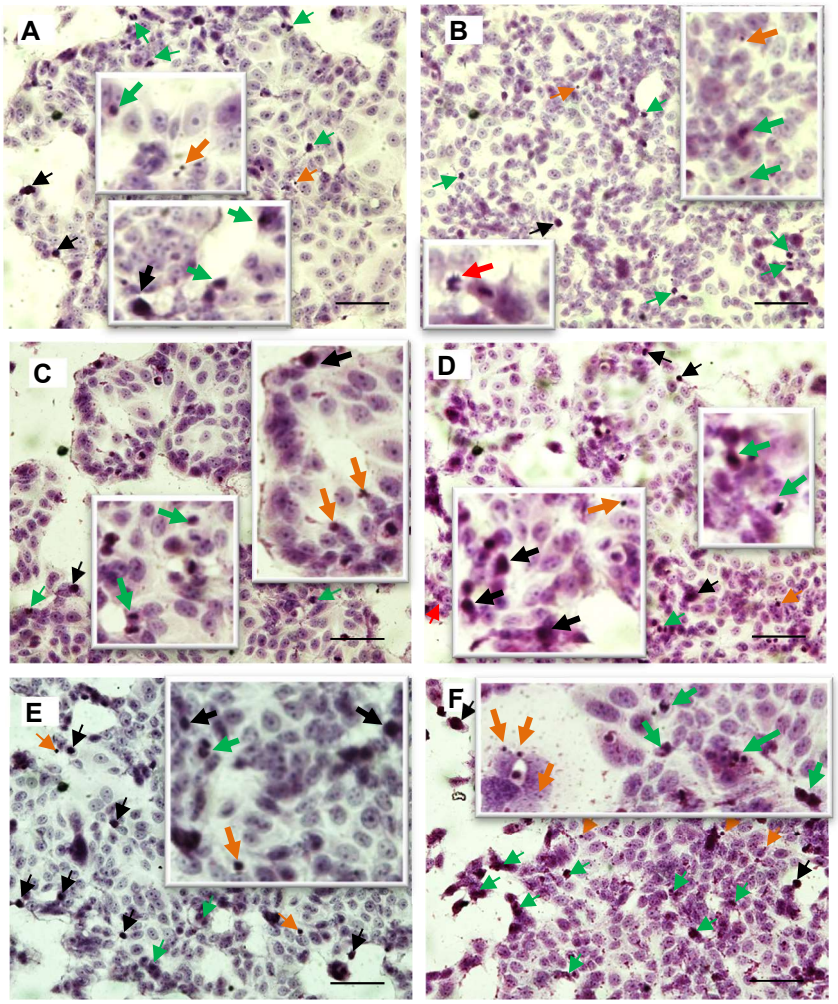


Figure 42 Microscopic images of hematoxylin and eosin (H and E) stained (A) untreated **MCF-7** and **MCF-7** treated with (B) TSA, (C) Zeb, (D) TSA and Zeb, (E) TRAIL for **48 h**; (F) TSA and Zeb for 12 h followed by TRAIL treatment for **48 h**. Scale bars represent 100 µm. The apoptotic morphologies are explained as follows: cell shrinkage and nuclear chromatin condensation (black arrows); cell membrane blebbing (red arrows); nuclear fragmentation (green arrows); apoptotic body (orange arrow). Images were captured at 20× magnification. Scale bars represent 100 µm. Insets are of same photo at higher magnification for clear view.

v

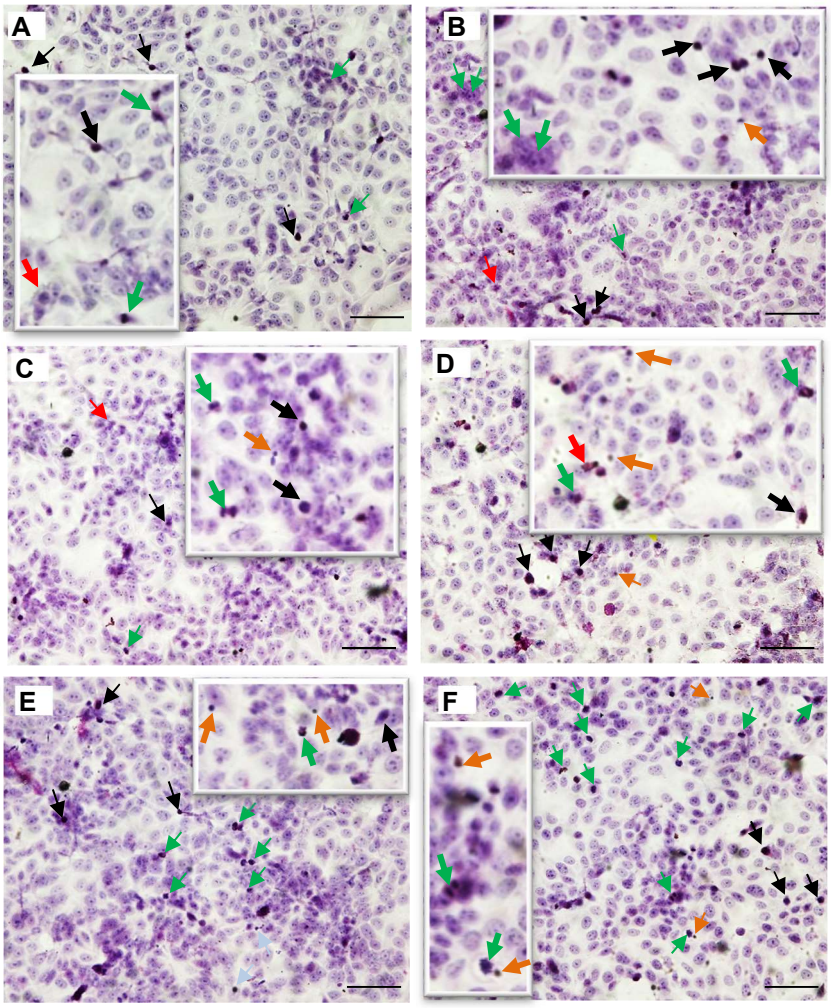


Figure 43 Microscopic images of hematoxylin and eosin (H and E) stained (A) untreated **MCF-7** and **MCF-7** treated with (B) TSA, (C) Zeb, (D) TSA and Zeb, (E) TRAIL for **72 h**; (F) TSA and Zeb for 12 h followed by TRAIL treatment for **72 h**. Scale bars represent 100 µm. The apoptotic morphologies are explained as follows: cell shrinkage and nuclear chromatin condensation (black arrows); cell membrane blebbing (red arrows); nuclear fragmentation (green arrows); apoptotic body (orange arrow). Images were captured at 20× magnification. Scale bars represent 100 µm. Insets are of same photo at higher magnification for clear view.

5.3.2 The effect of treatment on the cellular apoptosis of MDA MB-231

Apoptosis is a programmed cell death triggered by the activation of various caspases in damaged or senesced cells to maintain the body's homeostasis. Macrophages will phagocytose apoptotic cells on the basis of the translocation of phosphatidylserine (PtdSer) from the inner to the outer plasma membrane (Segawa and Nagata, 2015) in the early stage of apoptosis. Annexin V, a 35-36 kDa Ca2+ dependent phospholipid-binding protein, was shown to interact strongly and specifically with PtdSerand can be used after conjugation with fluorescein isothiocyanate (FITC) to detect apoptosis via flow cytometry by targeting for the aforementioned loss of plasma membrane asymmetry (van Engeland *et al.*, 1998). Cells being tracked from staining both Annexin V-FITC and PI negative (viable cells) to Annexin V-FITC positive, PI negative (early apoptosis) and Annexin V-FITC and PI positive (late apoptosis) are then deemed to have undergone apoptosis.

As shown in Figure 44a, TZ treatment on MDA-MB-231 for 24 h had induced the highest percentage of early and late apoptosis at 7.63% and 2.47%, respectively. TZT treatment had induced the second highest percentage of early apoptosis at 4.2% while TRAIL-treated MDA-MB-231 had a similar percentage of early and late apoptosis with that of untreated MDA-MB-231.

At 48 h post-treatment, TZ treatment remained the best inducer of apoptosis in MDA-MB-231 with 10.67% and 4.3% of early and late apoptosis, respectively. TZT-induced apoptosis remained similar to that at 24 h post-treatment (Figure 44b). From the preliminary findings at the 24 h and 48 h treatment time point, the minimal induction of apoptosis had guided us to attempt the 72 h treatment time point.

At 72 h post-treatment, TZ treatment had induced significantly ($p<0.05$) highest percentage of apoptosis in MDA-MB-231. Despite being insignificant, TZT had induced 7% more early apoptotic MDA-MB-231 population than that induced

by single TRAIL treatment (Figure 44c). The representative dot plots of MDA-MB-231 at the 24 h time point are shown in Appendix J.

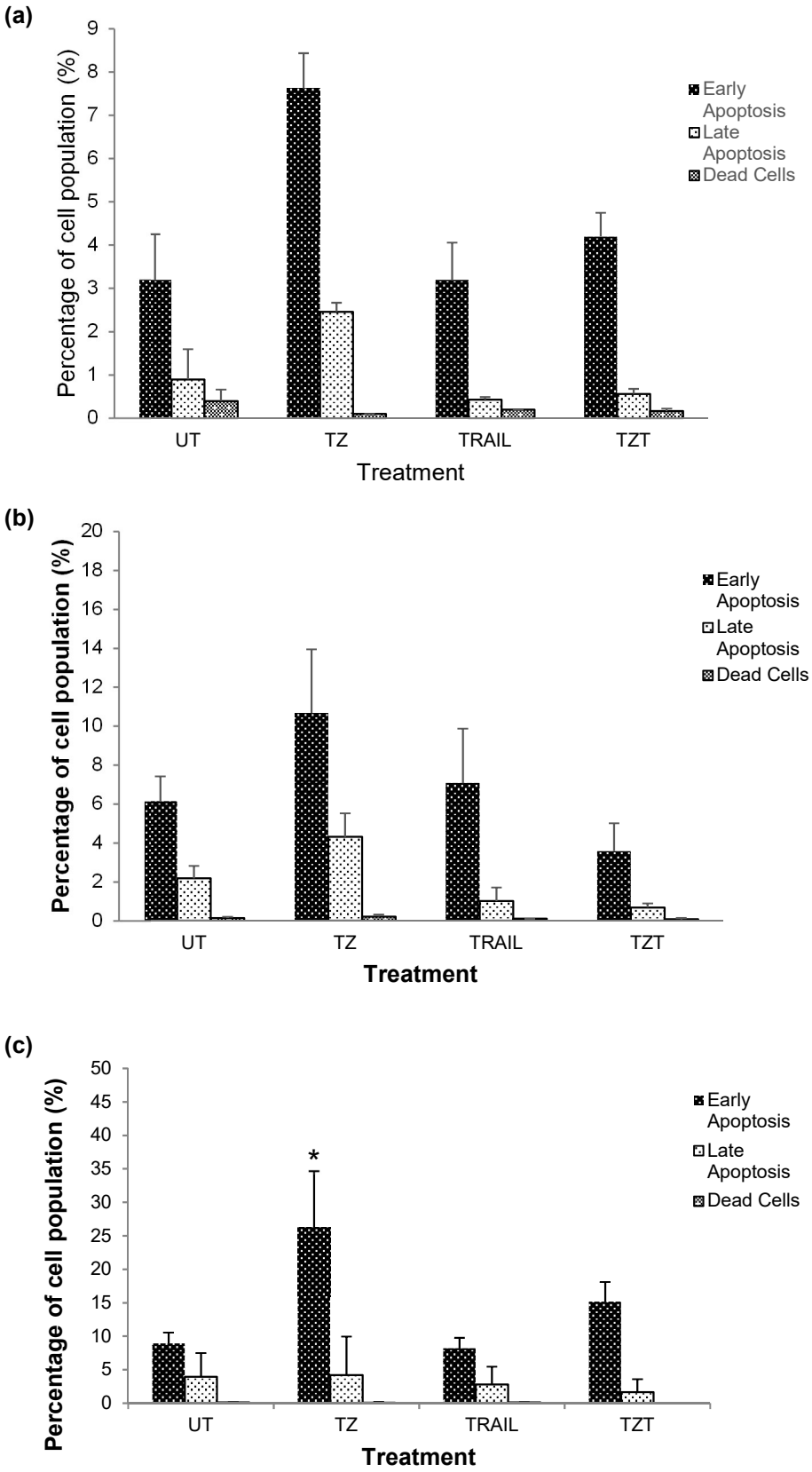


Figure 44 Percentage of cell population which has undergone early apoptosis, late apoptosis and dead from Annexin V-FITC/PI cellular apoptosis assay of different treatment groups on **MDA-MB-231** for **(a) 24**, **(b) 48 and (c) 72 h**. Data represents means ± standard deviation from one independent experiment of triplicates for (a) and (b). Data represents means ± SEM from two independent experiments of triplicates each for (c). *($p<0.05$) is significant difference from the untreated (UT) control and TRAIL treatment based on LSD mean separation.

5.3.3 The effect of treatment on the cellular apoptosis of E cadherin re-expressed MDA-MB-231 (231-EGFP)

Similar to that observed in MDA-MB-231, TZ had induced the highest percentage of apoptosis in 231-EGFP at the 24 h time point. However, in contrast to 7.63% and 2.47% of early and late apoptosis as induced by TZ treatment in MDA-MB-231, 2.2% and 0.6% of 231-EGFP had undergone early and late apoptosis, respectively, as induced by TZ treatment (Figure 45a). On the other hand, both the TRAIL and TZT treatment had not induced higher apoptosis rates as compared to the untreated 231-EGFP.

At 48 h, the trend remained the same as that of 24 h time point with TZ being most effective in inducing the highest (7.43%) percentage of cells undergoing early apoptosis while TRAIL and TZT remained ineffective in inducing appreciable higher apoptosis rate than that of untreated 231-EGFP (Figure 45b). Similar to MDA-MB-231, 72 h time point had been selected as the time point for experiment due to the preliminary finding of minimal apoptosis induction by the treatment at 24 and 48 h time points.

As treatment was prolonged to 72 h, the early apoptosis rates of 231-EGFP were similar across all experimental groups including the untreated control. On the other hand, the late apoptosis rate induced by TRAIL in 231-EGFP was the highest ($p<0.05$) among the other treatment groups. In addition, TRAIL had also significantly ($p<0.05$) induced the highest percentage of dead cells in 231-EGFP at this time point (Figure 45c). The representative dot plots of 231-EGFP at the 24 h time point are shown in Appendix K.

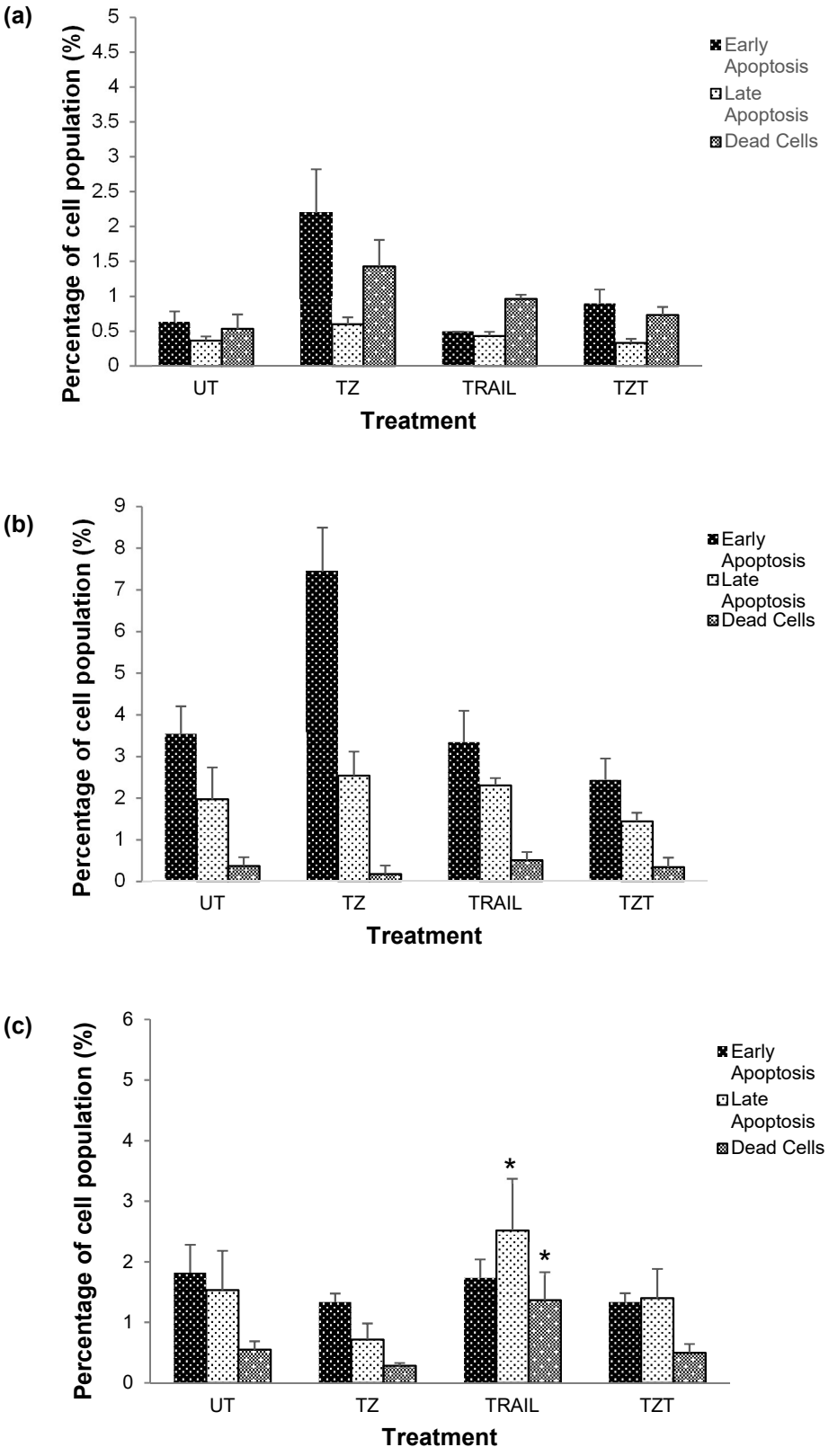


Figure 45 Percentage of cell population which are undergoing early apoptosis, late apoptosis and dead from Annexin V-FITC/PI cellular apoptosis assay of different treatment groups on **231-EGFP** for **(a) 24**, **(b) 48 and (c) 72 h**. Data represents means ± standard deviation from one independent experiment of triplicates for (a) and (b). Data represents means ± SEM from two independent experiments of triplicates each for (c). *($p<0.05$) is significant difference from the TZ treatment for late apoptosis and from all the other experimental groups for dead cells.

5.3.4 The effect of treatment on the cellular apoptosis of MCF7

At all three time points of 24, 48 and 72 h, only minimal late apoptosis events and dead cells were detected both in the untreated and treated MCF-7. Preliminary findings showed that at 24 h post-treatment, TZT did not induce appreciable increase in early apoptosis events as compared to the untreated control. TRAIL had induced the highest early apoptosis rate at 9.47% among the other experimental groups but this was only slightly higher than TZ-induced early apoptosis rate of 8.43% (Figure 46a).

At 48 h post-treatment, both the TZ and TRAIL treatments did not induce appreciable increase in early apoptosis events whereas TZT had induced approximately 3-fold increase (42.23%) in early apoptosis events in contrast to the untreated control (Figure 46b).

When the treatment was extended to 72 h, only TZ treatment significantly ($p<0.05$) doubled the early apoptosis rate from the background rate of the untreated MCF-7 while TRAIL and TZT did not significantly increase the early apoptosis rate higher than that of the background rate (Figure 46c). The representative dot plots of MCF-7 at the 24 h time point are shown in Appendix L.

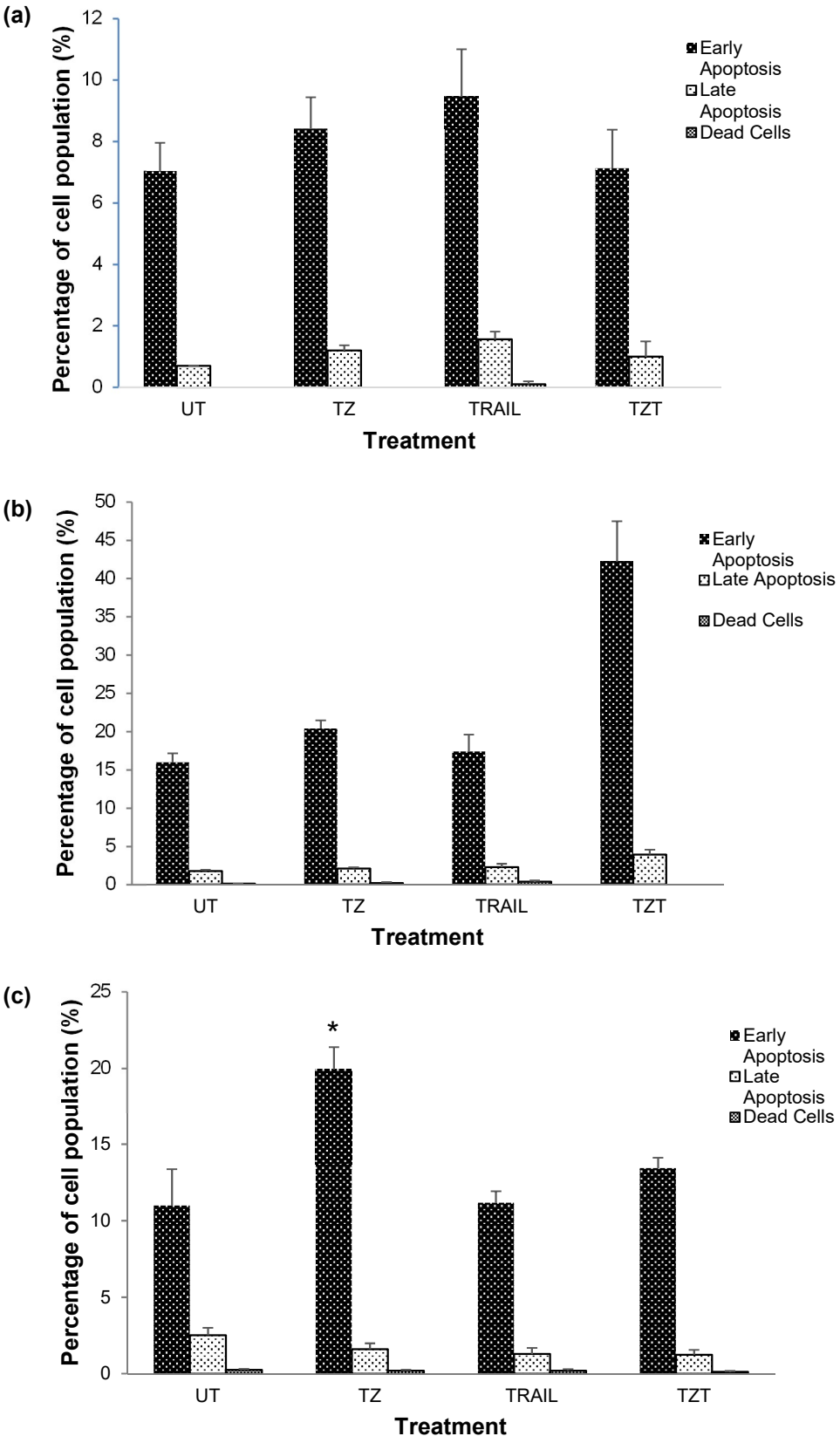


Figure 46 Percentage of cell population which are undergoing early apoptosis, late apoptosis and dead from Annexin V-FITC/PI cellular apoptosis assay of different treatment groups on **MCF-7** for **(a) 24**, **(b) 48 and (c) 72 h**. Data represents means ± standard deviation from one independent experiment of triplicates for (a) and (b). Data represents means ± SEM from two independent experiments of triplicates each. *($p<0.05$) is significant difference from all other experimental groups for early apoptosis for (c). *($p<0.05$) is significant difference from all other experimental groups for early apoptosis.

5.3.5 The effect of treatment on the protein expression of apoptosis-related genes in MDA-MB-231

Bcl-2 family is a protein family which comprises of three groups of proteins that are structurally and functionally related in the regulation of intrinsic apoptosis: 1) the pore formers, Bax and Bad, that oligomerize in the mitochondrial outer membrane (MOM), thereby permeabilizing it to release components to activate the executioner caspases; 2) the activator, BH3 proteins, which sense cellular stress and activates the pore formers and 3) the anti-apoptotic members like Bcl-2 and Bcl-xL which inhibit either the pore formers or the activators pro-apoptotic functions by interacting with them (Shamas-Din *et al.*, 2013).

At 72 h post-treatment, TZ treatment had induced a significant ($p<0.05$) increase in Bad expression and a significant *($p<0.05$) and very significant **($p<0.01$) decrease in Bcl-2 and Bcl-xL expression, respectively, in MDA-MB-231 as compared to the untreated control. TRAIL significantly *($p<0.05$) reduced Bcl-2 expression relative to the untreated control while TZT did not significantly alter the expression levels of any of the Bcl-2 family proteins investigated (Figure 47).

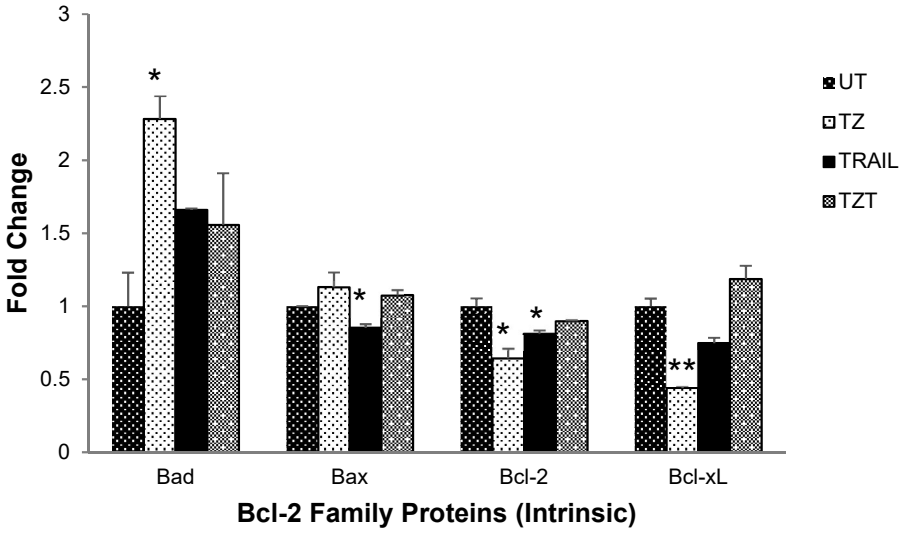


Figure 47 Bcl-2 family proteins expression in the untreated **MDA-MB-231** (UT) and MDA-MB-231 treated with TSA and Zeb (TZ), 50 ng/mL TRAIL (TRAIL) for **72 h** and TSA and Zeb for 12 h followed by TRAIL treatment for **72 h** (TZT). Data represents mean ± standard deviation. *($p<0.05$) is significant difference from UT using the Student's T-test.

On the other hand, the protein expression of some key apoptotic players in the extrinsic apoptosis pathway like TRAIL receptor 1 (TRAIL R1), TRAIL receptor 2 (TRAIL R2), Fas-associated death domain (FADD), Fas apoptosis ligand (Fas) and Tumour Necrosis Factor receptor 1 (TNF R1) had also been assessed. As shown in Figure 48 , both TZ and TRAIL treatments had significantly *($p<0.05$) increased TRAIL R1 expression at 1.68-fold and 1.39-fold, respectively, at 72 h post-treatment in MDA-MB-231. In addition, TZT had very significantly **($p<0.01$) increased TRAIL R2 expression as compared to untreated MDA-MB-231. Interestingly, TZT stood out as the only treatment that significantly *($p<0.05$) increased the expression of apoptosis ligand, Fas, in MDA-MB-231. However, none of the treatment groups had induced significant changes on the expression of FADD and TNF R1.

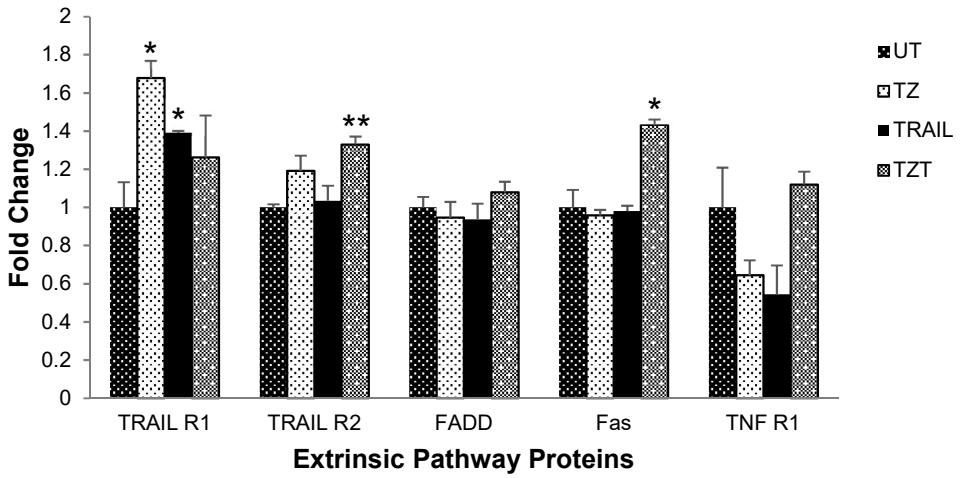


Figure 48 Extrinsic pathway proteins expression in the untreated **MDA-MB-231** (UT) and **MDA-MB-231** treated with TSA and Zeb (TZ), 50 ng/mL TRAIL (TRAIL) for **72 h** and TSA and Zeb for 12 h followed by TRAIL treatment for **72 h** (TZT). Data represents mean ± standard deviation. *($p<0.05$) and **($p<0.01$) are significant and very significant differences from UT using the Student's T-test.

Apart from the distinctive apoptosis players which constitute the extrinsic and intrinsic apoptosis pathways, respectively, the expression of other pro-apoptotic proteins like pro-caspase-3, cleaved caspase-3 and cytochrome c had also been analysed in MDA-MB-231 at 72 h post-treatment. Surprisingly, all treatment groups did not significantly enhance both the pro-caspase 3 and cleaved caspase-3 expression levels as compared to the untreated control. Intriguingly, cytochrome c expression levels had been significantly *($p<0.05$) downregulated by all the three treatment groups (Figure 49).

On the other hand, the anti-apoptotic proteins, catalase and paraoxonase-2 (PON2) remained largely at the basal expression levels with the exception of TZ treatment which induced a 2.2-fold increase in PON2 expression in contrast to that of the untreated MDA-MB-231. Conversely, the anti-apoptotic protein, clusterin, had been significantly *($p<0.05$) down-regulated for 50 to 60% by TZ, TRAIL and TZT treatments (Figure 49).

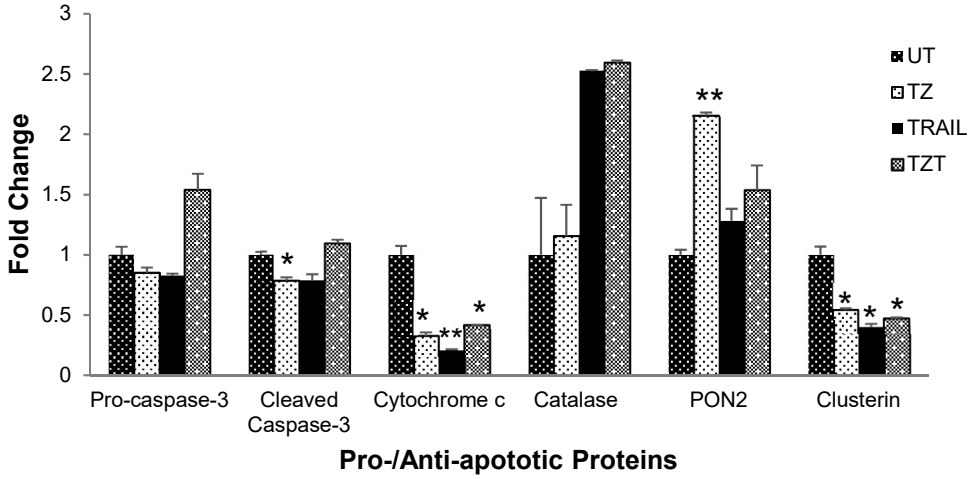


Figure 49 The expression of **pro-apoptotic proteins** (pro-caspase-3, cleaved caspase-3 and cytochrome c) and **anti-apoptotic proteins** (catalase, PON2, and clusterin) in the untreated **MDA-MB-231** (UT) and **MDA-MB-231** treated with TSA and Zeb (TZ), 50 ng/mL TRAIL (TRAIL) for **72 h** and TSA and Zeb for 12h followed by TRAIL treatment for **72 h** (TZT). Data represents mean ± standard deviation. *($p<0.05$) and **($p<0.01$) are significant and very significant differences from UT using the Student's T-test.

Subsequently, the protein expression of the family of inhibitors of apoptosis proteins (IAPs) and their inhibitors was also assessed to further delineate the apoptosis molecular events induced by the treatment groups. As shown in Figure 50, cellular inhibitor of apoptosis protein 1 (cIAP-1) and cellular inhibitor of apoptosis protein 2 (cIAP-2) were neither down-regulated not up-regulated in all the treatment groups. Nonetheless, TZ, TRAIL and TZT treatments had all consistently and significantly *($p<0.05$) down-regulated the IAPs, Livin, Survivin and X-linked inhibitor of apoptosis (XIAP). Concurrently, TZ and TZT but not TRAIL had significantly *($p<0.05$) up-regulated the second mitochondria-derived activator of caspase (SMAC). TZT had induced the highest SMAC expression at 1.19-fold relative to the untreated MDA-MB-231 (Figure 50).

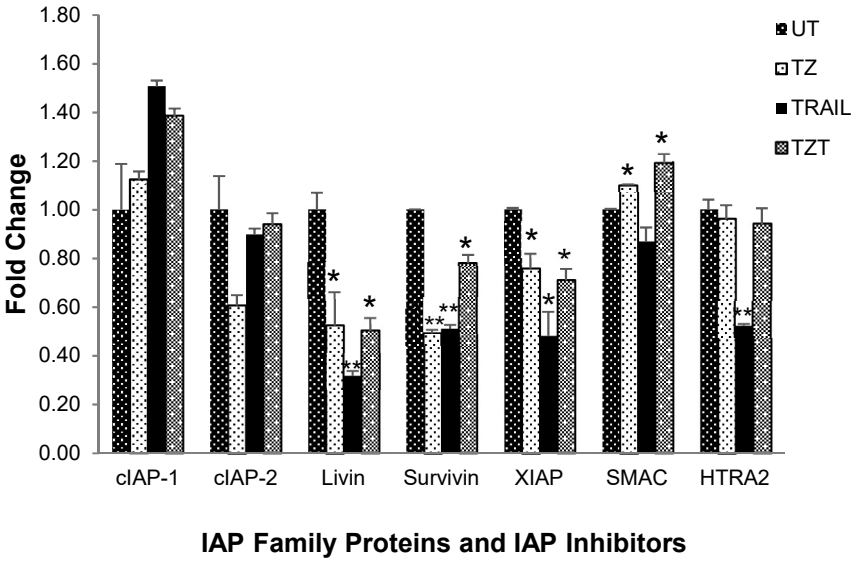


Figure 50 The protein expression of **IAP family proteins** (cIAP-1, cIAP-2, Livin, Survivin and XIAP) and **IAP inhibitors** (SMAC and HTRA2) in untreated MDA-MB-231 (UT) and MDA-MB-231 treated with TSA and Zeb (TZ), 50 ng/mL TRAIL (TRAIL) for **72 h** and TSA and Zeb for 12h followed by TRAIL treatment for **72 h** (TZT). Data represents mean ± standard deviation. *($p<0.05$) and **($p<0.01$) are significant and very significant differences from UT using the Student's T-test.

With regards to apoptosis study, it is worthwhile to also assess the cell cycle regulators because cell cycle checkpoint signalling can lead to the activation of apoptotic pathway in the event of cellular damage which is beyond reparable (Pietenpol and Stewart, 2002). As depicted in Figure 51, p21, cyclin-dependent kinase inhibitor 1, which induces G_0/G_1 cell cycle arrest upon induction (Wang *et al.*, 2013b), was significantly *($p<0.05$) up-regulated by the TZT treatment. On the other hand, among the differentially phosphorylated p53 forms, TZT had induced a very significant **($p<0.01$) 2.37-fold increase of phospho-p53 (Ser392) (p-p53 S392) relative to the untreated MDA-MB-231. In addition, TZT had also *($p<0.05$) significantly up-regulated another checkpoint inhibition activator for G_0/G_1 arrest, phospho-Rad17 (Ser635) (p-Rad17 S635), for 1.68-fold relative to untreated MDA-MB-231 (Figure 51).

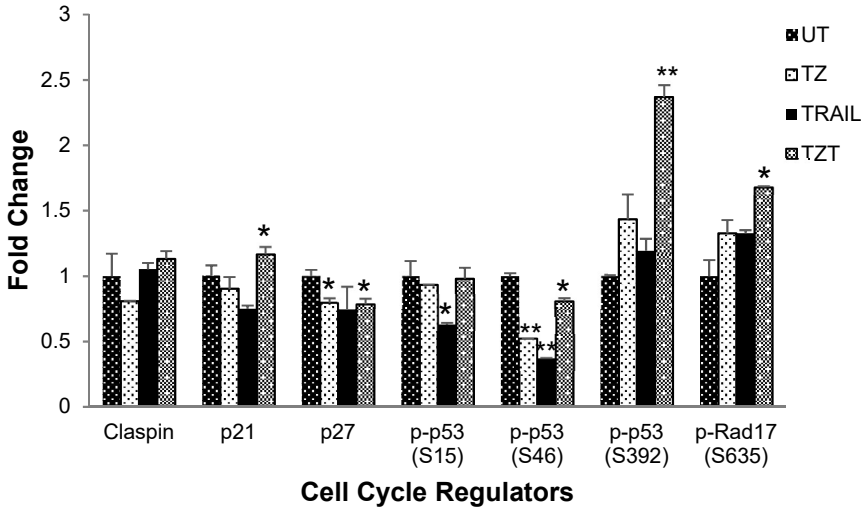


Figure 51 The expression of **cell cycle regulators** in the untreated MDA-MB-231 (UT) and MDA-MB-231 treated with TSA and Zeb (TZ), 50 ng/mL TRAIL (TRAIL) for **72 h** and TSA and Zeb for 12h followed by TRAIL treatment for **72 h** (TZT). Data represents mean ± standard deviation. *($p<0.05$) and **($p<0.01$) are significant and very significant differences from UT using the Student's T-test.

Eventually, several cell stress proteins had also been included in the apoptosis antibody array protein expression study due to the tight link of cellular stress response to cellular survivability or cellular demise (Fulda *et a.l*, 2010). The protein expression of Heme oxygenase (decycling) 1 (HMOX1) and heme oxygenase (decycling) 2 (HMOX2) remained largely unaltered by all the treatment groups (Figure 52). TZT treatment had induced a very significant **($p<0.01$) up-regulation of hypoxia-inducible factor 1-alpha (HIF-1-α) and a significant increase in the expression of heat shock protein 27 (HSP27) while significantly *($p<0.05$) down-regulating heat shock protein 70 (HSP70). On the other hand, both TZ and TRAIL had significantly *($p<0.05$) reduced the expression of HIF-1-α, HSP70 and heat shock protein 60 (HSP60) (Figure 52). The processed antibody array sheet image of MDA-MB-231 at the 72 h time point is shown in Appendix M.

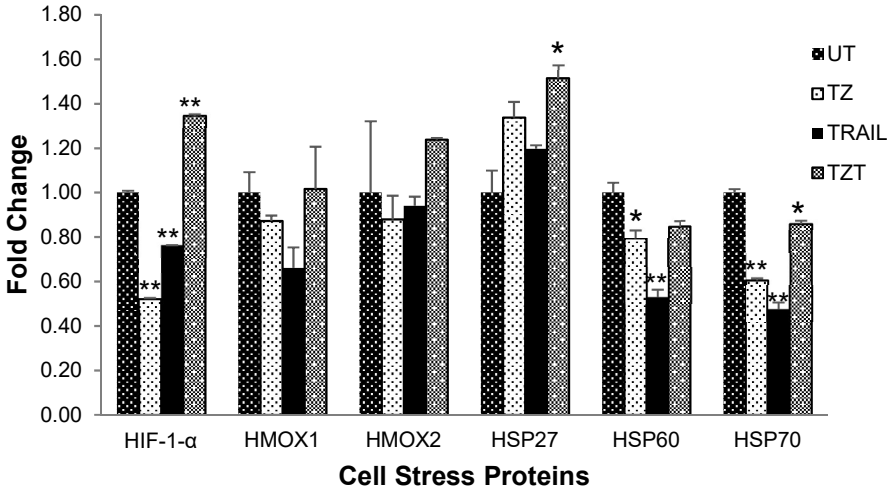


Figure 52 The protein expression of **cell stress proteins** in the untreated MDA-MB-231 (UT) and MDA-MB-231 treated with TSA and Zeb (TZ), 50 ng/mL TRAIL (TRAIL) for **72 h** and TSA and Zeb for 12h followed by TRAIL treatment for **72 h** (TZT). Data represents mean ± standard deviation. *($p<0.05$) and **($p<0.01$) are significant and very significant differences from UT using the Student's T-test.

5.3.6 The effect of treatment on the protein expression of apoptosis-related genes in 231-EGFP

Similar to the assessment on the protein expression of apoptosis-related genes done on MDA-MB-231 as reported above, the assessment on the protein expression of the same set of apoptosis-related genes had been made on MDA-MB-231 re-expressed with E-cadherin (231-EGFP). TZ treatment for 72 h had induced a very significant **($p<0.01$) increase in expression of the pro-apoptotic protein, Bad, in contrast to untreated 231-EGFP. Nonetheless, TZ had also concurrently elevated the expression of the anti-apoptotic proteins, Bcl-2 and Bcl-xL very significantly **($p<0.01$) and significantly *($p<0.05$), respectively, from the untreated 231-EGFP (Figure 53).

On the other hand, both TRAIL and TZT treatments for 72 h had significantly *($p<0.05$) and very significantly **($p<0.01$) reduced the expression of Bcl-xL and Bcl-2, respectively. However, both TRAIL and TZT treatments had also induced significant *($p<0.05$) and very significant **($p<0.01$) reduction in expression of the pro-apoptotic proteins, Bad and Bax, respectively (Figure 53).

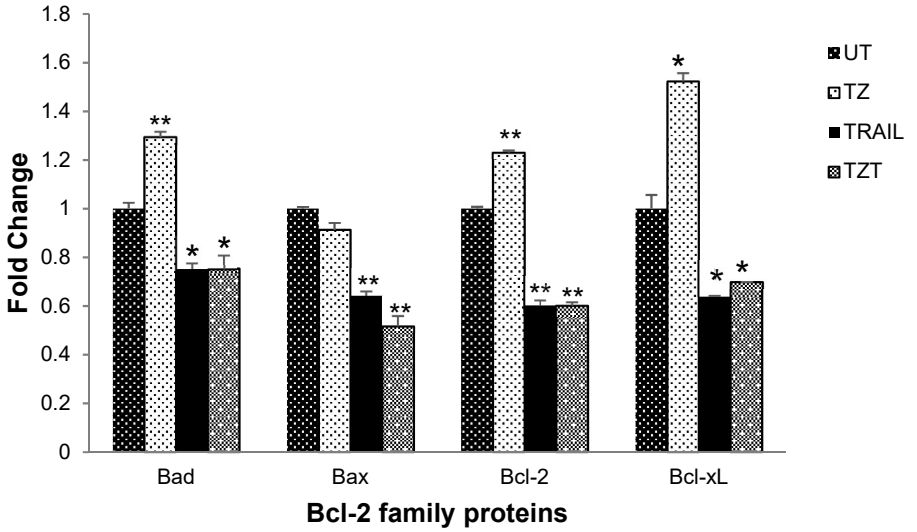


Figure 53 Bcl-2 family proteins expression in the untreated **231-EGFP** (UT) and **231-EGFP** treated with TSA and Zeb (TZ), 50 ng/mL TRAIL (TRAIL) for **72 h** and TSA and Zeb for 12h followed by TRAIL treatment for **72 h** (TZT). Data represents mean $\pm$ standard deviation. *($p<0.05$) and **($p<0.01$) are significant and very significant differences from UT using the Student's T-test.

The protein expression of some of the key extrinsic apoptotic players had also been studied in 231-EGFP. At 72 h post-treatment, TZ treatment had induced 1.62-fold **($p<0.01$), 1.45-fold *($p<0.05$) and 1.69-fold **($p<0.01$) increase in the expression of the extrinsic death receptors, TRAIL R1, TRAIL-R2, and TNF R1, respectively. Concurrently, TZ had also induced 1.23-fold **($p<0.01$) and 1.19-fold *($p<0.05$) increase in expression of FADD and Fas, respectively (Figure 54).

Intriguingly, TRAIL treatment for 72 h did not significantly alter TRAIL R1 and TRAIL-R2 expression but had significantly *($p<0.05$) reduced TNF R1 expression to 0.44-fold of the untreated 231-EGFP. At the same time, TRAIL treatment had also down-regulated FADD and Fas to 0.71-fold **($p<0.01$) and 0.65-fold *($p<0.05$), respectively, as compared to the untreated 231-EGFP (Figure 54). Similar trend had been observed for TZT treatment whereby it had very significantly **($p<0.01$) down-regulated the extrinsic death receptors of TRAIL R1, TRAIL R2 and TNF R1. Concurrently, it had also significantly *($p<0.05$) down-regulated FADD and Fas to 0.72-fold and 0.64-fold, respectively, in contrast to the untreated 231-EGFP (Figure 54).

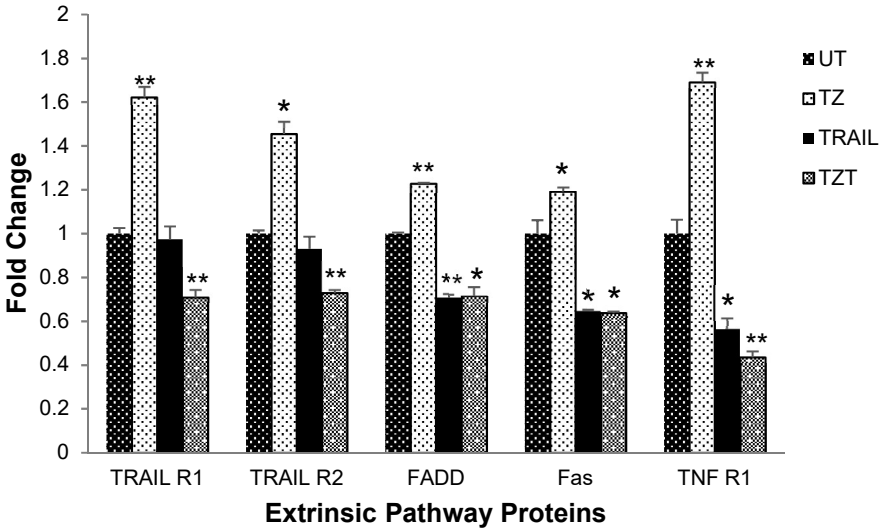


Figure 54 Extrinsic pathway proteins expression in the untreated **231-EGFP** (UT) and **231-EGFP** treated with TSA and Zeb (TZ), 50 ng/mL TRAIL (TRAIL) for **72 h** and TSA and Zeb for 12h followed by TRAIL treatment for **72 h** (TZT). Data represents mean ± standard deviation. *($p<0.05$) and **($p<0.01$) are significant and very significant differences from UT using the Student's T-test.

In addition to the key intrinsic and extrinsic apoptotic pathway players, the other pro-apoptotic proteins' expression levels like pro-caspase-3, cleaved caspase-3 and cytochrome c had also been investigated in 231-EGFP. At 72 h post-treatment, TZ had significantly *($p<0.05$) up-regulated the cleaved caspase-3 to 1.42-fold as compared to untreated 231-EGFP. TRAIL did not significantly alter the expression of pro-caspase-3 and cleaved caspase-3 but had significantly *($p<0.05$) reduced cytochrome c expression. In addition, TZT treatment had significantly *($p<0.05$) and very significantly *($p<0.01$) down-regulated pro-caspase-3 and cytochrome c, respectively, while having no significant alteration on cleaved caspase-3 expression (Figure 55).

On the other hand, the anti-apoptotic proteins, catalase, PON2 and clusterin, had also been studied their protein expression levels both in untreated 231-EGFP and treated 231-EGFP. Surprisingly, TZ treatment had significantly up-regulated all the anti-apoptotic proteins at 1.87-fold (catalase), 1.34-fold (PON2) and 1.52-fold (clusterin) in contrast to untreated 231-EGFP. On the other hand, TRAIL had significantly *($p<0.05$) down-regulated PON2 expression to 0.76-fold of the untreated control while TZT had significantly down-regulated all the anti-apoptotic proteins to 0.62-fold *($p<0.05$), 0.65-fold *($p<0.05$) and 0.62-fold **($p<0.01$) for catalase, PON2 and clusterin, respectively (Figure 55).

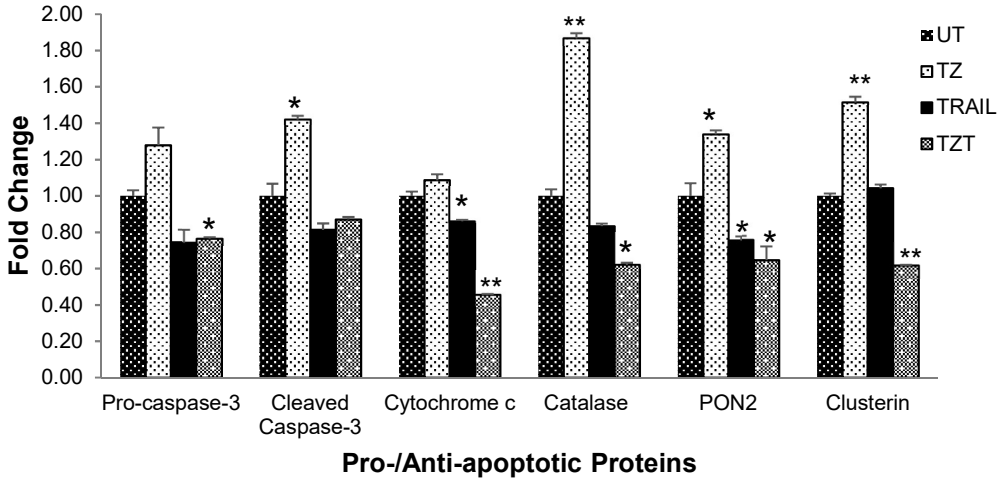


Figure 55 The expression of **pro-apoptotic proteins** (pro-caspase-3, cleaved caspase-3 and cytochrome c) and **anti-apoptotic proteins** (catalase, PON2, and clusterin) in the untreated **231-EGFP** (UT) and **231-EGFP** treated with TSA and Zeb (TZ), 50 ng/mL TRAIL (TRAIL) for **72 h** and TSA and Zeb for 12h followed by TRAIL treatment for **72 h** (TZT). Data represents mean ± standard deviation. *($p<0.05$) and **($p<0.01$) are significant and very significant differences from UT using the Student's T-test.

Next, the protein expression of the family of inhibitors of apoptosis proteins (IAPs) and their inhibitors was also assessed to further elucidate the apoptosis molecular events induced by the treatment groups in 231-EGFP. Surprisingly, TZ treatment for 72 h had very significantly **($p<0.01$) up-regulated both the IAPs (cIAP-1, cIAP-2, Survivin, XIAP) as well as their inhibitors SMAC and HTRA2. (Figure 56).

On the contrary, TRAIL treatment for 72 h had down-regulated cIAP-2, Livin and Survivin to 0.68-fold **($p<0.01$), 0.78-fold *($p<0.05$) and 0.87-fold *($p<0.05$), respectively while concomitantly reducing IAP inhibitor, HTRA2 to 0.72-fold **($p<0.01$) in comparison with the untreated control (Figure 56). As for TZT treatment, it had induced very significant **($p<0.01$) down-regulation of IAPs, cIAP-2, Livin, Survivin and XIAP to 0.69-fold, 0.45-fold, 0.77-fold and 0.57-fold, respectively. Nonetheless, TZT had also caused down-regulation of IAP inhibitors SMAC and HTRA2 to 0.8-fold *($p<0.05$) and 0.43-fold **($p<0.01$), respectively (Figure 56).

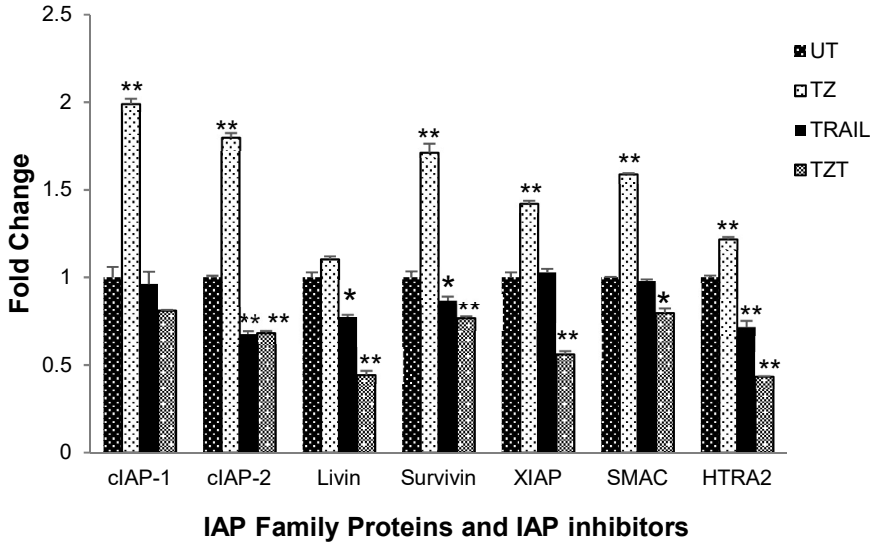


Figure 56 The protein expression of **IAP family proteins** (cIAP-1, cIAP-2, Livin, Survivin and XIAP) and **IAP inhibitors** (SMAC and HTRA2) in the untreated **231-EGFP** (UT) and **231-EGFP** treated with TSA and Zeb (TZ), 50 ng/mL TRAIL (TRAIL) for **72 h** and TSA and Zeb for 12 h followed by TRAIL treatment for **72 h** (TZT). Data represents mean $\pm$ standard deviation. *($p<0.05$) and **($p<0.01$) are significant and very significant differences from UT using the Student's T-test.

Besides, the protein expression levels of several cell cycle regulators that have shown to be tightly linked to apoptosis regulation had also been assessed in 231-EGFP. At 72 h post-treatment, TZ treatment had induced very significant **($p<0.01$) up-regulation of p21, p-p53 (S15), p-p53 (S46), p-p53 (S392) and p-Rad 17 (S635) and significant *($p<0.05$) up-regulation of p27 as compared to the untreated control. Claspin expression was not significantly altered by TZ treatment but had been very significantly **($p<0.01$) down-regulated by both TRAIL and TZT treatments (Figure 57).

In contrast to TZ treatment, TRAIL treatment had very significantly **($p<0.01$) down-regulated p21, p27, p-p53 (S15), p-p53 (S46) and significantly *($p<0.05$) down-regulated p-p53 (S392). TZT treatment had also induced similar trend of very significantly **($p<0.01$) down-regulating p21, p27, p-p53 (S15) and p-p53 (S392) while significantly *($p<0.05$) down-regulating p-Rad 17 (S635) (Figure 57).

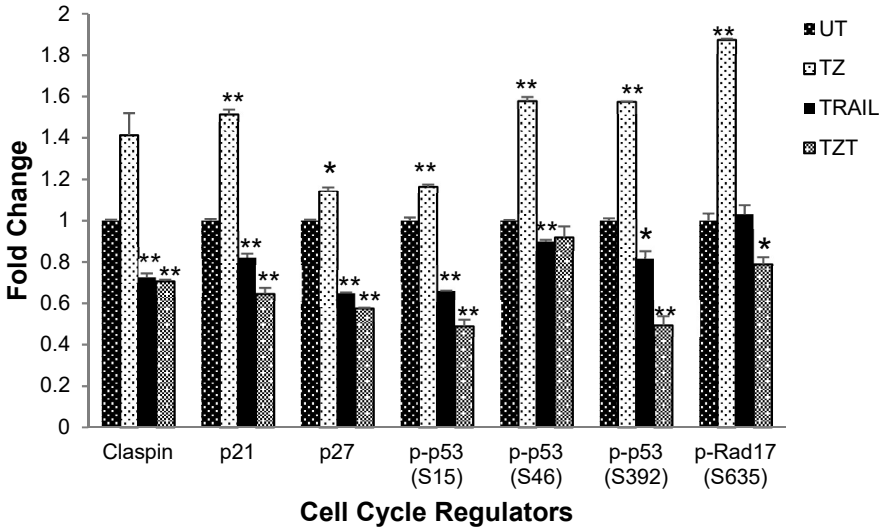


Figure 57 The expression of **cell cycle regulators** in the untreated **231-EGFP** (UT) and **231-EGFP** treated with TSA and Zeb (TZ), 50 ng/mL TRAIL (TRAIL) for **72 h** and TSA and Zeb for 12 h followed by TRAIL treatment for **72 h** (TZT). Data represents mean ± standard deviation. *($p<0.05$) and **($p<0.01$) are significant and very significant differences from UT using the Student's T-test.

Eventually, a few selected cell stress proteins had also been studied on their protein expression levels both in untreated and treated 231-EGFP. At the 72 h treatment time-point, HMOX1, HMOX2, HSP27 and HSP60 had been up-regulated by TZ treatment for 1.36-fold **($p<0.01$), 2.14-fold **($p<0.01$), 2.1-fold **($p<0.01$) and 1.32-fold *($p<0.05$), respectively (Figure 58).

On the other hand, TRAIL treatment did not have significant impact on the expression of HMOX2 and HSP27. However, TRAIL treatment had significantly down-regulated HIF-1-α, HMOX1, HSP60 and HSP70 to 0.71-fold **($p<0.01$), 0.6-fold *($p<0.05$), 0.61-fold *($p<0.05$) and 0.65-fold *($p<0.05$), respectively, of the untreated 231-EGFP. As for TZT treatment, it had down-regulated HIF-1-α, HMOX1, HSP27, HSP60 and HSP70 to 0.59-fold **($p<0.01$), 0.67-fold **($p<0.01$), 0.9-fold *($p<0.05$), 0.6-fold *(0.05) and 0.66-fold *($p<0.05$), respectively, in comparison with the untreated control (Figure 58). The processed antibody array sheet image of MDA-MB-231 at the 72 h time point is shown in Appendix N.

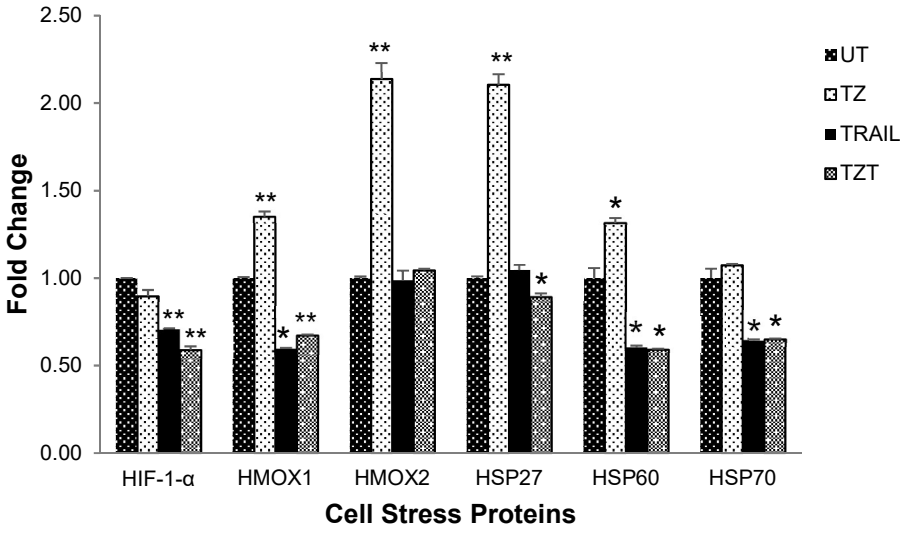


Figure 58 The protein expression of **cell stress proteins** in the untreated **231-EGFP** (UT) and **231-EGFP** treated with TSA and Zeb (TZ), 50 ng/mL TRAIL (TRAIL) for **72 h** and TSA and Zeb for 12 h followed by TRAIL treatment for **72 h** (TZT). Data represents mean ± standard deviation. *($p<0.05$) and **($p<0.01$) are significant and very significant differences from UT using the Student's T-test.

5.3.7 The effect of treatment on the protein expression of apoptosis-related genes in MCF-7

In this section, the protein expression of the same set of apoptosis-related genes had been assessed in the human breast adenocarcinoma cells, MCF-7, which inherently expresses E-cadherin, serving as an E-cadherin-positive control in comparison with 231-EGFP. Similar to that observed in 231-EGFP, TZ treatment had up-regulated the intrinsic pro-apoptotic proteins, Bad and Bax, for 1.56-fold *($p<0.05$) and 1.39-fold **($p<0.01$), respectively, with reference to the basal expression level in untreated MCF-7 (Figure 59). In addition, TZT had stimulated the highest up-regulation of Bad and Bax proteins at 1.72-fold *($p<0.05$) and 1.59-fold **($p<0.01$), respectively, in comparison with untreated MCF-7. On the other hand, single TRAIL treatment did not significantly increase the expression of both the pro-apoptotic proteins, Bad and Bax (Figure 59).

Nonetheless, TZ treatment had also concurrently induced up-regulation of the intrinsic anti-apoptotic proteins, Bcl-2 and Bcl-xL, to 1.61-fold **($p<0.01$) and 2.26-fold *($p<0.05$), respectively, in contrast to untreated MCF-7. Besides, TZT treatment had also caused up-regulation of Bcl-2 for 1.65-fold **($p<0.01$). However, single TRAIL treatment had very significantly **($p<0.01$) down-regulated Bcl-2 expression (Figure 59).

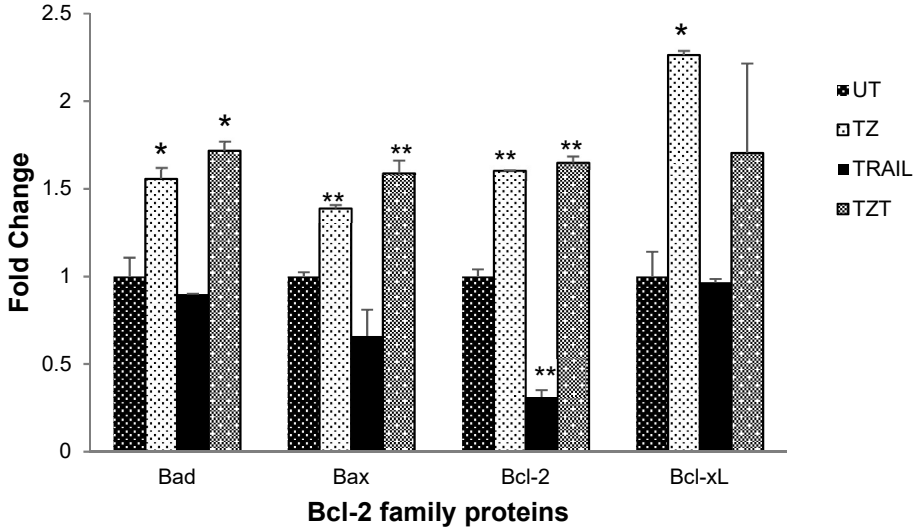


Figure 59 Bcl-2 family proteins expression in the untreated **MCF-7** (UT) and **MCF-7** treated with TSA and Zeb (TZ), 50 ng/mL TRAIL (TRAIL) for **72 h** and TSA and Zeb for 12h followed by TRAIL treatment for **72 h** (TZT). Data represents mean ± standard deviation. *($p<0.05$) and **($p<0.01$) are significant and very significant differences from UT using the Student's T-test.

In the axis of extrinsic apoptotic pathway, some of the key apoptotic ligands and their receptors had also been assessed for their protein expression levels both in the untreated and treated groups. Both TZ and TZT treatments had significantly up-regulated TRAIL R1 and TRAIL R2. The up-regulation stimulated by TZ was 1.43-fold **($p<0.01$) and 1.7-fold **($p<0.01$) for TRAIL R1 and TRAIL R2, respectively, which was slightly higher than that induced by TZT at 1.32-fold *($p<0.05$) and 1.51-fold **($p<0.01$), respectively. In addition, TZT was the only treatment that had significantly *($p<0.05$) up-regulated TNF R1 to 2.1-fold as compared to untreated MCF-7. On the other hand, single TRAIL treatment remained insignificant in the up-regulation of both TRAIL R1 and TRAIL R2 (Figure 60).

In terms of extrinsic apoptotic ligand, TZ treatment was the only treatment that had significantly *($p<0.05$) up-regulated the Fas ligand. It also remained as the only treatment that had significantly **($p<0.01$) up-regulated FADD despite the small increase in fold-change (Figure 60).

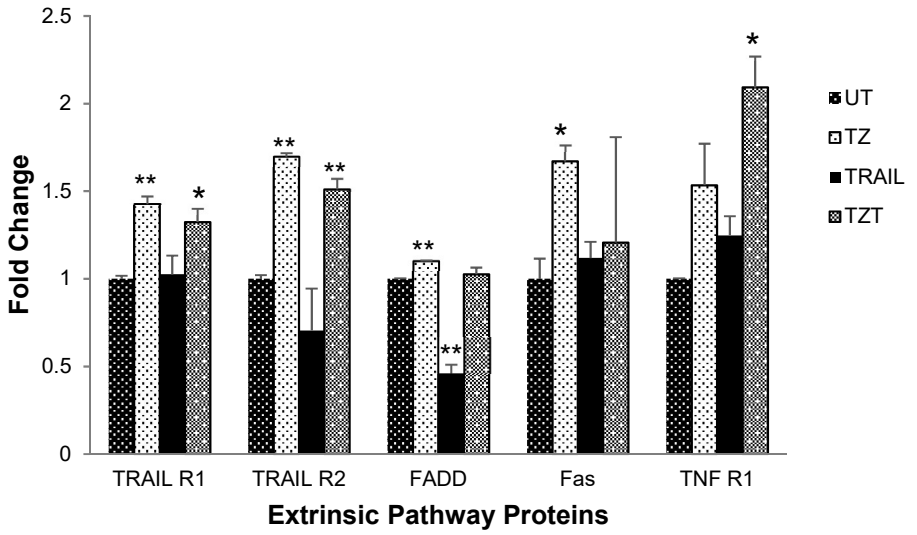


Figure 60 Extrinsic pathway proteins expression in the untreated **MCF-7** (UT) and **MCF-7** treated with TSA and Zeb (TZ), 50 ng/mL TRAIL (TRAIL) for **72 h** and TSA and Zeb for 12 h followed by TRAIL treatment for **72 h** (TZT). Data represents mean ± standard deviation. *($p<0.05$) and **($p<0.01$) are significant and very significant differences from UT using the Student's T-test.

The expression changes of some of the other pro- and anti-apoptotic proteins had also been investigated in MCF-7. As shown in Figure 61, TZ was the only treatment that had significantly *($p<0.05$) up-regulated pro-caspase-3 to 1.5-fold of the untreated MCF-7. Besides, both TRAIL and TZT treatments had significantly *($p<0.05$) induced 3.3-fold and 2.95-fold up-regulation of cytochrome c, respectively. Nevertheless, there were no significant changes induced by any of the treatment groups on the expression level of cleaved caspase-3 (Figure 61).

On the other hand, TZT treatment had significantly *($p<0.05$) down-regulated the anti-apoptotic protein, catalase to 0.8-fold of untreated MCF-7. Besides, TZT had also induced a very significant **($p<0.01$) down-regulation of the anti-apoptotic protein, PON2 at 0.85-fold. Concurrently, TRAIL had also significantly *($p<0.05$) down-regulated PON2 to 0.53-fold of the untreated control. However, TZ had up-regulated PON2, for 1.21-fold. Despite having a down-regulatory effect on the anti-apoptotic proteins, catalase and PON2, both TRAIL and TZT treatments had induced very significant **($p<0.01$) up-regulation of the anti-apoptotic protein, clusterin, at 2.23-fold and 2.65-fold, respectively (Figure 61).

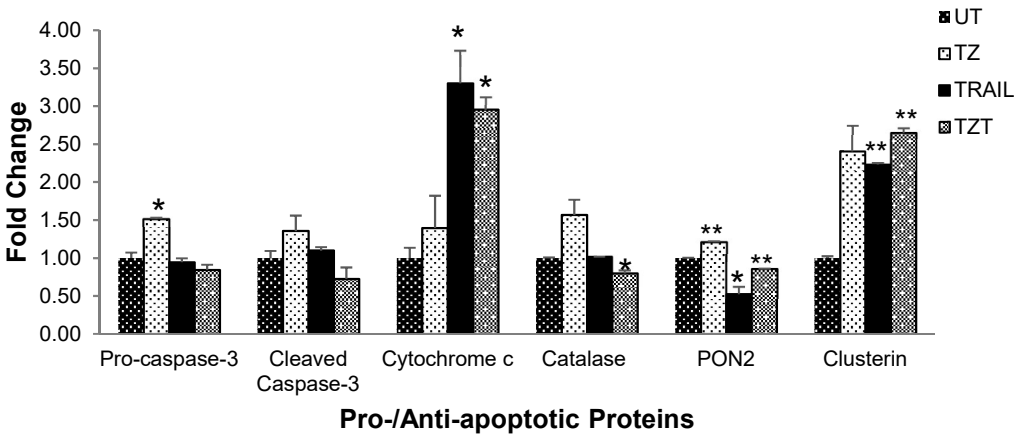


Figure 61 The expression of **pro-apoptotic proteins** (pro-caspase-3, cleaved caspase-3 and cytochrome c) and **anti-apoptotic proteins** (catalase, PON2, and clusterin) in the untreated **MCF-7** (UT) and **MCF-7** treated with TSA and Zeb (TZ), 50 ng/mL TRAIL (TRAIL) for **72 h** and TSA and Zeb for 12 h followed by TRAIL treatment for **72 h** (TZT). Data represents mean ± standard deviation. *($p<0.05$) and **($p<0.01$) are significant and very significant differences from UT using the Student's T-test.

The protein expression changes of several IAP family proteins and their inhibitors are depicted in Figure 62. Among the IAP family proteins that were investigated, only cIAP-1 had been significantly **($p<0.01$) down-regulated by TZT treatment to 0.54-fold of untreated MCF-7. The expression of Livin remained unchanged across all treatment groups while single TRAIL treatment alone had significantly *($p<0.05$) up-regulated XIAP (Figure 62). In addition, single TRAIL treatment had very significantly *($p<0.01$) up-regulated cIAP-1 to 1.4-fold while TZ and TZT treatments had induced up-regulation of cIAP-2 to 1.7-fold **($p<0.01$) and 1.35-fold *($p<0.05$), respectively. In the case of Survivin, all three treatments of TZ, TRAIL and TZT had induced very significant **($p<0.01$) increase in the expression of Survivin (Figure 62).

On the other hand, in terms of the expression changes of IAPs inhibitors, SMAC had been significantly up-regulated to 1.35-fold **($p<0.01$), 1.32-fold **($p<0.01$) and 1.22-fold *($p<0.05$) by TZ, TRAIL and TZT treatments, respectively. Nonetheless, only TRAIL and TZT treatments had induced significant up-regulation of HTRA2 at 1.45-fold **($p<0.01$) and 1.4-fold *($p<0.05$), respectively (Figure 62).

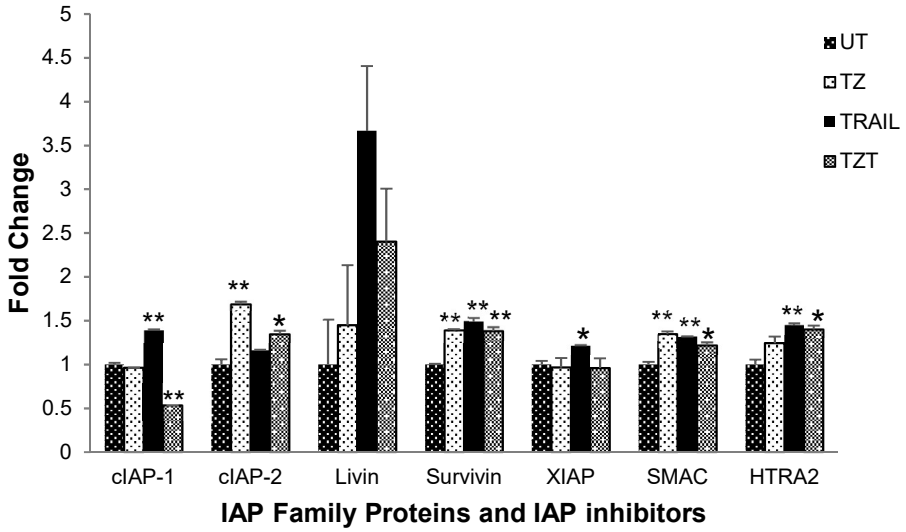


Figure 62 The protein expression of **IAP family proteins** (cIAP-1, cIAP-2, Livin, Survivin and XIAP) and **IAP inhibitors** (SMAC and HTRA2) in the untreated **MCF-7** (UT) and **MCF-7** treated with TSA and Zeb (TZ), 50 ng/mL TRAIL (TRAIL) for **72 h** and TSA and Zeb for 12 h followed by TRAIL treatment for **72 h** (TZT). Data represents mean ± standard deviation. *($p<0.05$) and **($p<0.01$) are significant and very significant differences from UT using the Student's T-test.

In addition, a set of cell cycle regulators had also been tested for their protein expression levels both in untreated and treated MCF-7, similar to that conducted in MDA-MB-231 and 231-EGFP. All the three treatments of TZ, TRAIL and TZT had induced very significant **($p<0.01$) increase in the expression of Claspin with TZT-induced up-regulation being the highest at 2.17-fold of untreated MCF-7. In addition, TZT treatment had also caused a surge in expression of p27 at 6.75-fold **($p<0.01$) of the untreated control. It had also caused a slight up-regulation of p-p53 (S46) of 1.28-fold *($p<0.05$) (Figure 63).

On the other hand, TZ treatment had significantly increased a number of cell cycle regulators which include p21 (1.94-fold), p27 (3.17-fold), p-p53 (S15) (2.05-fold), p-p53 (S46) (3.13-fold) and p-p53 (S392) (2.26-fold). Nonetheless, TRAIL had significantly up-regulated only p21 (1.18-fold) and p-p53 (S46) (1.63-fold) while down-regulating p27 to 0.47-fold of the untreated control. In all the treatments tested, no significant up-regulation or down-regulation of p-Rad 17(S635) was observed (Figure 63).

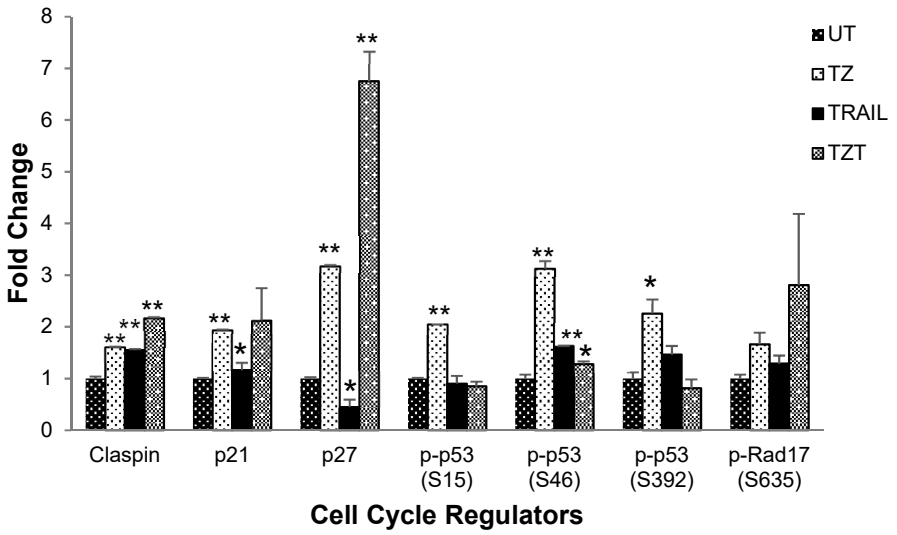


Figure 63 The expression of **cell cycle regulators** in the untreated **MCF-7** (UT) and **MCF-7** treated with TSA and Zeb (TZ), 50 ng/mL TRAIL (TRAIL) for **72 h** and TSA and Zeb for 12 h followed by TRAIL treatment for **72 h** (TZT). Data represents mean ± standard deviation. *($p<0.05$) and **($p<0.01$) are significant and very significant differences from UT using the Student's T-test.

Among the set of cell stress proteins being assessed, TZ treatment had significantly up-regulated HIF-1-α (1.31-fold), HMOX2 (1.51-fold), HSP27 (1.35-fold) and HSP60 (1.28-fold) while TRAIL treatment had induced significant increase in the expression of HMOX2 (1.3-fold), HSP27 (1.25-fold) and HSP60 (1.11-fold) (Figure 64).

On the other hand, TZT treatment had up-regulated HSP27 and HSP60 for 1.08-fold **($p<0.01$) and 1.15-fold **($p<0.01$), respectively, in contrast to the untreated control. Nonetheless, TZT had significantly *($p<0.05$) down-regulated HMOX1 to 0.36 as compared to untreated MCF-7. In all cases, HSP70 protein expression remained unchanged (Figure 64). The processed antibody array sheet image of MDA-MB-231 at the 72 h time point is shown in Appendix O.

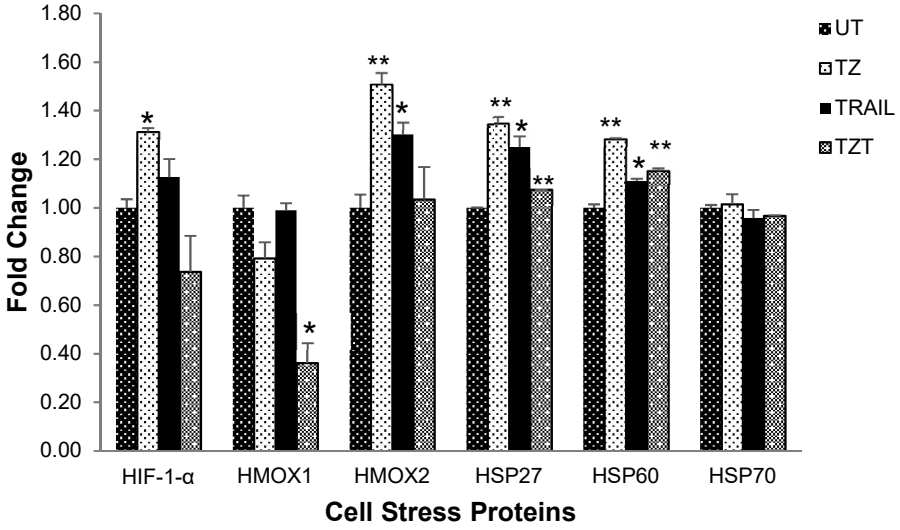


Figure 64 The protein expression of **cell stress proteins** in the untreated **MCF-7** (UT) and **MCF-7** treated with TSA and Zeb (TZ), 50 ng/mL TRAIL (TRAIL) for **72 h** and TSA and Zeb for 12 h followed by TRAIL treatment for **72 h** (TZT). Data represents mean $\pm$ standard deviation. *($p<0.05$) and **($p<0.01$) are significant and very significant differences from UT using the Student's T-test.

5.4 Discussion

5.4.1 TZT treatment had induced the up-regulation of cell cycle regulators p21 and p-p53 (S392) in MDA-MB-231

Apoptosis is an orchestrated cell death induced either by intracellular or extracellular cell death stimuli to eliminate damaged or stressed cells through phagocytosis which provokes minimal inflammatory reaction (Baig *et al.*, 2016). In the earliest stage of discovery, apoptosis had been studied through cellular morphological and biochemical changes using conventional histology and biochemical studies. In early apoptosis, cell shrinkage occurs and then followed by the typical morphological feature of nuclear condensation known as pyknosis (Elmore, 2007). In addition, phosphatidylserine will also be expressed on the outer layers rather than its usual occurrence on the inner layers of plasma membrane (Segawa and Nagata, 2015). Subsequently in the late stage of apoptosis, cell contracts and plasma membrane starts blebbing (Coleman *et al.*, 2001). Nuclear fragmentation (karyorrhexis) happens followed by nuclear fragments along with cellular organelles being packed into apoptotic bodies which then bud off from the dying cell before being phagocytosed (Saraste and Pulkki, 2000).

Similarly, both the histological and biochemical approaches on apoptosis assessment had been applied in this study. At the morphology level, apoptosis occurrence had been captured in MDA-MB-231 for all the treatment groups at all three time points of 24, 48 and 72 h (Figure 35, 36 and 37) as all displayed the typical apoptotic morphological changes as aforementioned. From the Annexin V-FITC/PI cellular apoptosis data as shown in Figure 44, TZ treatment was shown to be the most effective apoptosis inducer as a significant *($p<0.05$) 26% of cell population was undergoing early apoptosis. This data was backed by the proteome profiling of 35 apoptosis-related genes conducted in this study. TZ treatment had significantly *($p<0.05$) up-regulated the pro-apoptotic Bad

protein while concurrently down-regulating the anti-apoptotic proteins, Bcl-2 and Bcl-xL (Figure 47).

Bcl-2-Associated Death Promoter (Bad) is included in the pro-apoptotic sub-family of Bcl-2 protein family called the “BH3-only proteins” along with other members such as Puma, Noxa, Bim, Bid, Bmf, Hrk and Bik (Adams and Cory, 2007). Its death promoting function stems from its binding to the pro-survival Bcl-2, Bcl-xL and Bcl-w proteins via its BH3 domain, thereby ablating the inhibitory effects these pro-survival proteins have on the mitochondrial pore formers, Bax and Bak (Willis *et al.*, 2007). Our results are in agreement with literature evidence that TSA-induced apoptosis is mediated by up-regulation of Bad protein expression (Makki *et al.*, 2008; Sawa *et al.*, 2001). Besides, Zebularine was also shown by microarray analysis to activate Bad expression through demethylation of its silenced hyper-methylated promoter (Pompeia *et al.*, 2004).

In addition, the highest apoptosis rate induced by the TZ treatment in MDA-MB-231 was consistent with the up-regulation of the extrinsic apoptosis pathway member, TRAIL R1, observed in this study (Figure 48). The observation of TSA up-regulating TRAIL R1 but not TRAIL R2 can be explained by the similar observation of differential modulation of TRAIL R1 and TRAIL R2 expression induced by TSA in multiple myeloma cell lines (Fandy *et al.*, 2005). On the other hand, despite being statistically insignificant, TZT treatment had induced 15% early apoptosis events in MDA-MB-231 at the 72 h time point, which was higher than that induced by single TRAIL treatment (Figure 44). This could be explained by the enhanced Fas death receptor expression in addition to TRAIL R2 up-regulation as induced by TZT treatment (Figure 48) which could have resulted in enhanced caspase-8 activation in addition to the apoptosis signal signalled through TRAIL binding to TRAIL R2. Similar finding had been reported in H157 lung cancer cells whereby TSA had up-regulated Fas and Fas ligand which led to Bid cleavage and apoptosis (Kim

et al., 2006). Other similar reports have also highlighted the role of TSA in the epigenetic modulation of Fas which might predict tumour's chemo-sensitivity (Maecker *et al.*, 2002) and apoptosis occurrence in rheumatoid arthritis (Morinobu *et al.*, 2006).

Besides, TZ along with TRAIL and TZT treatments had consistently decreased the expression of anti-apoptotic clusterin protein (Figure 49). Several anti-apoptotic IAPs like Livin, Survivin and XIAP were also notably down-regulated by all the three treatments. Concurrently, TZ and TZT treatments had caused the increase in the pro-apoptotic SMAC expression but TZT had caused a higher induction of SMAC expression at 1.19-fold (Figure 50). This data collectively suggests that the ablation of IAPs and the induction of IAPs inhibitor, SMAC, play a role at the molecular level of the apoptotic events induced by the treatment. Our data concurs with the literature finding that small-molecule SMAC mimetics which are IAPs' antagonists could sensitize previously TRAIL-resistant human cancer cell lines to TRAIL (Bockbrader *et al.*, 2005; Finlay *et al.*, 2014). Moreover, TSA was shown to sensitize human renal carcinoma cells to TRAIL-induced apoptosis via the down-regulation of IAPs, XIAP and cIAP-1 (Han *et al.*, 2015). In another instance, decitabine-induced apoptosis in human leukemia cell lines was also correlated with the down-regulation of XIAP and cIAP-1 (Shin *et al.*, 2012). Therefore, the potential of TZ treatment prior to TRAIL administration (TZT) in our study had been validated.

As aforementioned, there is a tight link between cell cycle checkpoint signalling and cellular apoptosis. TZT-treated MDA-MB-231 had p21 being significantly *($p<0.05$) up-regulated (Figure 51). This is in agreement with several reports on TSA or other HDAC inhibitors being an effective sensitizer of cancer cells towards TRAIL-induced apoptosis with the involvement of increase in p21 expression in multiple myeloma cell lines (Fandy *et al.*, 2005) and breast cancer cell line (Chopin *et al.*, 2004; Varshochi *et al.*, 2005; Zuo *et al.*, 2014).

Moreover, the anti-lymphangiogenic effect of TSA was also shown to be dependent on its transcriptional activation of p21 promoter (Hrgovic *et al.*, 2016). Thus, this is considered an added therapeutic advantage of TZT treatment in our study in addition to its apoptosis-inducing effect.

Intriguingly, with TZ being the sensitizers prior to TRAIL treatment, there was a surge in the phosphorylated form of p53, p-p53 (S392), expression in MDA-MB-231 (Figure 51). Recently, a group had discovered through mutational studies that p-p53 (S392) aids the mitochondrial-translocation of p53 (Castrogiovanni *et al.*, 2018), thereby allowing its interaction with Bax and Bak to trigger the outer mitochondrial membrane permeabilization followed by cytochrome c release and apoptosis execution (Pietsch *et al.*, 2008). Despite p53 being largely mutated in MDA-MB-231 (Hui *et al.*, 2006), TZT treatment was shown to be useful in activating the transcription-independent apoptosis induction by p53 in this study. Along the same line, p53 could have also been stabilized through the TZT-induced up-regulation of HIF-1-α (Figure 52) as studies have shown that HIF-1-α interacts directly with p53 thereby resulting in p53 stabilization (Greijer and van der Wall, 2004; Piret *et al.*, 2002; Sermeus and Michiels, 2011).

Nonetheless, TZT had also up-regulated the pro-survival cell stress proteins, HSP27 (Figure 52). HSP27 was shown to interrupt the caspase activation by binding to caspase-3 and cytochrome c released from the mitochondria (Voss *et al.*, 2007). Therefore, this could possibly explain the insignificant percentage of apoptosis events (Figure 44) induced by TZT treatment in MDA-MB-231 as well as the lack of up-regulation of the cleaved caspase-3 and cytochrome c (Figure 49) observed in this study. Nonetheless, HSP70 which was shown to bind to TRAIL R1 and TRAIL R2, thereby inhibiting the formation of death-inducing silencing complex (DISC) (Wang *et al.*, 2014) had been slightly down-regulated by TZT treatment (Figure 52). Therefore, TZT had proven itself as a

positive sensitizer of MDA-MB-231 towards TRAIL-induced apoptosis at least at the DISC assembly stage upstream of caspase-3 activation.

5.4.2 TZT had down-regulated anti-apoptotic IAPs and cell stress proteins but induced insignificant apoptotic events in 231-EGFP

Paradoxical to our hypothesis, the re-expression of E-cadherin in 231-EGFP did not significantly enhance the TZT treatment-induced apoptosis (Figure 45). This cellular apoptosis data was supported by the apoptosis proteome profiling data obtained in this study for 231-EGFP. At 72 h post-treatment, TZT treatment had induced significant down-regulation of Bcl-2 (Figure 53). Since the TZT-induced decrease of Bcl-2 expression was not observed in the absence of E-cadherin in MDA-MB-231, E-cadherin re-expression in 231-EGFP could be seen as enhancing the TZT-induced pro-death effects by its known inverse relation with Bcl-2 in various carcinomas (Ferreira *et al.*, 2012; Sasaki *et al.*, 2000). Nonetheless, its pro-death down-regulation of the Bcl-2 protein had been offset by the concurrent down-regulation of the pro-apoptotic members, Bad and Bax (Figure 53). This could possibly be justified by the ligand-independent epidermal growth factor receptor (EGFR) activation mediated by E-cadherin (Fedor-Chaiken *et al.*, 2003; Reddy *et al.*, 2005; Shen and Kramer, 2004). EGFR-dependent MAPK signalling drives phosphorylation of Bad protein on serines 112 and 155, hence sequestering it from its interaction with Bcl-xL (Gilmore *et al.*, 2002). Both Bad and Bax which remained in the cytosol could have been degraded by the ubiquitin-proteasome system (Chen and Dou, 2010; Li and Dou, 2002).

In addition, TZT had also negatively regulated the extrinsic pro-apoptosis death receptors by decreasing the expression of TRAIL R1 and TRAIL R2 along with FADD (Figure 54). E-cadherin re-expression in MDA-MB-231 seemed to have abrogated the TZT-induced induction of TRAIL R2 as mentioned above (Figure

48). Lu *et al.* (2014) claimed that E-cadherin stably interacts with both TRAIL R1 and TRAIL R2 upon TRAIL ligation and facilitates the receptor clustering, recruitment of FADD and caspase-8 followed by DISC assembly via its connection to the actin skeleton via α-catenin. This had made E-cadherin a potent positive modulator of the death signalling through TRAIL R1 and TRAIL R2 as the constitutive endocytosis of both TRAIL R1 and TRAIL R2 was shown to contribute towards TRAIL resistance (Reis *et al.*, 2017; Zhang *et al.*, 2009) Nevertheless, immunohistochemistry study in human colorectal carcinomas showed that increased cytoplasmic and/or nuclear beta-catenin staining (loss of membranous staining) was associated with increased and stabilized expression of TRAIL R1 and TRAIL R2 (Jalving *et al.*, 2014). Therefore, despite TZ treatment prior to TRAIL (TZT) was useful in up-regulating TRAIL R1, TRAIL R2 as well as FADD in our study (Figure 54), E-cadherin re-expression might have sequestered most of the beta-catenin in the E-cadherin-beta-catenin complexes (Wong *et al.*, 2018), thereby reducing the beta-catenin pool available for interaction with other growth factor receptors c-Met and c-erbB2, the mucin MUC1 and the FOXO transcription factors, which could have stabilized or increased the expression of both the TRAIL receptors (Essers *et al.*, 2005; Hiscox and Jiang, 1999; Kanai *et al.*, 1995; Li *et al.*, 1998).

Furthermore, E-cadherin re-expression in 231-EGFP was also shown to enhance the death-inducing potential of TZT treatment with the down-regulation of anti-apoptotic proteins, catalse and PON2, in addition to clusterin induced in MDA-MB-231 (Figure 55). Nonetheless, this did not result in significant increase in apoptotic events (Figure 45) probably due to the concurrent down-regulation of pro-caspase-3 as well as cytochrome c (Figure 55). Similarly, the negative regulation on IAPs, Livin, cIAP-2, Survivin and XIAP, had also been counterbalanced by the concomitant down-regulation of the pro-apoptotic proteins, SMAC and HTRA2 (Figure 56). At the same time, most of the cell cycle checkpoint inhibitors like p21, p27, p-p53 (S15), p-p53 (S392) and p-Rad 17 (S635) had all been paradoxically down-regulated by TZT

treatment in 231-EGFP (Figure 57). As opposed to TZT treatment in MDA-MB-231 which up-regulated the pro-survival cell stress proteins, HSP27 (Figure 52), TZT treatment in 231-EGFP had down-regulated both HSP27 and HSP70 along with other cell stress proteins like HSP60, HIF-1-α and HMOX1 (Figure 58).

All these observations had collectively pointed us to reason that E-cadherin re-expression in 231-EGFP might have played more of a tumour promoting role rather than its usual tumour suppressor role in all the tested treatment groups. Anoikis, the anchorage-independent cell death, is usually suppressed by E-cadherin-mediated cell-to-cell adhesion via the activation of phosphatidylinositol 3-kinase-protein kinase B (PI3K-Akt) and ras-extracellular signal-regulated kinase (Raf-Erk) pathways (Grossmann, 2002). However, oncogenic *K-Ras* mutation in MDA-MB-231 (Kim *et al.*, 2015) could activate these pathways (Hymowitz and Malek, 2018; Sullivan and Kozuch, 2011), rendering anoikis-suppression no longer E-cadherin-dependent. Initially, it was hypothesized E-cadherin re-expression could render MDA-MB-231 to be more sensitive towards the TZT treatment due to its enhancement of TRAIL-induced apoptosis signalling in colon and pancreatic carcinomas (Lu *et al.*, 2014). On the contrary, the re-expression of E-cadherin had enhanced the pro-survival profile of MDA-MB-231 in our study, resembling the pro-survival E-cadherin re-expression followed by mesenchymal to epithelial reverting transition (MErT) in MDA-MB-231 when introduced into a secondary organ environment (Chao *et al.*, 2010, 2012; Chen *et al.*, 2015). The notion that E-cadherin re-expression in metastases promotes tumour survival is supported by the overexpression of E-cadherin in intravascular tumour emboli originated from the inflammatory breast cancer subtype (Rodriguez *et al.*, 2012).

In conclusion, TZT's anti-cancer therapeutic potential in E-cadherin re-expressed 231-EGFP could be supported by the down-regulation of anti-apoptotic proteins (catalase, PON2, clusterin) (Figure 55), IAPs (livin, cIAP-2,

survivin, XIAP1) (Figure 56) as well as the cell stress proteins (HMOX1, HSP27 and HSP70) (Figure 58) as these were not observed in MDA-MB-231 which expresses low or no E-cadherin. Nevertheless, the negligible increase in apoptotic events captured in this study showed that E-cadherin might enhance TRAIL receptors clustering and its apoptosis signalling in certain carcinoma cells lines but this regulation cannot be generalized across different cell lines.

5.4.3 MCF-7

MCF-7 is a human breast adenocarcinoma cell line that inherently expresses E-cadherin (Lu *et al.*, 2012) and was used in this study as the E-cadherin-positive control to assess the anti-cancer efficacy of the TZT treatment. At 48 h post-treatment, TZT had induced 42% of early apoptosis events in MCF-7. Nonetheless, the TZT-induced early apoptosis percentage had dropped to 13% at the 72 h time point (Figure 46). The initial spike in early apoptosis events of MCF-7 could be explained by the significant induction of Bad and Bax expression (Figure 59) and cytochrome c (Figure 61) by TZT treatment. Bad expression could have been induced by TSA and Zeb prior treatment similar to that observed in MDA-MB-231 as mentioned above. In another similar instance, the combination of 5-Aza-2-deoxycytidine (DNA demethylating agent) and TSA had also induced increase in Bax expression (Al-Rayyan *et al.*, 2014), further confirming the potential of TZ being the sensitizer towards TRAIL-induced apoptosis in our study.

In addition, TZT treatment had also significantly increased the expression of TRAIL R1 and TRAIL R2 (Figure 60). Concurrently, TZT had also induced down-regulation of anti-apoptotic proteins, catalase, PON2 (Figure 61) and cIAP-1 apart from increasing the pro-apoptotic SMAC and HTRA2 mitochondrial proteins (Figure 62). TZ's potential as sensitizers of MCF-7 cells towards TRAIL-induced apoptosis was supported by the increase in pro-apoptotic regulation engaged by both the extrinsic and the intrinsic pathways. Despite the lack of correlation between TRAIL receptors expression and TRAIL

sensitivity in MCF-7 (Zhang and Zhang, 2008), the inherent E-cadherin expression in MCF-7 was shown to sustain the TZ-mediated increase in expression of both TRAIL-R1 and -R2 in MCF-7 (Figure 60). Therefore, this observation showed that although *in vitro* E-cadherin over-expression might have counteracted against the TZ-mediated increase in TRAIL receptors as in the case of 231-EGFP mentioned above, the inherent E-cadherin re-expression remained a pro-apoptotic regulator towards TRAIL-induced apoptosis. This carries great potential as TRAIL treatment can be targeted not just towards primary tumour which mostly expresses E-cadherin (Kowalski *et al.*, 2003) but also invasive ductal carcinoma which is en route towards metastases formation as E-cadherin is majorly re-expressed in distant and lymph node metastases (Chen *et al.*, 2015; Fulga *et al.*, 2015).

On the other hand, TZT treatment had also up-regulated a number of pro-apoptotic cell cycle regulators, namely claspin, p27 and p-p53 (S46) (Figure 63). Based on our findings, the molecular determinants of TZ sensitization of MCF-7 towards TRAIL-induced apoptosis stemmed mainly from the cell cycle progression and DNA damage response regulatory pathways. During DNA damage response, Claspin contributes towards DNA damage-induced checkpoint kinase 1 (Chk1) activation (Ito *et al.*, 2018) which is commonly observed after DNA stress induction by genotoxic agent like cisplatin (Patil *et al.*, 2013). This signifies the pre-apoptosis stage as Chk is degraded after its initial activation (Patil *et al.*, 2013) while claspin was shown to be cleaved either by caspase-7 or proteasome during apoptosis (Clarke *et al.*, 2005; Semple *et al.*, 2007). Besides, the phosphorylation of p53 on S46 is an important determinant of p53-mediated regulation of apoptosis-related genes (Gibbons *et al.*, 2015; Smeenk *et al.*, 2011; Wu *et al.*, 2016). In addition, the significant increase in p27 in MCF-7 (Figure 63) showed that cell cycle arrest precedes the apoptosis event observed in MCF-7 and it is in agreement with reports on p27 up-regulation by the epigenetic drugs TSA (Fandy *et al.*, 2005) and Zeb (Billam *et al.*, 2010) used as sensitizers in the TZT treatment.

Last but not least, there was a slight up-regulation of both HSP27 and HSP60 induced by the TZT treatment in MCF-7 (Figure 64). Despite HSP27 being proven to inactivate cytochrome c by binding to it (Voss *et al.*, 2007), cytochrome c remained being up-regulated by TZT treatment probably due to only a slight up-regulation at 1.08-fold in MCF-7 (Figure 61) in contrast to 1.51-fold in MDA-MB-231 (Figure 52). In addition, the TZT-induced increase in HSP60 observed in our study explains that HSP60 might play a pro-death role in the treated MCF-7 via its cytosolic accumulation from mitochondrial release and interaction with caspase-3 (Chandra *et al.*, 2007). Notably, TZT had down-regulated HMOX1 to 0.36-fold of untreated MCF-7 (Figure 64). This outcome carries great significance as the anti-apoptotic HMOX1 is constantly over-expressed or can be induced by chemotherapeutic drugs like doxorubicin in breast cancer cells (Zhu *et al.*, 2015) Since TZ treatment prior to TRAIL (TZT) could target against HMOX1 both in 231-EGFP (Figure 58) and MCF-7 (Figure 64) but not in MDA-MB-231 (Figure 52), E-cadherin expression was again shown to be beneficial towards TZ-sensitized TRAIL-induced apoptosis in breast cancer cells.

Albeit the promising potential of TZT treatment shown in MCF-7 which inherently expresses E-cadherin, the dysfunctional caspase-3 in MCF-7 due to altered splicing followed by frame shift mutations (Kurokawa *et al.*, 1999) had resulted in high TRAIL-resistance despite the addition of IAPs and c-FLIP inhibitors (Huang *et al.*, 2016). Therefore, in order to validate the potential of TZT treatment in MCF-7 model, caspase-3 had to be reconstituted in MCF-7 prior to TZT treatment as caspase-3 reconstitution was shown to sensitize MCF-7 breast cancer cells towards doxorubicin- and etoposide-induced apoptosis (Yang *et al.*, 2001).

5.5 Concluding remarks

Collectively, the results from the apoptosis assessment reported in this chapter showed that TSA and Zeb sensitization prior to TRAIL treatment (TZT) had shown promising potential in enhancing TRAIL-induced apoptosis. TZ prior treatment had directed MDA-MB-231 towards cell cycle arrest before apoptosis occurrence. This was supported by the up-regulation of p21 and p-p53 (S392) in MDA-MB-231 by TZT. With the *in vitro* re-expression of E-cadherin in 231-EGFP, down-regulation of anti-apoptotic PON2, catalase, clusterin, IAPs as well as cell stress proteins had validated the notion that E-cadherin expression enhanced the TZT anti-cancer efficacy. Similarly, in E-cadherin-positive MCF-7, TZT treatment had down-regulated the anti-apoptotic proteins, increased the pro-apoptotic SMAC, HTRA2 as well as both the TRAIL receptors, TRAIL R1 and R2. Since *in vitro* re-expression of E-cadherin in 231-EGFP had negatively regulated TRAIL R1 and TRAIL R2 expression, we propose that MCF-7 with re-constituted caspase-3 might serve as a better model to study the effect of E-cadherin expression on the TZT apoptosis-inducing efficacy.

6. Immunohistochemistry staining of markers TRAIL-R2, CDH1 and TRAIL of sectioned breast cancer tissues and their association with the corresponding clinical parameters

6.1 Introduction

Breast cancer is a heterogeneous disease (Polyak, 2011; Turashvili and Brogi, 2017). Breast cancer cell lines have been commonly used in cancer research due to its convenience, however, its inherent functional heterogeneity (Olive *et al.*, 2018) might result in invalid or inconsistent experimental outcomes. Therefore, this chapter aims to assess the expression of three important markers, TRAIL-R2, TRAIL and E-cadherin relevant to previous chapters' studies, *in vivo*, in order to complement the *in vitro* findings on TRAIL-induced apoptosis in MDA-MB-231, with or without E-cadherin expression.

Despite TRAIL-R2 being part of the TRAIL-induced apoptosis mechanism, high expression of TRAIL-R2 had been associated with poor prognosis in breast cancer patients (Ganten *et al.*, 2009). Immunohistochemical staining revealed mostly intracellular distribution of both TRAIL-R2 receptors and this might be their escape mechanism from the immune surveillance by TRAIL-induced apoptosis (Fritsche *et al.*, 2015). The mislocalization of TRAIL receptor from membrane to intracellular also predicted resistance towards TRAIL-based therapy (Chen *et al.*, 2012). Moreover, high abundance of intracellular TRAIL-R2 also correlates with enhanced HMGA2 expression and increased cell proliferation (Kalthoff *et al.*, 2014).

On the other hand, E-cadherin had been a widely studied marker in breast cancer in terms of clinical-pathological associations (Singhai *et al.*, 2011; Younis *et al.*, 2007). E-cadherin had been used as a favourite marker in terms of histological typing in breast cancer (Nurismah *et al.*, 2008; Qureshi *et al.*, 2006). It was shown *in vitro* to physically associate with both TRAIL-R1 and TRAIL-R2 (Lu *et al.*, 2014), it is therefore worthwhile to assess the expression of E-cadherin alongside TRAIL-R2 expression at both the mRNA and protein

levels to decipher their expression levels and localization *in vivo* on breast cancer patient tissues.

In addition, TRAIL-TRAIL-R signalling can drive a tumour growth-supportive microenvironment in the case of TRAIL-resistant cancers (Hartwig *et al.*, 2017). TRAIL is also an important death ligand used in our *in vitro* studies. Therefore, it is also vital to include TRAIL as a biomarker in the investigation of its correlation with the biomarkers, TRAIL-R2 and E-cadherin, as well as patient's survival and prognosis.

In this chapter, both the bioinformatics and immunohistochemistry approaches have been utilized to investigate the expression patterns of TRAIL-R2, TRAIL and E-cadherin at both the mRNA and protein levels, respectively. The research objectives were as follow:

- To obtain the RNA sequencing data from The Cancer Genome Atlas (TCGA) breast invasive carcinoma data repository for normalized gene counts (mRNA) of TRAIL-R2, TRAIL, E-cadherin and conduct statistical analysis;
- To obtain the Molecular Taxonomy of Breast Cancer International Consortium (METABRIC) microarray mRNA expression data of TRAIL-R2, TRAIL, E-cadherin and conduct statistical analysis;
- To validate the specificity of anti-TRAIL-R2, anti-TRAIL and anti-E-cadherin monoclonal antibody using Western blotting;
- To stain the primary invasive breast cancer patients' formalin-fixed paraffin-embedded (FFPE) tissue sections via immunohistochemistry of the heat-induced epitope retrieval method;
- To score the immunohistochemically stained images of TRAIL-R2, TRAIL, and E-cadherin for H-scores calculation using the formula: (Percentage value × 3) + (Percentage value × 2) + (Percentage value × 1) + (Percentage value × 0) whereby 0=negative; 1=weak staining; 2=moderate staining; 3=strong staining) and conduct statistical analysis.

6.2 Methodology

6.2.1 Bioinformatics and statistical analysis of TRAIL-R2, E cadherin and TRAIL expression on published data

Next-generation RNA sequencing data (RNAseqv2) on *TNFSF10*, *TNFRSF10B* and *CDH1* along with their corresponding clinical parameters were obtained from The Cancer Genome Atlas (TCGA) breast invasive carcinoma data (portal.gdc.cancer.gov/projects/TCGA-BRCA). Patients were stratified based on the different clinic-pathological variables provided by TCGA-BRCA (n=1098). Normalized gene counts (gene counts rescaled according to library size) were compiled into a tab-delimited text file for analysis using the RobinA applying the Bioconductor-edgeR software.

In the Molecular Taxonomy of Breast Cancer International Consortium (METABRIC) cohort of 1980 invasive breast cancer patient, nucleic acids were isolated and transcriptionally profiled from fresh frozen samples using the Illumina HT-12v3 platforms with data being pre-processed and normalized as described by (Curtis *et al.*, 2012). The microarray transcriptomic data of T*NFSF10*, *TNFRSF10B* and *CDH1* were dichotomized using the X-tile software. The correlation between the expression of these genes and with the clinicopathological parameters provided by METABRIC were statistically analysed using IBM SPSS 25. Significance levels were set at *($P<0.05$), **($P<0.01$) and ***($P<0.001$).

6.2.2 Validation of anti-TRAIL-R2, anti-E-cadherin and anti-TRAIL primary antibody specificity using western blotting

Western blotting was performed using whole cell lysates of positive and negative expressor cells of E-cadherin to validate the specificity of the anti-*CDH1* antibody (clone 4A2C7) prior to immunohistochemistry. For this purpose, lysates of E-cadherin-expressing human breast ductal carcinoma and adenocarcinoma cell lines (T47D and MCF-7, American Type Culture

Collection (ATCC), USA), respectively, and E-cadherin-non-expressing human breast adenocarcinoma cell lines (MDA-MB-231, American Type Culture Collection (ATCC), USA) were used. As for the primary antibody specificity validation for anti-TRAIL (ab2056, Abcam, UK) and anti-TRAIL-R2 (HPA023625, Sigma-Aldrich, USA), whole cell lysates from a panel of cell lines which express TRAIL and TRAIL-R2 were used since both the markers are expressed in all tissue types. The panel of cell lines includes human cervical cancer HeLa CCL-2 (ATCC, USA), human breast adenocarcinoma MDA-MB-231, MCF7, SkBr3 (ATCC, USA), human breast ductal carcinoma T47D, human acute T cell leukemia Jurkat (ATCC, USA) and normal human mammary gland MCF10A (ATCC, USA). The primary antibody dilutions used were 1:300 (anti-E-cadherin, 1:500 (anti-TRAIL) and 1:250 (anti-TRAIL-R2). The IRDye® 800CW donkey anti-rabbit (926-32213, Li-cor Biosciences, Lincoln, NE, USA) and IRDye® 680RD donkey anti-mouse (926-68072, Li-cor Biosciences, Lincoln, NE, USA) secondary antibodies were used at 1:15 000 dilutions. Mouse anti-beta-actin (A2228, Sigma-Aldrich, USA) diluted at 1:5000 was used as the loading control. Blocking buffer (5% skim milk in 1x PBS with 0.1% (v/v) Tween-20) was used for both blocking and primary and secondary antibody incubations. Fluorescence was used to visualize the membrane. The images were developed via fluorescence using an Odyssey Fc (Li-cor Biosciences, Lincoln, NE, USA).

6.2.3 Immunohistochemistry

Patients at early-stage primary operable invasive breast cancer (BC) who aged ≤70 years, between 1986 and 1998 in Nottingham were selected for this study. Patient management was uniform and based on tumour characteristics by Nottingham Prognostic Index (NPI) and hormone receptor status. Patients within the NPI excellent prognostic group (score ≤3.4) received no adjuvant therapy, but those patients with NPI >3.4 received tamoxifen if ER-positive (± goserelin (Zoladex) in case the patients were premenopausal). Conversely,

classical cyclophosphamide, methotrexate and 5-fluorouracil (CMF) were used if the patients were ER-negative and fit enough to receive chemotherapy. None of the patients in this study received neoadjuvant therapy. Clinical history, tumour characteristics and information on therapy and outcomes are prospectively maintained.

For immunohistochemistry, heat-induced epitope retrieval was performed in citrate buffer pH 6.00 using microwave at 1000 W for 20 min. Novolink Max Polymer Detection System (RE7280-k, Leica, Newcastle, UK) was used to visualize the immunohistochemical reaction. Peroxidase block (Novolink Peroxidase Block) was added to the sections for 5 min to block endogenous peroxidase activity. Protein block (Novolink Protein Block) addition to the sections for 5 min was used to block the subsequent non-specific binding of the primary antibody, the post primary rabbit anti-mouse immunoglobulins (IgG) and the polymer. The primary antibodies are anti-*CDH1* (clone 4A2C7) (Thermo Fisher Scientific, U.S.A.), anti-*TNFRSF10B* (HPA023625) (Sigma-Aldrich, U.S.A.), and anti-*TNFSF10* (ab2056) (Abcam, U.K.). The dilution and incubation duration for the three markers are (*CDH1*, 1:25 for 24 h; *TNFSF10*, 1:500 for 1 h; *TNFRSF10B*, 1:400 for 20.5 h). The post primary (Novolink Post Primary) detects the mouse primary antibodies while the polymer (Novolink Polymer) detects both the post primary and any tissue-bound rabbit primary antibodies. Sections were then incubated with the substrate chromogen, 3,3'-diaminobenzidine (DAB), prepared from DAB Chromogen and Novolink DAB Substrate Buffer at 1:20 dilution for 5 min. Sections were counterstained with hematoxylin (Novolink Hematoxylin) for 6 min. Dehydration and clearing of the sections were carried out using the Leica ST5010 autostainer (Leica, Newcastle, UK). Cover slips were added with DPX mounting medium and slides were carefully mounted on them.

6.2.4 Statistical analyses

The 2000 BC cores from the section series have been scored and the H-scores were statistically analyzed using Pearson's correlation, Chi-square association tests, and Kaplan-Meier survival analyses. Mean and median values were used as dichotomization cut-off values of the tested markers' protein expression for normal and non-normal distribution of data, respectively.

6.3 Results

6.3.1 Bioinformatics and statistical analysis of TRAIL-R2, E-cadherin and TRAIL mRNA expression using RNA sequencing gene counts from TCGA-BRCA data

Based on the statistical analysis using RobinA applying the Bioconductor-edgeR on normalized gene counts of E-cadherin and TRAIL-R2 of stratified patients, E-cadherin was significantly ($P<0.001$) down-regulated while TRAIL-R2 was significantly ($P<0.01$) up-regulated in triple negative patients in comparison with triple positive patients as well as estrogen receptor positive (ER+) and progesterone receptor positive (PR+) patients who do not have human epidermal growth factor receptor 2 (HER2-) over-expression. A similar inverse correlation between the expression of E-cadherin and TRAIL-R2 had been observed in the non-tumour versus primary tumour analyses whereby the normalized gene counts of E-cadherin was significantly ($p<0.01$) increased while that of TRAIL-R2 was significantly ($p<0.05$) decreased in primary tumour of all BC subtypes. The inverse relationship between these two markers had been confirmed by Pearson correlation value of -0.165 ($p<0.001$) (Table 4). The expression of both E-cadherin and TRAIL-R2 in metastases remained statistically similar with that of non-tumour and primary tumour (Figure 65).

On the other hand, the normalized gene counts of TRAIL were significantly ($p<0.001$) higher in the triple positive as well as ER+, PR+, HER2- patients as compared to the triple negative patients. However, the TRAIL expression remained statistically similar across the patient groups of non-tumour, primary and metastases (Figure 65). In addition, TRAIL only had a weak positive correlation with *CDH1*, 0.065 while having no correlation with TRAIL-R2 (Table 4).

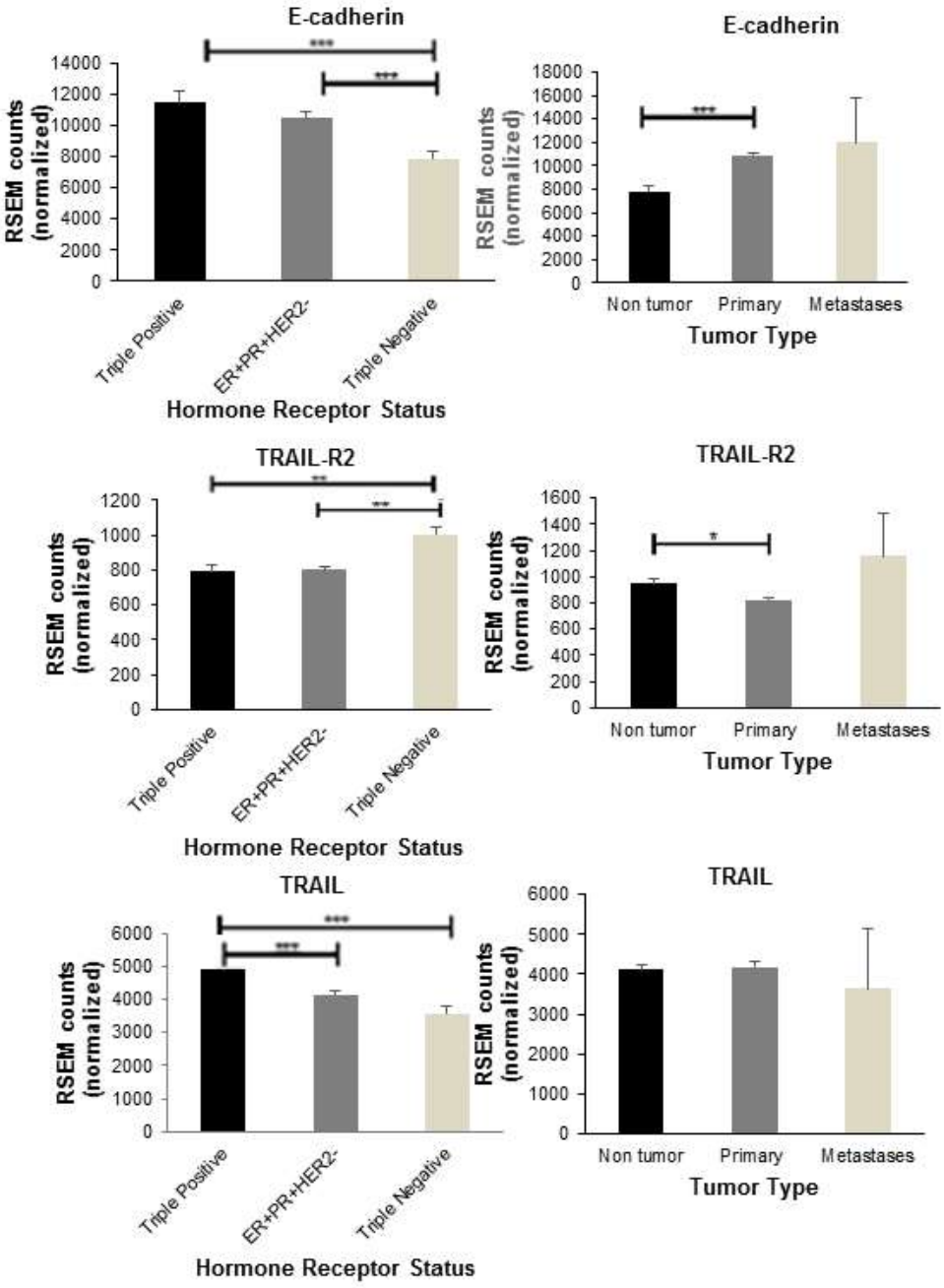


Figure 65 Differentially expressed E-cadherin and TRAIL-R2 across different hormone receptor (ER, PR, HER2) status and between non-tumour and primary breast tumour. Patients were sub-divided depending on the clinicopathological parameters provided by TCGA. Normalized gene counts (gene counts rescaled according to library size) were compiled into a tab-delimited text file for analysis using the RobinA applying the Bioconductor-edgeR software. Data represents means ± SEM. *, ** and *** are statistical significant differences at $p<0.05$, $p<0.01$ and $p<0.001$, respectively.

Table 4 Pearson correlation test between the normalized gene counts of *CDH1* (E-cadherin), *TNFRSF10B* (TRAIL-R2) and *TNFSF10* (TRAIL) from the TCGA data using SPSS analysis.

Correlations

		CDH1	*TNFRSF10B*
CDH1	Pearson Correlation	1	-.165**
	Sig. (2-tailed)		.000
	N	1202	1202
TNFRSF10B	Pearson Correlation	-.165**	1
	Sig. (2-tailed)	.000	
	N	1202	1202

**. Correlation is significant at the 0.01 level (2-tailed).

Correlations

		CDH1	*TNFSF10*
CDH1	Pearson Correlation	1	.065*
	Sig. (2-tailed)		.025
	N	1202	1202
TNFSF10	Pearson Correlation	.065*	1
	Sig. (2-tailed)	.025	
	N	1202	1202

*. Correlation is significant at the 0.05 level (2-tailed).

Correlations

		TNFSF10	*TNFRSF10B*
TNFSF10	Pearson Correlation	1	.004
	Sig. (2-tailed)		.896
	N	1202	1202
TNFRSF10B	Pearson Correlation	.004	1
	Sig. (2-tailed)	.896	
	N	1202	1202

6.3.2 Bioinformatics and statistical analysis of TRAIL-R2, E-cadherin and TRAIL mRNA expression using the microarray transcriptomic expression data from METABRIC and their correlation with the clinico-pathological parameters

Similar to that observed in the TCGA data, E-cadherin and TRAIL-R2 expression also assumed a significant ($p<0.001$) negative correlation with a Pearson correlation value of -0.14 in the METABRIC cohort (Table 5). In terms of their association with the clinico-pathological parameters, chi-square test of association showed that the mRNA expression of TRAIL-R2 was significantly ($p<0.001$) associated with tumour grade and lymph node stage. On the other hand, the mRNA expression of E-cadherin was significantly ($p<0.01$) associated with tumour grade and tumour size (Table 6).

Since breast cancer-specific survival (BCSS) is the ultimate outcome of interest from the study of association between the markers and the clinico-pathological parameters, the univariate and multivariate analyses of the prognostic variables of tumour grade, tumour size, lymph node stage and TRAIL-R2 and E-cadherin expression in relation to BCSS had been conducted as follows.

Table 5 Pearson correlation test between the normalized mRNA expression of *CDH1* (E-cadherin) and *TNFRSF10B* (TRAIL-R2) from the METABRIC data using SPSS analysis.

Correlations

		TNFRSF10B	*CDH1*
TNFRSF10B	Pearson Correlation	1	-.140**
	Sig. (2-tailed)		.000
	N	1981	1981
CDH1	Pearson Correlation	-.140**	1
	Sig. (2-tailed)	.000	
	N	1981	1981

**. Correlation is significant at the 0.01 level (2-tailed).

Table 6 Chi-square test association of *CDH1* (E-cadherin) and *TNFRSF10B* (TRAIL-R2) expression with the clinico-pathological variables in the METABRIC cohort using SPSS analysis.

	TNFRSF10B		***CDH1***	
Clinical parameters	**Pearson Chi-square**	**p-value**	**Pearson Chi-square**	**p-value**
Tumour grade	28.596	**P= 0.000 (<0.001)**	10.234	**p=0.006 (<0.01)**
Tumour size	123.659	P= 0.213	154.306	**p=0.004 (<0.01)**
Lymph node stage	19.554	**P= 0.000 (<0.001)**	2.797	p=0.247

As shown in Figure 66, high expression of TRAIL-R2 was significantly ($p<0.01$) associated with enhanced breast cancer-specific survival (BCSS) while low TRAIL-R2 expression was associated with worse survival. Similarly, high expression of E-cadherin was significantly ($p<0.05$) associated with improved survival while its low expression was associated with worse survival.

From the cox regression multivariate analysis results shown in Table 7, in addition to the independent ($p<0.01$) prognostic factors of tumour size and lymph node stage on BCSS, TRAIL-R2 was also an independent ($p<0.01$) prognostic factor on BCSS with a hazard ratio of 0.824 (less than 1) which signifies that the presence of TRAIL-R2 increases the chances of BCSS. On the other hand, both the variables E-cadherin and tumour grade were not independent predictors of BCSS with respect to the other variables. Despite not being an independent predictor of survival, E-cadherin also had a hazard ratio of 0.886 (less than 1), evidencing its positive effect on BCSS.

Based on the statistical analyses on the two independent repositories of transcriptomic data of TCGA and METABRIC, the importance of the markers, TRAIL-R2 and E-cadherin in impacting the clinico-pathological parameters and survival of the breast cancer patients was displayed at the mRNA level. Thus, this formed the basis of taking the study on these two markers further to the protein expression level using the method of immunohistochemistry (IHC) as followed. Despite TRAIL mRNA not being differentially expressed across non-tumour, primary tumour and metastases in the TCGA cohort, it had also been included in the following IHC studies since it is an important death ligand in this study and its potential impact on the clinical parameters at the protein expression level should not be neglected.

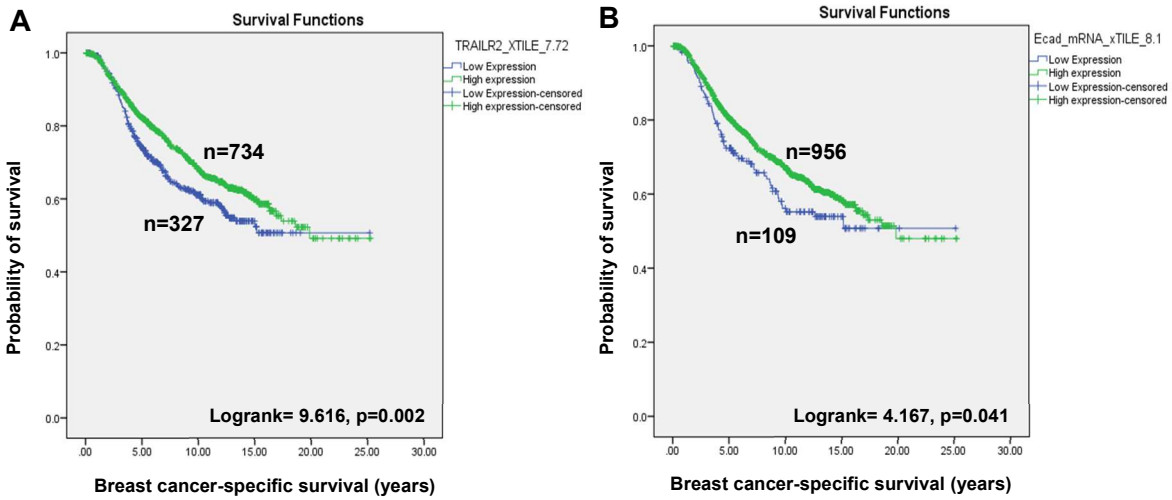


Figure 66 Kaplen-Meier survival plots of (A) *TNFRSF10B* (TRAIL-R2) and (B) *CDH1* (E-cadherin) vs breast cancer-specific survival (BCSS) in all cases of the METABRIC cohort. Dichotomization cut-off values of *TNFRSF10B* and *CDH1* mRNA expression were determined using the X-tile software to be at 7.72 and 8.1, respectively.

Table 7 Cox regression analysis on the effect of TRAIL-R2 (*TNFRSF10B*) and E-cadherin (*CDH1*) expression along with the prognostic factors, tumour grade, tumour size and lymph node stage on BCSS.

Variables	p-value	Hazard ratio (HR)	95% CI for HR	
			Lower	Upper
TNFRSF10B	**p = 0.001**	**0.824**	0.739	0.919
CDH1	p = 0.145	0.886	0.753	1.043
Tumour grade	p = 0.902	0.995	0.917	1.079
Tumour size	**p = 0.001**	**1.006**	1.002	1.009
LN_stage	**p = 0.000**	**1.391**	1.293	1.497

6.3.3 Validation of the TRAIL-R2, E-cadherin and TRAIL primary antibodies' specificity using western blotting and their immunohistochemistry staining on primary invasive BC series

As shown in Figure 67A, the expected band size of E-cadherin at 120 kDa was observed from Western blot assay on MCF-7 whole cell lysate. Nonetheless, in another E-cadherin-expressing cell line, invasive ductal carcinoma T47D, E-cadherin was detected at the band size of 55 kDa. This observation was aligned with the detection of cleaved extracellular E-cadherin form at 55 kDa in the supernatant of colorectal cancer which serves as an invasiveness marker (Christou *et al.*, 2017). On the other hand, no band was detected in thenon-E-cadherin-expressing cell line of MDA-MB-231. The specificity of the anti-E-cadherin (clone 4A2C7) antibody was hence, verified.

From the immunohistochemistry staining done on the primary invasive breast cancer cohort, several representative stained cores' images are shown in Figure 67B. A mixture of cytoplasmic and membranous staining of E-cadherin were observed. There was also a range of staining intensities from none and weak to moderate and strong as shown in Figure 67B.

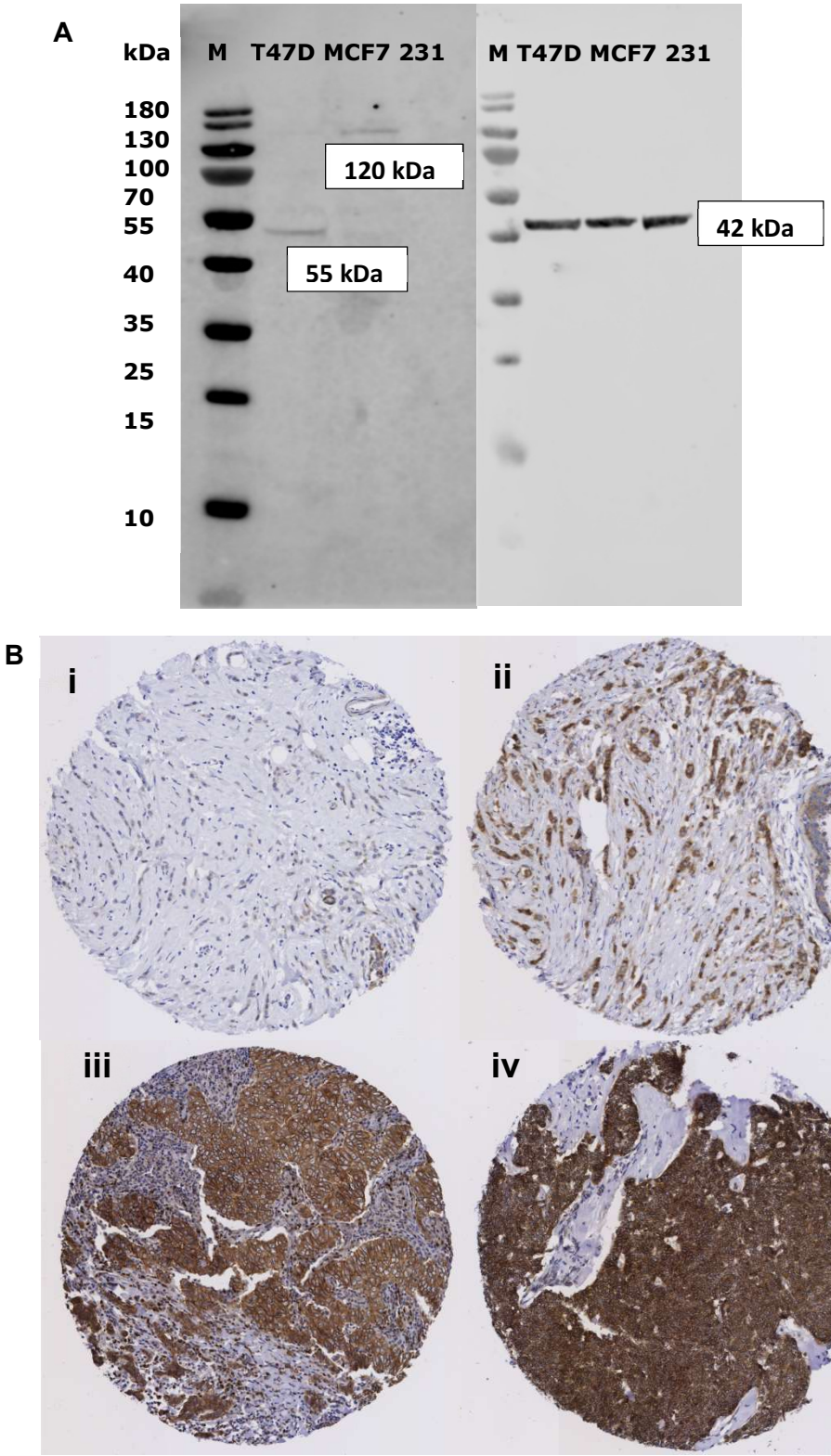


Figure 67 A) Western blot of E-cadherin (*CDH1*) expression in breast ductal carcinoma (T47D) and adenocarcinoma cell lines (MCF-7 and MDA-MB-231). The 42 kDa band on a separate blot (same gel) depicts the β-actin loading control. **B)** Immunohistochemical expression of *CDH1* in primary invasive breast cancer cores showing (i) negative, (ii) weak, (iii) moderate and (iv) strong staining of *CDH1*.

From the Western blot result shown in Figure 68A, the expected band sizes of 47.9 kDa and 45.1 kDa had been detected from the whole cell lysates of all the tested cell lines. In addition, the detected TRAIL-R2 band at approximately 130 kDa could be explained by its ability to self-assemble (Clancy *et al.*, 2005) and cross-assemble with other receptor family members (Smulski *et al.*, 2017). The assembled receptor complex might not have been fully denatured from the heat denaturation step during Western blot. On the other hand, from Uniprot darabase, TRAIL-R2 isoform could be produced from alternative splicing. Therefore, the faint 35 kDa band could have resulted from low levels of mRNA read-through escaping the nonsense-mediated decay of splice variant containing premature stop codon.

Immunohistochemistry staining of TRAIL-R2 showed that TRAIL-R2 could be detected mostly in the cytoplasm with a small percentage of membranous and nuclear staining observed in this study. There was also a range of staining intensities from none and weak to moderate and strong (Figure 68B).

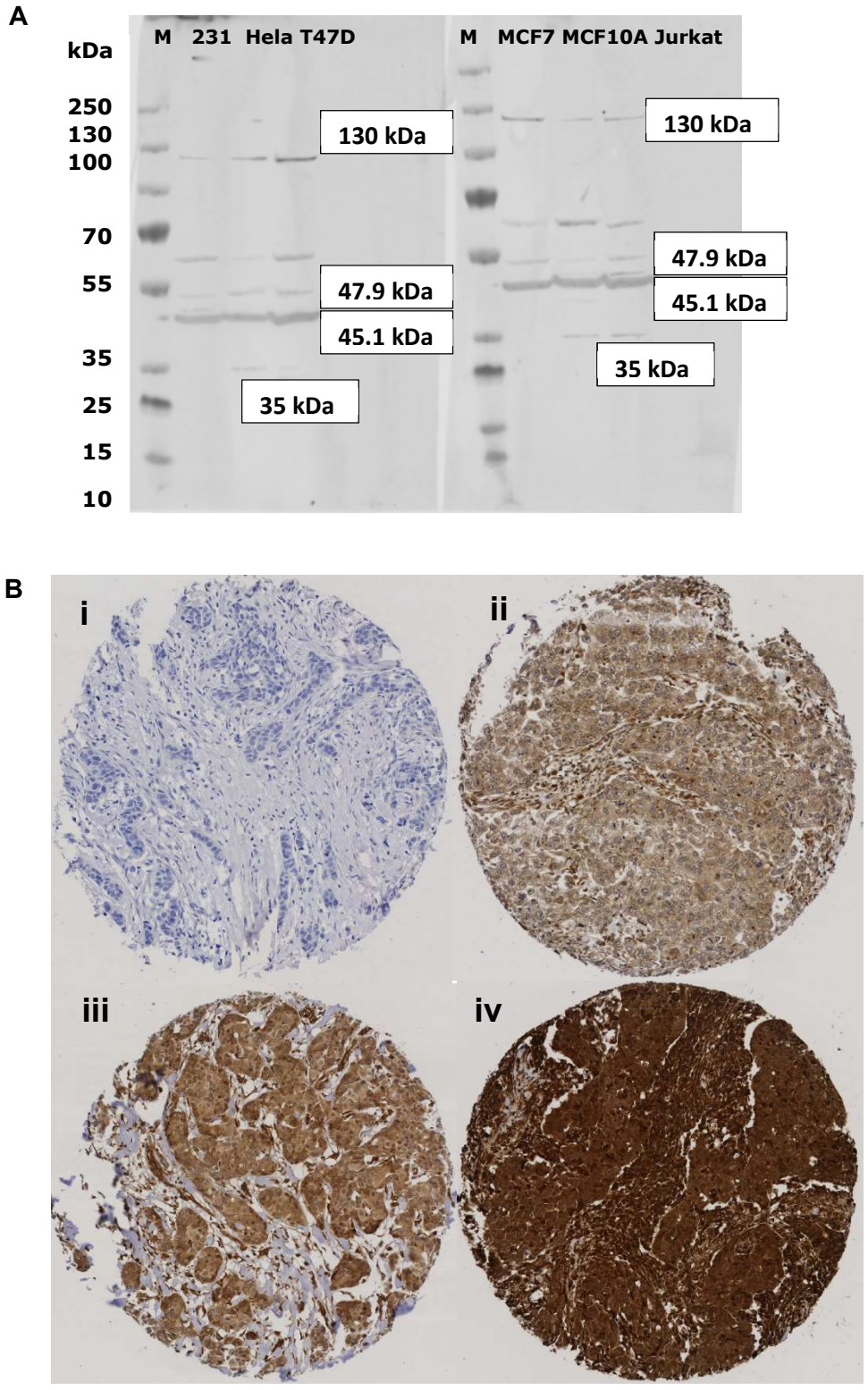


Figure 68 **A)** Western blot of TRAIL-R2 (*TNFRSF10B*) expression in human cervical cancer (HeLa CCL-2), human breast adenocarcinoma (MDA-MB-231, MCF-7), human breast ductal carcinoma (T47D), human acute T cell leukemia (Jurkat) and normal human mammary gland (MCF10A). The 42 kDa band on the same blot depicts the β-actin loading control. **B)** Immunohistochemical expression of *TNFRSF10B* in primary invasive breast cancer cores showing (i) negative, (ii) weak, (iii) moderate and (iv) strong staining of *TNFRSF10B*.

In the Western blot test on the specificity of TRAIL, a 120 kDa band was detected in all the tested cell lines of HeLa CCL-2, MDA-MB-231, MCF-7, SkBr3, T47D, Jurkat and MCF10A (Figure 69A). In addition, the expected band size of 32 kDa was detected in MDA-MB-231, MCF10A and T47D whole cell lysates in addition to the 120 kDa band. The 120 kDa band was believed to be the trimerized (Bodmer *et al.*, 2000) and glycosylated (Micheau, 2018) form of TRAIL.

As for the immunohistochemistry staining of TRAIL, mostly cytoplasmic staining was observed. A smaller percentage of staining was observed to be nuclear. Similar to E-cadherin and TRAIL-R2, a range of none and weak to moderate and strong staining events were observed (Figure 69B).

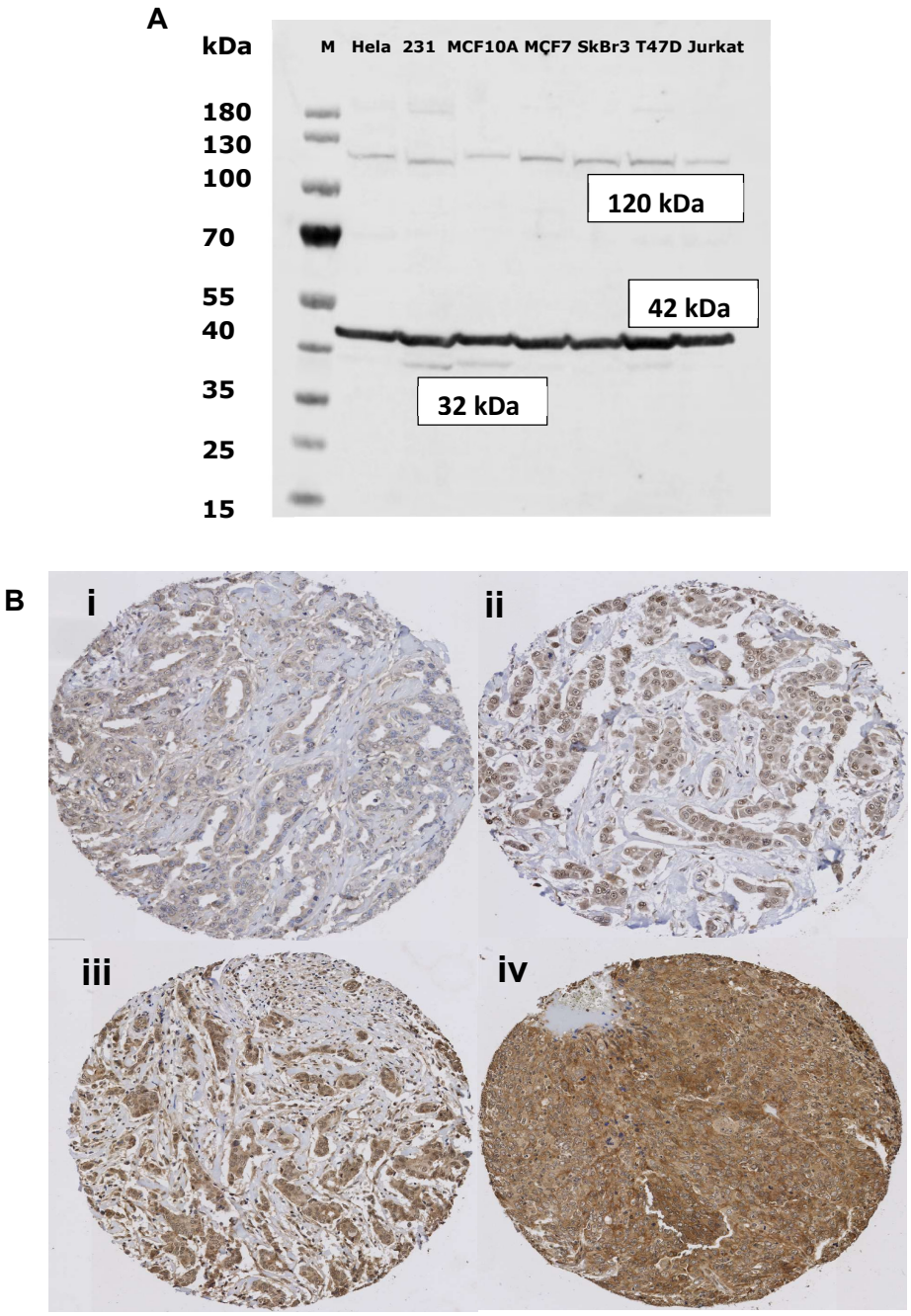


Figure 69 **A)** Western blot of TRAIL (*TNFSF10*) expression in human cervical cancer (HeLa CCL-2), human breast adenocarcinoma (MDA-MB-231, MCF-7, SkBr3), human breast ductal carcinoma (T47D), human acute T cell leukemia (Jurkat) and normal human mammary gland (MCF10A). The 42 kDa band on the same blot depicts the β-actin loading control. **B)** Immunohistochemical expression of *TNFSF10* in primary invasive breast cancer cores showing (i) negative, (ii) weak, (iii) moderate and (iv) strong staining of *TNFSF10*.

6.3.4 Correlation between the H-scores of immunohistochemistry stained TRAIL-R2, E-cadherin and TRAIL on the primary invasive BC series

From the H-scores obtained from the 2000 primary invasive BC cores, cytoplasmic TRAIL-R2 protein expression was positively correlated ($p<0.0001$) with both the cytoplasmic and membranous E-cadherin protein expression. In addition, nuclear expression of TRAIL-R2 protein was also positively correlated with cytoplasmic ($p<0.05$) and membranous ($p<0.0001$) expression of E-cadherin protein. However, the membranous expression of TRAIL-R2 protein was not significantly correlated with either cytoplasmic or membranous E-cadherin protein expression (Table 8).

With respect to the marker, TRAIL protein, both the cytoplasmic ($p<0.0001$) and nuclear ($p<0.05$) TRAIL protein expressions were positively correlated with cytoplasmic E-cadherin protein expression. Similarly, TRAIL protein expression of the two respective aforementioned localizations were also significantly ($p<0.0001$) correlated with the membranous E-cadherin protein expression (Table 8).

Table 8 Pearson correlation test between the H-scores of *CDH1* (E-cadherin) with H-scores of *TNFRSF10B* (TRAIL-R2) and *TNFSF10* from the primary invasive BC series using SPSS analysis.
N.B. p-values in bold are significant differences.

	CDH1* protein** ***Pearson R value ***(p-value)***	
	Cytoplasm	Membrane
***TNFRSF10B* protein**		
Cytoplasm	0.221 (**<0.0001**)	0.107 (**<0.0001**)
Nuclear	0.06 (**0.018**)	0.118 (**<0.0001**)
Membrane	-0.03 (0.232)	0.02 (0.437)
***TNFSF10* protein**		
Cytoplasm	0.139 (**<0.0001**)	0.109 (**<0.0001**)
Nuclear	0.063 (**0.015)**	0.103 (**<0.0001**)

6.3.5 The association between the protein expression of TRAIL-R2, E-cadherin, TRAIL and the clinico-pathological parameters of the primary invasive BC series

6.3.5.1 Clinico-pathological associations of TRAIL-R2, E-cadherin, and TRAIL in breast cancer

As shown in Table 9, high expression of TRAIL-R2 in the cytoplasm was associated with high tumour grade ($p<0.001$), high pleomorphism score ($p<0.001$) and high mitosis score ($p<0.001$). In addition, high cytoplasmic TRAIL-R2 expression was also associated with the histological BC types of ductal and medullary-like ($p<0.001$). On the other hand, low TRAIL-R2 expression was associated with the lobular BC type ($p<0.001$). Nonetheless, cytoplasmic TRAIL-R2 expression was not significantly associated with tumour size, tubule formation, lymph node stage and Nottingham Prognostic Index (NPI).

On the other hand, low TRAIL-R2 expression in the plasma membrane was associated with high tumour grade ($p<0.001$), high tubule formation score ($p<0.05$), high pleomorphism score ($p<0.01$), low mitosis score ($p<0.001$) and moderate NPI ($p<0.01$). Besides, low membranous TRAIL-R2 expression was also associated with all BC type groups except that of tubular. However, membranous TRAIL-R2 expression was not significantly associated with tumour size and lymph node stage in BC (Table 9). Nuclear TRAIL-R2 expression was found to be not significantly associated to any of the clinico-pathological parameters (Table 9).

Table 9 Clinico-pathological associations of TRAIL-R2 (*TNFRSF10B*) cytoplasmic, nuclear and membranous expression in breast cancer.
N.B. p-values in bold are significant differences.

	TRAIL-R2 (*TNFRSF10B*) protein						
	Cytoplasm		**Nuclear**		**Membrane**		
	Low n (%)	**High n (%)**	**Low n (%)**	**High n (%)**	**Low n (%)**	**High n (%)**	**χ^2 (p-value)**
Tumour size							
< 2 cm	370 (38.8%)	584 (61.2%)	883 (92.6%)	71 (7.4%)	906 (95%)	48 (5%)	Cytoplasm: 3.311 (0.069) Nuclear: 1.668 (0.196) Membrane: 0.993 (0.319)
≥ 2 cm	264 (43.4%)	344 (56.6%)	573 (94.2%)	35 (5.8%)	584 (96.1%)	24 (3.9%)	
Tumour grade							
1	77 (37.2%)	130 (62.8%)	191 (92.3%)	16 (7.7%)	205 (99%)	2 (1%)	Cytoplasm: 24.298 (**<0.0001**) Nuclear: 0.336 (0.845) Membrane: 19.236 (**<0.0001**)
2	309 (47.8%)	337 (52.2%)	603 (93.3%)	43 (6.7%)	626 (96.9%)	20 (3.1%)	
3	248 (35%)	461 (65%)	662 (93.4%)	47 (6.6%)	659 (92.9%)	50 (7.1%)	
Tubule formation							
1	27 (32.9%)	55 (67.1%)	75 (91.5%)	7 (8.5%)	81 (98.8%)	1 (1.2%)	Cytoplasm: 4.047 (0.132) Nuclear: 2.552 (0.279) Membrane: 6.821 (**0.033**)
2	173 (38.2%)	280 (61.8%)	429 (94.7%)	24 (5.3%)	439 (96.9%)	14 (3.1%)	
3	427 (42.1%)	587 (57.9%)	939 (92.6%)	75 (7.4%)	957 (94.4%)	57 (5.6%)	
Pleomorphism							
1	2 (18.2%)	9 (81.8%)	10 (90.9%)	1 (9.1%)	11 (100%)	0 (0%)	Cytoplasm: 22.696 (**<0.0001**) Nuclear: 2.751 (0.253) Membrane: 12.57 (**0.002**)
2	222 (49.4%)	227 (50.6%)	411 (91.5%)	38 (8.5%)	441 (98.2%)	8 (1.8%)	
3	403 (37%)	686 (63%)	1022 (93.8%)	67 (6.2%)	1025 (94.1%)	64 (5.9%)	
Mitosis							
1	337 (45.2%)	409 (54.8%)	691 (92.6%)	55 (7.4%)	726 (97.3%)	20 (2.7%)	Cytoplasm: 20.428 (**<0.0001**) Nuclear: 0.75 (0.687) Membrane: 17.127 (**<0.0001**)
2	124 (42.2%)	170 (57.8%)	274 (93.2%)	20 (6.8%)	281 (95.6%)	13 (4.4%)	
3	165 (32.5%)	342 (67.5%)	476 (93.9%)	31 (6.1%)	468 (92.3%)	39 (7.7%)	

Lymph node stage							
1	402 (41.1%)	576 (58.9%)	904 (92.4%)	74 (7.6%)	931 (95.2%)	47 (4.8%)	Cytoplasm: 0.475 (0.788)
2	169 (39.7%)	257 (60.3%)	402 (94.4%)	24 (5.6%)	411 (96.5%)	15 (3.5%)	Nuclear: 2.478 (0.29)
3	60 (38.7%)	95 (61.3%)	147 (94.8%)	8 (5.2%)	146 (94.2%)	9 (5.8%)	Membrane: 1.747 (0.417)
Nottingham Prognostic Index (NPI)							
Good	212 (41.3%)	301 (58.7%)	468 (91.2%)	45 (8.8%)	502 (97.9%)	11 (2.1%)	Cytoplasm: 1.018 (0.601)
Moderate	326 (40.9%)	472 (59.1%)	751 (94.1%)	47 (5.9%)	747 (93.6%)	51 (6.4%)	Nuclear: 4.688 (0.096)
Poor	93 (37.7%)	154 (62.3%)	233 (94.3%)	14 (5.7%)	238 (96.4%)	9 (3.6%)	Membrane: 13.511 (**0.001**)
Histological type							
Ductal (including mixed)	532 (39%)	833 (61%)	1270 (93%)	95 (7%)	1300 (95.2%)	65 (4.8%)	
Lobular	82 (61.7%)	51 (38.3%)	126 (94.7%)	7 (5.3%)	131 (98.5%)	2 (1.5%)	Cytoplasm: 34.284 (**<0.0001**)
Medullary	4 (28.6%)	10 (71.4%)	13 (92.9%)	1 (7.1%)	12 85.7%)	2 (14.3%)	Nuclear: 1.429 (0.964)
Miscellaneous	5 (55.6%)	4 (44.4%)	9 (100%)	0 (0%)	8 (88.9%)	1 (11.1%)	Membrane: 27.9 (**<0.0001**)
Special type	9 (23.7%)	29 (76.3%)	35 (92.1%)	3 (7.9%)	37 (97.4%)	1 (2.6%)	
Tubular	0 (0%)	1 (100%)	1 (100%)	0 (0%)	0 (0%)	1 (100%)	

In Table 10, the clinico-pathological associations of E-cadherin expression in breast cancer were depicted. High E-cadherin expression in cytoplasm was associated with small tumour size ($p<0.01$) and low tumour grade ($p<0.001$). In addition, high cytoplasmic E-cadherin expression was also associated with the BC histological types of ductal, special type and tubular ($p<0.001$). On the other hand, low cytoplasmic E-cadherin expression was associated with high tubule formation score ($p<0.001$), lobular, medullary-like and miscellaneous BC histological type groups ($p<0.001$). However, cytoplasmic E-cadherin expression was not significantly associated with pleomorphism score, mitosis score, lymph node stage and NPI.

Similarly, high membranous E-cadherin expression was associated with low tumour grade ($p<0.01$) and ductal BC histological type group ($p<0.001$). In contrast to cytoplasmic E-cadherin expression, high E-cadherin expression at the plasma membrane was associated with high lymph node stage ($p<0.01$) (Table 10). On the other hand, low membranous E-cadherin expression was associated with high tubule formation score ($p<0.001$), high pleomorphism score ($p<0.05$) and low lymph node stage ($p<0.01$). Besides, similar to low cytoplasmic E-cadherin expression, low membranous E-cadherin expression was associated with the BC histological type groups of lobular and medullary-like. However, membranous E-cadherin expression was not significantly associated with tumour size, mitosis score and NPI (Table 10).

Table 10 Clinico-pathological associations of E-cadherin (*CDH1*) cytoplasmic and membranous expression in breast cancer. N.B. p-values in bold are significant differences.

	E-cadherin (*CDH1*) protein				
	Cytoplasm		**Membrane**		
	Low n (%)	**High n (%)**	**Low n (%)**	**High n (%)**	**χ^2 (p-value)**
Tumour size					
< 2 cm	500 (48%)	542 (52%)	533 (51.2%)	509 (48.8%)	Cytoplasm: 10.1 (**0.001**)
≥ 2 cm	371 (55.9%)	293 (44.1%)	370 (55.7%)	294 (44.3%)	Membrane: 3.402 (0.065)
Tumour grade					
1	95 (38.6%)	151 (61.4%)	112 (45.5%)	134 (54.5%)	Cytoplasm: 17.875 (**<0.0001**)
2	372 (53.1%)	328 (46.9%)	402 (57.4%)	298 (42.6%)	Membrane: 11.959 (**0.003**)
3	405 (53.2%)	356 (46.8%)	390 (51.2%)	371 (48.8%)	
Tubule formation					
1	35 (35.7%)	63 (64.3%)	45 (45.9%)	53 (54.1%)	Cytoplasm: 33.369 (**<0.0001**)
2	214 (42.9%)	285 (57.1%)	232 (46.5%)	267 (53.5%)	Membrane: 16.351 (**<0.0001**)
3	614 (56%)	482 (44%)	621 (56.7%)	475 (43.3%)	
Pleomorphism					
1	7 (41.2%)	10 (58.8%)	9 (52.9%)	8 (47.1%)	Cytoplasm: 1.067 (0.587)
2	267 (52.3%)	244 (47.7%)	297 (58.1%)	214 (41.9%)	Membrane: 7.612 (**0.022**)
3	589 (50.6%)	576 (49.4%)	592 (50.8%)	573 (49.2%)	
Mitosis					
1	417 (50.2%)	414 (49.8%)	463 (55.7%)	368 (44.3%)	Cytoplasm: 0.494 (0.781)
2	164 (51.6%)	154 (48.4%)	154 (48.4%)	164 (51.6%)	Membrane: 5.414 (0.067)
3	282 (52%)	260 (48%)	281 (51.8%)	261 (48.2%)	

Lymph node stage					
1	545 (51.1%)	522 (48.9%)	591 (55.4%)	476 (44.6%)	Cytoplasm: 0.028 (0.986)
2	236 (50.8%)	229 (49.2%)	218 (46.9%)	247 (53.1%)	Membrane: 9.563 (**0.008**)
3	88 (51.5%)	83 (48.5%)	93 (54.4%)	78 (45.6%)	
Nottingham Prognostic Index (NPI)					
Good	270 (47.4%)	300 (52.6%)	299 (52.5%)	271 (47.5%)	Cytoplasm: 4.88 (0.087)
Moderate	450 (52.3%)	410 (47.7%)	470 (54.7%)	390 (45.3%)	Membrane: 2.847 (0.241)
Poor	148 (54.4%)	124 (45.6%)	133 (48.9%)	139 (51.1%)	
Histological type					
Ductal (including mixed)	710 (48.1%)	766 (51.9%)	729 (49.4%)	747 (50.6%)	
Lobular	128 (84.2%)	24 (15.8%)	131 (86.2%)	21 (13.8%)	Cytoplasm: 82.86 (**<0.0001**)
Medullary	10 (71.4%)	4 (28.6%)	10 (71.4%)	4 (28.6%)	Membrane: 78.695 (**<0.0001**)
Miscellaneous	6 (60%)	4 (40%)	4 (40%)	6 (60%)	
Special type	18 (35.3%)	33 (64.7%)	28 (54.9%)	23 (45.1%)	
Tubular	0 (0%)	2 (100%)	1 (50%)	1 (50%)	

In the aspect of clinico-pathological associations of TRAIL expression in breast cancer, high cytoplasmic expression of TRAIL was associated with high tumour grade ($p<0.001$) and high mitosis score ($p<0.001$). On the other hand, low cytoplasmic TRAIL expression was associated with high pleomorphism score ($p<0.01$) (Table 11). Nonetheless, cytoplasmic TRAIL expression was not significantly associated with tumour size, tubule formation, lymph node stage, NPI and BC histological types (Table 11).

On the other hand, low nuclear TRAIL expression was associated with small tumour size ($p<0.01$), moderate NPI ($p<0.05$), low mitosis score ($p<0.01$) but high tumour grade ($p<0.01$). In addition, low nuclear TRAIL expression was associated with all BC type groups except special type. Nevertheless, there was no significant association between nuclear TRAIL expression with tubule formation, pleomorphism, and lymph node stage in BC (Table 11).

Table 11 Clinico-pathological associations of TRAIL (*TNFSF10*) cytoplasmic and nuclear expression in breast cancer.
N.B. p-values in bold are significant differences.

	TRAIL (*TNFSF10*) protein				
	Cytoplasm		**Nuclear**		
	Low n (%)	**High n (%)**	**Low n (%)**	**High n (%)**	**χ^2 (p-value)**
Tumour size					
< 2 cm	492 (53.5%)	428 (46.5%)	601 (65.3%)	319 (34.7%)	Cytoplasm: 0.032 (0.857)
≥ 2 cm	321 (53.9%)	274 (46.1%)	429 (72.2%)	165 (27.8%)	Nuclear: 7.893 (**0.005**)
Tumour grade					
1	124 (61.1%)	79 (38.9%)	128 (63.1%)	75 (36.9%)	Cytoplasm: 16.644 (**<0.0001**)
2	354 (57.5%)	262 (42.5%)	399 (64.8%)	217 (35.2%)	Nuclear: 11.347 (**0.003**)
3	335 (48.1%)	361 (51.9%)	503 (72.4%)	192 (27.6%)	
Tubule formation					
1	42 (53.8%)	36 (46.2%)	50 (64.1%)	28 (35.9%)	Cytoplasm: 0.107 (0.948)
2	242 (54.5%)	202 (45.5%)	293 (66%)	151 (34%)	Nuclear: 2.076 (0.354)
3	525 (53.6%)	455 (46.4%)	678 (59.3%)	301 (30.7%)	
Pleomorphism					
1	5 (45.5%)	6 (54.5%)	6 (54.5%)	5 (45.5%)	Cytoplasm: 10.896 (**0.004**)
2	258 (60.6%)	168 (39.4%)	273 (64.1%)	153 (35.9%)	Nuclear: 5.393 (0.067)
3	546 (51.3%)	519 (48.7%)	742 (69.7%)	322 (30.3%)	
Mitosis					
1	422 (58.9%)	294 (41.1%)	455 (63.5%)	261 (36.5%)	Cytoplasm: 23.114 (**<0.0001**)
2	160 (56.1%)	125 (43.9%)	201 (70.5%)	84 (29.5%)	Nuclear: 12.969 (**0.002**)
3	226 (45.2%)	274 (54.8%)	364 (72.9%)	135 (27.1%)	

Lymph node stage					
1	496 (52.8%)	443 (47.2%)	630 (67.2%)	308 (32.8%)	Cytoplasm: 0.858 (0.651)
2	228 (54.4%)	191 (45.6%)	290 (69.2%)	129 (30.8%)	Nuclear: 0.905 (0.636)
3	87 (56.5%)	67 (43.5%)	108 (70.1%)	46 (29.9%)	
Nottingham Prognostic Index (NPI)					
Good	277 (56.9%)	210 (43.1%)	308 (63.2%)	179 (36.8%)	Cytoplasm: 3.622 (0.164)
Moderate	400 (51.4%)	378 (48.6%)	543 (69.9%)	234 (30.1%)	Nuclear: 8.101 (**0.017**)
Poor	133 (54.1%)	113 (45.9%)	177 (72%)	69 (28%)	
Histological type					
Ductal (including mixed)	708 (53.1%)	625 (46.9%)	917 (68.8%)	416 (31.2%)	
Lobular	75 (63%)	44 (37%)	74 (62.2%)	45 (37.8%)	Cytoplasm: 7.846 (0.165)
Medullary	4 (33.3%)	8 (66.7%)	11 (91.7%)	1 (8.3%)	Nuclear: 11.931 (**0.036**)
Miscellaneous	4 (44.4%)	5 (55.6%)	6 (75%)	2 (25%)	
Special type	22 (55%)	18 (45%)	20 (50%)	20 (50%)	
Tubular	0 (0%)	1 (100%)	1 (100%)	0 (0%)	

6.3.5.2 Expression of TRAIL-R2, E-cadherin and TRAIL in breast cancer and the expression of other molecular biomarkers

Aside from the clinico-pathological associations test conducted in the previous section, the expression of TRAIL-R2, E-cadherin and TRAIL were also studied along with the expression of estrogen receptor (ER), progesterone receptor (PR), and human epidermal growth factor receptor 2 (HER2) overexpression in breast cancer (BC). From the results summarized in Table 12, high cytoplasmic TRAIL-R2 expression was associated with positive ER expression (ER+) ($p<0.001$) and negative HER2 overexpression (HER2-) ($p<0.001$). In addition, high cytoplasmic TRAIL-R2 expression was also concurrently associated with the non-triple negative patient group ($p<0.01$). Similarly, low membranous TRAIL-R2 expression was associated with ER+ ($p<0.001$), positive PR expression (PR+) ($p<0.001$) and HER2- ($p<0.01$). Likewise, low membranous TRAIL-R2 expression was associated with the non-triple negative patient group ($p<0.01$).

Table 12 The cytoplasmic, nuclear and membranous expression of TRAIL-R2 (*TNFRSF10B*) in breast cancer and the expression of other molecular biomarkers. N.B. p-values in bold are significant differences.

	TRAIL-R2 (*TNFRSF10B*) protein						
	Cytoplasm		**Nuclear**		**Membrane**		
	Low n (%)	**High n (%)**	**Low n (%)**	**High n (%)**	**Low n (%)**	**High n (%)**	**χ^2 (p-value)**
ER							
Negative	94 (30.2%)	217 (69.8 %)	290 (93.2%)	21 (6.8%)	279 (89.7%)	32 (10.3%)	Cytoplasm: 17.329 (**<0.0001**) Nuclear: 0.000 (0.984) Membrane: 28.576 (**<0.0001**)
Positive	541 (43.2%)	712 (56.8%)	1168 (93.2%)	85 (6.8%)	1213 (96.8%)	40 (3.2%)	
PR							
Negative	247 (38.2%)	399 (61.8%)	595 (92.1%)	51 (7.9%)	593 (91.8%)	53 (8.2%)	Cytoplasm: 3.094 (0.079) Nuclear: 2.022 (0.155) Membrane: 31.968 (**<0.0001**)
Positive	388 (42.7%)	521 (57.3%)	854 (93.9%)	55 (6.1%)	890 (97.9%)	19 (2.1%)	
HER2							
Negative	577 (42.5%)	782 (57.5%)	1266 (93.2%)	93 (6.8%)	1305 (96%)	54 (4%)	Cytoplasm: 14.82 (**<0.0001**) Nuclear: 0.071 (0.79) Membrane: 9.372 (**0.002**)
Positive	58 (28.3%)	147 (71.7%)	192 (93.7%)	13 (6.3%)	187 (91.2%)	18 (8.8%)	
Triple negative							
No	564 (42.2%)	773 (57.8%)	1246 (93.2%)	91 (6.8%)	1284 (96%)	53 (4%)	Cytoplasm: 9.571 (**0.002**) Nuclear: 0.012 (0.912) Membrane: 8.578 (**0.003**)
Yes	71 (31.3%)	156 (68.7%)	212 (93.4%)	15 (6.6%)	208 (91.6%)	19 (8.4%)	

In terms of E-cadherin expression along with the expression of ER, PR and HER2, high cytoplasmic E-cadherin expression was associated with ER+ ($p<0.05$), PR+ ($p<0.001$) and HER2- ($p<0.01$). On the other hand, high membranous E-cadherin expression was associated with HER2+ ($p<0.05$) but not significantly associated with ER or PR expression. In addition, both the cytoplasmic and membranous expression of E-cadherin were neither associated with the triple negative nor the non-triple negative patient group (Table 13).

With regards to TRAIL expression, low cytoplasmic TRAIL expression was associated with ER+ ($p<0.001$) and the non-triple negative patient group ($p<0.001$). On the other hand, low nuclear TRAIL expression was associated with ER+ ($p<0.001$), HER2- ($p<0.001$) and the non-triple negative patient group ($p<0.001$) (Table 14).

Table 13 The cytoplasmic and membranous expression of *CDH1* in breast cancer and the expression of other molecular biomarkers.
N.B. p-values in bold are significant differences.

	E-cadherin (*CDH1*) protein				
	Cytoplasm		**Membrane**		
	Low n (%)	**High n (%)**	**Low n (%)**	**High n (%)**	**χ^2 (p-value)**
ER					
Negative	187 (56.3%)	145 (43.7%)	181 (54.5%)	151 (45.5%)	Cytoplasm: 4.532 (**0.033**)
Positive	686 (49.8%)	691 (50.2%)	724 (52.6%)	653 (47.4%)	Membrane: 0.404 (0.525)
PR					
Negative	392 (56.1%)	307 (43.9%)	366 (52.4%)	333 (47.6%)	Cytoplasm: 12.124 (**<0.0001**)
Positive	474 (47.5%)	524 (52.5%)	533 (53.4%)	465 (46.6%)	Membrane: 0.181 (0.671)
HER2					
Negative	741 (49.7%)	749 (50.3%)	803 (53.9%)	687 (46.1%)	Cytoplasm: 8.492 (**0.004**)
Positive	132 (60.3%)	87 (39.7%)	102 (46.6%)	117 (53.4%)	Membrane: 4.104 (**0.043**)
Triple negative					
No	738 (50.4%)	726 (49.6%)	766 (52.3%)	698 (47.7%)	Cytoplasm: 1.849 (0.174)
Yes	135 (55.1%)	110 (44.9%)	139 (56.7%)	106 (43.3%)	Membrane: 1.64 (0.200)

Table 14 The cytoplasmic and nuclear expression of TRAIL (*TNFSF10*) in breast cancer and the expression of other molecular biomarkers. N.B. p-values in bold are significant differences.

	TRAIL (*TNFSF10*) protein				
	Cytoplasm		**Nuclear**		
	Low n (%)	**High n (%)**	**Low n (%)**	**High n (%)**	**χ^2 (p-value)**
ER					
Negative	123 (40.5%)	181 (59.5%)	240 (78.9%)	64 (21.1%)	Cytoplasm: 26.362 (**<0.0001**)
Positive	690 (56.9%)	523 (43.1%)	792 (65.3%)	420 (34.7%)	Nuclear: 20.686 (**<0.0001**)
PR					
Negative	322 (50.8%)	312 (49.2%)	448 (70.8%)	185 (29.2%)	Cytoplasm: 3.764 (0.052)
Positive	488 (55.8%)	386 (44.2%)	578 (66.1%)	296 (33.9%)	Nuclear: 3.639 (0.056)
HER2					
Negative	699 (53.4%)	610 (46.6%)	916 (70%)	393 (30%)	Cytoplasm: 0.143 (0.705)
Positive	114 (54.8%)	94 (45.2%)	116 (56%)	91 (44%)	Nuclear: 15.978 (**<0.0001**)
Triple negative					
No	733 (56.5%)	564 (43.5%)	846 (65.3%)	450 (34.7%)	Cytoplasm: 30.711 (**<0.0001**)
Yes	80 (36.4%)	140 (63.6%)	186 (84.5%)	34 (15.5%)	Nuclear: 32.126 (**<0.0001**)

6.3.5.3 The effect of TRAIL-R2, E-cadherin, and TRAIL protein expression on breast cancer specific survival (BCSS)

From the Kaplan-Meier analysis on BCSS of all the markers' parameters, only membranous TRAIL-R2 expression had a significant effect on breast cancer-specific survival (BCSS). Low membranous TRAIL-R2 expression was associated with better BCSS, as shown in (Figure 70A).

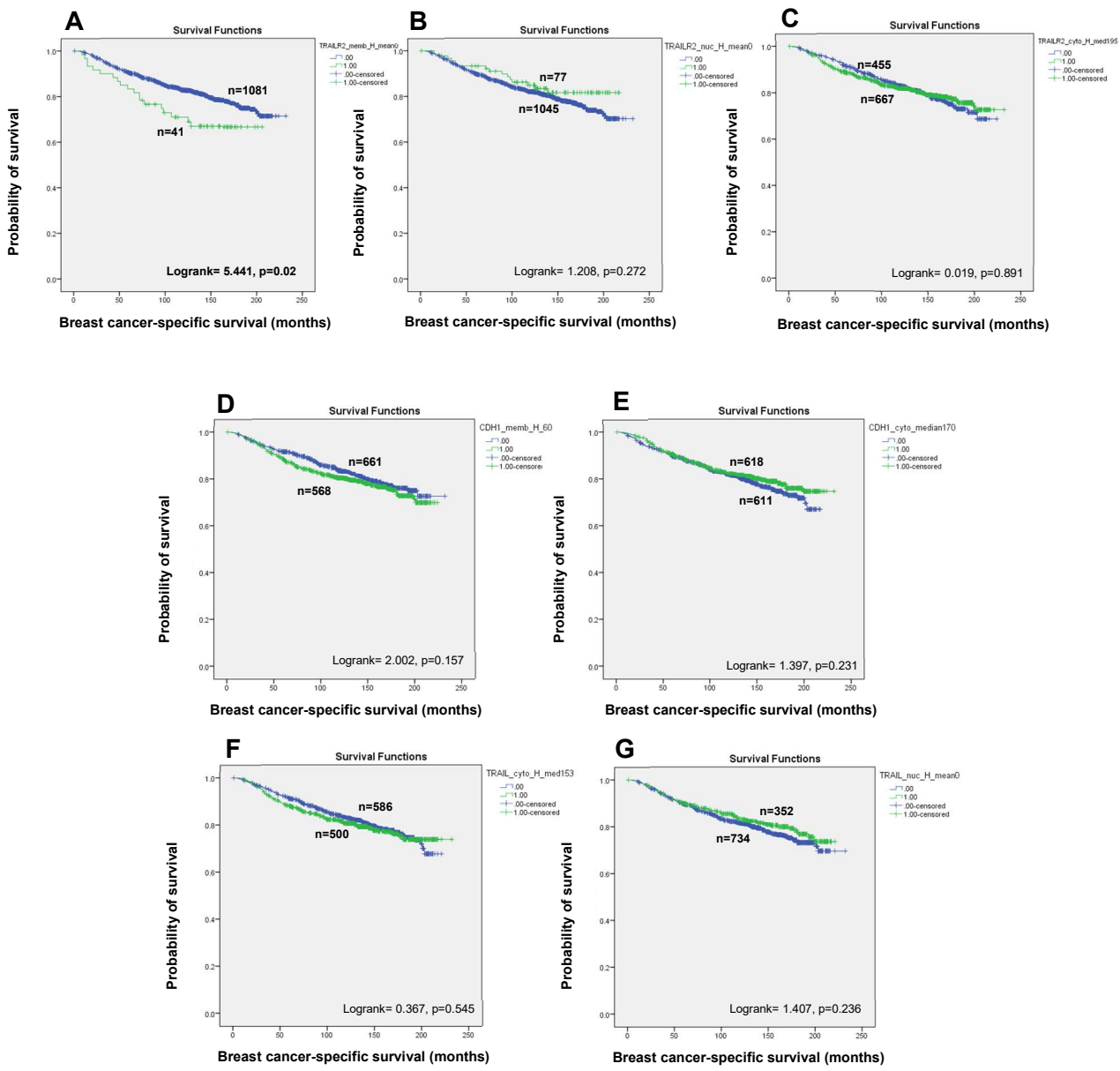


Figure 70 Effect of *TNFRSF10B*, *CDH1* and *TNFSF10* protein expression on breast cancer patient outcome. **(A)** membranous TRAIL-R2 (*TNFRSF10B*) vs BCSS; **(B)** nuclear TRAIL-R2 (*TNFRSF10B*) vs BCSS; **(C)** cytoplasmic TRAIL-R2 (*TNFRSF10B*) vs BCSS; **(D)** membranous E-cadherin (*CDH1*) vs BCSS; **(E)** cytoplasmic E-cadherin (*CDH1*) vs BCSS; **(F)** cytoplasmic TRAIL (*TNFSF10*) vs BCSS; **(G)** nuclear TRAIL (*TNFSF10*) vs BCSS in all cases. N.B. p-values in bold are significant differences. 0= low expression; 1= high expression

6.4 Discussion

Breast cancer (BC) is a disease known for its heterogeneity, both intra-tumourous and inter-tumourous, in terms of stages, histopathological classifications and expression of prognostic biomarkers like hormone receptors and HER2 (Turashvili and Brogi, 2017). This heterogeneity in BC had resulted in heterogeneity of drug response even among different clones from a single cancer cell (Wang *et al.*, 2017), making the recent invent of anti-cancer drug sensitivity assay with quantitative heterogeneity testing (Zhang *et al.*, 2018) relevant.

In this study, TRAIL sensitivity had been tested *in vitro* on breast adenocarcinoma cells, MDA-MB-231 (without E-cadherin expression), 231-EGFP (transfected with E-cadherin) and MCF-7 (with E-cadherin expression), as reported in the previous chapters. With the aforementioned heterogeneity in BC, it was deemed more relevant to complement the *in vitro* findings with the *ex vivo* findings via bioinformatics analysis of established BC patient mRNA data and immunohistochemistry on sections of formalin-fixed paraffin-embedded BC tissue cores array of the biomarkers, TRAIL-R2, E-cadherin and TRAIL.

The mRNA expression of TRAIL-R2 and E-cadherin were inversely correlated in the TCGA cohort in the comparisons between the triple negative versus non-triple negative patient groups and the non-tumour versus primary tumour groups (Figure 65, Table 4). This finding had also been corroborated by the METABRIC cohort in which the negative correlation between TRAIL-R2 and E-cadherin was also observed (Table 5). At the protein expression level, low membranous TRAIL-R2 expression was significantly associated with the non-triple negative patient (positive E-cadherin expression) group (Table 12). This inverse correlation between the expression of TRAIL-R2 and E-cadherin was also supported by the observation of increased E-cadherin expression in TRAIL-R2 knock-down in MDA-MB-231 of another study (Kalthoff *et al.*, 2014).

Nonetheless, both the cytoplasmic and nuclear expression of TRAIL-R2 but not membranous were positively correlated with both the cytoplasmic and membranous E-cadherin expression (Table 8). The disparity in correlation of the two markers between mRNA and protein expression could potentially be explained by the differential regulatory impact of different TRAIL-R2 isoforms on E-cadherin expression whereby the over-expression of short-TRAIL-R2-isoform down-regulated E-cadherin while the over-expression of long TRAIL-R2 isoform up-regulated E-cadherin (Fritsche *et al.*, 2015).

On the other hand, TRAIL mRNA expression was positively correlated with E-cadherin mRNA expression in the TCGA cohort (Table 4). This mRNA data was condoned by the positive correlation between both cytoplasmic and nuclear TRAIL expression with the cytoplasmic and membranous E-cadherin expression from the IHC analyses (Table 8). However, high cytoplasmic TRAIL expression was associated with the high tumour grade and high mitosis score while its low nuclear expression was associated with better prognosis of smaller tumour size, moderate NPI and low mitosis score (Table 11). This finding showed that regardless of its localization, TRAIL overexpression was associated with poor prognosis in this BC and it was supported by another study in hepatocarcinoma cells whereby TRAIL surface overexpression could be hijacked by cancer cells to evade immune surveillance by inducing apoptosis of activated tumour-infiltrating lymphocytes (Shiraki *et al.*, 2005). Moreover, low nuclear and cytoplasmic TRAIL expression were also correlated with ER+ and the non-triple negative patient groups which signified better prognosis (Table 14). These findings were in agreement with another previous finding that high TRAIL cytoplasmic expression was correlated with nuclear grade in carcinoma (Bilski *et al.*, 2010), showing that overexpression of TRAIL, regardless of its localization, might be part of an escape mechanism established by cancer cells against tumour surveillance by inducing apoptosis in tumour-infiltrating lymphocytes (Koyama *et al.*, 2002).

High TRAIL-R2 expression was constantly shown to be associated with decreased survival in breast cancer (McCarthy *et al.*, 2005) and human pancreatic ductal adenocarcinoma as well as other tumour cells (Hadelmann *et al.*, 2014). Similarly in this study on a large BC cohort, high cytoplasmic expression of TRAIL-R2 was associated with the negative prognostic markers like high tumour grade ($p<0.001$), high pleomorphism score ($p<0.001$) and high mitosis score ($p<0.001$) (Table 9). Concurrently, low membranous TRAIL-R2 expression was also similarly associated with the unfavourable prognostic markers like higher tumour grade, higher tubule formation and higher pleomorphism score. This phenomenon could possibly be explained by the mis-localization of TRAIL-R2 from its canonical plasma membrane to other cell parts like cytosol and nuclear, limiting its apoptosis-induction capacity. A recent finding showing that TRAIL-R2 mislocalized to the nucleus could prevent primary let-7 miRNA maturation and enhance tumour cell proliferation (Bertsch *et al.*, 2014; Hadelmann *et al.*, 2014) had verified the aforementioned explanation. Nonetheless, overall, low membranous TRAIL-R2 expression was associated with moderate NPI (Table 9) and enhanced BCSS (Figure 70A). This could be attributed to the pro-invasive role of TRAIL-R2 repeatedly being reported in breast cancer which was shown to stem from up-regulation of CXCR4 levels and enhanced stromal cell-derived factor 1-directed migration in BC (Fritsche *et al.*, 2015; Malin *et al.*, 2011).

Therefore, the observation that TRAIL-R2 (Bertsch *et al.*, 2014) and other plasma membrane receptor like fibroblast growth factor receptor-1 (Dunham-Ems *et al.*, 2006) having compartmentalized and distinct functions across different cellular localizations had approved our study approach in measuring the nuclear, cytoplasmic and membranous expression of the markers in this study. For instance, the finding that high cytoplasmic and low membranous TRAIL-R2 expression were associated with poor prognosis in this study showed that the mis-localization of TRAIL-R2 from its canonical plasma membrane localization could be part of the mechanism with which BC cells

escape from TRAIL-induced apoptosis. Nonetheless, the overall association of low membranous TRAIL-R2 expression with moderate NPI and enhanced BCSS depicts that TRAIL-R2 was more weighted towards the pro-invasive role in BC.

On the other hand, E-cadherin is commonly being recognized as a tumour-suppressor gene (Jeanes *et al.*, 2008; Pećina-Šlaus, 2003). Li *et al.* (2017) have reported that reduced E-cadherin expression was correlated with higher histological tumour grade, larger tumour size and negative progesterone receptor status. Similarly, in our study, high cytoplasmic E-cadherin expression was significantly correlated with favourable prognosis like smaller tumour size and lower tumour grade. High membranous E-cadherin expression was also associated with lower tumour grade while low membranous E-cadherin expression correlated with higher tubule formation and higher pleomorphism score which signified worse prognosis (Table 10). From these findings, it was shown that E-cadherin, regardless of its localization in the membrane or cytoplasm, functions as a tumour suppressor gene as its expression contributes towards favourable prognosis in BC. E-cadherin's tumour suppressing role could be attributed to its regulation on cancer cells apoptosis shown in gall bladder carcinoma (Sasatomi *et al.*, 1996) and melanoma cells (Hsu *et al.*, 2000) which potentially involves its negative regulation on β-catenin's activation of the Wnt signalling pathway which increases cell proliferation

In terms of correlation between E-cadherin expression and hormone receptor status, high cytoplasmic expression of E-cadherin was significantly associated with ER+, PR+ and HER2- (Luminal A). This finding complemented the aforementioned results that E-cadherin expression serves the tumour suppressor role because breast cancer subtype luminal A commonly grows slower and gives better survival in contrast to TNBC which does not present with any hormone receptor expression (Fallahpour *et al.*, 2017). Nonetheless,

membranous expression of E-cadherin was only associated with the over-expression of HER2 (HER2+) (Table 13). HER2+, mostly localized at the plasma membrane (Jeong *et al.*, 2017), alone was shown to be correlated with worse prognosis in breast cancer patients as its overexpression promoted malignant behavior in human mammary epithelial cell lines (Jeong *et al.*, 2017; Karray-Chouayekh *et al.*, 2012). In addition, high membranous E-cadherin expression was also associated with higher LN stage (Table 10). This finding was condoned by the numerous reports on the pro-invasive role of membranous E-cadherin expression in enhancing breast cancer metastases (Chao *et al.*, 2010; Palen *et al.*, 2016; Repetto *et al.*, 2014) by its dynamic expression changes from loss in EMT to gain in MET, thereby facilitating the cancer cells' survival and colonization in establishing secondary metastases (Wong *et al.*, 2018). Therefore, despite cytoplasmic expression of E-cadherin contributed towards better BC prognosis, membranous E-cadherin expression had been harnessed by BC cells to fuel their survival and metastatic potential.

6.5 Concluding remarks

In conclusion, in the BC patient cohorts tested, TRAIL-R2 and E-cadherin assumed a negative correlation at both the mRNA and protein levels. However, at the protein level, different TRAIL-R2 isoforms might have differential regulation on E-cadherin. Low membranous TRAIL-R2 expression was correlated with unfavourable prognostic markers, showing that membranous TRAIL-R2 could be a marker for good prognosis in BC. Nonetheless, its high membranous expression was yet associated with poor BCSS, potentially due to TRAIL-R2 being harnessed by cancer cells for a pro-invasive role. Similarly, despite being associated with an overall good prognosis, membranous E-cadherin expression was also shown to be pro-invasive by its association with higher LN stage in our study. Last but not least, over-expression of TRAIL, regardless of its localization, was associated with high tumour grade and high mitosis score, demonstrating that the escape mechanism from tumour surveillance might be in place in this study. Thus, these findings showed that the tumour suppressor genes, TRAIL-R2, TRAIL and E-cadherin markers' anti-cancer functions had been hijacked by BC cells to facilitate their survival (TRAIL) and metastatic potential (TRAIL-R2, E-cadherin). Both their over-expression and localization could potentially serve as markers for BC prognosis and treatment regime selection.

7. Conclusion and Future Perspectives

At the beginning of this study, the *CDH1*-GFP gene was successfully delivered into MDA-MB-231 using the non-viral, chemical-based transfection method as it had low cytotoxicity and better versatility. Lipofectamine LTX reagent gave an 11.5% of transfection efficiency while *Trans*IT-X2® reagent produced only 7.6% of transfection efficiency. *Trans*IT-X2® reagent was chosen despite its inferiority in terms of transfection efficiency due to the much less cytotoxicity induced on transfected MDA-MB-231 cells. As miRNA silencing could have contributed to the low *CDH1*-GFP expression in MDA-MB-231, the low *CDH1*-GFP expressing MDA-MB-231 cell population could only be maintained under G4-18 selection for up to a month's time, resulting in transient expression. Therefore, after transfection, selection and expansion of *CDH1*-GFP expressing MDA-MB-231 cell population, all following cellular and molecular assays were conducted within a month before another transfection of delivering the gene *CDH1*-GFP into MDA-MB-231 cells was performed and followed by the cellular and molecular assays.

When the efficacy of epigenetic drugs, TSA and Zeb sensitization of MDA-MB-231 human breast adenocarcinoma cells towards TRAIL anti-cancer effects were probed into, E-cadherin expression was shown to enhance the TZT-induced growth inhibition and G_0/G_1 cell cycle arrest. The anti-cancer effects were shown to be mediated by the suppression of PCNA and CDK2 expression by the TZT treatment alongside E-cadherin expression. Nonetheless, future prospective study design on TRAIL needs to highlight the pro-invasiveness nature of TRAIL in order that TRAIL can be applied to the cancer therapy field with more promising versatility.

With the promising results from Chapter 4, the research was brought further to analysing the potential of the treatment regime in apoptosis induction. Collectively, the results from the apoptosis assessment reported in Chapter 5 showed that TZT had shown promising potential in enhancing TRAIL-induced apoptosis on the basis that TZ prior treatment had directed MDA-MB-231 towards cell cycle arrest before apoptosis occurrence. This was supported by the up-regulation of p21 and p-p53 (S392) in MDA-

MB-231 by TZT. With the *in vitro* re-expression of E-cadherin in 231-EGFP, down-regulation of anti-apoptotic PON2, catalase, clusterin, IAPs as well as cell stress proteins had validated the notion that E-cadherin expression enhanced the TZT anti-cancer efficacy. Similarly, in E-cadherin-positive MCF-7, the anti-apoptotic proteins had been down-regulated while the pro-apoptotic SMAC, HTRA2 as well as both the TRAIL receptors, TRAIL R1 and R2 had been up-regulated by TZT. Nonetheless, *in vitro* re-expression of E-cadherin in 231-EGFP had negatively down-regulated TRAIL R1 and TRAIL R2 expression, demonstrating that *in vitro* re-expression of E-cadherin in MDA-MB-231 might not be the most feasible model in terms of studying TRAIL-based anti-cancer activities in breast cancer.

From the *in vitro* studies, it could be concluded that TZ treatment had displayed itself as a potential sensitizer of human breast adenocarcinoma cells towards TRAIL-induced growth inhibition, G_0/G_1 cell cycle arrest and apoptosis, both with and without E-cadherin expression. In the case of MDA-MB-231, TZT-induced apoptosis could be increased with the prolonging of TZ prior treatment from 12 to 24 h. In Chapter 4, it was shown that the delayed reduction in cell viability of MDA-MB-231 on TZT treatment at 48 h (Figure 24b) could be explained by the cell cycle arrest induced from the first 24 h of TZT treatment. Therefore, with the prolongation of TZ sensitization period prior to TRAIL treatment, sufficient time would then be given for cell cycle arrest to occur. This adds value to TRAIL-based therapy as it can then be used to target the resting, non-proliferative tumour cells which are usually recalcitrant towards treatment and stimulate relapse after an extended period of time (Ehrhardt *et al.*, 2015). On the other hand, since 231-EGFP was seen as the inferior E-cadherin-positive model due to its down-regulatory effect on TRAIL-R1 and TRAIL-R2, it is therefore proposed that for future work, MCF-7 with re-constituted caspase-3 might serve as a better model to study the effect of E-cadherin expression on the TZT apoptosis-inducing efficacy in future. The value of caspase-3 reconstitution in MCF-7 as a drug efficacy model was also shown in a recent study (Nan *et al.*, 2019).

As for the *in vivo* findings, TRAIL-R2 and E-cadherin were inversely correlated with each other both at the mRNA and protein levels, despite the possible differential regulation on E-cadherin by the different TRAIL-R2 isoforms. This finding was aligned with the *in vitro* observation that E-cadherin re-expression had down-regulated TRAIL-R1 and TRAIL-R2, potentially due to the sequestration of beta-catenin (Wong *et al.*, 2018) pool that is available for interaction with other growth factors and transcription factors which could stabilize or increase the expression of both TRAIL receptors (Essers *et al.*, 2005; Hiscox and Jiang, 1999; Kanai *et al.*, 1995; Li *et al.*, 1998). In addition, despite low membranous TRAIL-R2 expression being correlated with poor prognostic factors, it was counter-intuitively correlated with better BCSS, possibly due to TRAIL-R2 being hijacked to become pro-invasive in breast cancer cells. In the same vein, E-cadherin, being a tumour suppressor protein, was also associated with higher LN stage in this study cohort. The notion that E-cadherin re-expression aids metastases formation (Chao *et al.*, 2010) in breast cancer is condoned by this finding. Moreover, the over-expression of the death ligand, TRAIL, was also associated with high tumour grade and high mitosis score, showing that cancers could have developed the escape mechanism from tumour surveillance.

In short, in the feat of enhancing the efficacy of TRAIL-based cancer therapy, future research directions should be more diversified rather than monolithic. Since this study had revealed that supposedly tumour suppressor genes like TRAIL, TRAIL-R2 and E-cadherin could be hijacked by cancer cells towards fuelling their survival, research goals should be focused not only on growth inhibition or apoptosis enhancement but also on anti-invasiveness because most of the breast cancer deaths could have been caused by the primary breast cancer cells gaining invasiveness and forming distant metastases tremendously improve cancer cells survivability and sturdiness (Al-Mahmood *et al.*, 2018).

References

Abou-Ghali M, Stiban J (2015). Regulation of ceramide channel formation and disassembly: Insights on the initiation of apoptosis. *Saudi J Biol Sci* **22**: 760–772.

Abramson VG, Lehmann BD, Ballinger TJ, Pietenpol JA (2015). Subtyping of triple-negative breast cancer: implications for therapy. *Cancer* **121**: 8–16.

Adams JM, Cory S (2007). The Bcl-2 apoptotic switch in cancer development and therapy. *Oncogene* **26**: 1324–1337.

Agarwal G, Pradeep P V., Aggarwal V, Yip CH, Cheung PSY (2007). Spectrum of breast cancer in Asian women. *World J Surg* **31**: 1031–1040.

Ahmed K, Koval A, Xu J, Bodmer A, Katanaev VL (2019). Towards the first targeted therapy for triple-negative breast cancer: Repositioning of clofazimine as a chemotherapy-compatible selective Wnt pathway inhibitor. *Cancer Lett* **449**: 45–55.

Al-Mahmood S, Sapiezynski J, Garbuzenko OB, Minko T (2018). Metastatic and triple-negative breast cancer: challenges and treatment options. *Drug Deliv Transl Res* **8**: 1483–1507.

Al-Rayyan N, Litchfield LM, Ivanova MM, Radde BN, Cheng A, Elbedewy A, *et al* (2014). 5-Aza-2-deoxycytidine and trichostatin A increase COUP-TFII expression in antiestrogen-resistant breast cancer cell lines. *Cancer Lett* **347**: 139–50.

Allensworth JL, Aird KM, Aldrich AJ, Batinic-Haberle I, Devi GR (2012). XIAP inhibition and generation of reactive oxygen species enhances TRAIL sensitivity in inflammatory breast cancer cells. *Mol Cancer Ther* **11**: 1518–1527.

Allensworth JL, Sauer SJ, Lyerly HK, Morse MA, Devi GR (2013). Smac mimetic Birinapant induces apoptosis and enhances TRAIL potency in inflammatory breast cancer cells in an IAP-dependent and TNF-α-independent mechanism. *Breast Cancer Res Treat* **137**: 359–371.

Almasan A, Ashkenazi A (2003). Apo2L/TRAIL: apoptosis signaling, biology, and potential for cancer therapy. *Cytokine Growth Factor Rev* **14**: 337–348.

Anampa J, Makower D, Sparano JA (2015). Progress in adjuvant chemotherapy for breast cancer: an overview. *BMC Med* **13**: 195.

Antczak C, Mahida JP, Singh C, Calder PA, Djaballah H (2014). A high content assay to assess cellular fitness. *Comb Chem High Throughput Screen* **17**: 12–24.

Antiabong JF, Ngoepe MG, Abechi AS (2016). Semi-quantitative digital analysis of polymerase chain reactionelectrophoresis gel: Potential applications in low-income veterinary laboratories. *Vet World* **9**: 935–939.

Ashkenazi A (2008). Targeting the extrinsic apoptosis pathway in cancer. *Cytokine Growth Factor Rev* **19**: 325–331.

Ashkenazi A (2015). Targeting the extrinsic apoptotic pathway in cancer: lessons learned and future directions. *J Clin Invest* **125**: 487–489.

Ashkenazi A, Pai RC, Fong S, Leung S, Lawrence DA, Marsters SA, *et al* (1999). Safety and antitumor activity of recombinant soluble Apo2 ligand. *J Clin Invest* **104**: 155–162.

Azijli K, Roosmalen IAM van, Smit J, Pillai S, Fukushima M, Jong S de, *et al* (2014). The novel thymidylate synthade inhibitor trifluorothymidine (TFT) and TRAIL synergistically eradicate non-small cell lung cancer cells. *Cancer Chemother Pharmacol* **73**: 1273–1283.

Azijli K, Weyhenmeyer B, Peters GJ, Jong S de, Kruyt FAE (2013). Non-canonical kinase signaling by the death ligand TRAIL in cancer cells: discord in the death receptor family. *Cell Death Differ* **20**: 858–868.

Azijli K, Yuvaraj S, Peppelenbosch MP, Würdinger T, Dekker H, Joore J, *et al* (2012).

Kinome profiling of non-canonical TRAIL signaling reveals RIP1–Src–STAT3-dependent invasion in resistant non-small cell lung cancer cells. *J Cell Sci* **125**: 4651–4661.

Azimzadeh M, Rahaie M, Nasirizadeh N, Ashtari K, Naderi-Manesh H (2016). An electrochemical nanobiosensor for plasma miRNA-155, based on graphene oxide and gold nanorod, for early detection of breast cancer. *Biosens Bioelectron* **77**: 99–106.

Baig S, Seevasant I, Mohamad J, Mukheem A, Huri HZ, Kamarul T (2016). Potential of apoptotic pathway-targeted cancer therapeutic research: Where do we stand? *Cell Death Dis* **7**: e2058.

Barber AG, Castillo-Martin M, Bonal DM, Jia AJ, Rybicki BA, Christiano AM, *et al* (2015). PI3K/AKT pathway regulates E-cadherin and Desmoglein 2 in aggressive prostate cancer. *Cancer Med* **4**: 1258–1271.

BARTEL D (2004). MicroRNAsGenomics, Biogenesis, Mechanism, and Function. *Cell* **116**: 281–297.

Belch A, Sharma A, Spencer A, Tarantolo S, Bahlis NJ, Doval D, *et al* (2010). A Multicenter Randomized Phade II Trial of Mapatumumab, a TRAIL-R1 Agonist Monoclonal Antibody, In Combination with Bortezomib In Patients with Relapsed/Refractory Multiple Myeloma (MM). *Blood* **116**: 5031.

Berry DA, Cronin KA, Plevritis SK, Fryback DG, Clarke L, Zelen M, *et al* (2005). Effect of screening and adjuvant therapy on mortality from breast cancer. *N Engl J Med* **353**: 1784–1792.

Bertsch U, Röder C, Kalthoff H, Trauzold A (2014). Compartmentalization of TNF-related apoptosis-inducing ligand (TRAIL) death receptor functions: emerging role of nuclear TRAIL-R2. *Cell Death Dis* **5**: e1390.

Berx G, Staes K, Hengel J van, Molemans F, Bussemakers MJ, Bokhoven a van, *et al* (1995). Cloning and characterization of the human invasion suppressor gene E-cadherin (CDH1). *Genomics* **26**: 281–289.

Billam M, Sobolewski MD, Davidson NE (2010). Effects of a novel DNA methyltransferase inhibitor zebularine on human breast cancer cells. *Breast Cancer Res Treat* **120**: 581–592.

Bilski A, Pasz-Walczak G, Kubiak R, Sek P, Chalubinska J, Fendler W, *et al* (2010). TRAIL protein expression in breast cancer cells correlates with nuclear grade. *Arch Med Sci* **6**: 545–551.

Blackburn SA, Parks RM, Cheung K-L (2018). Fulvestrant for the treatment of advanced breast cancer. *Expert Rev Anticancer Ther* **18**: 619–628.

Bockbrader KM, Tan M, Sun Y (2005). A small molecule Smac-mimic compound induces apoptosis and sensitizes TRAIL- and etoposide-induced apoptosis in breast cancer cells. *Oncogene* **24**: 7381–7388.

Bodmer JL, Meier P, Tschopp J, Schneider P (2000). Cysteine 230 is essential for the structure and activity of the cytotoxic ligand TRAIL. *J Biol Chem* **275**: 20632–20637.

Bray F, Ferlay J, Soerjomataram I, Siegel RL, Torre LA, Jemal A (2018). Global cancer statistics 2018: GLOBOCAN estimates of incidence and mortality worldwide for 36 cancers in 185 countries. *CA Cancer J Clin* **68**: 394–424.

Bremnes RM, Veve R, Hirsch FR, Franklin WA (2002). The E-cadherin cell-cell adhesion complex and lung cancer invasion, metastasis, and prognosis. *Lung cancer* **36**: 115–124.

Burstein MD, Tsimelzon A, Poage GM, Covington KR, Contreras A, Fuqua SAW, *et al* (2015). Comprehensive genomic analysis identifies novel subtypes and targets of triple-negative breast cancer. *Clin Cancer Res* **21**: 1688–1698.

Butler LM, Liapis V, Bouralexis S, Welldon K, Hay S, Thai LM, *et al* (2006). The histone deacetylase inhibitor, suberoylanilide hydroxamic acid, overcomes

resistance of human breast cancer cells to Apo2L/TRAIL. *Int J Can* **119**: 944–954.

Camidge DR, Herbst RS, Gordon MS, Eckhardt SG, Kurzrock R, Durbin B, *et al* (2010). A Phade I Safety and Pharmacokinetic Study of the Death Receptor 5 Agonistic Antibody PRO95780 in Patients with Advanced Malignancies. *Clin Cancer Res* **16**: 1256–1263.

Capaldo CT, Farkas AE, Nusrat A (2014). Epithelial adhesive junctions. *F1000Prime Rep* **6**: 1.

Cardarelli F, Digiacomo L, Marchini C, Amici A, Salomone F, Fiume G, *et al* (2016). The intracellular trafficking mechanism of Lipofectamine-based transfection reagents and its implication for gene delivery. *Sci Rep* **6**: 25879.

Castrogiovanni C, Waterschoot B, Backer O De, Dumont P (2018). Serine 392 phosphorylation modulates p53 mitochondrial translocation and transcription-independent apoptosis. *Cell Death Diff* **25**: 190–203.

Celià-Terrassa T, Meca-Cortés Ó, Mateo F, Martínez de Paz A, Rubio N, Arnal-Estapé A, *et al* (2012). Epithelial-mesenchymal transition can suppress major attributes of human epithelial tumor-initiating cells. *J Clin Invest* **122**: 1849–1868.

Chandra D, Choy G, Tang DG (2007). Cytosolic accumulation of HSP60 during apoptosis with or without apparent mitochondrial release: evidence that its pro-apoptotic or pro-survival functions involve differential interactions with caspase-3. *J Biol Chem* **282**: 31289–31301.

Chao Y, Wu Q, Acquafondata M, Dhir R, Wells A (2012a). Partial mesenchymal to epithelial reverting transition in breast and prostate cancer metastases. *Cancer Microenviron* **5**: 19–28.

Chao Y, Wu Q, Shepard C, Wells A (2012b). Hepatocyte induced re-expression of E-cadherin in breast and prostate cancer cells increases chemoresistance. *Clin Exp Metastasis* **29**: 39–50.

Chao YL, Shepard CR, Wells A (2010). Breast carcinoma cells re-express E-cadherin during mesenchymal to epithelial reverting transition. *Mol Cancer* **9**: 179.

Chen D, Dou QP (2010). The ubiquitin-proteasome system as a prospective molecular target for cancer treatment and prevention. *Curr Protein Pept Sci* **11**: 459–470.

Chen JJ, Shen HCJ, Rivera Rosado LA, Zhang Y, Di X, Zhang B (2012). Mislocalisation of death receptors correlates with cellular resistance to their cognate ligands in human breast cancer cells. *Oncotarget* **3**: 833–842.

Chen L, Jian W, Lu L, Zheng L, Yu Z, Zhou D (2015). Elevated expression of E-cadherin in primary breast cancer and its corresponding metastatic lymph node. *Int J Clin Exp Med* **8**: 11752–11758.

Chen Q, Kang J, Fu C (2018). The independence of and associations among apoptosis, autophagy, and necrosis. *Signal Transduct Target Ther* **3**: 1-18.

Chen X, Kandasamy K, Srivastava RK (2003). Differential Roles of RelA (p65) and c-Rel Subunits of Nuclear Factor {kappa}B in Tumor Necrosis Factor-related Apoptosis-inducing Ligand Signaling. *Cancer Res* **63**: 1059–1066.

Chen Z, Zhao X, Wang J, Li B, Wang Z, Sun J, *et al* (2011). microRNA-92a promotes lymph node metastasis of human esophageal squamous cell carcinoma via E-cadherin. *J Biol Chem* **286**: 10725–10734.

Cheng JC, Yoo CB, Weisenberger DJ, Chuang J, Wozniak C, Liang G, *et al* (2004). Preferential response of cancer cells to zebularine. *Cancer Cell* **6**: 151–158.

Cheng L, Nagabhushan M, Pretlow TP, Amini SB, Pretlow TG (1996). Expression of E-cadherin in primary and metastatic prostate cancer. *Am J Pathol* **148**: 1375–1380.

Chopin V, Slomianny C, Hondermarck H, Bourhis X Le (2004). Synergistic induction of apoptosis in breast cancer cells by cotreatment with butyrate and TNF-alpha, TRAIL, or anti-Fas agonist antibody involves enhancement of death receptors' signaling and requires P21waf1. *Exp Cell Res* **298**: 560–573.

Christou N, Perraud A, Blondy S, Jauberteau M-O, Battu S, Mathonnet M (2017). The extracellular domain of E cadherin linked to invasiveness in colorectal cancer: a new resistance and relapses monitoring serum-bio marker? *J Cancer Res Clin Oncol* **143**: 1177–1190.

Ciuleanu T, Bazin I, Lungulescu D, Miron L, Bondarenko I, Deptala A, *et al* (2016). A randomized, double-blind, placebo-controlled phade II study to assess the efficacy and safety of mapatumumab with sorafenib in patients with advanced hepatocellular carcinoma. *Ann Oncol* **27**: 680–687.

Clancy L, Mruk K, Archer K, Woelfel M, Mongkolsapaya J, Screaton G, *et al* (2005). Preligand assembly domain-mediated ligand-independent association between TRAIL receptor 4 (TR4) and TR2 regulates TRAIL-induced apoptosis. *Proc Natl Acad Sci USA* **102**: 18099–18104.

Clarke CAL, Bennett LN, Clarke PR (2005). Cleavage of claspin by caspase-7 during apoptosis inhibits the Chk1 pathway. *J Biol Chem* **280**: 35337–35345.

Coleman ML, Sahai EA, Yeo M, Bosch M, Dewar A, Olson MF (2001). Membrane blebbing during apoptosis results from caspase-mediated activation of ROCK I. *Nat Cell Biol* **3**: 339–345.

Conticello C, Adamo L, Vicari L, Giuffrida R, Iannolo G, Anastasi G, *et al* (2008). Antitumor activity of bortezomib alone and in combination with TRAIL in human acute myeloid leukemia. *Acta Haematol* **120**: 19–30.

Criscitiello C, Fumagalli D, Saini KS, Loi S (2010). Tamoxifen in early-stage estrogen receptor-positive breast cancer: overview of clinical use and molecular biomarkers for patient selection. *Onco Targets Ther* **4**: 1–11.

Curtis C, Shah SP, Chin S-F, Turashvili G, Rueda OM, Dunning MJ, *et al* (2012). The genomic and transcriptomic architecture of 2,000 breast tumours reveals novel subgroups. *Nature* **486**: 346-352.

Dalby B, Cates S, Harris A, Ohki EC, Tilkins ML, Price PJ, *et al* (2004). Advanced transfection with Lipofectamine 2000 reagent: primary neurons, siRNA, and high-throughput applications. *Methods* **33**: 95–103.

Daniels DL, Weis WI (2005). β-catenin directly displaces Groucho/TLE repressors from Tcf/Lef in Wnt-mediated transcription activation. *Nat Struct Mol Biol* **12**: 364–371.

Danish L, Imig D, Allgöwer F, Scheurich P, Pollak N (2018). Bcl-2-mediated control of TRAIL-induced apoptotic response in the non-small lung cancer cell line NCI-H460 is effective at late caspase processing steps. *PLoS One* **13**: e0198203.

Dantuma NP, Lindsten K, Glas R, Jellne M, Masucci MG (2000). Short-lived green fluorescent proteins for quantifying ubiquitin/proteasome-dependent proteolysis in living cells. *Nat Biotechnol* **18**: 538–543.

Davis MA, Ireton RC, Reynolds AB (2003). A core function for p120-catenin in cadherin turnover. *J Cell Biol* **163**: 525–534.

Demetri GD, Cesne A Le, Chawla SP, Brodowicz T, Maki RG, Bach BA, *et al* (2012). First-line treatment of metastatic or locally advanced unresectable soft tissue sarcomas with conatumumab in combination with doxorubicin or doxorubicin alone: A Phade I/II open-label and double-blind study. *Eur J Cancer* **48**: 547–563.

Dent R, Hanna WM, Trudeau M, Rawlinson E, Sun P, Narod SA (2009). Pattern of metastatic spread in triple-negative breast cancer. *Breast Cancer Res Treat* **115**: 423–428.

Dent R, Trudeau M, Pritchard KI, Hanna WM, Kahn HK, Sawka CA, *et al* (2007).

Triple-negative breast cancer: clinical features and patterns of recurrence. *Clin Cancer Res* **13**: 4429–4434.

Di X, Zhang G, Zhang Y, Takeda K, Rivera Rosado LA, Zhang B (2013). Accumulation of autophagosomes in breast cancer cells induces TRAIL resistance through downregulation of surface expression of death receptors 4 and 5. *Oncotarget* **4**: 1349–1364.

Dijk M van, Halpin-McCormick A, Sessler T, Samali A, Szegezdi E (2013). Resistance to TRAIL in non-transformed cells is due to multiple redundant pathways. *Cell Death Dis* **4**: e702.

Dimberg LY, Anderson CK, Camidge R, Behbakht K, Thorburn A, Ford HL (2013). On the TRAIL to successful cancer therapy? Predicting and counteracting resistance against TRAIL-based therapeutics. *Oncogene* **32**: 1341–1350.

Doi T, Murakami H, Ohtsu A, Fuse N, Yoshino T, Yamamoto N, *et al* (2011). Phade 1 study of conatumumab, a pro-apoptotic death receptor 5 agonist antibody, in Japanese patients with advanced solid tumors. *Cancer Chemother Pharmacol* **68**: 733–741.

Dunham-Ems SM, Pudavar HE, Myers JM, Maher PA, Prasad PN, Stachowiak MK (2006). Factors controlling fibroblast growth factor receptor-1's cytoplasmic trafficking and its regulation as revealed by FRAP analysis. *Mol Biol Cell* **17**: 2223–2235.

Ehrhardt H, Alves CC, Wachter F, Jeremias I (2015). TRAIL Preferentially Affects Cell Cycle-Arrested Tumor Cells Including Stem- and Progenitor Cells From Patients with Acute Lymphoblastic Leukemia. *Blood* **120**: 1879.

Elmore S (2007). Apoptosis: A Review of Programmed Cell Death. *Toxicol Pathol* **35**: 495–516.

Engeland M van, Nieland LJ, Ramaekers FC, Schutte B, Reutelingsperger CP (1998). Annexin V-affinity assay: a review on an apoptosis detection system based on phosphatidylserine exposure. *Cytometry* **31**: 1–9.

Engesæter B, Sathermugathevan M, Hellenes T, Engebråten O, Holm R, Flørenes VA, *et al* (2011). Targeting inhibitor of apoptosis proteins in combination with dacarbazine or TRAIL in melanoma cells. *Cancer Biol Ther* **12**: 47–58.

Essers MAG, Vries-Smits LMM de, Barker N, Polderman PE, Burgering BMT, Korswagen HC (2005). Functional interaction between beta-catenin and FOXO in oxidative stress signaling. *Science (80-)* **308**: 1181–1184.

Fallahpour S, Navaneelan T, De P, Borgo A (2017). Breast cancer survival by molecular subtype: a population-based analysis of cancer registry data. *C open* **5**: E734–E739.

Fandy TE, Shankar S, Ross DD, Sausville E, Srivastava RK (2005). Interactive effects of HDAC inhibitors and TRAIL on apoptosis are associated with changes in mitochondrial functions and expressions of cell cycle regulatory genes in multiple myeloma. *Neoplasia* **7**: 646–657.

Fang Y, Liang X, Jiang W, Li J, Xu J, Cai X (2015). Cyclin B1 suppresses colorectal cancer invasion and metastasis by regulating E-Cadherin. *PLoS One* **10**: e0126875.

Fedor-Chaiken M, Hein PW, Stewart JC, Brackenbury R, Kinch MS (2003). E-cadherin binding modulates EGF receptor activation. *Cell Commun Adhes* **10**: 105–118.

Ferreira AC, Suriano G, Mendes N, Gomes B, Wen X, Carneiro F, *et al* (2012). E-cadherin impairment increases cell survival through Notch-dependent upregulation of Bcl-2. *Hum Mol Genet* **21**: 334–343.

Ferreira P, Oliveira MJ, Beraldi E, Mateus AR, Nakajima T, Gleave M, *et al* (2005). Loss of functional E-cadherin renders cells more resistant to the apoptotic agent taxol in vitro. *Exp Cell Res* **310**: 99–104.

Finlay D, Vamos M, Gonzalez-Lopez M, Ardecky RJ, Ganji SR, Yuan H, *et al* (2014). Small-molecule IAP antagonists sensitize cancer cells to TRAIL-induced apoptosis: roles of XIAP and cIAPs. *Mol Cancer Ther* **13**: 5–15.

Fisher ML, Adhikary G, Grun D, Kaetzel DM, Eckert RL (2016). The Ezh2 polycomb group protein drives an aggressive phenotype in melanoma cancer stem cells and is a target of diet derived sulforaphane. *Mol Carcinog* **55**: 2024–2036.

Florean C, Schnekenburger M, Lee J-Y, Kim KR, Mazumder A, Song S, *et al* (2016). Discovery and characterization of Isofistularin-3, a marine brominated alkaloid, as a new DNA demethylating agent inducing cell cycle arrest and sensitization to TRAIL in cancer cells. *Oncotarget* **7**: 24027–24049.

Forero-Torres A, Infante JR, Waterhouse D, Wong L, Vickers S, Arrowsmith E, *et al* (2013). Phade 2, multicenter, open-label study of tigatuzumab (CS-1008), a humanized monoclonal antibody targeting death receptor 5, in combination with gemcitabine in chemotherapy-naive patients with unresectable or metastatic pancreatic cancer. *Cancer Med* **2**: 925–932.

Forero-Torres A, Shah J, Wood T, Posey J, Carlisle R, Copigneaux C, *et al* (2010). Phade I Trial of Weekly Tigatuzumab, an Agonistic Humanized Monoclonal Antibody Targeting Death Receptor 5 (DR5). *Cancer Biother Radiopharm* **25**: 13–19.

Forero A, Bendell JC, Kumar P, Janisch L, Rosen M, Wang Q, *et al* (2017). First-in-human study of the antibody DR5 agonist DS-8273a in patients with advanced solid tumors. *Invest New Drugs* **35**: 298–306.

Frew AJ, Lindemann RK, Martin BP, Clarke CJP, Sharkey J, Anthony DA, *et al* (2008). Combination therapy of established cancer using a histone deacetylase inhibitor and a TRAIL receptor agonist. *Proc Natl Acad Sci U S A* **105**: 11317–11322.

Fritsche H, Heilmann T, Tower RJ, Hauser C, Au A von, El-Sheikh D, *et al* (2015). TRAIL-R2 promotes skeletal metastasis in a breast cancer xenograft mouse model. *Oncotarget* **6**: 9502–9516.

Frixen UH, Behrens J, Sachs M, Eberle G, Voss B, Warda A, *et al* (1991). E-cadherin-mediated cell-cell adhesion prevents invasiveness of human carcinoma cells. *J Cell Biol* **113**: 173–185.

Fujita Y, Krause G, Scheffner M, Zechner D, Leddy HE, Behrens J, *et al* (2002). Hakai, a c-Cbl-like protein, ubiquitinates and induces endocytosis of the E-cadherin complex. *Nat Cell Biol* **4**: 222–231.

Fulda S (2015). Safety and tolerability of TRAIL receptor agonists in cancer treatment. *Eur J Clin Pharmacol* **71**: 525–527.

Fulda S, Debatin K-M (2005). HDAC inhibitors: Double edge sword for TRAIL cancer therapy? *Cancer Biol Ther* **4**: 1113–1115.

Fulda S, Debatin KM (2006). Extrinsic versus intrinsic apoptosis pathways in anticancer chemotherapy. *Oncogene* **25**: 4798–4811.

Fulda S, Gorman AM, Hori O, Samali A (2010). Cellular stress responses: cell survival and cell death. *Int J Cell Biol* **2010**: 1-23.

Fulga V, Rudico L, Balica AR, Cimpean AM, Saptefrati L, Margan M-M, *et al* (2015). Differential expression of e-cadherin in primary breast cancer and corresponding lymph node metastases. *Anticancer Res* **35**: 759–765.

Ganten TM, Sykora J, Koschny R, Batke E, Aulmann S, Mansmann U, *et al* (2009). Prognostic significance of tumour necrosis factor-related apoptosis-inducing ligand (TRAIL) receptor expression in patients with breast cancer. *J Mol Med* **87**: 995–1007.

Gibbons JA, Kanwar JR, Kanwar RK (2015). Iron-free and iron-saturated bovine lactoferrin inhibit survivin expression and differentially modulate apoptosis in breast cancer. *BMC Cancer* **15**: 425.

Gilmore AP, Valentijn AJ, Wang P, Ranger AM, Bundred N, O'Hare MJ, *et al* (2002). Activation of BAD by therapeutic inhibition of epidermal growth factor receptor and transactivation by insulin-like growth factor receptor. *J Biol Chem* **277**: 27643–27650.

Gonzalvez F, Ashkenazi A (2010). New insights into apoptosis signaling by Apo2L/TRAIL. *Oncogene* **29**: 4752–4765.

Greco FA, Bonomi P, Crawford J, Kelly K, Oh Y, Halpern W, *et al* (2008). Phade 2 study of mapatumumab, a fully human agonistic monoclonal antibody which targets and activates the TRAIL receptor-1, in patients with advanced non-small cell lung cancer. *Lung Cancer* **61**: 82–90.

Greijer AE, Wall E van der (2004). The role of hypoxia inducible factor 1 (HIF-1) in hypoxia induced apoptosis. *J Clin Pathol* **57**: 1009–1014.

Grossmann J (Kluwer Academic Publishers: 2002). Molecular mechanisms of "detachment-induced apoptosis-Anoikis." *Apoptosis* **7**: 247-260.

Gu H, Tang H, Xiong P, Zhou Z (2019). Biomarkers-based Biosensing and Bioimaging with Graphene for Cancer Diagnosis. *Nanomater* **9**: 130.

Guan B, Yue P, Lotan R, Sun S-Y (2002). Evidence that the human death receptor 4 is regulated by activator protein 1. *Oncogene* **21**: 3121–9.

Guilford P, Hopkins J, Harraway J, McLeod M, McLeod N, Harawira P, *et al* (1998). E-cadherin germline mutations in familial gastric cancer. *Nature* **392**: 402–405.

Gunasinghe NP, Wells A, Thompson EW, Hugo HJ (2012). Mesenchymal-epithelial transition (MET) as a mechanism for metastatic colonisation in breast cancer. *Cancer Metastasis Rev* **31**: 469–478.

Gyrd-Hansen M, Meier P (2010). IAPs: From caspase inhibitors to modulators of NF-κB, inflammation and cancer. *Nat Rev Cancer* **10**: 561–574.

Han MH, Park C, Kwon TK, Kim G-Y, Kim W-J, Hong SH, *et al* (2015). The Histone Deacetylase Inhibitor Trichostatin A Sensitizes Human Renal Carcinoma Cells to TRAIL-Induced Apoptosis through Down-Regulation of c-FLIPL. *Biomol Ther* **23**: 31–38.

Harrison OJ, Jin X, Hong S, Bahna F, Ahlsen G, Brasch J, *et al* (2011). The extracellular architecture of adherens junctions revealed by crystal structures of type I cadherins. *Structure* **19**: 244–256.

Hartwig T, Montinaro A, Karstedt S von, Sevko A, Surinova S, Chakravarthy A, *et al* (2017). The TRAIL-Induced Cancer Secretome Promotes a Tumor-Supportive Immune Microenvironment via CCR2. *Mol Cell* **65**: 730–742.e5.

Hadelmann V, Kurz A, Bertsch U, Hübner S, Olempska-Müller M, Fritsch J, *et al* (2014). Nuclear death receptor TRAIL-R2 inhibits maturation of let-7 and promotes proliferation of pancreatic and other tumor cells. *Gastroenterology* **146**: 278–290.

Häussinger D, Ahrens T, Aberle T, Engel J, Stetefeld J, Grzesiek S (2004). Proteolytic E-cadherin activation followed by solution NMR and X-ray crystallography. *EMBO J* **23**: 1699–1708.

He B, Lu N, Zhou Z (2009). Cellular and nuclear degradation during apoptosis. *Curr Opin Cell Biol* **21**: 900–912.

He G, Wang Y, Pang X, Zhang B (2014). Inhibition of autophagy induced by TSA sensitizes colon cancer cell to radiation. *Tumor Biol* **35**: 1003–1011.

He TC, Sparks AB, Rago C, Hermeking H, Zawel L, Costa LT da, *et al* (1998). Identification of c-MYC as a target of the APC pathway. *Science (80-)* **281**: 1509–1512.

Herbst RS, Eckhardt SG, Kurzrock R, Ebbinghaus S, O'Dwyer PJ, Gordon MS, *et al* (2010a). Phade I dose-escalation study of recombinant human Apo2L/TRAIL, a dual proapoptotic receptor agonist, in patients with advanced cancer. *J Clin*

Oncol **28**: 2839–2846.

Herbst RS, Kurzrock R, Hong DS, Valdivieso M, Hsu C-P, Goyal L, *et al* (2010b). A First-in-Human Study of Conatumumab in Adult Patients with Advanced Solid Tumors. *Clin Cancer Res* **16**: 5883–5891.

Hetschko H, Voss V, Horn S, Seifert V, Prehn JHM, Kögel D (2008). Pharmacological inhibition of Bcl-2 family members reactivates TRAIL-induced apoptosis in malignant glioma. *J Neurooncol* **86**: 265–272.

Hiscox S, Jiang WG (1999). Association of the HGF/SF Receptor, c-met, with the Cell-Surface Adhesion Molecule, E-Cadherin, and Catenins in Human Tumor Cells. *Biochem Biophys Res Commun* **261**: 406–411.

Hochstrasser M (1996). Ubiquitin-dependent protein degradation. *Annu Rev Genet* **30**: 405–39.

Holland PM (2013). Targeting Apo2L/TRAIL receptors by soluble Apo2L/TRAIL. *Cancer Lett* **332**: 156–162.

Hong H, Yang K, Zhang Y, Engle JW, Feng L, Yang Y, *et al* (2012). In vivo targeting and imaging of tumor vasculature with radiolabeled, antibody-conjugated nanographene. *ACS Nano* **6**: 2361–2370.

Hotte SJ, Hirte HW, Chen EX, Siu LL, Le LH, Corey A, *et al* (2008). A phade 1 study of mapatumumab (fully human monoclonal antibody to TRAIL-R1) in patients with advanced solid malignancies. *Clin Cancer Res* **14**: 3450–3455.

Hrgovic I, Doll M, Kleemann J, Wang X-F, Zoeller N, Pinter A, *et al* (2016). The histone deacetylase inhibitor trichostatin a decreases lymphangiogenesis by inducing apoptosis and cell cycle arrest via p21-dependent pathways. *BMC Cancer* **16**: 763.

Hsu MY, Meier FE, Nesbit M, Hsu JY, Belle P Van, Elder DE, *et al* (2000). E-Cadherin expression in melanoma cells restores keratinocyte-mediated growth control and down-regulates expression of invasion-related adhesion receptors. *Am J Pathol* **156**: 1515–1525.

Huang S, Okumura K, Sinicrope FA (2009). BH3 mimetic obatoclax enhances TRAIL-mediated apoptosis in human pancreatic cancer cells. *Clin Cancer Res* **15**: 150–159.

Huang Y, Yang X, Xu T, Kong Q, Zhang Y, Shen Y, *et al* (2016). Overcoming resistance to TRAIL-induced apoptosis in solid tumor cells by simultaneously targeting death receptors, c-FLIP and IAPs. *Int J Oncol* **49**: 153–163.

Hui L, Zheng Y, Yan Y, Bargonetti J, Foster DA (2006). Mutant p53 in MDA-MB-231 breast cancer cells is stabilized by elevated phospholipase D activity and contributes to survival signals generated by phospholipase D. *Oncogene* **25**: 7305–7310.

Huiping C, Kristjansdottir S, Jonasson JG, Magnusson J, Egilsson V, Ingvarsson S (2001). Alterations of E-cadherin and beta-catenin in gastric cancer. *BMC Cancer* **1**: 16.

Hulsken J, Birchmeier W, Behrens J (1994). E-cadherin and APC compete for the interaction with beta-catenin and the cytoskeleton. *J Cell Biol* **127**: 2061–2069.

Hussain AR, Siraj AK, Ahmed M, Bu R, Pratheeshkumar P, Alrashed AM, *et al* (2017). XIAP over-expression is an independent poor prognostic marker in Middle Eastern breast cancer and can be targeted to induce efficient apoptosis. *BMC Cancer* **17**: 1–13.

Hymowitz SG, Malek S (2018). Targeting the MAPK Pathway in RAS Mutant Cancers. *Cold Spring Harb Perspect Med* **8**: a031492.

Iglesias JM, Beloqui I, Garcia-Garcia F, Leis O, Vazquez-Martin A, Eguiara A, *et al* (2013). Mammosphere formation in breast carcinoma cell lines depends upon expression of E-cadherin. *PLoS One* **8**: e77281.

Inoue S, MacFarlane M, Harper N, Wheat LMC, Dyer MJS, Cohen GM (2004). Histone deacetylase inhibitors potentiate TNF-related apoptosis-inducing ligand (TRAIL)-induced apoptosis in lymphoid malignancies. *Cell Death Differ* **11**: S193–S206.

Ishiyama N, Lee SH, Liu S, Li GY, Smith MJ, Reichardt LF, *et al* (2010). Dynamic and static interactions between p120 catenin and E-cadherin regulate the stability of cell-cell adhesion. *Cell* **141**: 117–128.

Ito F, Yoshimoto C, Yamada Y, Sudo T, Kobayashi H (2018). The HNF-1β-USP28-Claspin pathway upregulates DNA damage-induced Chk1 activation in ovarian clear cell carcinoma. *Oncotarget* **9**: 17512–17522.

Jalving M, Heijink DM, Koornstra JJ, Boersma-van Ek W, Zwart N, Wesseling J, *et al* (2014). Regulation of TRAIL receptor expression by -catenin in colorectal tumours. *Carcinogenesis* **35**: 1092–1099.

Jeanes A, Gottardi CJ, Yap AS (2008). Cadherins and cancer: how does cadherin dysfunction promote tumor progression? *Oncogene* **27**: 6920–6929.

Jelovac D, Emens LA (2013). HER2-directed therapy for metastatic breast cancer. *Oncol (willist Park* **27**: 166–175.

Jeong J, Kim W, Kim LK, VanHouten J, Wysolmerski JJ (2017). HER2 signaling regulates HER2 localization and membrane retention. *PLoS One* **12**: e0174849.

Jiang WG (1996). E-cadherin and its associated protein catenins, cancer invasion and metastasis. *Br J Surg* **83**: 437–446.

Jin H-O, Lee Y-H, Park J-A, Kim J-H, Hong S-E, Kim H-A, *et al* (2014). Blockage of Stat3 enhances the sensitivity of NSCLC cells to PI3K/mTOR inhibition. *Biochem Biophys Res Commun* **444**: 502–508.

Jou TS, Stewart DB, Stappert J, Nelson WJ, Marrs JA (1995). Genetic and biochemical dissection of protein linkages in the cadherin-catenin complex. *Proc Natl Acad Sci U S A* **92**: 5067–5071.

Kale J, Osterlund EJ, Andrews DW (2018). BCL-2 family proteins: changing partners in the dance towards death. *Cell Death Diff* **25**: 65–80.

Kalthoff H, Hadelmann V, Kurz A, Bertsch U, Huebner S, Fritsche H, *et al* (2014). Abstract 2955: Trail-R2: A death receptor turns malignant upon nuclear localization. *Cancer Res* **74**: 2955–2955.

Kaminskyyy VO, Surovay O V., Vaculova A, Zhivotovsky B (2011). Combined inhibition of DNA methyltransferase and histone deacetylase restores caspase-8 expression and sensitizes SCLC cells to TRAIL. *Carcinogenesis* **32**: 1450–1458.

Kanai Y, Ochiai A, Shibata T, Oyama T, Ushijima S, Akimoto S, *et al* (1995). c-erbB-2 Gene Product Directly Associates with β-Catenin and Plakoglobin. *Biochem Biophys Res Commun* **208**: 1067–1072.

Kantari C, Walczak H (2011). Caspase-8 and bid: caught in the act between death receptors and mitochondria. *Biochim Biophys Acta* **1813**: 558–563.

Karray-Chouayekh S, Trifa F, Khabir A, Sellami-Boudawara T, Frikha M, Gargouri A, *et al* (2012). Negative/low HER2 expression alone or combined with E-cadherin positivity is predictive of better prognosis in patients with breast carcinoma. *Histol Histopathol* **27**: 377–385.

Kaya-Aksoy E, Cingoz A, Senbabaoglu F, Seker F, Sur-Erdem I, Kayabolen A, *et al* (2019). The pro-apoptotic Bcl-2 family member Harakiri (HRK) induces cell death in glioblastoma multiforme. *Cell Death Dis* **5**: 1-12.

Kelley SK, Ashkenazi A (2004). Targeting death receptors in cancer with Apo2L/TRAIL. *Curr Opin Pharmacol* **4**: 333–339.

Kim CS, Lee CH, Shin JS, Chung YS, Hyung NI (1997). A Simple and Rapid Method for Isolation of High Quality Genomic DNA from Fruit Trees and Conifers Using

PVP. *Nucleic Acids Res* **25**: 1085–1086.

Kim E, Kim A, Kim SK, Kim HJ, Chang J, Ahn CM, *et al* (2014). Inhibition of mTORC1 induces loss of E-cadherin through AKT/GSK-3β signaling-mediated upregulation of E-cadherin repressor complexes in non-small cell lung cancer cells. *Respir Res* **15**: 1-9.

Kim H-R, Kim E-J, Yang S-H, Jeong E-T, Park C, Lee J-H, *et al* (2006). Trichostatin A induces apoptosis in lung cancer cells via simultaneous activation of the death receptor-mediated and mitochondrial pathway. *EXP MOL MED* **38**: 616–624.

Kim J, Krichevsky A, Grad Y, Hayes GD, Kosik KS, Church GM, *et al* (2004). Identification of many microRNAs that copurify with polyribosomes in mammalian neurons. *Proc Natl Acad Sci U S A* **101**: 360–365.

Kim R-K, Suh Y, Yoo K-C, Cui Y-H, Kim H, Kim M-J, *et al* (2015). Activation of KRAS promotes the mesenchymal features of basal-type breast cancer. *Exp Mol Med* **47**: 1-9.

Kindler HL, Richards DA, Garbo LE, Garon EB, Stephenson JJ, Rocha-Lima CM, *et al* (2012). A randomized, placebo-controlled phade 2 study of ganitumab (AMG 479) or conatumumab (AMG 655) in combination with gemcitabine in patients with metastatic pancreatic cancer. *Ann Oncol* **23**: 2834–2842.

King TD, Suto MJ, Li Y (2012). The Wnt/β-catenin signaling pathway: a potential therapeutic target in the treatment of triple negative breast cancer. *J Cell Biochem* **113**: 13–18.

Kisim A, Atmaca H, Cakar B, Karabulut B, Sezgin C, Uzunoglu S, *et al* (2012). Pretreatment with AT-101 enhances tumor necrosis factor-related apoptosis-inducing ligand (TRAIL)-induced apoptosis of breast cancer cells by inducing death receptors 4 and 5 protein levels. *J Cancer Res Clin Oncol* **138**: 1155–1163.

Kohler BA, Sherman RL, Howlader N, Jemal A, Ryerson AB, Henry KA, *et al* (2015). Annual Report to the Nation on the Status of Cancer, 1975-2011, Featuring Incidence of Breast Cancer Subtypes by Race/Ethnicity, Poverty, and State. *J Natl Cancer Inst* **107**: djv048.

Kosaka N, Iguchi H, Hagiwara K, Yoshioka Y, Takeshita F, Ochiya T (2013). Neutral sphingomyelinase 2 (nSMase2)-dependent exosomal transfer of angiogenic microRNAs regulate cancer cell metastasis. *J Biol Chem* **288**: 10849–10859.

Kowalski PJ, Rubin M a, Kleer CG (2003). E-cadherin expression in primary carcinomas of the breast and its distant metastases. *Breast Cancer Res* **5**: R217–R222.

Koyama S, Koike N, Adachi S (2002). Expression of TNF-related apoptosis-inducing ligand (TRAIL) and its receptors in gastric carcinoma and tumor-infiltrating lymphocytes: a possible mechanism of immune evasion of the tumor. *J Cancer Res Clin Oncol* **128**: 73–79.

Kurokawa H, Nishio K, Fukumoto H, Tomonari A, Suzuki T, Saijo N (1999). Alteration of caspase-3 (CPP32/Yama/apopain) in wild-type MCF-7, breast cancer cells. *Oncol Rep* **6**: 33–37.

Kwon S, Lee S (2016). Recent Advances in Microwave Imaging for Breast Cancer Detection. *J Biomed Imag* **2016**: 1–26.

Leckband D, Prakasam A (2006). Mechanism and dynamics of cadherin adhesion. *Annu Rev Biomed Eng* **8**: 259–287.

Lehmann BD, Bauer JA, Chen X, Sanders ME, Chakravarthy AB, Shyr Y, *et al* (2011). Identification of human triple-negative breast cancer subtypes and preclinical models for selection of targeted therapies. *J Clin Invest* **121**: 2750–67.

Lemke J, Karstedt S von, Zinngrebe J, Walczak H (2014). Getting TRAIL back on track for cancer therapy. *Cell Death Differ* **21**: 1350–1364.

Leong S, Cohen RB, Gustafson DL, Langer CJ, Camidge DR, Padavic K, *et al* (2009). Mapatumumab, an Antibody Targeting TRAIL-R1, in Combination With Paclitaxel and Carboplatin in Patients With Advanced Solid Malignancies: Results of a Phade I and Pharmacokinetic Study. *J Clin Oncol* **27**: 4413–4421.

Leong SPL, Shen Z-Z, Liu T-J, Agarwal G, Tajima T, Paik N-S, *et al* (2010). Is breast cancer the same disease in Asian and Western countries? *World J Surg* **34**: 2308–2324.

Li B, Dou QP (2002). Bax degradation by the ubiquitin/proteasome-dependent pathway: Involvement in tumor survival and progression. *Proc Natl Acad Sci U S A* **97**: 3850–3855.

Li E (2002). Chromatin modification and epigenetic reprogramming in mammalian development. *Nat Rev Genet* **3**: 662–673.

Li H, Wang X, Li N, Qiu J, Zhang Y, Cao X (2007). hPEBP4 resists TRAIL-induced apoptosis of human prostate cancer cells by activating Akt and deactivating ERK1/2 pathways. *J Biol Chem* **282**: 4943–4950.

Li J-W, Liu G-Y, Ji Y-J, Yan X, Pang D, Jiang Z-F, *et al* (2019). Switching to anastrozole plus goserelin vs continued tamoxifen for adjuvant therapy of premenopausal early-stage breast cancer: preliminary results from a randomized trial. *Cancer Manag Res* **11**: 299–307.

Li LN, Zhang HD, Yuan SJ, Yang DX, Wang L, Sun ZX (2008). Differential sensitivity of colorectal cancer cell lines to artesunate is associated with expression of beta-catenin and E-cadherin. *Eur J Pharmacol* **588**: 1–8.

Li Y, Bharti A, Chen D, Gong J, Kufe D (1998). Interaction of glycogen synthade kinase 3beta with the DF3/MUC1 carcinoma-associated antigen and beta-catenin. *Mol Cell Biol* **18**: 7216–7224.

Li Z, Yin S, Zhang L, Liu W, Chen B (2017). Prognostic value of reduced E-cadherin expression in breast cancer: a meta-analysis. *Oncotarget* **8**: 16445–16455.

Lin NU, Claus E, Sohl J, Razzak AR, Arnaout A, Winer EP (2008). Sites of distant recurrence and clinical outcomes in patients with metastatic triple-negative breast cancer: high incidence of central nervous system metastases. *Cancer* **113**: 2638–2645.

Lincoln FA, Imig D, Boccellato C, Juric V, Noonan J, Kontermann RE, *et al* (2018). Sensitization of glioblastoma cells to TRAIL-induced apoptosis by IAP- and Bcl-2 antagonism. *Cell Death Dis* **9**: 1112.

Liu X, Huang H, Remmers N, Hollingsworth MA (2014). Loss of E-cadherin and epithelial to mesenchymal transition is not required for cell motility in tissues or for metastasis. *Tissue Barriers* **2**: 1-6.

Lopes RB, Gangeswaran R, McNeish IA, Wang Y, Lemoine NR (2007). Expression of the IAP protein family is dysregulated in pancreatic cancer cells and is important for resistance to chemotherapy. *Int J Cancer* **120**: 2344–2352.

Louie E, Chen XF, Coomes A, Ji K, Tsirka S, Chen EI (2013). Neurotrophin-3 modulates breast cancer cells and the microenvironment to promote the growth of breast cancer brain metastasis. *Oncogene* **32**: 4064–4077.

Lowy AM, Knight J, Groden J (2002). Restoration of E-cadherin/beta-catenin expression in pancreatic cancer cells inhibits growth by induction of apoptosis. *Surgery* **132**: 141–148.

Lu L, Zhou D, Jiang X, Song K, Li K, Ding W (2012). Loss of E-cadherin in multidrug resistant breast cancer cell line MCF-7/Adr: possible implication in the enhanced invasive ability. *Eur Rev Med Pharmacol Sci* **16**: 1271–1279.

Lu M, Kwan T, Yu C, Chen F, Freedman B, Schafer JM, *et al* (2005). Peroxisome proliferator-activated receptor gamma agonists promote TRAIL-induced apoptosis by reducing survivin levels via cyclin D3 repression and cell cycle arrest. *J Biol Chem* **280**: 6742–6751.

Lu M, Marsters S, Ye X, Luis E, Gonzalez L, Ashkenazi A (2014). E-cadherin couples death receptors to the cytoskeleton to regulate apoptosis. *Mol Cell* **54**: 987–998.

Luo M, Li Z, Wang W, Zeng Y, Liu Z, Qiu J (2013). Long non-coding RNA H19 increases bladder cancer metastasis by associating with EZH2 and inhibiting E-cadherin expression. *Cancer Lett* **333**: 213–221.

Ma L, Young J, Prabhala H, Pan E, Mestdagh P, Muth D, *et al* (2010). miR-9, a MYC/MYCN-activated microRNA, regulates E-cadherin and cancer metastasis. *Nat Cell Biol* **12**: 247–256.

MacDonald BT, Tamai K, He X (2009). Wnt/beta-Catenin Signaling: components, mechanisms, and diseases. *Dev Cell* **17**: 9–26.

Mady MM (2011). Cationic liposomes as gene delivery system. *African J Pharm Pharmacol* **5**: 2007–2012.

Maecker HL, Yun Z, Maecker HT, Giaccia AJ (2002). Epigenetic changes in tumor Fas levels determine immune escape and response to therapy. *Cancer Cell* **2**: 139–148.

Makki MS, Heinzel T, Englert C (2008). TSA downregulates Wilms tumor gene 1 (Wt1) expression at multiple levels. *Nucleic Acids Res* **36**: 4067–4078.

Malin D, Chen F, Schiller C, Koblinski J, Cryns VL (2011). Enhanced Metastasis Suppression by Targeting TRAIL Receptor 2 in a Murine Model of Triple-Negative Breast Cancer. *Cancer Ther Preclin* **17**: OF1-OF11.

Marsters SA (1996). Induction of Apoptosis by Apo-2 Ligand, a New Member of the Tumor Necrosis Factor Cytokine Family. *J Biol Chem* **271**: 12687–12690.

Martinez-Ruiz G, Maldonado V, Ceballos-Cancino G, Grajeda JPR, Melendez-Zajgla J (2008). Role of Smac/DIABLO in cancer progression. *J Exp Clin Cancer Res* **27**: 1-7.

Masuda H, Baggerly KA, Wang Y, Zhang Y, Gonzalez-Angulo AM, Meric-Bernstam F, *et al* (2013). Differential pathologic complete response rates after neoadjuvant chemotherapy among molecular subtypes of triple-negative breast cancer. *ASCO Meet Abstr* **31**: 1-16.

Mayer B, Johnson JP, Leitl F, Jauch KW, Heiss MM, Schildberg FW, *et al* (1993). E-Cadherin expression in primary and metastatic gastric cancer: down-regulation correlates with cellular dedifferentiation and glandular disintegration. *Cancer Res* **53**: 1690–1695.

Mayes PA, Campbell L, Ricci MS, Plastaras JP, Dicker DT, El-Deiry WS, *et al* (2005). Modulation of TRAIL-induced tumor cell apoptosis in a hypoxic environment. *Cancer Biol Ther* **4**: 1068-1074.

McCarthy MM, Sznol M, DiVito KA, Camp RL, Rimm DL, Kluger HM (2005). Evaluating the Expression and Prognostic Value of TRAIL-R1 and TRAIL-R2 in Breast Cancer. *Clin Can Res* **11**: 5188–5194.

Merchant MS, Geller JI, Baird K, Chou AJ, Galli S, Charles A, *et al* (2012). Phade I Trial and Pharmacokinetic Study of Lexatumumab in Pediatric Patients With Solid Tumors. *J Clin Oncol* **30**: 4141–4147.

Mérino D, Lalaoui N, Morizot A, Schneider P, Solary E, Micheau O (2006). Differential inhibition of TRAIL-mediated DR5-DISC formation by decoy receptors 1 and 2. *Mol Cell Biol* **26**: 7046–7055.

Meyer AS, Miller MA, Gertler FB, Lauffenburger DA (2013). The receptor AXL diversifies EGFR signaling and limits the response to EGFR-targeted inhibitors in triple-negative breast cancer cells. *Sci Signal* **6**: 1-26.

Micheau O (2018). Regulation of TNF-Related Apoptosis-Inducing Ligand Signaling by Glycosylation. *Int J Mol Sci* **19**: 1-23.

Migowski A (2015). [Early detection of breast cancer and the interpretation of results of survival studies]. *Ciên Saúde Colet* **20**: 1309.

Miyoshi E, Moriwaki K, Terao N, Tan C-C, Terao M, Nakagawa T, *et al* (2012). Fucosylation Is a Promising Target for Cancer Diagnosis and Therapy. *Biomolecules* **2**: 34–45.

Mizushima N, Ohsumi Y, Yoshimori T (2002). Autophagosome Formation in Mammalian Cells. *Cell Struct Funct* **27**: 421–429.

Mom CH, Verweij J, Oldenhuis CNAM, Gietema JA, Fox NL, Miceli R, *et al* (2009). Mapatumumab, a Fully Human Agonistic Monoclonal Antibody That Targets TRAIL-R1, in Combination with Gemcitabine and Cisplatin: a Phade I Study. *Clin Cancer Res* **15**: 5584–5590.

Morales JC, Ruiz-Magaña MJ, Carranza D, Ortiz-Ferrón G, Ruiz-Ruiz C (2010). HDAC inhibitors with different gene regulation activities depend on the mitochondrial pathway for the sensitization of leukemic T cells to TRAIL-induced apoptosis. *Cancer Lett* **297**: 91–100.

Morinobu A, Wang B, Liu J, Yoshiya S, Kurosaka M, Kumagai S (2006). Trichostatin A cooperates with Fas-mediated signal to induce apoptosis in rheumatoid arthritis synovial fibroblasts. *J Rheumatol* **33**: 1052–1060.

Moriwaki K, Miyoshi E (2010). Fucosylation and gastrointestinal cancer. *World J Hepatol* **2**: 151–161.

Moriwaki K, Narisada M, Imai T, Shinzaki S, Miyoshi E (2010). The effect of epigenetic regulation of fucosylation on TRAIL-induced apoptosis. *Glycocoj J* **27**: 649–659.

Moriwaki K, Noda K, Furukawa Y, Ohshima K, Uchiyama A, Nakagawa T, *et al* (2009). Deficiency of GMDS leads to escape from NK cell-mediated tumor surveillance through modulation of TRAIL signaling. *Gastroenterology* **137**: 188–98, 198.e1–2.

Moriwaki K, Shinzaki S, Miyoshi E (2011). GDP-mannose-4,6-dehydratase (GMDS) deficiency renders colon cancer cells resistant to tumor necrosis factorrelated apoptosis-inducing ligand (TRAIL) receptor- and CD95-mediated apoptosis by inhibiting complex II formation. *J Biol Chem* **286**: 43123–43133.

Mougalian SS, Soulos PR, Killelea BK, Lannin DR, Abu-Khalaf MM, DiGiovanna MP, *et al* (2015). Use of neoadjuvant chemotherapy for patients with stage I to III breast cancer in the United States. *Cancer* **121**: 2544–2552.

Nagane M, Huang HJ, Cavenee WK (2001). The potential of TRAIL for cancer chemotherapy. *Apoptosis* **6**: 191–197.

Nagar B, Overduin M, Ikura M, Rini JM (1996). Structural basis of calcium-induced E-cadherin rigidification and dimerization. *Nature* **380**: 360–364.

Nan M-L, Wang X, Li H-J, Yu D-H, Sun W-Y, Xu H-M, *et al* (2019). Rotundic acid induces Cas3-MCF-7 cell apoptosis through the p53 pathway. *Oncol Lett* **17**: 630–637.

Nascimento JCF do, Ferreira S de A, Vasconcelos JL de A, Silva-Filho JLQ da, Barbosa BT, Bezerra MF, *et al* (2015). Fut3 role in breast invasive ductal carcinoma: Investigating its gene promoter and protein expression. *Exp Mol Pathol* **99**: 409–415.

Nebbioso A, Carafa V, Conte M, Tambaro FP, Abbondanza C, Martens J, *et al* (2017). c-Myc Modulation and Acetylation Is a Key HDAC Inhibitor Target in Cancer. *Clin Cancer Res* **23**: 2542–2555.

Nieset JE, Redfield AR, Jin F, Knudsen KA, Johnson KR, Wheelock MJ (1997). Characterization of the interactions of α -catenin with α -actinin and β-catenin/plakoglobin. *J Cell Sci* **110**: 1013–1022.

Nounou MI, ElAmrawy F, Ahmed N, Abdelraouf K, Goda S, Syed-Sha-Qhattal H (2015). Breast Cancer: Conventional Diagnosis and Treatment Modalities and Recent Patents and Technologies. *Breast Cancer (Auckl)* **9**: 17–34.

Nurismah MI, Noriah O, Suryati MY, Sharifah NA (2008). E-cadherin expression

correlates with histologic type but not tumour grade in invasive breast cancer. *Asian Pac J Cancer Prev* **9**: 699–702.

O'Leary L, Sloot AM van der, Reis CR, Deegan S, Ryan AE, Dhami SPS, *et al* (2016). Decoy receptors block TRAIL sensitivity at a supracellular level: the role of stromal cells in controlling tumour TRAIL sensitivity. *Oncogene* **35**: 1261–1270.

Ogou SI, Yoshida-Noro C, Takeichi M (1983). Calcium-dependent cell-cell adhesion molecules common to hepatocytes and teratocarcinoma stem cells. *J Cell Biol* **97**: 944–948.

Oka H, Shiozaki H, Kobayashi K, Inoue M, Tahara H, Kobayashi T, *et al* (1993). Expression of E-cadherin cell adhesion molecules in human breast cancer tissues and its relationship to metastasis. *Cancer Res* **53**: 1696–1701.

Olive JF, Qin Y, DeCristo MJ, Laszewski T, Greathouse F, McAllister SS (2018). Accounting for tumor heterogeneity when using CRISPR-Cas9 for cancer progression and drug sensitivity studies. *PLoS One* **13**: 1-23.

Ouyang X, Shi M, Jie F, Bai Y, Shen P, Yu Z, *et al* (2017). Phade III study of dulanermin (recombinant human tumor necrosis factor-related apoptosis-inducing ligand/Apo2 ligand) combined with vinorelbine and cisplatin in patients with advanced non-small-cell lung cancer. *Invest New Drugs* **36**:315-322.

Ozawa M, Kemler R (1990). Correct proteolytic cleavage is required for the cell adhesive function of uvomorulin. *J Cell Biol* **111**: 1645–1650.

Ozören N, El-Deiry WS (2002). Defining characteristics of Types I and II apoptotic cells in response to TRAIL. *Neoplasia* **4**: 551–557.

Palen K, Weber J, Dwinell MB, Johnson BD, Ramchandran R, Gershan JA (2016). E-cadherin re-expression shows in vivo evidence for mesenchymal to epithelial transition in clonal metastatic breast tumor cells. *Oncotarget* **7**: 43363–43375.

Palmer HG, Gonzalez-Sancho JM, Espada J, Berciano MT, Puig I, Baulida J, *et al* (2001). Vitamin D3 promotes the differentiation of colon carcinoma cells by the induction of E-cadherin and the inhibition of beta-catenin signaling. *J Cell Biol* **154**: 369–387.

Pandey SS, Singh S, Pathak C, Tiwari BS (2018). "Programmed Cell Death: A Process of Death for Survival" – How Far Terminology Pertinent for Cell Death in Unicellular Organisms. *J Cell Death* **11**: 1179066018790259.

Park JS, Choi SY, Lee J-H, Lee M, Nam ES, Jeong AL, *et al* (2013). Interleukin-32β stimulates migration of MDA-MB-231 and MCF-7cells via the VEGF-STAT3 signaling pathway. *Cell Oncol (Dordr)* **36**: 493–503.

Pathy NB, Yip CH, Taib NA, Hartman M, Saxena N, Iau P, *et al* (2011). Breast cancer in a multi-ethnic Asian setting: results from the Singapore-Malaysia hospital-based breast cancer registry. *Breast* **Suppl 2**: S75-S80.

Patil M, Pabla N, Dong Z (2013). Checkpoint kinase 1 in DNA damage response and cell cycle regulation. *Cell Mol Life Sci* **70**: 4009–4021.

Pawel J von, Harvey JH, Spigel DR, Dediu M, Reck M, Cebotaru CL, *et al* (2014). Phade II Trial of Mapatumumab, a Fully Human Agonist Monoclonal Antibody to Tumor Necrosis Factor-Related Apoptosis-Inducing Ligand Receptor 1 (TRAIL-R1), in Combination With Paclitaxel and Carboplatin in Patients With Advanced Non–Small-Cell Lung Cancer. *Clin Lung Cancer* **15**: 188–196.e2.

Pawel J Von, Harvey JH, Spigel DR, Dediu M, Reck M, Cebotaru CL, *et al* (2010). A randomized phade II trial of mapatumumab, a TRAIL-R1 agonist monoclonal antibody, in combination with carboplatin and paclitaxel in patients with advanced NSCLC. *J Clin Oncol* **28**: LBA7501.

Pećina-Šlaus N (2003). Tumor suppressor gene E-cadherin and its role in normal and malignant cells. *Cancer Cell Int* **3**: 1-7.

Pennati M, Sbarra S, Cesare M De, Lopergolo A, Locatelli SL, Campi E, *et al* (2015).

YM155 sensitizes triple-negative breast cancer to membrane-bound TRAIL through p38 MAPK- and CHOP-mediated DR5 upregulation. *Int J cancer* **136**: 299–309.

Petrucci E, Pasquini L, Bernabei M, Saulle E, Biffoni M, Accarpio F, *et al* (2012). A small molecule SMAC mimic LBW242 potentiates TRAIL- and anticancer drug-mediated cell death of ovarian cancer cells. *PLoS One* **7**: 1-14.

Pietenpol J., Stewart Z. (2002). Cell cycle checkpoint signaling:: Cell cycle arrest versus apoptosis. *Toxicology* **181**–**182**: 475–481.

Pietsch EC, Perchiniak E, Canutescu AA, Wang G, Dunbrack RL, Murphy ME (2008). Oligomerization of BAK by p53 utilizes conserved residues of the p53 DNA binding domain. *J Biol Chem* **283**: 21294–21304.

Piret J-P, Mottet D, Raes M, Michiels C (2002). Is HIF-1α a pro- or an anti-apoptotic protein? *Biochem Pharmacol* **64**: 889–892.

Plummer R, Attard G, Pacey S, Li L, Razak A, Perrett R, *et al* (2007). Phade 1 and Pharmacokinetic Study of Lexatumumab in Patients with Advanced Cancers. *Clin Cancer Res* **13**: 6187–6194.

Polyak K (2011). Heterogeneity in breast cancer. *J Clin Invest* **121**: 3786–3788.

Pompeia C, Hodge DR, Plass C, Wu Y-Z, Marquez VE, Kelley JA, *et al* (2004). Microarray analysis of epigenetic silencing of gene expression in the KAS-6/1 multiple myeloma cell line. *Cancer Res* **64**: 3465–3473.

Portanova P, Notaro A, Pellerito O, Sabella S, Giuliano M, Calvaruso G (2013). Notch inhibition restores TRAIL-mediated apoptosis via AP1-dependent upregulation of DR4 and DR5 TRAIL receptors in MDA-MB-231 breast cancer cells. *Int J Oncol* **43**: 121–130.

Prabhu V V, Allen JE, Dicker DT, El-Deiry WS (2015). Small-Molecule ONC201/TIC10 Targets Chemotherapy-Resistant Colorectal Cancer Stem-like Cells in an Akt/Foxo3a/TRAIL-Dependent Manner. *Cancer Res* **75**: 1423–32.

Pribic J, Brazill D (2012). Paxillin phosphorylation and complexing with Erk and FAK are regulated by PLD activity in MDA-MB-231 cells. *Cell Signal* **24**: 1531–40.

Quast SA, Steinhorst K, Plötz M, Eberle J (2015). Sensitization of Melanoma Cells for Death Ligand TRAIL Is Based on Cell Cycle Arrest, ROS Production, and Activation of Proapoptotic Bcl-2 Proteins. *J Invest Dermatol* **135**: 2794–2804.

Qureshi HS, Linden MD, Divine G, Raju UB (2006). E-cadherin status in breast cancer correlates with histologic type but does not correlate with established prognostic parameters. *Am J Clin Pathol* **125**: 377–385.

Rahman M, Davis SR, Pumphrey JG, Bao J, Nau MM, Meltzer PS, *et al* (2009). TRAIL induces apoptosis in triple-negative breast cancer cells with a mesenchymal phenotype. *Breast Cancer Res Treat* **113**: 217–230.

Rathore R, McCallum JE, Varghese E, Florea AM, Büsselberg D (2017). Overcoming chemotherapy drug resistance by targeting inhibitors of apoptosis proteins (IAPs). *Apoptosis* **22**: 898–919.

Ravi R, Bedi GC, Engstrom LW, Zeng Q, Mookerjee B, Gélinas C, *et al* (2001). Regulation of death receptor expression and TRAIL/Apo2L-induced apoptosis by NF-kappaB. *Nat Cell Biol* **3**: 409–416.

Reck M, Krzakowski M, Chmielowska E, Sebastian M, Hadler D, Fox T, *et al* (2013). A randomized, double-blind, placebo-controlled phade 2 study of tigatuzumab (CS-1008) in combination with carboplatin/paclitaxel in patients with chemotherapy-naïve metastatic/unresectable non-small cell lung cancer. *Lung Cancer* **82**: 441–448.

Reddy P, Liu L, Ren C, Lindgren P, Boman K, Shen Y, *et al* (2005). Formation of E-cadherin-mediated cell-cell adhesion activates AKT and mitogen activated protein kinase via phosphatidylinositol 3 kinase and ligand-independent activation of epidermal growth factor receptor in ovarian cancer cells. *Mol*

Endocrinol **19**: 2564–2578.

Reis CR, Chen P-H, Bendris N, Schmid SL (2017). TRAIL-death receptor endocytosis and apoptosis are selectively regulated by dynamin-1 activation. *Proc Natl Acad Sci U S A* **114**: 504–509.

Repetto O, Paoli P De, Re V De, Canzonieri V, Cannizzaro R (2014). Levels of soluble E-cadherin in breast, gastric, and colorectal cancers. *BioMed Res Int* **2014**: 1-8.

Rocha Lima CM, Bayraktar S, Flores AM, MacIntyre J, Montero A, Baranda JC, *et al* (2012). Phade Ib Study of Drozitumab Combined With First-Line mFOLFOX6 Plus Bevacizumab in Patients with Metastatic Colorectal Cancer. *Cancer Invest* **30**: 727–731.

Rodriguez FJ, Lewis-Tuffin LJ, Anastasiadis PZ (2012). E-cadherin's dark side: possible role in tumor progression. *Biochim Biophys Acta* **1826**: 23–31.

Saraei R, Soleimani M, Movassaghpour Akbari AA, Farshdousti Hagh M, Hadsanzadeh A, Solali S (2018). The role of XIAP in resistance to TNF-related apoptosis-inducing ligand (TRAIL) in Leukemia. *Biomed Pharmacother* **107**: 1010–1019.

Saraste A, Pulkki K (2000). Morphologic and biochemical hallmarks of apoptosis. *Cardiovasc Res* **45**: 528–537.

Sasaki CY, Lin H c, Passaniti A (2000). Expression of E-cadherin reduces bcl-2 expression and increases sensitivity to etoposide-induced apoptosis. *Int J Cancer* **86**: 660–666.

Sasatomi E, Tokunaga O, Miyazaki K (1996). Spontaneous apoptosis in gallbladder carcinoma: Relationships with clinicopathologic factors, expression of E-cadherin,bcl-2 protooncogene, and p53 oncosuppressor gene. *Cancer* **78**: 2101–2110.

Sattler M, Liang H, Nettesheim D, Meadows RP, Harlan JE, Eberstadt M, *et al* (1997). Structure of Bcl-xL-Bak peptide complex: recognition between regulators of apoptosis. *Sci* **275**: 983–986.

Sawa H, Murakami H, Ohshima Y, Sugino T, Nakajyo T, Kisanuki T, *et al* (2001). Histone deacetylase inhibitors such as sodium butyrate and trichostatin A induce apoptosis through an increase of the bcl-2-related protein Bad. *Brain Tumor Pathol* **18**: 109–114.

Sawada K, Mitra AK, Radjabi AR, Bhadkar V, Kistner EO, Tretiakova M, *et al* (2008). Loss of E-Cadherin promotes ovarian cancer metastasis via alpha 5-Integrin, which is a therapeutic target. *Cancer Res* **68**: 2329–2339.

Saxena S, Jónsson ZO, Dutta A (2003). Small RNAs with imperfect match to endogenous mRNA repress translation. Implications for off-target activity of small inhibitory RNA in mammalian cells. *J Biol Chem* **278**: 44312–44319.

Schulze-Osthoff K, Ferrari D, Los M, Wesselborg S, Peter ME (1998). Apoptosis signaling by death receptors. *Eur J Biochem* **254**: 439–459.

Sedlak TW, Oltvai ZN, Yang E, Wang K, Boise LH, Thompson CB, *et al* (1995). Multiple Bcl-2 family members demonstrate selective dimerizations with Bax. *Proc natl Acad Sci U S A* **92**: 7834–7838.

Segawa K, Nagata S (2015). An Apoptotic "Eat Me" Signal: Phosphatidylserine Exposure. *Trends Cell Biol* **25**: 639–650.

Selli C, Sims AH (2019). Neoadjuvant Therapy for Breast Cancer as a Model for Translational Research. *Breast Cancer (Auckl)* **13**: 1178223419829072.

Semple JI, Smits VAJ, Fernaud J-R, Mamely I, Freire R (2007). Cleavage and degradation of Claspin during apoptosis by caspases and the proteasome. *Cell Death Diff* **14**: 1433–1442.

Sermeus A, Michiels C (2011). Reciprocal influence of the p53 and the hypoxic

pathways. *Cell Death Dis* **2**: 1-11.

Shamas-Din A, Kale J, Leber B, Andrews DW (2013). Mechanisms of action of Bcl-2 family proteins. *Cold Spring Harb Perspect Biol* **5**: 1-21.

Sharma S, Kelly TK, Jones PA (2009). Epigenetics in cancer. *Carcinogenesis* **31**: 27–36.

Sharma S, Vries EG de, Infante JR, Oldenhuis CN, Gietema JA, Yang L, *et al* (2014). Safety, pharmacokinetics, and pharmacodynamics of the DR5 antibody LBY135 alone and in combination with capecitabine in patients with advanced solid tumors. *Invest New Drugs* **32**: 135–144.

Shen M, Jiang Y-Z, Wei Y, Ell B, Sheng X, Esposito M, *et al* (2019). Tinagl1 Suppresses Triple-Negative Breast Cancer Progression and Metastasis by Simultaneously Inhibiting Integrin/FAK and EGFR Signaling. *Cancer Cell* **35**: 64–80.

Shen X, Kramer RH (2004). Adhesion-mediated squamous cell carcinoma survival through ligand-independent activation of epidermal growth factor receptor. *Am J Pathol* **165**: 1315–1329.

Shin D, Park Y-S, Yang K, Kim W-J, Han MH, Kang HS, *et al* (2012). Decitabine, a DNA methyltransferase inhibitor, induces apoptosis in human leukemia cells through intracellular reactive oxygen species generation. *Int J Oncol* **41**: 910–918.

Shin H-R, Boniol M, Joubert C, Hery C, Haukka J, Autier P, *et al* (2010). Secular trends in breast cancer mortality in five East Asian populations: Hong Kong, Japan, Korea, Singapore and Taiwan. *Cancer Sci* **101**: 1241–1246.

Shiraki K, Yamanaka T, Inoue H, Kawakita T, Enokimura N, Okano H, *et al* (2005). Expression of TNF-related apoptosis-inducing ligand in human hepatocellular carcinoma. *Int J Oncol* **26**: 1273–1281.

Shoeb M, Ramana K V, Srivastava SK (2013). Aldose reductase inhibition enhances TRAIL-induced human colon cancer cell apoptosis through AKT/FOXO3a-dependent upregulation of death receptors. *Free Radic Biol Med* **63**: 280–290.

Sikic B, Wakelee H, Mehren M Von, Lewis N, Plummer ER, Calvert AH, *et al* (2007). [Meeting Abstract] A Phade 1b study to assess the safety of lexatumumab, a human monoclonal antibody that activates TRAIL-R2, in combination with gemcitabine, pemetrexed, doxorubicin or FOLFIRI. *Mol Cancer Ther* **6**.

Silke J, Meier P (2013). Inhibitors of Apoptosis (IAP) Proteins- Modulators of Cell Death and Inflammation. *Cold Spring Harb Perspect Biol* **5**: 1-19.

Singh G (2012). Oophorectomy in breast cancer-controversies and current status. *Indian J Surg* **74**: 210–212.

Singh TR, Shankar S, Srivastava RK (2005). HDAC inhibitors enhance the apoptosis-inducing potential of TRAIL in breast carcinoma. *Oncogene* **24**: 4609–4623.

Singhai R, Patil VW, Jaiswal SR, Patil SD, Tayade MB, Patil A V (2011). E-Cadherin as a diagnostic biomarker in breast cancer. *N Am J Med Sci* **3**: 227–233.

Smeenk L, Heeringen SJ van, Koeppel M, Gilbert B, Janssen-Megens E, Stunnenberg HG, *et al* (2011). Role of p53 serine 46 in p53 target gene regulation. *PLoS One* **6**: 1-14.

Smulski CR, Decossas M, Chekkat N, Beyrath J, Willen L, Guichard G, *et al* (2017). Hetero-oligomerization between the TNF receptor superfamily members CD40, Fas and TRAILR2 modulate CD40 signalling. *Cell Death Dis* **8**: e2601–e2601.

Soria J-C, Márk Z, Zatloukal P, Szima B, Albert I, Juhász E, *et al* (2011). Randomized phade II study of dulanermin in combination with paclitaxel, carboplatin, and bevacizumab in advanced non-small-cell lung cancer. *J Clin Oncol* **29**: 4442–4451.

Soria J-C, Smit E, Khayat D, Besse B, Yang X, Hsu C-P, *et al* (2010). Phade 1b study

of dulanermin (recombinant human Apo2L/TRAIL) in combination with paclitaxel, carboplatin, and bevacizumab in patients with advanced non-squamous non-small-cell lung cancer. *J Clin Oncol* **28**: 1527–1533.

Stadel D, Mohr A, Ref C, MacFarlane M, Zhou S, Humphreys R, *et al* (2010). TRAIL-Induced Apoptosis Is Preferentially Mediated via TRAIL Receptor 1 in Pancreatic Carcinoma Cells and Profoundly Enhanced by XIAP Inhibitors. *Clin Cancer Res* **16**: 5734–5749.

Stockinger A, Eger A, Wolf J, Beug H, Foisner R (2001). E-cadherin regulates cell growth by modulating proliferation-dependent β -catenin transcriptional activity. *J Cell Biol* **154**: 1185–1196.

Stuckey DW, Shah K (2013). TRAIL on trial: preclinical advances in cancer therapy. *Trends Mol Med* **19**: 685–694.

Sullivan KM, Kozuch PS (2011). Impact of KRAS Mutations on Management of Colorectal Carcinoma. *Pathol Res Int* **2011**: 1–11.

Tabernero J, Chawla SP, Kindler H, Reckamp K, Chiorean EG, Azad NS, *et al* (2015). Anticancer activity of the type I insulin-like growth factor receptor antagonist, ganitumab, in combination with the death receptor 5 agonist, conatumumab. *Target Oncol* **10**: 65–76.

Tang S-N, Fu J, Nall D, Rodova M, Shankar S, Srivastava RK (2012). Inhibition of sonic hedgehog pathway and pluripotency maintaining factors regulate human pancreatic cancer stem cell characteristics. *Int J Cancer* **131**: 30–40.

Tetsu O, McCormick F (1999). Beta-Catenin regulates expression of cyclin D1 in colon carcinoma cells. *Nature* **398**: 422–426.

Tolcher AW, Mita M, Meropol NJ, Mehren M von, Patnaik A, Padavic K, *et al* (2007). Phade I Pharmacokinetic and Biologic Correlative Study of Mapatumumab, a Fully Human Monoclonal Antibody With Agonist Activity to Tumor Necrosis Factor–Related Apoptosis-Inducing Ligand Receptor-1. *J Clin Oncol* **25**: 1390–1396.

Trarbach T, Moehler M, Heinemann V, Köhne C-H, Przyborek M, Schulz C, *et al* (2010). Phade II trial of mapatumumab, a fully human agonistic monoclonal antibody that targets and activates the tumour necrosis factor apoptosis-inducing ligand receptor-1 (TRAIL-R1), in patients with refractory colorectal cancer. *Br J Cancer* **102**: 506–512.

Trivedi R, Mishra DP (2015). Trailing TRAIL Resistance: Novel Targets for TRAIL Sensitization in Cancer Cells. *Front Oncol* **5**: 1–20.

Tsai JH, Yang J (2013). Epithelial-mesenchymal plasticity in carcinoma metastasis. *Genes Dev* **27**: 2192–2206.

Turashvili G, Brogi E (2017). Tumor Heterogeneity in Breast Cancer. *Front Med* **4**: 1-11.

Turner NC, Reis-Filho JS (2013). Tackling the Diversity of Triple-Negative Breast Cancer. *Clin Cancer Res* **19**: 6380–6388.

Twomey JD, Kim S-R, Zhao L, Bozza WP, Zhang B (2015). Spatial dynamics of TRAIL death receptors in cancer cells. *Drug Resist Updat* **19**: 13–21.

Twomey JD, Zhang B (2019). Circulating Tumor Cells Develop Resistance to TRAIL-Induced Apoptosis Through Autophagic Removal of Death Receptor 5: Evidence from an In Vitro Model. *Cancers (Basel)* **11**: 1-16.

VanOosten RL, Moore JM, Karacay B, Griffith TS (2005a). Histone Deacetylase Inhibitors Modulate Renal Cell Carcinoma Sensitivity to TRAIL/Apo-2L-Induced Apoptosis by Enhancing TRAIL-R2 Expression. *Cancer Biol Ther* **4**: 1104–1112.

VanOosten RL, Moore JM, Ludwig AT, Griffith TS (2005b). Depsipeptide (FR901228) Enhances the Cytotoxic Activity of TRAIL by Redistributing TRAIL Receptor to Membrane Lipid Rafts. *Mol Ther* **11**: 542–552.

Varshochi R, Halim F, Sunters A, Alao JP, Madureira PA, Hart SM, *et al* (2005). ICI182,780 induces p21Waf1 gene transcription through releasing histone deacetylase 1 and estrogen receptor alpha from Sp1 sites to induce cell cycle arrest in MCF-7 breast cancer cell line. *J Biol Chem* **280**: 3185–3196.

Vidula N, Bardia A (2017). Targeted therapy for metastatic triple negative breast cancer: The next frontier in precision oncology. *Oncotarget* **8**: 106167–106168.

Vleminckx K, Vakaet L, Mareel M, Fiers W, Roy F van (1991). Genetic manipulation of E-cadherin expression by epithelial tumor cells reveals an invasion suppressor role. *Cell* **66**: 107–119.

Voss OH, Batra S, Kolattukudy SJ, Gonzalez-Mejia ME, Smith JB, Doseff AI (2007). Binding of caspase-3 prodomain to heat shock protein 27 regulates monocyte apoptosis by inhibiting caspase-3 proteolytic activation. *J Biol Chem* **282**: 25088–25099.

Wagner KW, Punnoose EA, Januario T, Lawrence DA, Pitti RM, Lancaster K, *et al* (2007). Death-receptor O-glycosylation controls tumor-cell sensitivity to the proapoptotic ligand Apo2L/TRAIL. *Nat Med* **13**: 1070–1077.

Wakelee HA, Patnaik A, Sikic BI, Mita M, Fox NL, Miceli R, *et al* (2010). Phade I and pharmacokinetic study of lexatumumab (HGS-ETR2) given every 2 weeks in patients with advanced solid tumors. *Ann Oncol* **21**: 376–381.

Wang D, Liu D, Gao J, Liu M, Liu S, Jiang M, *et al* (2013a). TRAIL-induced miR-146a expression suppresses CXCR4-mediated human breast cancer migration. *FEBS J* **280**: 3340–3353.

Wang F, Lin J, Xu R (2014a). The molecular mechanisms of TRAIL resistance in cancer cells: help in designing new drugs. *Curr Pharm Des* **20**: 6714–6722.

Wang L (2017). Early Diagnosis of Breast Cancer. *Sensors (Basel)* **17**: 1-20.

Wang L, Wang G, Yang D, Guo X, Xu Y, Feng B, *et al* (2013b). Euphol arrests breast cancer cells at the G1 phade through the modulation of cyclin D1, p21 and p27 expression. *Mol Med Rep* **8**: 1279–1285.

Wang R, Jin C, Hu X (2017). Evidence of drug-response heterogeneity rapidly generated from a single cancer cell. *Oncotarget* **8**: 41113–41124.

Wang X, Chen M, Zhou J, Zhang X (2014b). HSP27, 70 and 90, anti-apoptotic proteins, in clinical cancer therapy. *Int J Oncol* **45**: 18–30.

Wheelock MJ, Johnson KR (2003). Cadherins as modulators of cellular phenotype. *Annu Rev Cell Dev Biol* **19**: 207–235.

Wiley SR, Schooley K, Smolak PJ, Din WS, Huang C-P, Nicholl JK, *et al* (1995). Identification and characterization of a new member of the TNF family that induces apoptosis. *Immunity* **3**: 673–682.

Willis SN, Fletcher JI, Kaufmann T, Delft MF van, Chen L, Czabotar PE, *et al* (2007). Apoptosis Initiated When BH3 Ligands Engage Multiple Bcl-2 Homologs, Not Bax or Bak. *Science (80-)* **315**: 856–859.

Wong SHM, Fang CM, Chuah L-H, Leong CO, Ngai SC (2018). E-cadherin: Its dysregulation in carcinogenesis and clinical implications. *Crit Rev Oncol Hematol* **121**: 11–22.

Wu S-Y, Wu ATH, Liu S-H, Wu S-Y, Wu ATH, Liu S-H, *et al* (2016). MicroRNA-17-5p regulated apoptosis-related protein expression and radiosensitivity in oral squamous cell carcinoma caused by betel nut chewing. *Oncotarget* **7**: 51482–51493.

Yan S, Qu X, Xu C, Zhu Z, Zhang L, Xu L, *et al* (2012). Down-regulation of Cbl-b by bufalin results in up-regulation of DR4/DR5 and sensitization of TRAIL-induced apoptosis in breast cancer cells. *J Cancer Res Clin Oncol* **138**: 1279–1289.

Yang P-M, Lin Y-T, Shun C-T, Lin S-H, Wei T-T, Chuang S-H, *et al* (2013). Zebularine inhibits tumorigenesis and stemness of colorectal cancer via p53-

dependent endoplasmic reticulum stress. *Sci Rep* **3**: 1-11.

Yang XH, Sladek TL, Liu X, Butler BR, Froelich CJ, Thor AD (2001). Reconstitution of caspase 3 sensitizes MCF-7 breast cancer cells to doxorubicin- and etoposide-induced apoptosis. *Cancer Res* **61**: 348–354.

Yao D, Peng S, Dai C (2013). The role of hepatocyte nuclear factor 4alpha in metastatic tumor formation of hepatocellular carcinoma and its close relationship with the mesenchymal–epithelial transition markers. *BMC Cancer* **13**: 1-11.

Yates CC, Shepard CR, Stolz DB, Wells A (2007). Co-culturing human prostate carcinoma cells with hepatocytes leads to increased expression of E-cadherin. *Br J Cancer* **96**: 1246–1252.

Yerbes R, López-Rivas A, Reginato MJ, Palacios C (2012). Control of FLIP(L) expression and TRAIL resistance by the extracellular signal-regulated kinase1/2 pathway in breast epithelial cells. *Cell Death Differ* **19**: 1908–1916.

Yip CH, Bhoo Pathy N, Teo SH (2014). A review of breast cancer research in malaysia. *Med J Malaysia* **69 Suppl A**: 8–22.

Yoshida T, Zhang Y, Rivera Rosado L a, Zhang B (2009). Repeated treatment with subtoxic doses of TRAIL induces resistance to apoptosis through its death receptors in MDA-MB-231 breast cancer cells. *Mol Cancer Res* **7**: 1835–1844.

Youlden DR, Cramb SM, Dunn NAM, Muller JM, Pyke CM, Baade PD (2012). The descriptive epidemiology of female breast cancer: An international comparison of screening, incidence, survival and mortality. *Cancer Epidemiol* **36**: 237–248.

Youlden DR, Cramb SM, Yip CH, Baade PD (2014). Incidence and mortality of female breast cancer in the Asia-Pacific region. *Cancer Biol Med* **11**: 101–115.

Younis LK, Sakka H El, Haque I (2007). The Prognostic Value of E-cadherin Expression in Breast Cancer. *Int J Heal Sci* **1**: 43–51.

Zhang B, Roosmalen IAM van, Reis CR, Setroikromo R, Quax WJ (2019). Death receptor 5 is activated by fucosylation in colon cancer cells. *FEBS J* **286**: 555–571.

Zhang L, Fang B (2005). Mechanisms of resistance to TRAIL-induced apoptosis in cancer. *Cancer Gene Ther* **12**: 228–237.

Zhang Y, Xu J, Yu Y, Shang W, Ye A (2018). Anti-Cancer Drug Sensitivity Assay with Quantitative Heterogeneity Testing Using Single-Cell Raman Spectroscopy. *Mol* **23**: 1-14.

Zhang Y, Yoshida T, Zhang B (2009). TRAIL induces endocytosis of its death receptors in MDA-MB-231 breast cancer cells. *Cancer Biol Ther* **8**: 917–922.

Zhang Y, Zhang B (2008). TRAIL resistance of breast cancer cells is associated with constitutive endocytosis of death receptors 4 and 5. *Mol Cancer Res* **6**: 1861–1871.

Zhang Y, Zhu J, Tang Y, Li F, Zhou H, Peng B, *et al* (2011). X-linked inhibitor of apoptosis positive nuclear labeling: A new independent prognostic biomarker of breast invasive ductal carcinoma. *Diagn Pathol* **6**: 1-9.

Zhou LL, Zhou LY, Luo KQ, Chang DC (2005). Smac/DIABLO and cytochrome c are released from mitochondria through a similar mechanism during UV-induced apoptosis. *Apoptosis* **10**: 289–299.

Zhou W, Feng X, Han Han H, Guo S, Wang G (2016). Synergistic effects of combined treatment with histone deacetylase inhibitor suberoylanilide hydroxamic acid and TRAIL on human breast cancer cells. *Sci Rep* **6**: 1-16.

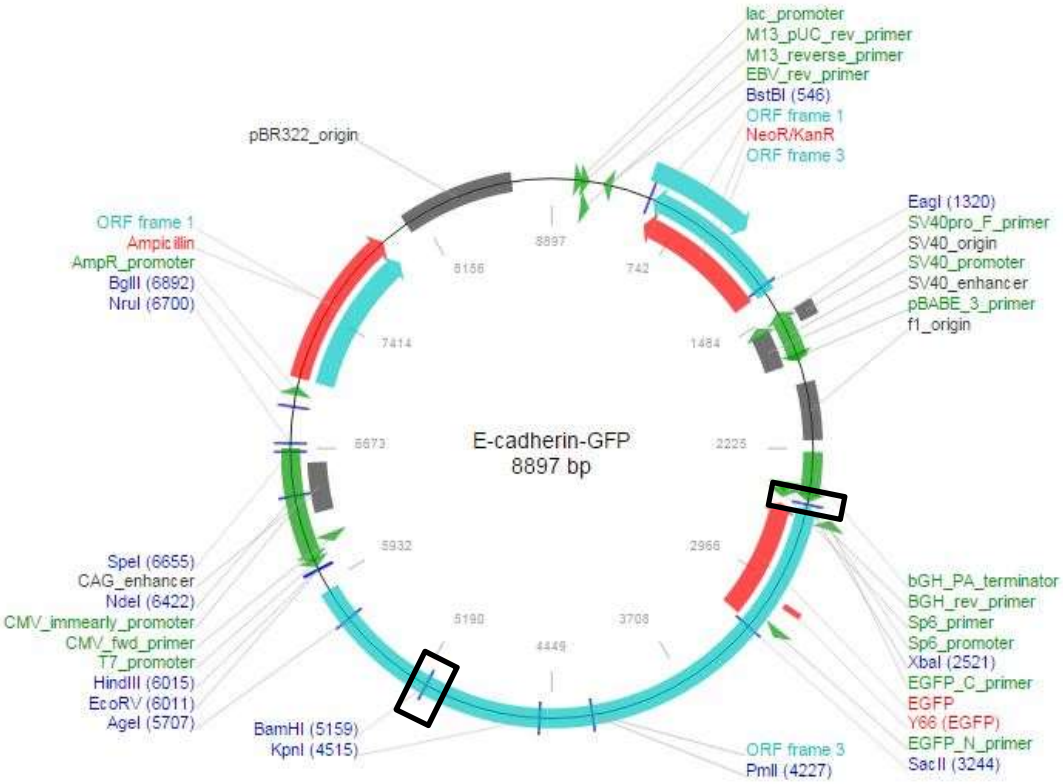
Zhu X-F, Li W, Ma J-Y, Shao N, Zhang Y-J, Liu R-M, *et al* (2015). Knockdown of heme oxygenase-1 promotes apoptosis and autophagy and enhances the cytotoxicity of doxorubicin in breast cancer cells. *Oncol Lett* **10**: 2974–2980.

Zuhorn IS, Kalicharan R, Hoekstra D (2002). Lipoplex-mediated transfection of

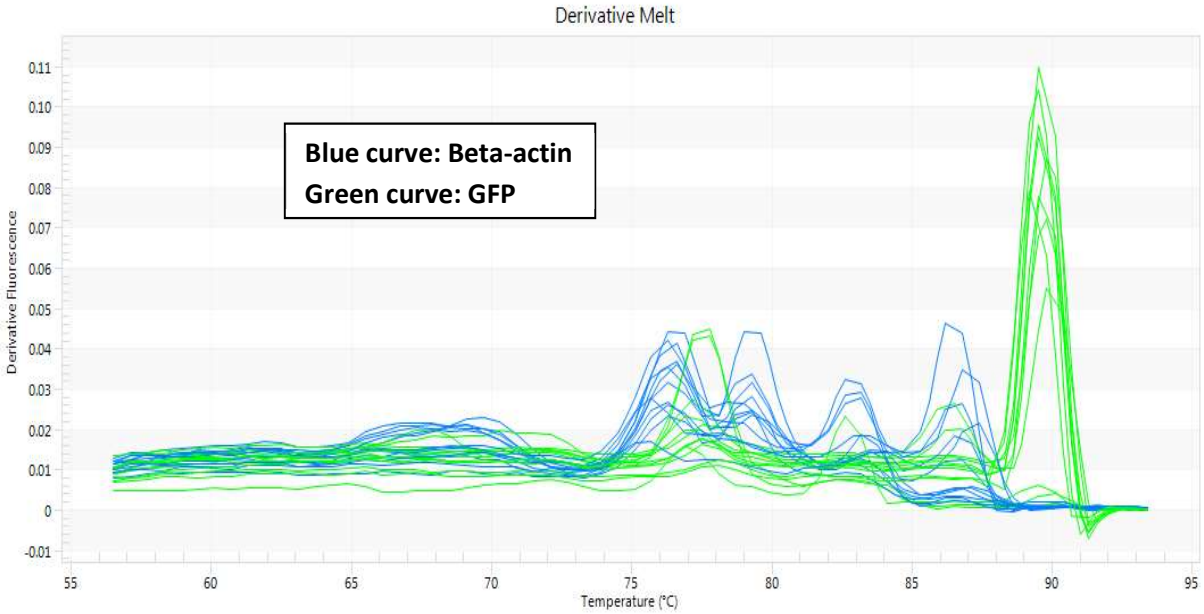
mammalian cells occurs through the cholesterol-dependent clathrin-mediated pathway of endocytosis. *J Biol Chem* **277**: 18021–18028.

Zuo X, Qin Y, Zhang X, Ning Q, Shao S, Luo M, *et al* (2014). Breast cancer cells are arrested at different phades of the cell cycle following the re-expression of ARHI. *Oncol Rep* **31**: 2358–2364.

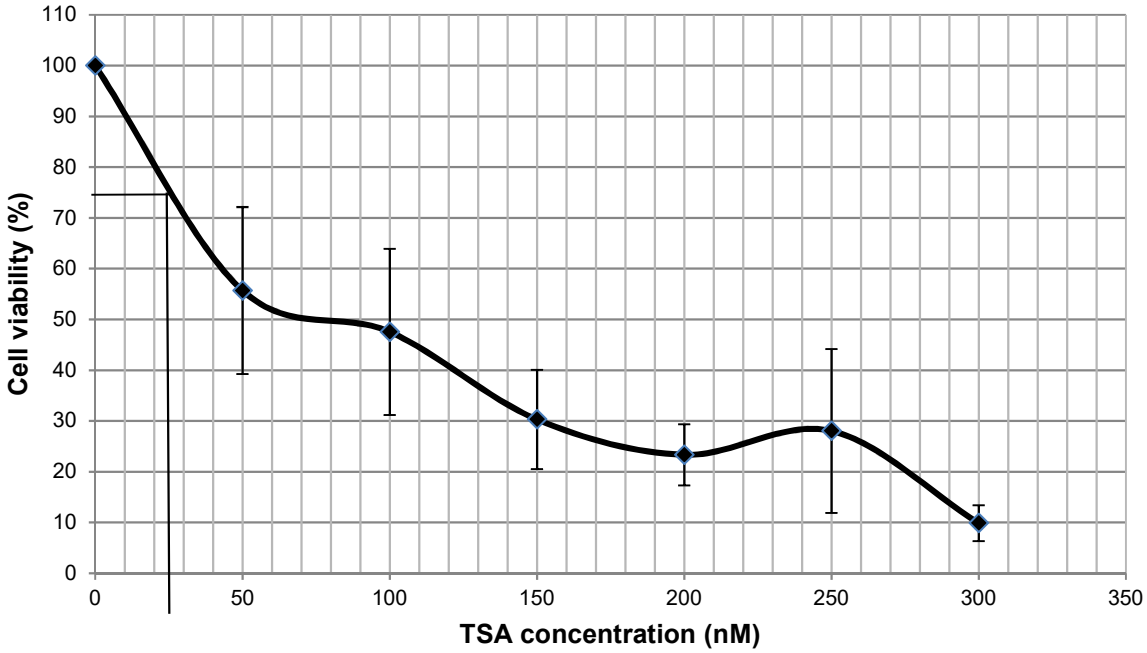
Appendices



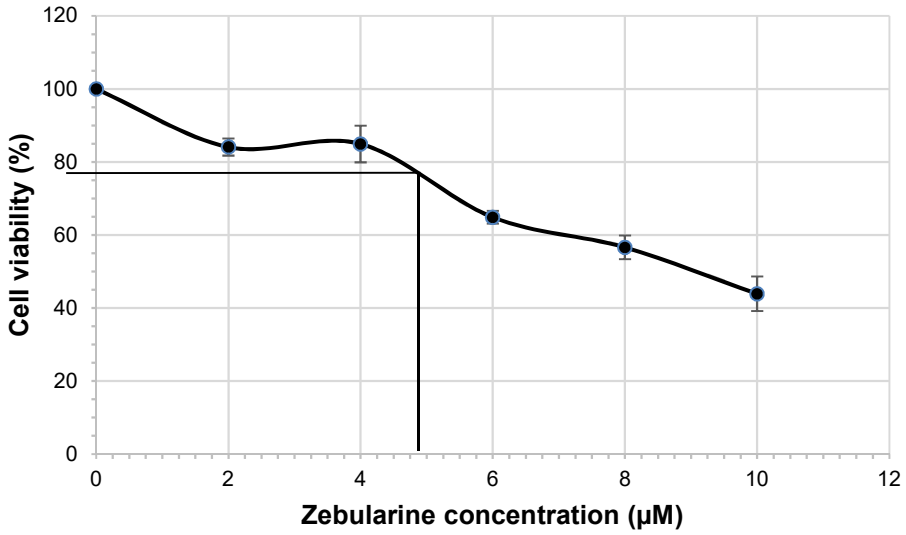
Appendix A E-cadherin-GFP (EGFP) plasmid sequence map with total length of 8897 base pairs (bp). *Bam*HI and *Xba*I restrictions sites at 5159 bp and 2521 bp, respectively are shown (black rectangle).



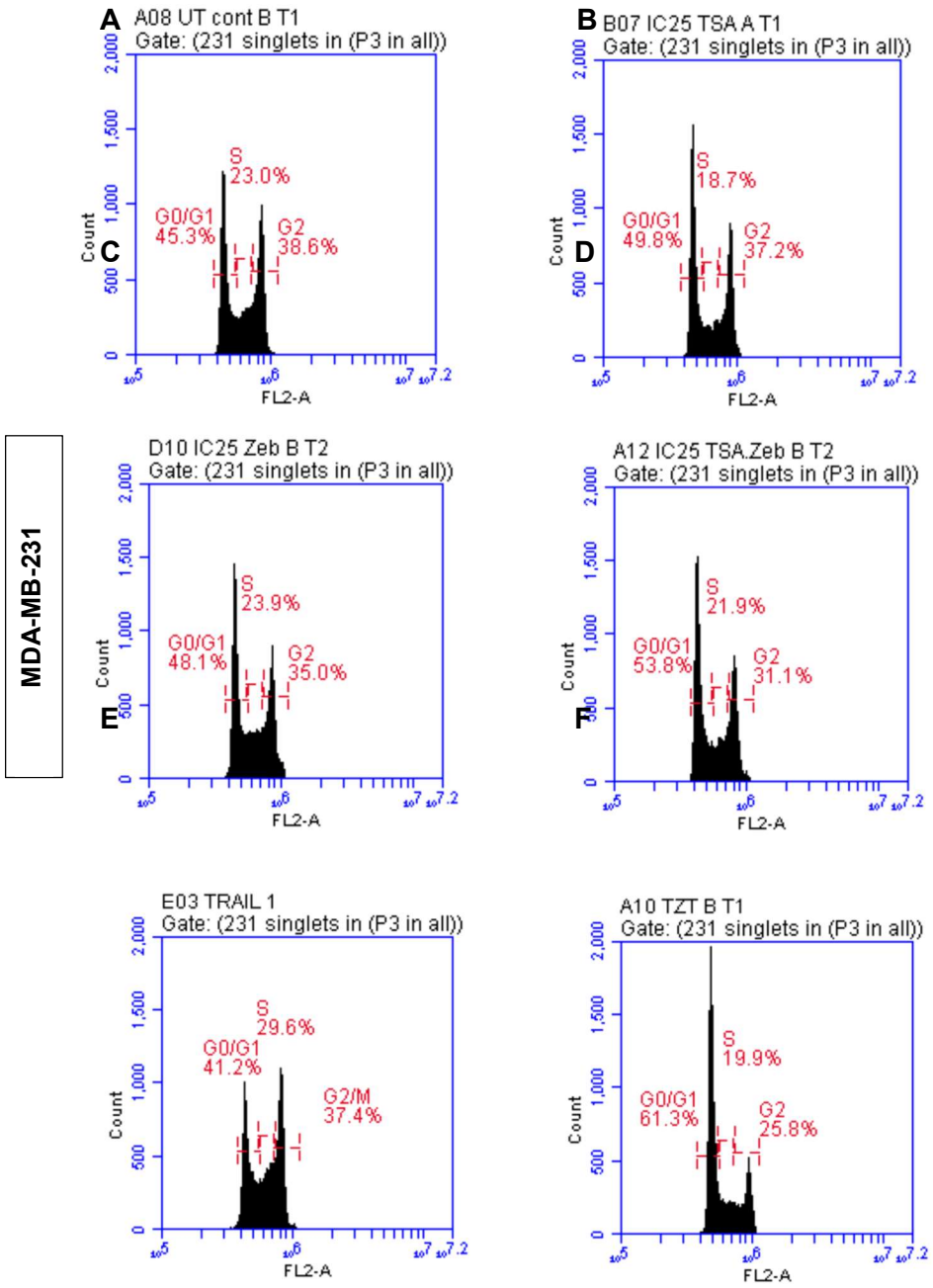
Appendix B Melt curve analysis of the qPCR reaction. The peak (green curve) at approximately 90˚C shows the potential GFP product while the peak (blue curve) at approximately 77˚C shows the potential beta-actin product. Unspecific binding of beta-actin primer is also depicted from the blue curve. The melt curve analysis conditions were 95˚C for 15s, 55˚C for 15s and eventually 95˚C for 15 s.



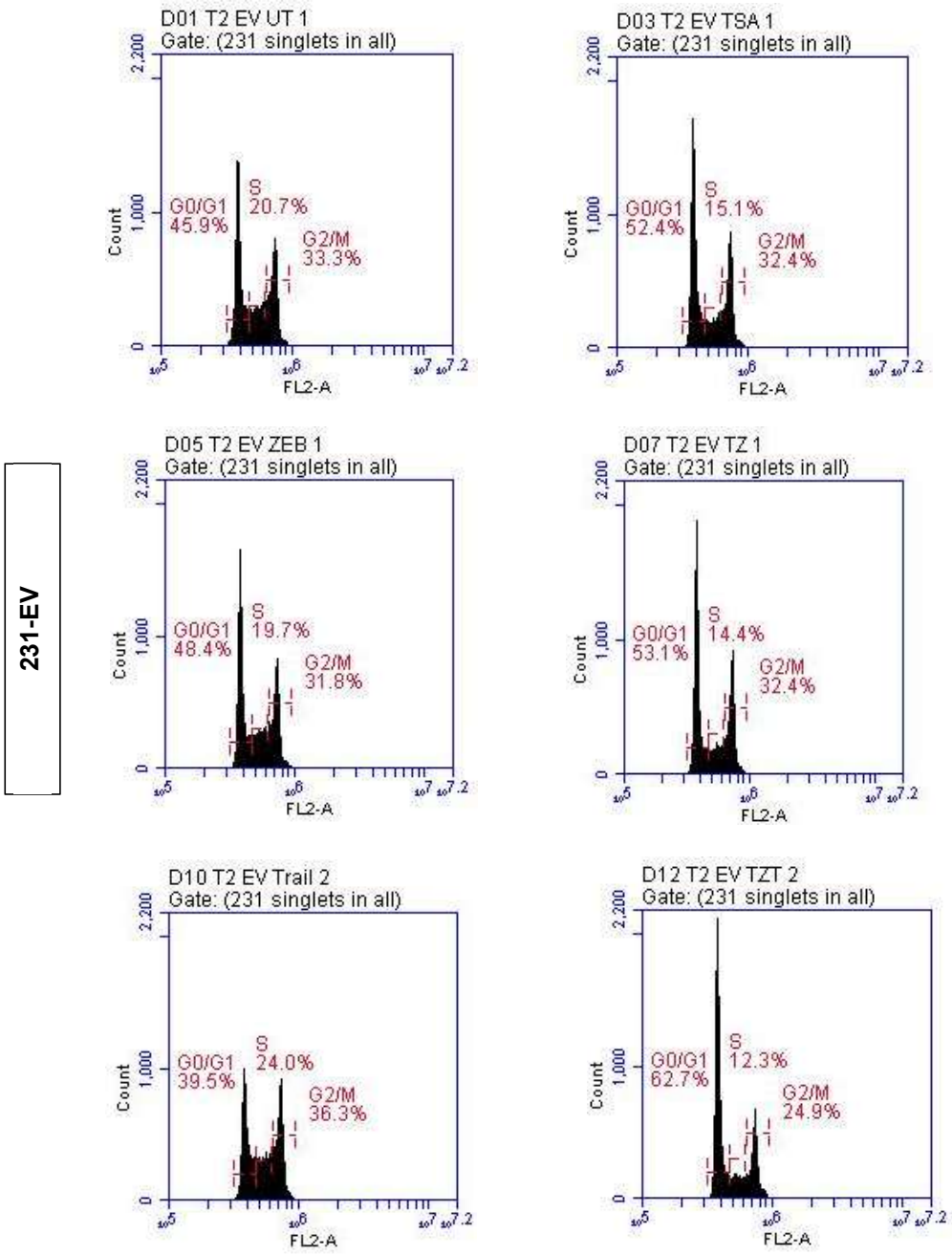
Appendix C Cell viability curve of MDA-MB-231 treated with 50, 100, 150, 200, 250 and 300 nM TSA. Data represents means ± SEM from three independent experiments.



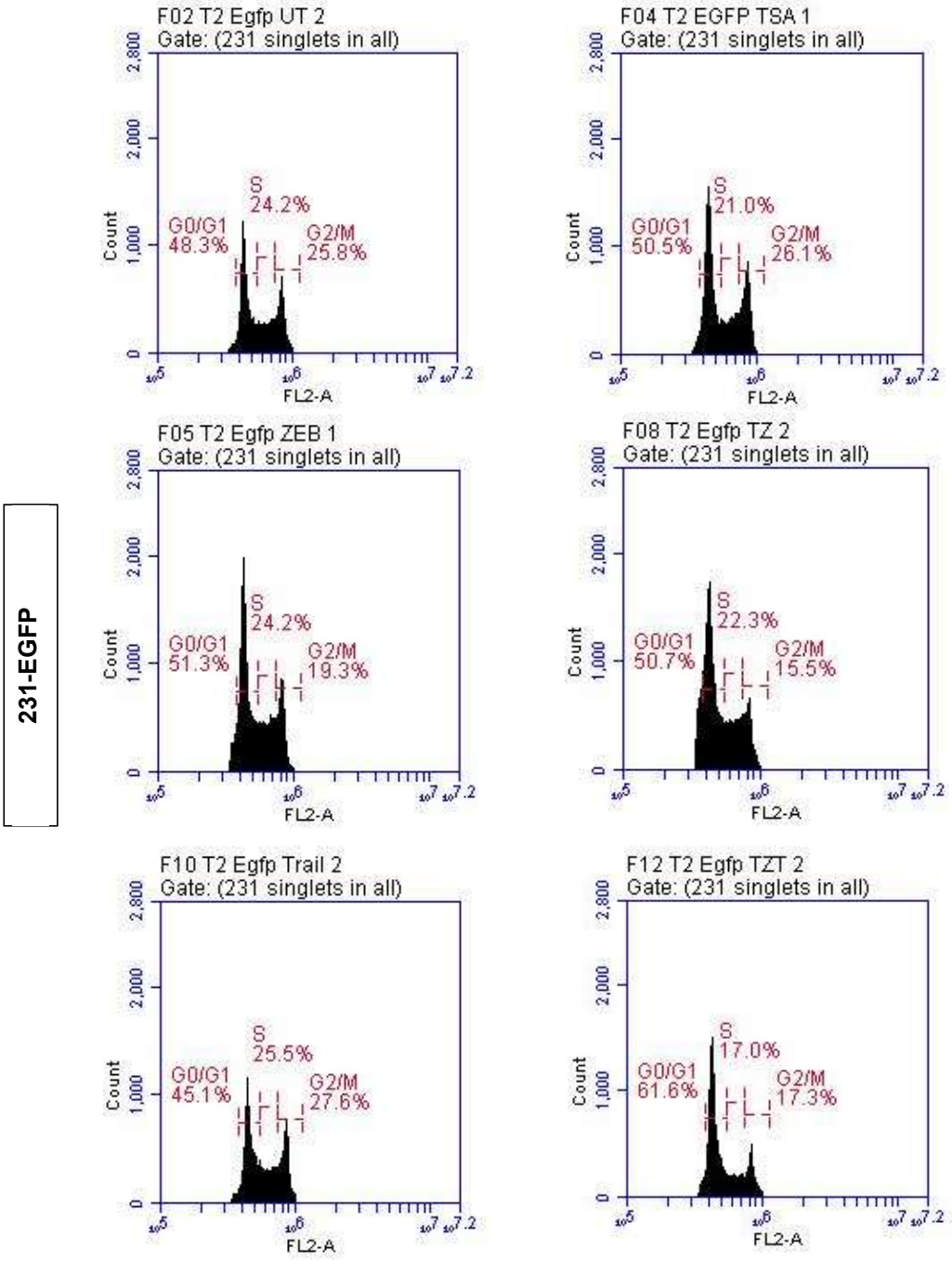
Appendix D Cell viability curve of MDA-MB-231 treated with 2, 4, 6, 8 and 10 µM Zeb. Data represents means ± SEM from three independent experiments.



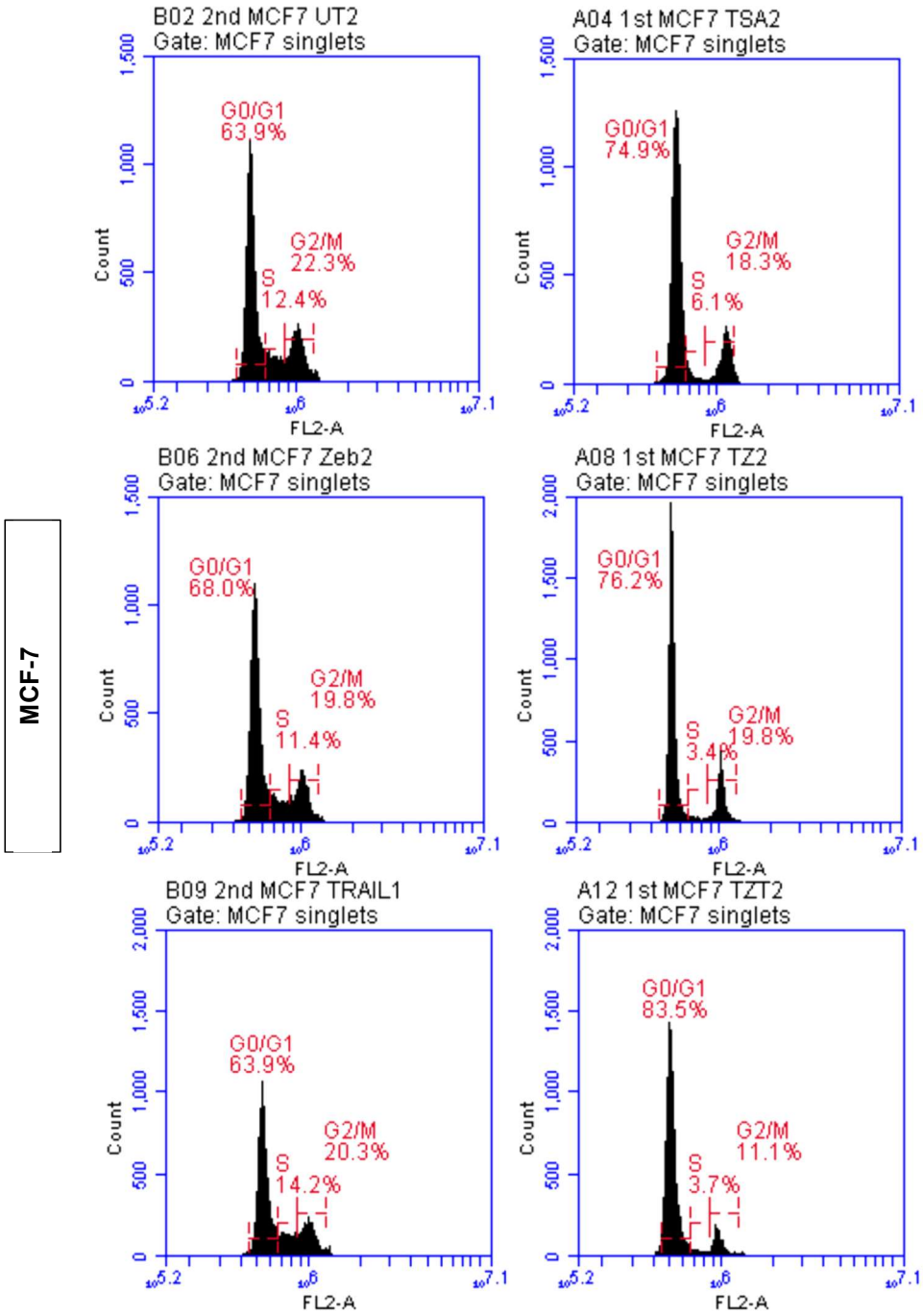
Appendix E Histogram representation of cell cycle analysis on (A) **untreated MDA-MB-231** cells and **MDA-MB-231 treated with** (B) IC_{25} of TSA , (C) IC_{25} of Zeb, (D) IC_{25} of TSA and Zeb combination, (E) 50 ng/mL TRAIL for 24h and (F) IC_{25} of TSA and Zeb combination for 12h followed by 50 ng/mL TRAIL for **24 h**.



Appendix F Histogram representation of cell cycle analysis on (A) **untreated 231-empty vector (231-EV)** cells and **231-EV cells treated with** (B) IC_{25} of TSA , (C) IC_{25} of Zeb, (D) IC_{25} of TSA and Zeb combination, (E) 50 ng/mL TRAIL for 24h and (F) IC_{25} of TSA and Zeb combination for 12h followed by 50 ng/mL TRAIL for **24 h**.

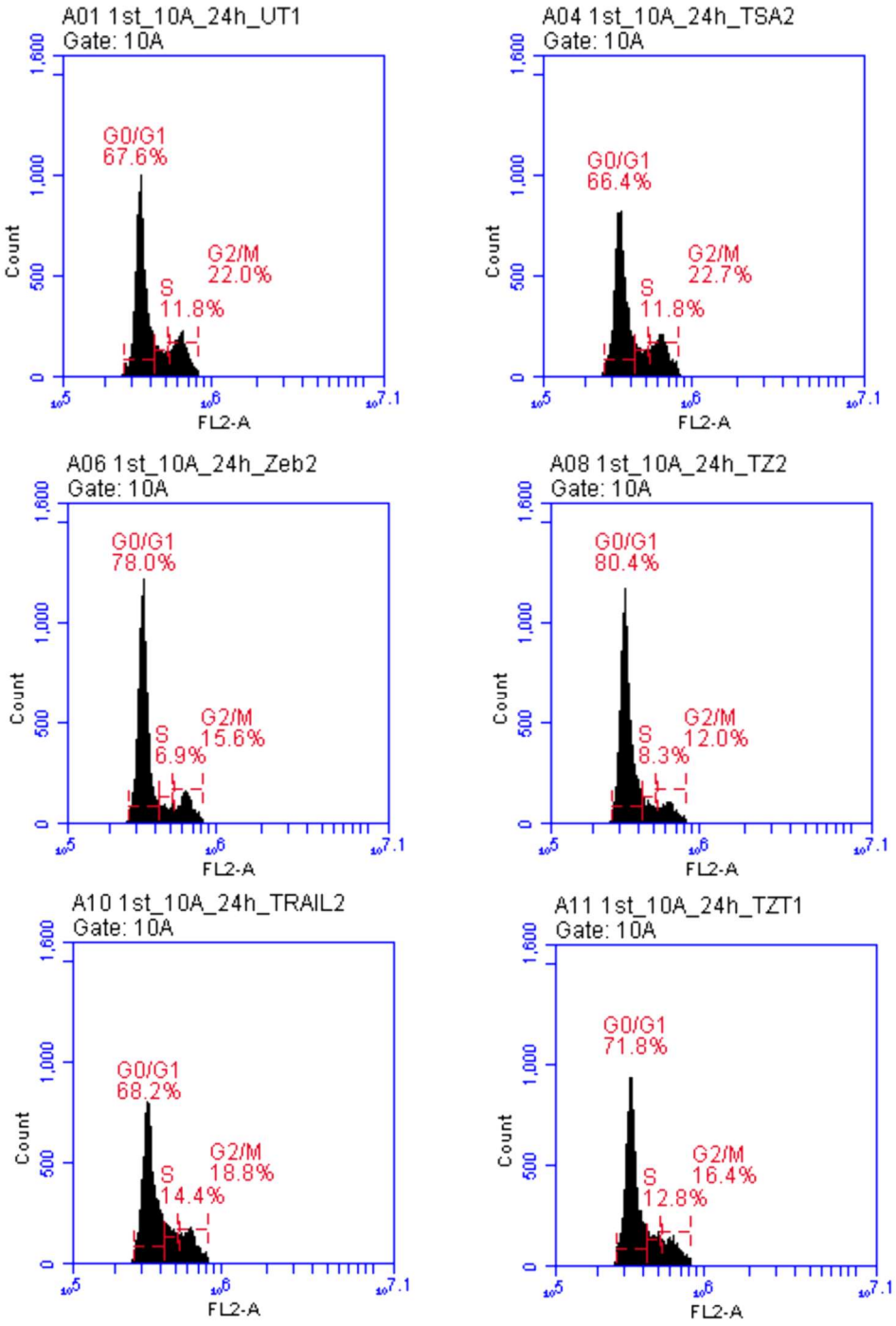


Appendix G Histogram representation of cell cycle analysis on (A) **untreated 231-E-cadherin-GFP (231-EGFP)** cells and **231-EGFP cells treated with** (B) IC_{25} of TSA , (C) IC_{25} of Zeb, (D) IC_{25} of TSA and Zeb combination, (E) 50 ng/mL TRAIL for **24 h** and (F) IC_{25} of TSA and Zeb combination for 12h followed by 50 ng/mL TRAIL for **24 h.**

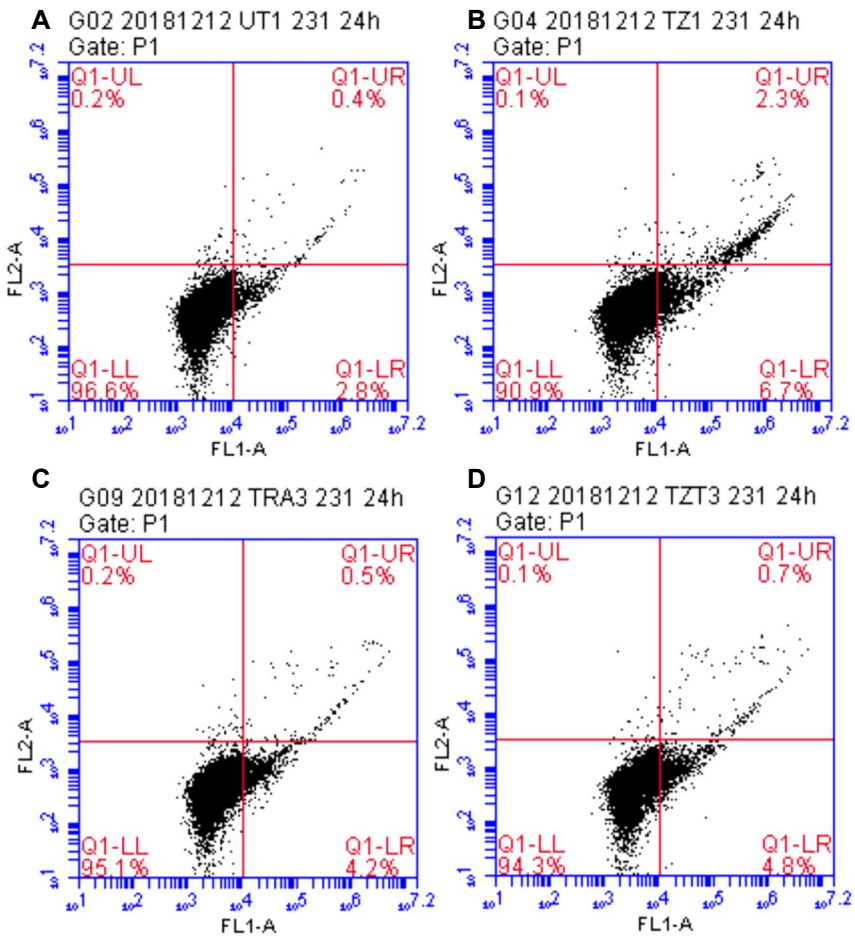


Appendix H Histogram representation of cell cycle analysis on (A) **MCF-7** cells and **MCF-7 cells treated with** (B) IC_{25} of TSA , (C) IC_{25} of Zeb, (D) IC_{25} of TSA and Zeb combination, (E) 50 ng/mL TRAIL for **24 h** and (F) IC_{25} of TSA and Zeb combination for 12h followed by 50 ng/mL TRAIL for **24 h.**

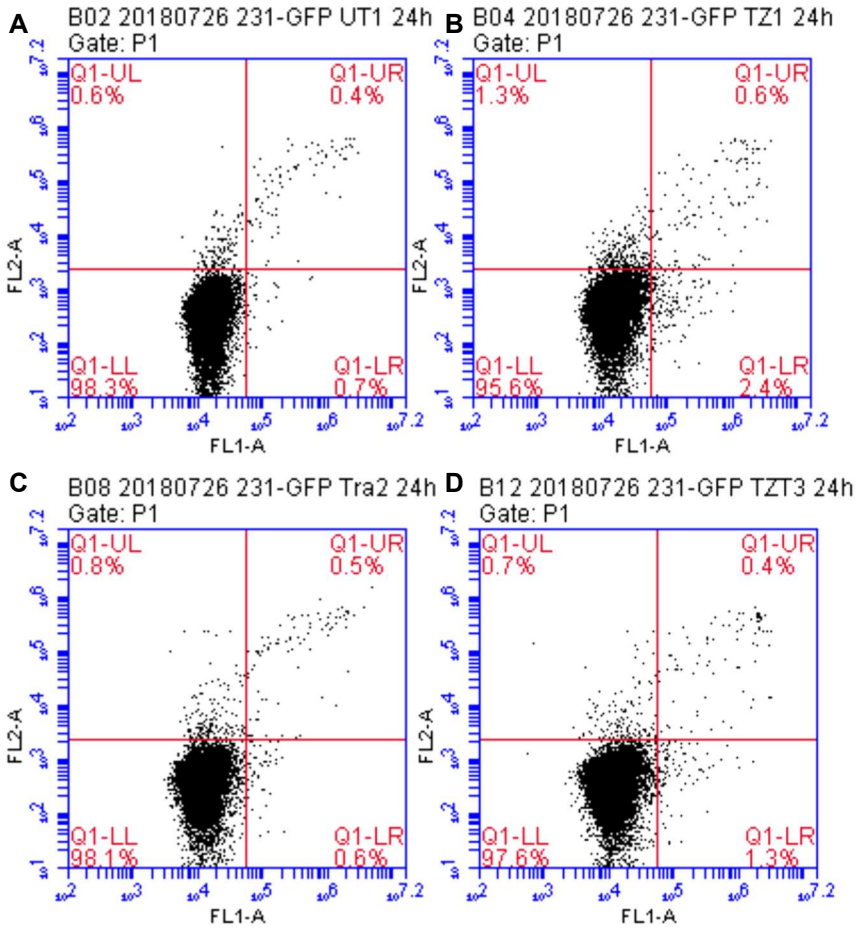
MCF10A



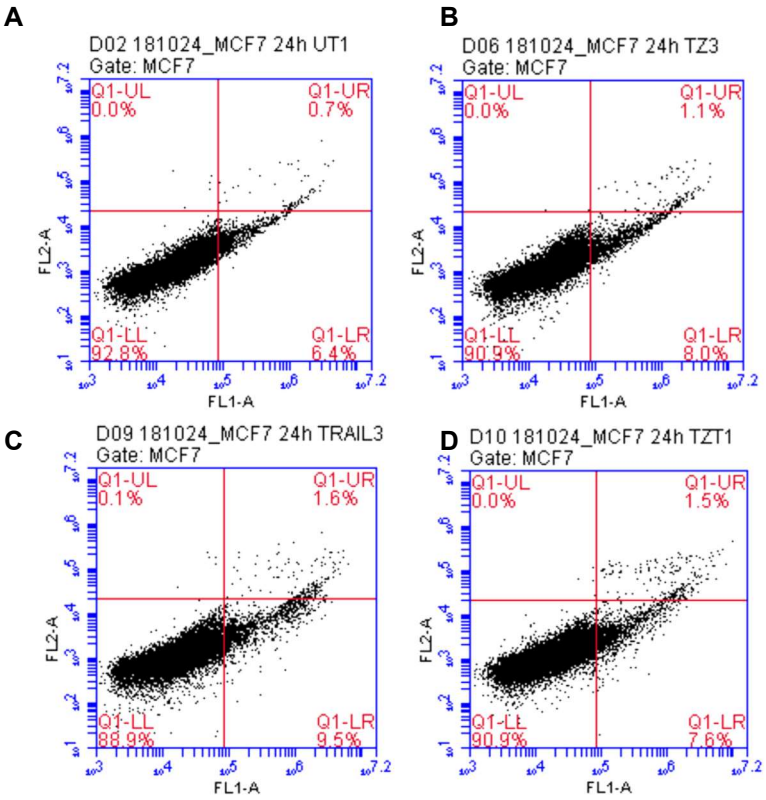
Appendix I Histogram representation of cell cycle analysis on (A) **MCF10A** cells and **MCF10A cells treated with** (B) IC_{25} of TSA , (C) IC_{25} of Zeb, (D) IC_{25} of TSA and Zeb combination, (E) 50 ng/mL TRAIL for **24 h** and (F) IC_{25} of TSA and Zeb combination for 12h followed by 50 ng/mL TRAIL for **24 h.**



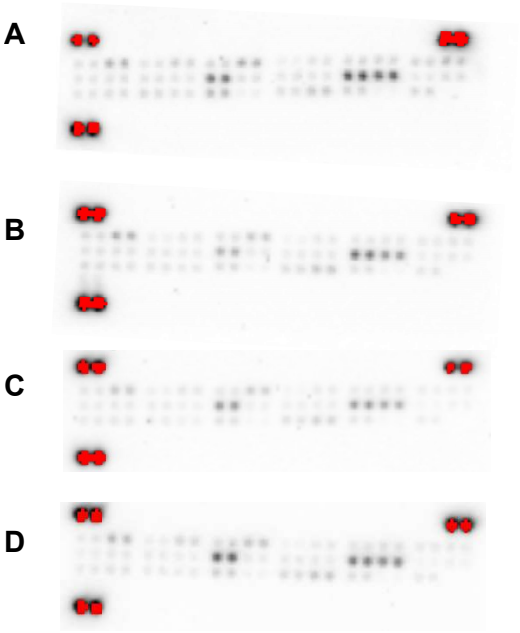
Appendix J Histogram representation of Annexin V-FITC/PI cellular apoptosis assay on (A) **MDA-MB-231** cells and **MDA-MB-231 cells treated with** (B) IC_{25} of TSA and Zeb combination, (C) 50 ng/mL TRAIL for **24 h** and (D) IC_{25} of TSA and Zeb combination for 12h followed by 50 ng/mL TRAIL for **24 h.**



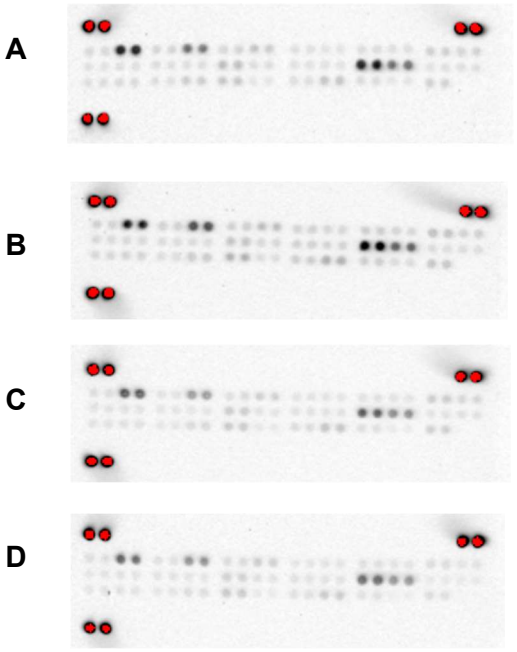
Appendix K Histogram representation of Annexin V-FITC/PI cellular apoptosis assay on (A) **231-EGFP** cells and **231-EGFP cells treated with** (B) IC_{25} of TSA and Zeb combination, (C) 50 ng/mL TRAIL for **24 h** and (D) IC_{25} of TSA and Zeb combination for 12h followed by 50 ng/mL TRAIL for **24 h.**



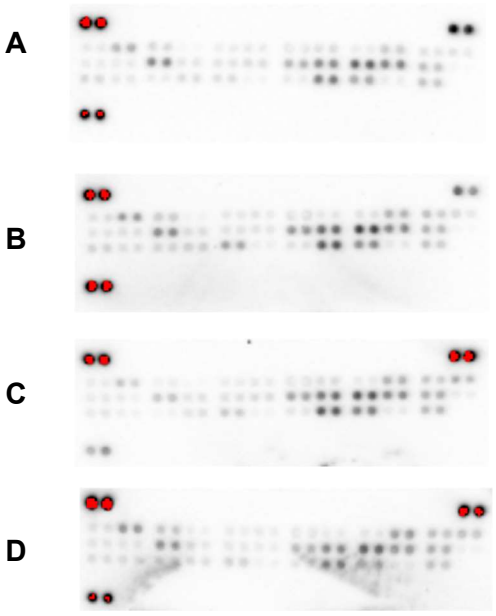
Appendix L Histogram representation of Annexin V-FITC/PI cellular apoptosis assay on (A) **MCF-7** cells and **MCF-7 cells treated with** (B) IC_{25} of TSA and Zeb combination, (C) 50 ng/mL TRAIL for **24 h** and (D) IC_{25} of TSA and Zeb combination for 12h followed by 50 ng/mL TRAIL for **24 h.**



Appendix M The processed apoptosis antibody array sheets of (A) **MDA-MB-231** cells and **MDA-MB-231 cells treated with** (B) IC_{25} of TSA and Zeb combination, (C) 50 ng/mL TRAIL for **72h** and (D) IC_{25} of TSA and Zeb combination for 12 h followed by 50 ng/mL TRAIL for **72h.**



Appendix N The processed apoptosis antibody array sheets of (A) **231-EGFP** cells and **231-EGFP cells treated with** (B) IC_{25} of TSA and Zeb combination, (C) 50 ng/mL TRAIL for **72h** and (D) IC_{25} of TSA and Zeb combination for 12 h followed by 50 ng/mL TRAIL for **72h.**



Appendix O The processed apoptosis antibody array sheets of (A) **MCF-7** cells and **MCF-7 cells treated with** (B) IC_{25} of TSA and Zeb combination, (C) 50 ng/mL TRAIL for **72h** and (D) IC_{25} of TSA and Zeb combination for 12 h followed by 50 ng/mL TRAIL for **72h.**